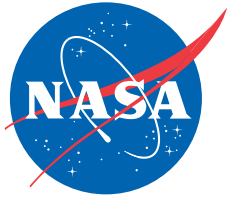


NASA/TP-2014-218374



## **Rotorcraft Airloads Measurements—Extraordinary Costs, Extraordinary Benefits**

*William G. Bousman  
U.S. Army Aeroflightdynamics Directorate  
Ames Research Center, Moffett Field, California*

---

**August 2014**

## The NASA STI Program Office . . . in Profile

Since its founding, NASA has been dedicated to the advancement of aeronautics and space science. The NASA Scientific and Technical Information (STI) Program Office plays a key part in helping NASA maintain this important role.

The NASA STI Program Office is operated by Langley Research Center, the Lead Center for NASA's scientific and technical information. The NASA STI Program Office provides access to the NASA STI Database, the largest collection of aeronautical and space science STI in the world. The Program Office is also NASA's institutional mechanism for disseminating the results of its research and development activities. These results are published by NASA in the NASA STI Report Series, which includes the following report types:

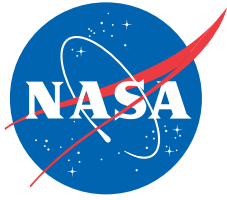
- **TECHNICAL PUBLICATION.** Reports of completed research or a major significant phase of research that present the results of NASA programs and include extensive data or theoretical analysis. Includes compilations of significant scientific and technical data and information deemed to be of continuing reference value. NASA's counterpart of peer-reviewed formal professional papers but has less stringent limitations on manuscript length and extent of graphic presentations.
- **TECHNICAL MEMORANDUM.** Scientific and technical findings that are preliminary or of specialized interest, e.g., quick release reports, working papers, and bibliographies that contain minimal annotation. Does not contain extensive analysis.
- **CONTRACTOR REPORT.** Scientific and technical findings by NASA-sponsored contractors and grantees.

- **CONFERENCE PUBLICATION.** Collected papers from scientific and technical conferences, symposia, seminars, or other meetings sponsored or cosponsored by NASA.
- **SPECIAL PUBLICATION.** Scientific, technical, or historical information from NASA programs, projects, and missions, often concerned with subjects having substantial public interest.
- **TECHNICAL TRANSLATION.** English-language translations of foreign scientific and technical material pertinent to NASA's mission.

Specialized services that complement the STI Program Office's diverse offerings include creating custom thesauri, building customized databases, organizing and publishing research results . . . even providing videos.

For more information about the NASA STI program, see the following:

- Access the NASA STI program home page at <http://www.sti.nasa.gov>
- E-mail your question via the Internet to [help@sti.nasa.gov](mailto:help@sti.nasa.gov)
- Fax your question to the NASA STI Help Desk at 443-757-5803
- Telephone the NASA STI Help Desk at 443-757-5802
- Write to:  
NASA Center for AeroSpace Information (CASI)  
7115 Standard Drive  
Hanover, MD 21076-1320



## **Rotorcraft Airloads Measurements—Extraordinary Costs, Extraordinary Benefits**

*William G. Bousman  
U.S. Army Aeroflightdynamics Directorate  
Ames Research Center, Moffett Field, California*

National Aeronautics and  
Space Administration

Ames Research Center  
Moffett Field, California 94035-1000

## **Acknowledgments**

I obtained a great deal of help from many people while preparing this report. I thank them all, including Ed Austin, Ken Bartie, Ed Beno, Mahendra Bhagwat, Dave Conner, Jeff Cross, Joe Chambers, Bruce Charles, Frank Harris, Danny Hoad, Euan Hooper, Terry Hornbuckle, Larry Jenkins, Wayne Johnson, Andy Kerr, Bob Kufeld, Tom Lawrence, Al Lizak, Tom Maier, Wayne Mantay, Bobby Mathew, Jim McCroskey, Don Merkley, Jorge Morillo, Tom Norman, Bob Ormiston, Ray Piziali, Ray Prouty, Art Ragosta, Nischint Rajmohan, Mike Scully, Marilyn Smith, Karen Studebaker, Barbara Trippe, John Vorvald, John Ward, Bill Warmbrodt, Bob Wood, Gloria Yamauchi, and Hyeonsoo Yeo.

This publication is an expanded version of the 31st Alexander Nikolsky Honorary Lecture, originally presented at the American Helicopter Society 66th Annual Forum, Virginia Beach, VA, May 3–5, 2011.

Available from:

NASA Center for Aerospace Information  
7115 Standard Drive  
Hanover, MD 21076-1320

National Technical Information Service  
5301 Shawnee Road  
Alexandria, VA 22312



## TABLE OF CONTENTS

<p>SUMMARY ..... 1</p> <p>INTRODUCTION ..... 1</p> <p>ROTORCRAFT AIRLOADS ..... 2</p> <p>EXTRAORDINARY COSTS, EXTRAORDINARY BENEFITS ..... 3</p> <p>HISTORY OF AIRLOADS TESTING ..... 4</p> <p style="padding-left: 20px;">Flight Envelope Limits ..... 4</p> <p style="padding-left: 20px;">Early NACA Research Into Rotor Loads ..... 6</p> <p style="padding-left: 20px;">The Twelve Airloads Tests ..... 7</p> <p style="padding-left: 20px;">Technology and Airloads Testing ..... 9</p> <p style="padding-left: 20px;">Data Validation ..... 13</p> <p style="padding-left: 40px;">Repeat Cases ..... 13</p> <p style="padding-left: 40px;">Steady Thrust Comparisons ..... 15</p> <p style="padding-left: 40px;">Test-on-Test Cases ..... 17</p> <p>BENEFITS OBTAINED FROM AIRLOADS TESTING ..... 20</p> <p style="padding-left: 20px;">Citations as a Measure of Benefits ..... 21</p> <p style="padding-left: 20px;">Understanding Airloads ..... 22</p> <p style="padding-left: 40px;">First Problem: Vortex Wake Loading at Low Speed ..... 22</p> <p style="padding-left: 40px;">Second Problem: Dynamic Stall ..... 23</p> <p style="padding-left: 40px;">Third Problem: High-Speed Structural Loads ..... 25</p> <p style="padding-left: 20px;">UH-60A Airloads Program and Workshops ..... 29</p> <p style="padding-left: 40px;">UH-60A Airloads Program ..... 30</p> <p style="padding-left: 40px;">UH-60A Airloads Workshop ..... 31</p> <p style="padding-left: 40px;">Airloads Workshops and the New Calculations ..... 31</p> <p style="padding-left: 40px;">The Airloads Workshops Transformation ..... 33</p> <p>CONCLUDING REMARKS ..... 37</p> <p>THE FIVE CHALLENGES ..... 38</p> <p style="padding-left: 20px;">Integrating the New Methods ..... 38</p>	<p>Nonlinear Aerodynamics—Each Rotor is Different ..... 38</p> <p>Remaining Deficiencies ..... 39</p> <p>Loss of Experimental Data ..... 40</p> <p>Alternatives to Full-Scale Airloads Tests ..... 42</p> <p style="padding-left: 20px;">Model Rotor Tests ..... 42</p> <p style="padding-left: 20px;">Full-Scale Rotor Tests With Limited Instrumentation ..... 43</p> <p style="padding-left: 20px;">Simplified Measurements ..... 44</p> <p style="padding-left: 20px;">New Measurement Techniques and Technologies ..... 44</p> <p>APPENDIX 1—AIRLOADS TEST DESCRIPTIONS ..... 45</p> <p style="padding-left: 20px;">Introduction ..... 45</p> <p style="padding-left: 20px;">NACA 15-Foot-Diameter Model Rotor ..... 45</p> <p style="padding-left: 20px;">CH-34 Flight Test ..... 47</p> <p style="padding-left: 20px;">UH-1A Flight Test ..... 50</p> <p style="padding-left: 20px;">CH-34 Wind Tunnel Test ..... 53</p> <p style="padding-left: 20px;">CH-47A Flight Test ..... 54</p> <p style="padding-left: 20px;">NH-3A Compound Flight Test ..... 57</p> <p style="padding-left: 20px;">XH-51A Compound Flight Test ..... 59</p> <p style="padding-left: 20px;">CH-53A Flight Test ..... 62</p> <p style="padding-left: 20px;">AH-1G/Operational Loads Survey ..... 64</p> <p style="padding-left: 20px;">AH-1G/Tip Aerodynamics and Acoustics Test ..... 67</p> <p style="padding-left: 20px;">UH-60A Airloads Program Flight Test ..... 70</p> <p style="padding-left: 20px;">UH-60A Airloads Wind Tunnel Test ..... 74</p> <p>APPENDIX 2—CORRELATION ACCURACY ..... 78</p> <p style="padding-left: 20px;">Introduction ..... 78</p> <p style="padding-left: 20px;">Steady Data ..... 78</p> <p style="padding-left: 20px;">Time History Data ..... 79</p> <p>REFERENCES ..... 81</p>
--	--



# Rotorcraft Airloads Measurements—Extraordinary Costs, Extraordinary Benefits

William G. Bousman<sup>1</sup>

Ames Research Center

## SUMMARY

The first airloads measurements were made in the 1950s at NACA Langley on a 15.3-foot-diameter model rotor, stimulated by the invention of miniaturized pressure transducers. The inability to predict higher harmonic loads in those early years led the U.S. Army to fund airloads measurements on the CH-34 and the UH-1A aircraft. Nine additional comprehensive airloads tests have been done since that early work, including the recent test of an instrumented UH-60A rotor in the 40- by 80-Foot Wind Tunnel at NASA Ames. This historical paper discusses the 12 airloads tests and how the results were integrated with analytical efforts. The recent history of the UH-60A Airloads Workshops is presented, and it is shown that new developments in analytical methods have transformed our capability to predict airloads that are critical for design.

## INTRODUCTION

It is traditional for the Nikolsky Lecturer to draw some connection between the lecturer and Professor Nikolsky, something that becomes more difficult to do with each passing year. I have no such connection, but I do have a link to the start of the honorary lectureship and that will have to suffice.

In 1978, Dewey Hodges and I wrote a paper on the correlation of theory and experiment for helicopter rotor aeromechanical stability (Bousman and Hodges, 1979). I had the opportunity to present the paper at the Fourth European Rotorcraft Forum in Stresa, Italy, in September of that year. The plenary session was a presentation of “Early Development of the Helicopter at Sikorsky.” Sergei Sikorsky gave the presentation based on his and Bill Paul’s delving into the Sikorsky archives (fig. 1). Most of the lecture focused on Igor Sikorsky’s notebooks. It was a marvelous talk and very stimulating for a young engineer. Unfortunately there was no written version.

That winter, I think in January, Bart Kelley (fig. 2) presented a talk to the San Francisco Bay Area Chapter of the American Helicopter Society (AHS) on Art Young, Larry Bell, and the early history of the Bell two-bladed rotor. I found this talk amazing as well, and wondered why we could not have some of this fascinating history written down.

In the summer of 1979, I became the President of the San Francisco Bay Area Chapter. In quiet moments in the test area behind our offices at Ames Research Center, I started thinking whether there might be a way to create



Figure 1. Sergei Sikorsky (left) and Bill Paul (courtesy of Sikorsky Aircraft).



Figure 2. Bart Kelley (AHS International Archive).

<sup>1</sup>U.S. Army Aeroflightdynamics Directorate (retired), Moffett Field, CA 94035

a history-oriented lecture and ensure that it was written down. I had a vague notion of the American Institute of Aeronautics and Astronautics (AIAA) lecture series, so I called the AIAA office and asked how they had structured their Dryden Lectureship in Research. The AIAA staffer I spoke with was very kind and sent me considerable information on the award. I then called the AHS and asked Kim Smith how we could go about proposing a new honorary award. She explained the process of making a formal proposal and then presenting it to the board.

The chapter and I put together a proposal for an honorary lectureship that would include both a lecture and a subsequent written manuscript to be published in the AHS Journal. Bob Wood was the AHS Western Region Vice President at the time, and he agreed to take the proposal to the next AHS board meeting. The board approved our proposal and named it in honor of Professor Alexander A. Nikolsky. The first recipient of the Alexander A. Nikolsky Honorary Lectureship was Steppy Stepniewski of Boeing Vertol. He presented this inaugural lecture at the 37th Annual Forum in New Orleans in 1981. Subsequently, a biography of Professor Nikolsky and that first lecture were published in the journal (Stepniewski, 1982a,b).

### ROTORCRAFT AIRLOADS

Airloads are the aerodynamic forces on a rotor blade and can be measured by installing pressure transducers at the blade's surface. Figure 3 shows the planforms of the 12 instrumented rotor blades used in the airloads tests that are the focus of this paper. These tests used at least five radial stations for the measured airloads, and the average number of transducers at any station ranged from 5 to about 12. After the individual pressures are measured and recorded, they are integrated along the blade chord to provide normal force and pitching moment (and in some cases chord force). The normal forces at the radial stations can then be integrated to provide the blade loads.

The airloads on the rotor are important for performance, flight control, fatigue loading, vibration, and acoustics. The steady or zeroth harmonic forces determine the helicopter's lift and propulsive force. First harmonic airloads are essential for control. The oscillatory airloads, usually the first to third harmonics, determine the fatigue loading on the blade and controls. Higher harmonics of airloading that are not cancelled at the rotor hub are important for vibration. Still higher harmonics of the airloads are important for radiated acoustic noise.

This paper begins by addressing the extraordinary costs of these airloads tests, in part, by describing how they fit into the concept of "Big Science." It also discusses what these experiments must achieve to bring about benefits that are comparable to their costs.

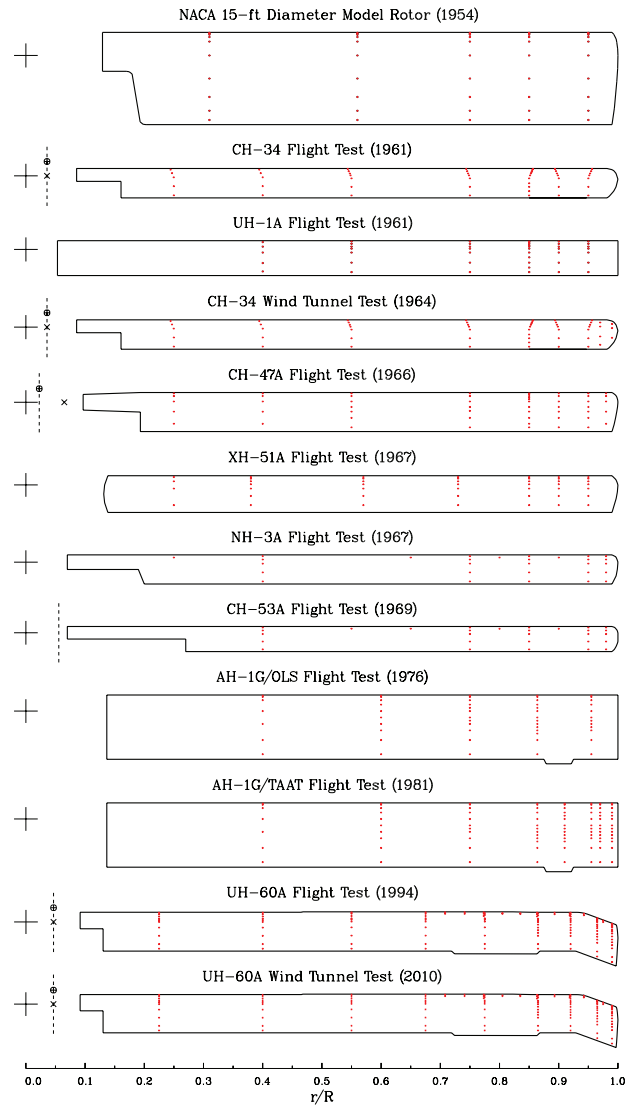


Figure 3. Blade planforms for 12 airloads tests showing locations of upper surface pressure transducers.

The primary theme of this paper is a history of airloads testing, from the first experiment by Jack Rabbott and Gary Churchill around 1954 (Rabbott and Churchill, 1956) to the recent wind tunnel test of the UH-60A blades in 2010 (Norman et al., 2011). To understand these experiments it is also essential to understand the development of airloads theory over the same time period. I am an engineer, not a philosopher, but I am attracted to the oriental concept of yin yang, which suggests that conflicting forces are interconnected and must achieve balance. I see experimentation as yin and theoretical developments as yang. But these are both just two sides of one problem. In the last decade the UH-60A Airloads Workshops have been successful in bringing these two sides together, and a discussion of those workshops and the transformation in our predictive capabilities is an important part of this paper.

In addition, the influence of technology is felt throughout this period, both on the experimental and the theoretical sides. Here there is also conflict, this time between new technological capabilities that offer sometimes too much or sometimes too little. Both the experimentalist and theoretician need to balance their needs with the new possibilities, so the subtheme of technology development weaves in and out of this paper.

Finally, this paper concludes with five challenges. These are areas where we need to focus if we are to use our new methods, tools, and understanding from the last decade to obtain a transformation.

By including only the 12 airloads tests that are the core of this paper, many excellent test programs based on pressure transducer measurements were excluded. These include full-scale flight tests with measurements at a limited number of radial stations and numerous model rotor tests. Many of these tests deserve their own history.

### EXTRAORDINARY COSTS, EXTRAORDINARY BENEFITS

A useful perspective of the costs of major research programs is that of “Big Science.” In the world of national and international science, projects that fit the moniker of Big Science are those that are too large to fund from conventional national research budgets. Each of these projects requires long and painstaking negotiations to develop the mission and funding. The promise that is made in all of these projects is that when overruns occur, the project will not eat everyone else’s resources.

Table 1 lists a sampling of Big Science programs (<http://www.msnbc.msn.com/id/14505278/>). A typical mix, some of these are currently operating (the International Space Station and the Large Hadron Collider (LHC)), one has been cancelled (the Superconducting Super Collider (SSC)), and two are in development (the International Thermonuclear Experimental Reactor (ITER) and the new space telescope). For the Webb Space Telescope, an independent panel reported a \$1.7 billion overrun in November 2010, bringing the cost to \$6.8 billion. “The overrun is \$700 million more than NASA now spends each year on all astronomy projects.” (Lawler and Bhattacharjee, 2010). There is currently an effort in congress to terminate the project (Bhattacharjee, 2011). Most of these projects are multinational—the expenses are simply too great for any one country to afford.

In the world of helicopter development, the numbers associated with Big Science are in the millions, not the billions, as shown in table 2. The Integrated Technology Rotor/Flight Research Rotor (ITR/FRR) project in the mid-1980s was for the development and test of two prototype

TABLE 1. BIG SCIENCE PROGRAMS

Project	Cost
International Space Station	\$35–100 billion
International Thermonuclear Experimental Reactor (ITER)	\$13 billion
Superconducting Super Collider (SSC)	\$8–11 billion
Large Hadron Collider (LHC)	\$8 billion
James Webb Space Telescope	\$6.8 billion

rotors that would employ the most recent technology developments, updating industrial capabilities since the development of the Utility Tactical Transport Aircraft System (UTTAS) and Advanced Attack Helicopter (AAH) programs. But after a few preliminary technology studies, the program was cancelled.

The XV-15 and Rotor Systems Research Aircraft (RSRA) developments occurred in the 1970s (Ward, 2010). The XV-15, a tiltrotor technology demonstrator, was a notable success and led to the eventual development of the V-22 Osprey. The RSRA, a “flying wind tunnel,” was brought to flight status, but never achieved its intended purpose (Snyder et al., 1990).

The UH-60A Airloads Program (Bugos, 2010), by comparison, was less costly than these others but had the same characteristics of many Big Science projects in its ability to overrun costs. As with so many of these types of programs, it was also cancelled, and that cancellation, followed by subsequent success, is part of this paper.

The extraordinary costs of airloads test programs must be matched by extraordinary benefits. It is not sufficient to simply collect data and publish a few test reports. Rather, it is essential that the data be useful for the rotorcraft designer and be able to affect future aircraft designs.

Larry Jenkins, Director of Research and Technology at Bell Helicopter Textron, briefed the National Research Council in 1995 about the essential knowledge that was required by the rotorcraft designer for improved helicopter

TABLE 2. BIG SCIENCE PROGRAMS IN THE HELICOPTER WORLD

Project	Cost
Integrated Technology Rotor/Flight Research Rotor (ITR/FRR)	\$60 million
Tiltrotor Research Aircraft (XV-15)	\$46 million
Rotor Systems Research Aircraft (RSRA)	\$42 million
UH-60A Airloads Program	\$6 million



designs in the disciplines of aeromechanics. Larry's requirements of essential knowledge are shown in figure 4, overlaid on the power-required curve of a typical helicopter as a function of advance ratio.

In the discipline of aeromechanics, the helicopter designer must consider performance, critical design and fatigue loads, vibration, and acoustics—all in a balanced approach. In hover, the designer must be able to accurately compute hover performance (1), the most unique attribute for a helicopter. For military aircraft there is also the need to predict the vertical climb capability of a helicopter (2), a required increment in installed power to give helicopters additional maneuver capability at their hover ceiling. Similarly, at cruise or maximum level flight speed, the designer must be able to accurately calculate the power required (3). For multiengine aircraft, it is also necessary to compute the one engine inoperative (OEI) performance (4). This is important for civilian designs where the OEI performance is critical for engine failures while leaving a landing platform and for military designs in defining the rotorcraft's service ceiling.

Critical design loads occur in maneuvers (5); these may occur infrequently but are the most severe loads encountered by a rotorcraft in flight. Fatigue loads (6), normally the first three harmonics, influence component safe lives or on-condition replacement. These loads cannot be allowed to occur in normal operation, lest excessive fatigue damage and early part replacement result.

Vibration typically occurs at high speed (7) and at the transition speed (8), about  $\mu = 0.1$ . For a four-bladed rotor, vibration is caused mostly by the third to fifth harmonics of rotor loads. Excessive vibration reduces mission capability and reduces crew and passenger comfort. Where the designer cannot reduce these vibratory loads in the design, he must accommodate them with some form of vibration reduction equipment.

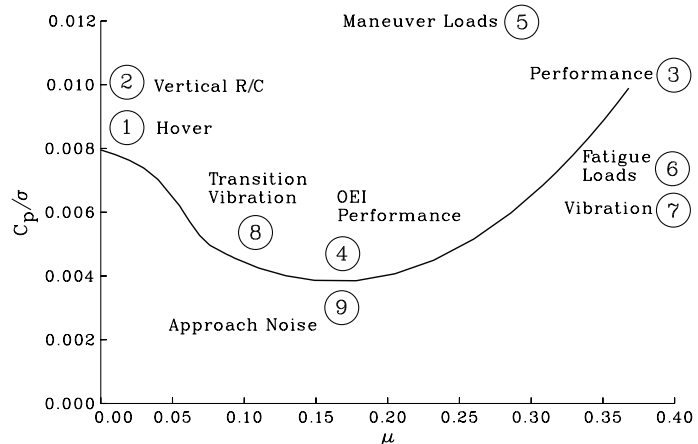


Figure 4. Knowledge requirements for rotorcraft designer for new aircraft designs.

Finally, the designer must account for radiated acoustic noise (9), whether at approach as illustrated here or for other conditions such as at high speed.

Improvements in designer capability were the objective of all of the airloads testing of the last half century. To provide the extraordinary benefits in the title of this paper, a significant improvement in designer capability must be shown.

## HISTORY OF AIRLOADS TESTING

### Flight Envelope Limits

It is essential that airloads testing include flight conditions throughout the flight envelope, but there is a special benefit for testing at the boundary limits. The thrust limits are for the most part caused by dynamic stall, and the propulsive limits are caused both by dynamic stall on the retreating side of the rotor and supersonic flows on the advancing side.

Figure 5 shows the flight envelope of the UH-60A as it was tested in 1993–94. The ordinate is the product of the nondimensional weight coefficient over solidity,  $C_w/\sigma$ , and the aircraft load factor (acceleration),  $n_z$ . Typically in flight testing, rotor thrust,  $C_T$ , is not accurately measured, whereas the weight is. For most purposes the two coefficients are roughly the same. By including the product of load factor, it is possible to include both level flight cases ( $n_z = 1.0$ ) and maneuvers. The abscissa is the advance ratio,  $\mu$ .

McHugh's thrust boundary (McHugh, 1978; McHugh et al., 1977) is used to define the flight envelope thrust limit for a helicopter rotor. That experiment used a 5.92-foot-diameter, three-bladed model rotor that was designed and built such that rotor's aerodynamic limits were encountered before the structural limits. Hence, at each trim condition in the tunnel, the rotor collective was increased until the rotor balance showed a thrust reversal, that is, the rotor thrust boundary. This test uniquely defined the rotor thrust boundary in level flight and hence the lifting flight envelope. In maneuvers, however, it is possible to exceed the thrust boundary, at least for short periods of time. As shown in figure 5, this occurs in both transient maneuvers such as the UTTAS pull-up and in steady diving turns.

The thrust boundary shown in figure 5 has been examined recently in the test of the UH-60A pressure-instrumented rotor in the NASA Ames 40- by 80-Foot Wind Tunnel by Norman et al. (2011). Figure 6 shows the measured rotor thrust as a function of collective pitch angle at  $\mu = 0.30$ . As the collective is increased, the incremental increase in rotor thrust with collective pitch angle decreases until it approaches zero at the thrust boundary. There is

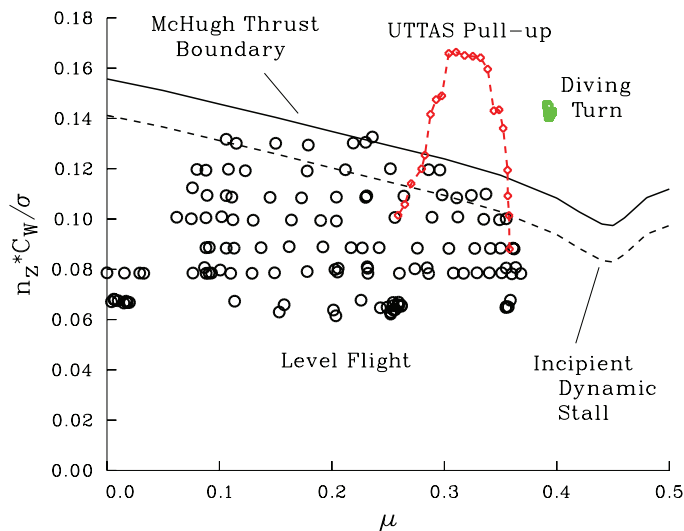


Figure 5. Nondimensional weight coefficient over solidity (including effect of load factor) as a function of advance ratio for UH-60A Airloads Program. Level flight data, a UTTAS pull-up maneuver, and a diving turn are compared with McHugh's thrust boundary and an incipient dynamic stall boundary.

fairly good agreement of the measured thrust boundary in figure 6 with McHugh (1978). The UH-60A data show a boundary at  $C_T/\sigma$  of 0.126, and McHugh's measurements show about 0.124. But McHugh's thrust boundary was determined for a constant propulsive force, whereas the UH-60A's boundary was for a zero shaft angle.

The thrust boundary (flight envelope limit) is caused by dynamic stall. Figure 7 shows the measured section pitching moments at  $r/R = 0.92$  as a function of eight collective pitch values for the UH-60A rotor in the wind tunnel test. At the thrust boundary, the pitching moment shows two cycles of deep stall in the fourth quadrant, and the rotor has run out of lift. But at lower collective pitch angles, the stall is less severe. The lowest pitch angle where there is evidence of dynamic stall is about  $9.1^\circ$ . At this angle there is a single cycle of incipient dynamic stall. The thrust at this point of incipient stall is about 12 percent below the thrust boundary. In the flight envelopes shown in this paper, this incipient dynamic stall line is used to show how dynamic stall becomes progressively more severe as the thrust boundary is approached (see figure 5).

The propulsive force limits for the helicopter may depend on the thrust boundary or transonic loading. The level flight data shown in figure 5 were obtained for six airspeed sweeps, roughly from  $C_W/\sigma = 0.08$  to 0.13 in increments of  $C_W/\sigma = 0.01$ . The pitching moments on the blade at  $r/R = 0.865$  are shown in figure 8 for the six limiting conditions. In all six sweeps, the UH-60A is power limited at these propulsive limits (some helicopters may be structurally limited at these loading conditions). At the highest thrust conditions, both the lift and propulsive force are

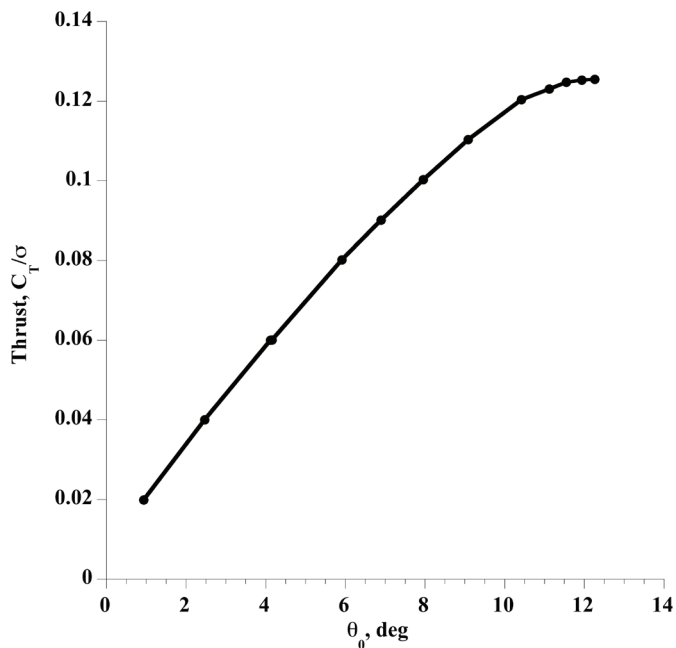


Figure 6. Nondimensional thrust coefficient over solidity as a function of collective pitch for the UH-60A in the 40-by 80-Foot Wind Tunnel;  $\mu = 0.30$ ,  $\alpha_s = 0$  (Norman et al., 2011).

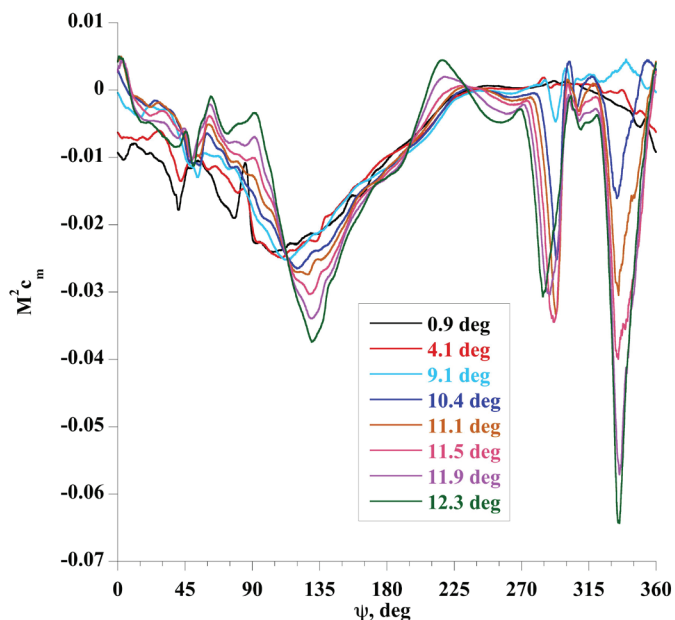


Figure 7. Nondimensional pitching moment as a function of azimuth angle for the UH-60A in the 40-by 80-Foot Wind Tunnel for eight collective pitch angles;  $\mu = 0.30$ ,  $\alpha_s = 0$ ,  $r/R = 0.92$  (Norman et al., 2011).

limited by dynamic stall. Although figure 8 shows section pitching moment and not power, the extent of the dynamic stall cycles are a good indicator of the loss of lift and the significant increase in drag that occur in severe dynamic stall.

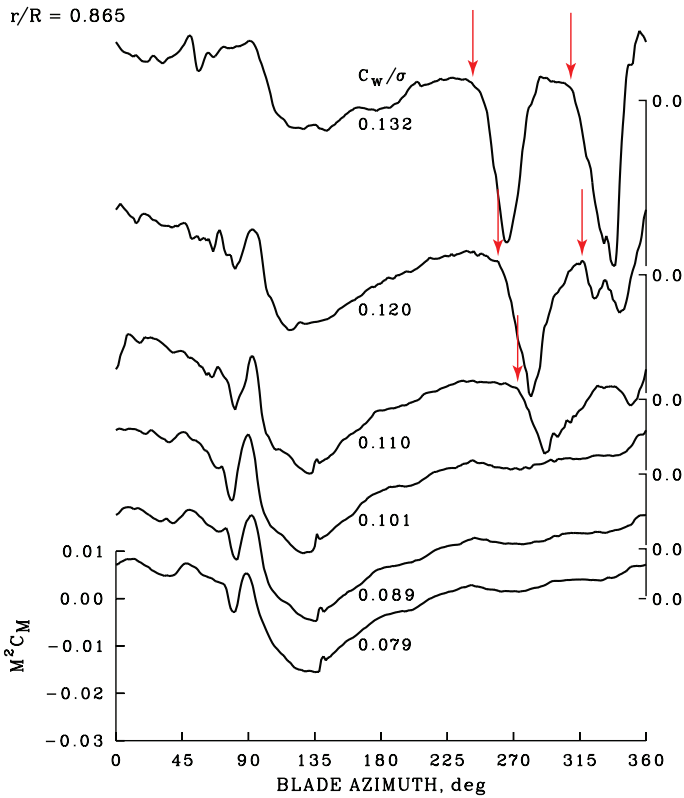


Figure 8. Nondimensional pitching moment as a function of azimuth angle for the UH-60A at the propulsive force limit in level flight;  $r/R = 0.865$ , 0–120 harmonics. Red arrows show the dynamic stall cycles.

At lower thrust conditions the aircraft is power limited, not because of dynamic stall (there is none) but because of the supercritical flows on the advancing side of the rotor. As the blade starts into the first quadrant there is a rapid increase in Mach number while at the same time the blade pitch angle is being reduced. At the limit conditions shown in figure 8, supersonic flow forms on the forward section of the upper surface of the airfoil and is followed by a shock. As the blade pitch angle becomes negative, supersonic flow and its associated shock form on the lower surface. The relative motions of the supersonic flows on the upper and lower surfaces cause rapid variations in the section pitching moments (as shown on the advancing side in figure 8) and are a good indicator of the high drag occurring near the tip of the blade for these conditions.

The high-speed capability of a helicopter is thus limited by either dynamic stall on the retreating side or supersonic flow on the advancing side. If rotor speed is reduced, this reduces the supersonic drag but makes dynamic stall worse. If the rotor speed is increased, the effects of dynamic stall may be eliminated but the supersonic drag increases. As in the Merle Travis song “16 Tons,” made popular by Tennessee Ernie Ford in the 1950s,

“One fist of iron, the other of steel  
If the right one don’t a-get you  
Then the left one will”

No matter, at the propulsive force limit, either dynamic stall or supersonic drag and the associated loads will get you.

The McHugh thrust boundary limit is to some extent idealized. Both McHugh’s model-scale measurements and the 40- by 80-Foot Wind Tunnel test data show that the thrust boundary is reduced by trim changes, such as an increase in propulsive force or an increase in shaft angle. But these shifts are small and do not diminish the value of the thrust boundary.

### Early NACA Research Into Rotor Loads

Fred Gustafson reported on early performance tests of a Sikorsky YR-4B in forward flight (Gustafson, 1945) and in hover with Al Gessow (Gustafson and Gessow, 1945). Figure 9 shows a photograph of that aircraft at Langley Field. The primary purpose of these tests was to obtain performance data, but Gustafson also looked at rotor speed variation as a means of identifying the stall boundaries. In this sense, these experiments and subsequent analysis of the data (Gustafson and Myers, 1946; Gustafson and Gessow, 1947) represent one of the earliest formal studies of rotor loading.

In the initial tests, Gustafson obtained steady level flight data, as shown in figure 10, with a maximum speed of  $\mu = 0.24$ . From the maximum speed condition, the engine speed “was carried to the lowest rotational speed at which the pilot could control the aircraft.” The decrease in rotor speed,  $N_R$ , provided for an increase in advance ratio, but also increased the thrust coefficient by the square of the rotor speed. Although no individual blade measurements were obtained, it appears that this test approach did allow the test aircraft to encounter dynamic stall.

Gustafson and his co-workers were under no illusions that a helicopter in forward flight was limited only by dynamic stall. Gustafson and Myers (1946) wrote, “Tip stall and compressibility thus ultimately limit the high speed of the helicopter.”

In the late 1950s, LeRoy Ludi published a series of reports on flight tests of a U.S. Army Sikorsky H-19A bailed to the National Advisory Committee for Aeronautics (NACA) at Langley Field (Ludi, 1958a,b; Ludi, 1959; Ludi, 1961). Figure 11 is a photo of the H-19A (Sikorsky Aircraft S-55). One blade of the H-19A was instrumented with strain gauges. Flap and chord bending and torsion moments were measured at  $0.14R$ , and flap bending moments were also obtained at  $0.40R$ .

Flight data were obtained both for relatively benign conditions as well as for severe loading cases including dynamic stall in maneuvers and level flight, vertical descents in the vortex ring state, and landing approaches.





Figure 9. Sikorsky YR-4B tested at the NACA in the mid-1940s; figure 2 of Gustafson (1945). (NASA photo, courtesy of Teresa Hornbuckle.)



Figure 11. Sikorsky H-19A tested at the NACA in the late 1950s; figure 1 of Ludi (1958a). (NASA photo, courtesy of Teresa Hornbuckle.)

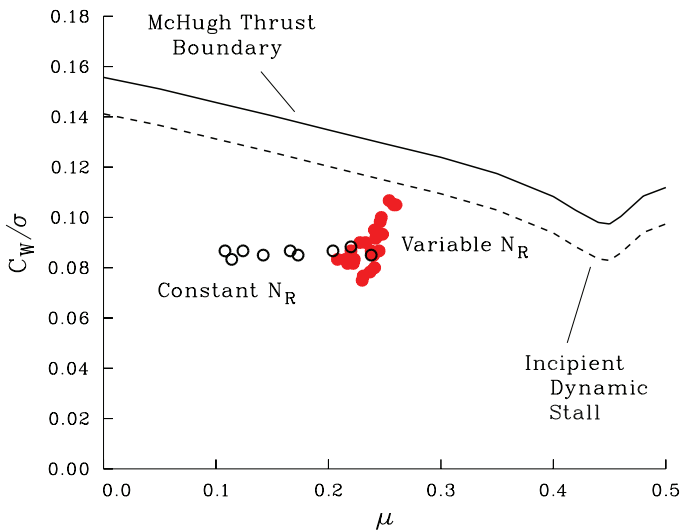


Figure 10. YR-4B performance test points compared to typical helicopter flight envelope. Steady level flight data at constant rotor speed as open circles (Flt 5) and reduced rotor speed cases as solid circles (Flt 9), Gustafson (1945).

To examine dynamic stall, Ludi used the same approach that Gustafson (1945) had used with the YR-4B, that is, reducing the rotor speed to increase both  $\mu$  and  $C_w/\sigma$ . The test aircraft achieved advance ratios as high as 0.36, and values of  $C_w/\sigma$  as great as 0.148. Plots of the torsion moments show substantial increases in the moments under dynamic stall conditions (Ludi, 1958b).

By looking at many different flight conditions for the H-19A, Ludi was able to identify those that had the greatest impact on blade loads. These publications were helpful in providing the industry with a better focus on critical flight conditions, as well as for the test planning for the first airloads flight tests in the following years.

## The Twelve Airloads Tests

Twelve rotorcraft airloads tests were accomplished, starting in 1953 and extending to 2010, a span of 57 years. The stimulus for these tests began with the work of John Patterson at the iconic NACA Instrumentation Research Division at Langley Aeronautical Laboratory in the early 1950s (Patterson, 1952). Patterson developed a miniaturized differential pressure transducer with high bandwidth and minimum sensitivity to g-forces (see figure 12).

Patterson's objective was to devise a miniature transducer that would fit within the wings of high-speed aircraft wind tunnel models, would have high-frequency response suitable for measurements of wing buffet, and would be insensitive to g-forces, either vibratory or centrifugal. Wind tunnel and propeller tests were the primary "customers" for the new transducer, but rotorcraft researchers immediately saw the potential for the new device. By 1953 Jack Rabbott had a two-bladed teetering rotor constructed, and 50 of Patterson's transducers were installed in the blade at 5 radial stations (Rabbott, 1956).

From the starting point of the NACA differential pressure transducers of the early 1950s on the two-bladed teetering rotor tested in the 30- by 60-Foot Wind Tunnel (Rabbott and Churchill, 1956), there have been 11 additional airloads tests. The sequence of these tests by year is shown in figure 13. The date is the final test date (if recorded) or an appropriate estimate based on contract or report dates. Descriptive parameters for the test rotors and their instrumentation are shown in table 3. A detailed description of each test is provided in Appendix 1.

The sponsors of the airloads tests are shown in figure 13, although the actual cost sharing is unknown where there was more than one sponsor. Unlike the other test programs, the CH-34 wind tunnel test included some funding from Sikorsky Aircraft. All the other tests were funded by U.S. Government agencies, one indicator of the extraordinary costs of these programs.

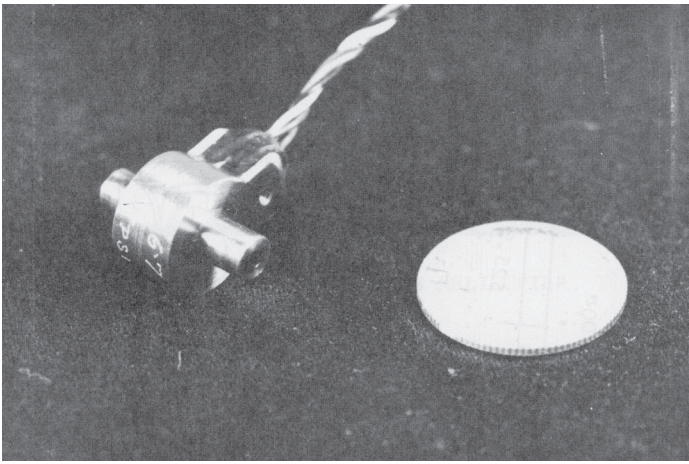


Figure 12. Patterson's miniaturized differential pressure transducer (a dime is shown on the right). Photo from Burpo and Lynn (1962).

Seven of the 12 airloads rotors were tested in the decade of the 1960s. This concentration of testing was probably a result of the enabling technology of the new pressure transducers, but may have been affected by other factors. The U.S. Army took responsibility for their own aircraft development programs in this decade rather than relying on the Navy or Air Force for these projects. Two of the airloads tests were compound helicopters, the Sikorsky NH-3A and Lockheed XH-51A, and these tests were a part of a larger effort to look at this technology on four different flight vehicles (Prouty, 2009). After the initial test activity in the 1960s, there were only four additional tests in the next 40 years, two of the Bell AH-1G Cobra and two of the Sikorsky UH-60A Black Hawk.

Table 3 provides details about the 12 airloads tests. The first several rows contain information about the rotor or aircraft whereas the remaining rows show information about the instrumentation. The number of radial stations refers to those stations where there were at least five pressure

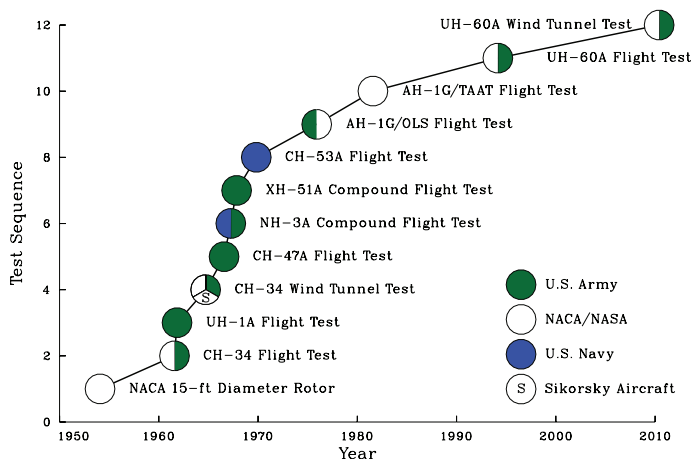


Figure 13. Sequence of 12 airloads tests.

transducers along the blade chord (with the exception of the two tip stations on the CH-34 rotor tested in the 40- by 80-Foot Wind Tunnel at Ames). In a few tests, additional pressure transducers were used at other radial stations. Single pressure transducers were added at  $0.09c$  at four radial stations on both the NH-3A and the CH-53A flight test programs. The UH-60A rotor had additional absolute pressure transducers added near the leading edge on both surfaces at eight radial stations to better quantify blade-vortex interactions

The number of pressure transducers per station (“X’ducers/station”) in table 3 is an average of the number of installed transducers over all radial stations. For the tests that used differential pressure transducers (or absolutes wired as differentials), the average is just the number of pressure transducers divided by the number of stations. For the last four tests, which used absolute pressure transducers, there were sometimes more transducers installed on the upper surface than the lower. The average for these tests is half the number of transducers divided by the number of stations. Thus, there is equivalency between the two types of transducers.

Rotating sensors are those whose signals were transferred from the rotating system to the fixed system, usually by a set of slip rings. These sensors include the pressure transducers, strain-gauge bridges on the blade, accelerometers, pitch-link loads, and a number of other measurements as described for each test in Appendix 1.

The bandwidth is defined in table 3 as the number of harmonics. The number of azimuthal samples per revolution is twice the bandwidth. The azimuthal step size is  $360^\circ$  divided by the number of azimuthal samples.

The number of rotating samples is the sum of the number of samples for each sensor for one revolution times the number of test points. In a number of these tests more than one revolution of data were recorded, but the “Rotating samples” in table 3 are for a single revolution for each test point.

For the UH-1A test, four test points were obtained with the bandwidth increased to 12 harmonics instead of 6. To obtain this increased bandwidth it was necessary to reduce the number of sensors that were recorded. These changes are shown in table 3 in parentheses. The purpose of the increased bandwidth is discussed below.

Both rotors on the CH-47A were instrumented for that test so there were many more rotating sensor measurements than in prior tests and more rotating samples as well.

The two AH-1G Cobra tests used multiplex frequency modulation (FM) analog tape recording. The bandwidth, therefore, depended on which FM band the instrumentation

TABLE 3. DESCRIPTION OF AIRLOADS ROTOR TESTS, PART 1

Test	1	2	3	4	5	6
Aircraft	model rotor	CH-34	UH-1A	CH-34	CH-47A	NH-3A
Type	wind tunnel	flight	flight	wind tunnel	flight	flight, compound
Sponsor	NACA	NASA, Army	Army	NASA, Army, Sikorsky	Army	Navy, Army
Manufacturer	NACA	Sikorsky	Bell	Sikorsky	Boeing	Sikorsky
No. blades	2	4	2	4	3 (×2)	5
Airfoil	0012	0012	0015	0012	mod 0012	0012
Twist, deg	0.0	-8.0	-15.0	-8.0	-9.0	-4.0
Solidity	0.0974	0.0622	0.0369	0.0622	0.0619	0.0781
Diameter, ft	15.3	56.0	43.8	56.0	51.9	62.0
Tip speed, ft/sec	481.	650.	716.	650.	712.	660.
Radial stations	5	7	6 (5)	9	8	5
X'ducers/station	10.0	7.0	7.3 (7.4)	6.2	6.8	5.0
Rotating sensors	57	67	78 (49)	70	166	90
Test points	6	129	17 (4)	10	121	74
Bandwidth, harm.	24	12	6 (12)	36	8	36
Rotating samples	15,936	205,110	20,015	48,480	316,052	479,520
Test hours	—	<10.0	6.4	—	—	16.4
Completion date	1954	1961	1961	1964	1966	1967
References	Rabbott, 1956; Rabbott and Churchill, 1956; Mayo, 1959	Scheiman and Ludi, 1963; Scheiman, 1964	Burpo and Lynn, 1962	Rabbott et al., 1966a,b	Golub and McLachlan, 1967; Grant and Pruyn, 1967; Obbard, 1967; Pruyn, 1967; Pruyn, 1968	Fenaughty and Beno, 1970a,b

was assigned to. There were three bandwidths, roughly 9 harmonics for structural parameters, 37 harmonics for inboard pressure transducers, and 78 harmonics for outboard pressure transducers.

### Technology and Airloads Testing

Improvements in technology have had a significant impact on airloads testing over the half century covered in this paper. In many cases the technology improvements have enabled major advances in the amount of data that could be obtained in these tests, but there has been a downside as well. Sometimes the industry and the government simply were not able to handle some of the new technologies, and control of the data was lost.

The test measurements that were made in the 12 tests are characterized into 2 groups in figures 14 and 15. Figure

14 shows the number of instrumented radial stations, the number of chordwise pressure transducers, and the total number of rotating sensors over time. Figure 15 shows the natural logarithm of the number of test points, the harmonic bandwidth, and the number of rotating samples over time.

As shown in figure 14, the number of radial stations has varied from five to nine over the last half century. Reducing the number of radial stations has the advantage of a consequent reduction for modern tests of 20 to 30 pressure transducers, but too few instrumented radial stations means that there will be unexamined aerodynamic events on the rotor.

The first test installed 10 differential pressure transducers at each radial station. Subsequent tests dropped this number, soon reaching a basement level of only five transducers. This number has climbed for the most recent tests and the average number is about 12 (for absolute pressure transducer measurements, that means 24 transducers at each

TABLE 3. DESCRIPTION OF AIRLOADS ROTOR TESTS, PART 2

Test	7	8	9	10	11	12
Aircraft	XH-51A	CH-53A	AH-1G	AH-1G	UH-60A	UH-60A
Type	flight, compound	flight	flight	flight	flight	wind tunnel
Sponsor	Army	Navy	Army, NASA	NASA	NASA, Army	NASA, Army
Manufacturer	Lockheed	Sikorsky	Bell	Bell	Sikorsky	Sikorsky
No. blades	4	6	2	2	4	4
Airfoil	mod 0012	mod 0011	mod 0009	mod 0009	SC1095, SC1094 R8	SC1095, SC1094 R8
Twist, deg	-4.0	-6.0	-10.0	-10.0	-16.0	-16.0
Solidity	0.0788	0.1150	0.0690	0.0690	0.0826	0.0826
Diameter, ft	35.0	72.0	44.0	44.0	53.7	53.7
Tip speed, ft/sec	651.	709.	746.	746.	719.	719.
Radial stations	7	5	5	8	9	9
X'ducers/station	6.6	5.0	11.0	11.8	12.3	12.3
Rotating sensors	85	109	285	363	354	322
Test points	49	56	238	312	962	2,755
Bandwidth, harm.	10	36	9, 37, 78	9, 37, 78	120	1028
Rotating samples	60,760	439,438	2,527,798	4,220,674	64,198,493	1,444,243,200
Test hours	-	10.8	28.0	35.0	57.0	83.0
Completion date	1967	1969	1976	1981	1994	2010
References	Bartsch, 1968a,b; Sweers, 1968	Beno, 1970a,b	Shockey et al., 1977	Cross and Watts, 1988; Cross and Tu, 1990	Kufeld et al., 1994; Bousman and Kufeld, 2005	Norman et al., 2011

radial station). The impetus to install more pressure transducers at each radial station is largely a result of attempting to better understand transonic flow over the rotor airfoil as well as the progression of the dynamic stall vortices, both nonlinear phenomena.

Once the number of radial stations and chordwise pressure transducers have been selected, the total number of rotating sensors is roughly determined. Figure 14 shows that the average number of pressure transducers at each station closely matches the total number of sensors. The one exception is for the CH-47A flight test where both rotors were instrumented.

Figure 15 shows the natural logarithm of the number of harmonics, test points, and the total rotating samples. Each of these parameters has shown exponential growth over the last half century, albeit at different rates. Much of this increase was enabled by improvements in the technologies that deal with acquiring, recording, and storing the measured data.

The first experiment was based on Patterson's development work at the NACA Langley Aeronautical Laboratory

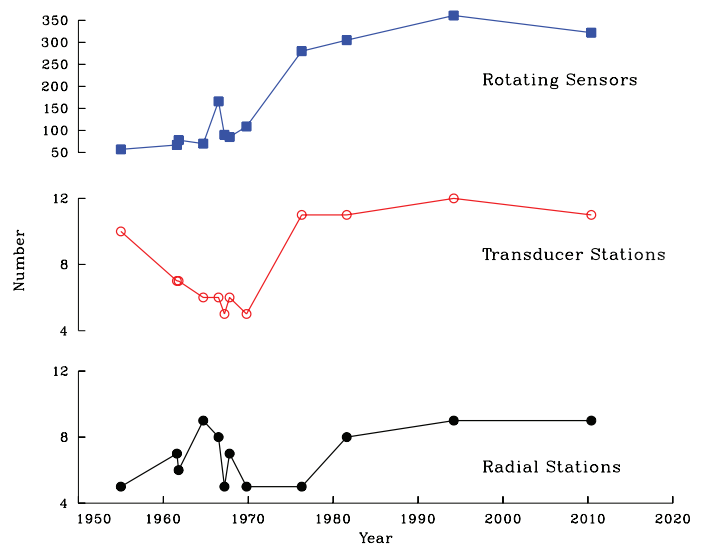


Figure 14. Number of instrumented radial stations and chordwise pressure transducers, and total number of rotating sensors for 12 airloads tests as a function of years.



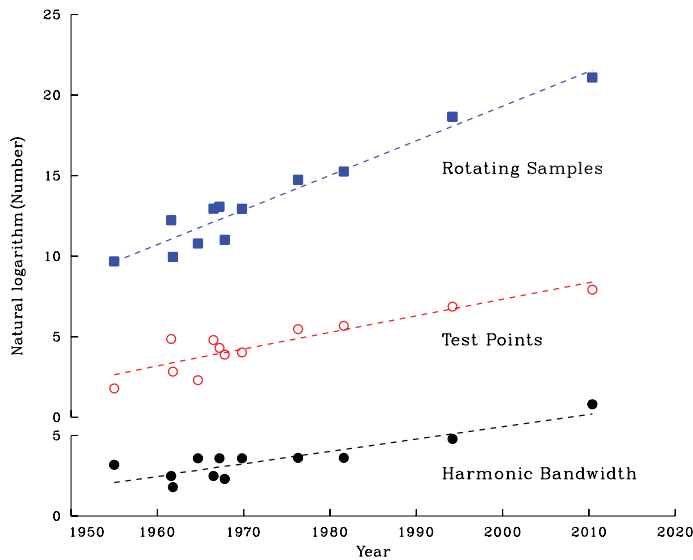


Figure 15. Natural logarithm of number of recorded harmonics, test points, and rotating samples per rev for 12 airloads tests as a function of years.

(Patterson, 1952). As shown in figure 16, the early airloads tests all used differential pressure transducers. These miniaturized transducers were suitable for installation in full-scale rotor blades, but the major drawback was that drilling holes in the blade spar significantly reduced the blade's fatigue life.

There is no discussion of the fatigue design and testing for the CH-34 rotor (Scheiman, 1964; Rabbott et al., 1966a), but John Ward (*pers. comm.*) recalls that the responsibility for this testing was his first job after joining the Vertical Takeoff and Landing (VTOL) Branch at NASA Langley. They tested a single specimen of the blade with holes drilled in the spar, and analysis indicated that the blades were good for a 10-hour lifetime (Ward, *pers. comm.*). The blades were flown successfully and were later used in the wind tunnel test.

Engineers at Bell Helicopter Textron (UH-1A) and Lockheed California Company (XH-51A) also fatigue tested blade specimens and calculated appropriate safe lifetimes (Burpo and Lynn, 1962; Bartsch, 1968a).

By the 1960s, a number of commercial businesses had begun to design and manufacture miniaturized absolute pressure transducers. For the helicopter manufacturers involved with airloads measurements, the new absolute pressure transducers solved the fatigue-damage problem with the differential pressure transducers because these new transducers could be surface-mounted on the blade and did not affect its structural integrity.

The three tests in the 1960s that used absolute pressure transducers on the blade structural spars treated the upper- and lower-surface pressure measurements as though

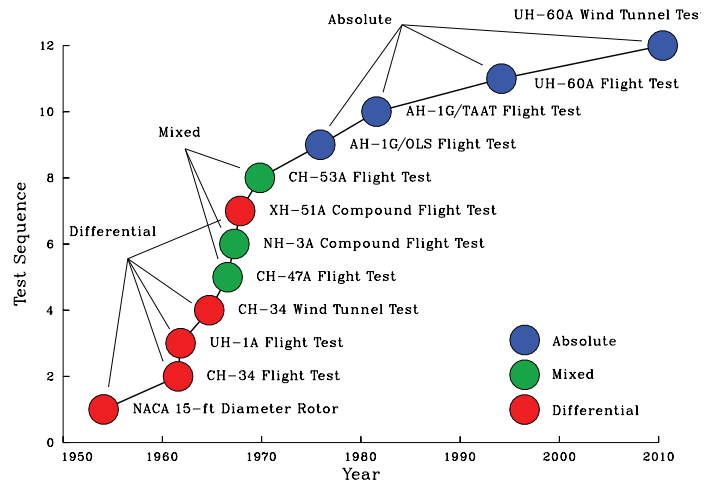


Figure 16. Pressure transducer developments over the last half century.

they represented a differential pressure measurement. They either wired the transducers such that the output was a differential measurement, or they recorded the absolute pressures separately and computed the differential pressure during data reduction.

The first test to use absolute pressure transducers at all spanwise and chordwise locations was the AH-1G/Operational Loads Survey (OLS) test (Shockey et al., 1977). Under U.S. Army sponsorship in 1965, Bell started on a series of technology demonstration programs that defined the necessary instrumentation and data processing that would provide an improved understanding of aerodynamic and structural loads in normal flight. The most important test was the instrumentation of one radial station of a UH-1H blade that was then tested in the NASA Ames 40- by 80-Foot Wind Tunnel (Bowden and Shockey, 1970). This test demonstrated that differential pressure transducers did not adequately characterize the aerodynamics over the rotor blade, and absolute pressure transducers were required. All subsequent airloads tests have used absolute pressure transducers to measure the rotor blade pressures.

The technology of recording the pressure measurements has also changed over the last half century (fig. 17). Lunn and Knopp (1981) provided a history of the changes that occurred over the decades of the 1960s and 1970s when most of the 12 airloads tests were run:

“The evolution to our present data system in this 20 yr period has progressed from oscillograph recording, frequency modulated analog tape recording to programmable pulse code modulation (PCM) digital recording and telemetry from the aircraft, complemented by data-handling techniques which have progressed from colored pencils and hand analysis to large scale, real time computer analysis.”

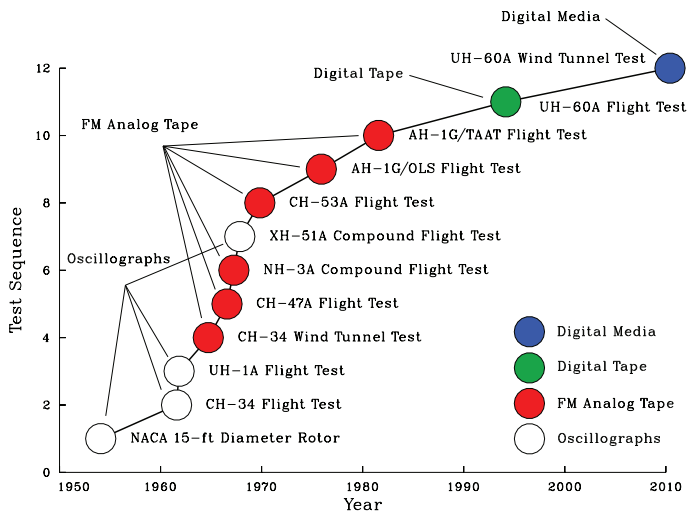


Figure 17. Data recording developments over the last half century.

As shown in figure 17, the early tests, the NACA model rotor, the CH-34 in flight, and the UH-1A, plus the later XH-51A compound flight test, all recorded data on one or more oscillograph recorders. The oscillograph rolls were then “processed” using an optical device with a set of cross-hairs that would transfer the signal amplitude and time to punched cards each time the operator clicked a digitization button.

The introduction of multiplex FM analog tape simplified the recording of pressure data and increased the accuracy. The technology capability in the new multiplex FM analog systems also encouraged flight test organizations to record greater amounts of data.

In some cases, the signal conditioning was done on the rotor hub, in other cases, in the aircraft. The early tests multiplexed the signals in the aircraft and then recorded them on analog tape, but the AH-1G tests did the multiplexing in a hub-mounted bucket (“mux bucket”).

The analog-to-digital (A/D) conversion of the multiplexed FM tapes was done in a ground station for all of the tests using analog tapes. Considerable effort was taken to keep the slip rings clean because contamination could lead to dropouts or spikes in the pressure data. As Lunn and Knopp (1981) noted, “Pulse code modulation (PCM) became an option and A/D was then done in the rotating system and the PCM stream could be sent down through the slip rings and there were far fewer problems with the pressure data.” In the most recent rotor test in the National Full-Scale Aerodynamics Complex (NFAC), the PCM streams were brought into the fixed system with a noncontacting capacitive data coupler.

The technology for data storage has changed significantly over the last 50 or so years (fig. 18). Data storage for the NACA model rotor were simply the data points plotted

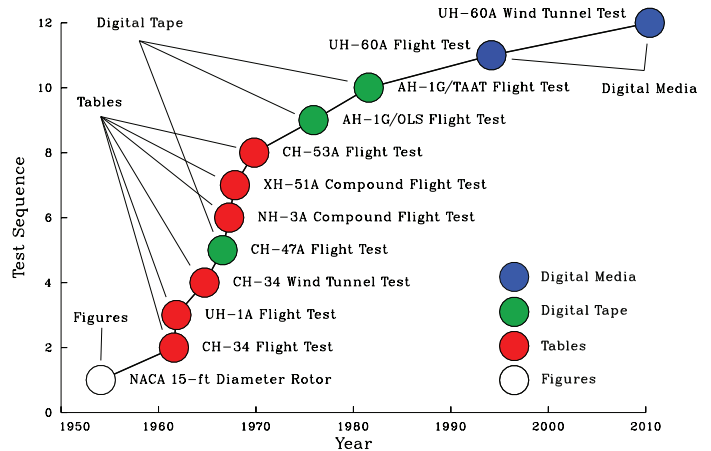


Figure 18. Data storage developments over the last half century.

on the graphs in the report, roughly a total of 16 kilobytes. Today, these data are stored in large computers. The data from the UH-60A wind tunnel test occupies roughly 5 terabytes. The Particle Image Velocimetry (PIV) and blade deflection images probably occupy another 10 terabytes (Tom Norman, *pers. comm.*).

The early tests that used multiplexed FM analog tape data, for the most part, did not attempt to create a permanent database of digital data following the A/D conversion in their ground-based computers. Rather, they processed the data in one or more passes and wrote the results to tables, most made with the IBM chain printers of the time. Unfortunately, some of the tabulated data are barely legible because of too much or too little ink, and the setup of the printer (see Fenaughty and Beno, 1970b; Beno, 1970b).

The next big step was to write the data to digital tape for permanent storage. This was apparently done with the CH-47A airloads data, although the details are obscure. For the AH-1G/OLS test, the analog data were processed and then recorded on about 173 9-track digital tapes. For the AH-1G/Tip Aerodynamic and Acoustic Test (TAAT), there were a total of 350 tapes (from the original 23 FM analog tapes). The low data density of the 9-track digital tapes of the era created data handling problems. For the OLS data, it was initially left to the user to access the digital data using the complex Data Definition statements, and this was quite awkward (Don Merkley, *pers. comm.*). The Army contracted with Bell to provide a user interface program called DATAMAP (Philbrick and Eubanks, 1979; Philbrick, 1980). Access to the database was much improved with the use of DATAMAP (Don Merkley, *pers. comm.*).

Eventually, the large tape machines that could access the OLS and TAAT digital tapes became obsolete. Once this happened, the digital tapes could no longer be read and they were discarded.

A decade later, when the UH-60A flight test was conducted, there had been a number of advances in the technology. The A/D was done in a bucket mounted in the rotating system, the Rotating Data Acquisition System (RDAS). The digital data were then a PCM stream that was passed through the slip rings and recorded on digital tape. The data from individual flights were processed in a ground station, very much like the prior tests that used FM analog tapes. After processing, the digital data were written to a magnetic disk. There were roughly 16 times more data for the UH-60A flight program than for the AH-1G/TAAT test. Even with advances in the intervening years, the storage of the data was costly. Eventually, the 30 gigabytes of data were written to optical disks stacked in a “juke box.”

The UH-60A wind tunnel test also did the A/D in the rotating system, but it was transferred to the fixed system using a capacitive data coupler. Once in the main computer, all the processing and storage was on that computer. At last the storage technology had caught up with the recording technology.

But digital data storage is ephemeral. Technical obsolescence, as with the two AH-1G tests, can make data disappear almost overnight, regardless of the original expense incurred in acquiring the data. Management changes can have the same effect. As Wayne Johnson has said (Hooper, 1985):

“We have had paper for a couple of thousand years, printing presses for a couple of hundred, computers have been with us for maybe a couple of decades ... I think actually putting things down on paper and saving them has a lot to be recommended.”

### Data Validation

The basic procedures for experimental measurements are well established. All transducers must be accurately calibrated. Signal conditioning, recording, signal processing and all of the associated steps also require careful calibration. Everything must be documented. Throughout the entire process, one must remain vigilant, for there are a thousand ways that measurements can go wrong.

Even when appropriate procedures have been followed, the experimentalist continues to look for approaches that can be used to validate the measurements. At the simplest level, one can just do repeat tests with the expectation that the original and repeat measurements will agree. With complex experiments such as airloads tests, there are other possibilities. Considering only the steady loads, the calculation of rotor lift based on pressure measurements can be compared with the vehicle weight for a flight test or the rotor balance for a tunnel test. And, if two independent

experiments using the same rotor have been made, a test-on-test comparison of the two experiments can be made.

All of these comparisons between measurements require a means of evaluating the accuracy of the comparison, that is, a quantitative metric. Bousman and Norman (2010) have used a metric based on linear regression and applied it to numerous aeromechanics problems for both steady and unsteady conditions. Briefly, they use one set of measurements as a reference condition and a second set (or theoretical calculations) as a dependent condition. They then calculate a linear regression between the two sets and compute the slope,  $m$ , between the sets as a measure of accuracy ( $m = 1$  for perfect correlation) and the coefficient of determination,  $r^2$ , as a measure of scatter ( $r^2 = 1$  for no variance). The use of this approach is explained in Appendix 2 with a number of examples.

### Repeat Cases

Repeat cases deal with two problems that are, to some degree, independent. The first problem is the necessity of establishing trim conditions for a baseline and repeat case that are identical. The second problem is dealing with unsteadiness in the data. In this section, a number of instances are examined where the principal investigators (of subsequent researchers) used repeat data to validate the measurements.

The trim problem requires that there be an accurate measurement of all trim parameters for the baseline case and that these are accurately reproduced for the repeat case.

Unsteadiness becomes a problem when there is some sort of inherent unsteadiness in the data that is not readily quantified or easily handled. The most obvious example for a rotor airloads test is the effect of dynamic stall where sequential rotor revolutions may not show identical stall cycles. Averaging the data on a per-revolution basis may provide a baseline case, but in that event there are implicit assumptions made about the stochastic nature of the unsteadiness and these may not be accurate.

One or more of the repeat case types were examined for the NACA model rotor, the CH-34 wind tunnel test, the XH-51A compound flight test, the UH-60A flight test, and the UH-60A wind tunnel test. Some examples are described below.

**NACA model rotor.** In the first airloads test in the 1950s, Rabbott and Churchill (1956) obtained baseline data for five radial stations for the six advance ratios that they tested in the Langley 30- by 60-Foot Wind Tunnel. In addition, they included a repeat case at the  $0.75R$  radial station for each of the six advance ratios. For the baseline data, the section normal forces were obtained from an integration of the average differential pressures over 10 consecutive

revolutions. Presumably, the repeat data were obtained in the same manner and for the same trim conditions. The linear regression of the baseline and repeat conditions were computed to assess the accuracy. The independent variables are the baseline normal forces, and the dependent variables are the repeat case normal forces. The combined linear regression for all of the six advance ratio cases was also computed. The results are shown in the accuracy map in figure 19, which shows the slope,  $m$ , as a function of the coefficient of determination,  $r^2$ .

The repeatability results for five of the six advance ratios are very good—the five cases are within an accuracy circle of about of 3 percent. But the results at  $\mu = 0.20$  are poor. The combined analysis, however, shows that overall, the repeatability for this test was very good, fitting in an accuracy circle of 1.7 percent.

**CH-34 Wind Tunnel Test.** Rabbott et al. (1966a,b) provided data for 10 conditions for their wind tunnel test of the CH-34 rotor. They repeated the sixth test condition,  $\mu = 0.39$  and  $\alpha_s = 0$ , and compared the normal force measurements at three radial stations:  $0.25R$ ,  $0.75R$ , and  $0.90R$  (fig. 10, Rabbott et al., 1966a). The trim for the baseline and the trim for the repeat condition were different as shown in table 4, particularly for the propulsive force.

The baseline and repeat case normal force data from figure 10 of Rabbott et al. (1966a) was digitized, and the linear regression between the baseline and repeat cases computed. The accuracy map in figure 20 shows that there was very good repeatability at  $0.25R$  and  $0.90R$ . Both radial stations are within an accuracy circle of 3.0 percent, but there is considerably more scatter at  $0.75R$ , and the accuracy circle is about 11 percent. The combined analysis of the three sections together shows very good results that are within an accuracy circle of less than 2 percent.

**UH-60A Flight Test.** Data from approximate repeat conditions on each flight were used to evaluate the health of the pressure transducer measurements (Bousman and Kufeld, 2005). Limited level flight repeat data were obtained on two of the later flights during the program, but these have not been examined.

But unsteadiness aspects of repeatability have been examined by comparing normal force and pitching moments within a single test point (counter). For the UH-60A flight test, most counters included either 19 or 20 revolutions of data. From this time history, the mean, mean+ $\sigma$ , and mean- $\sigma$  time histories of a single revolution were computed. The linear regression considered the mean- $\sigma$  time history as the baseline (independent variable) and the mean+ $\sigma$  time history as the repeat (dependent variable).

Figure 21 shows accuracy maps for normal force and pitching moment for Counter 8534, a high-speed,

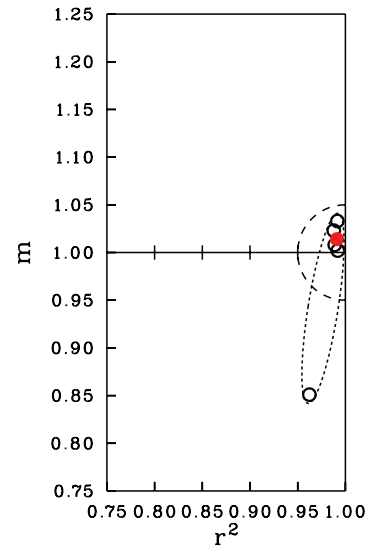


Figure 19. Accuracy map for section normal forces for repeat case at  $0.75R$  for six advance ratios; outlier is for  $\mu = 0.20$ . Fifteen-foot-diameter model rotor in the NACA Langley 30- by 60-Foot Wind Tunnel (Rabbott and Churchill, 1956).

moderately loaded, level flight case. Except for the pitching moment at one radial station ( $0.40R$ , where there is no change in the moment around the azimuth), there is very good agreement.

The agreement is not as good in a case with dynamic stall, where there is substantial variance from revolution to revolution for the pitching moments in the rotor’s fourth quadrant. Figure 22 shows the normal force and pitching moment accuracy maps for Counter 9017, a highly loaded case with severe dynamic stall. The normal force is slightly degraded from the level flight case, but still within an accuracy circle of 5 percent. But the accuracy map for pitching moment shows a great deal of scatter. Current computational methods have shown good agreement with the mean response in cases like this but have not demonstrated that they can predict revolution-to-revolution changes in pitching moments.

**UH-60A Wind Tunnel Test.** Norman et al. (2011) showed the variance in measured pitching moments for a moderate loading condition,  $\mu = 0.30$ ,  $C_T/\sigma = 0.10$ , and a highly loaded dynamic stall case,  $\mu = 0.30$ ,  $C_T/\sigma = 0.125$ , both at the  $0.865R$  radial station. Unlike the flight test, which had 19 or 20 revolutions of data, they obtained 128 revolutions of data for these steady rotor conditions. In

TABLE 4. COMPARISON OF TRIM CONDITIONS FOR CH-34 WIND TUNNEL REPEAT CASE

	Baseline	Repeat	Difference, %
Lift, lb	8400	8650	3.0
Drag, lb	-250	-300	20.0



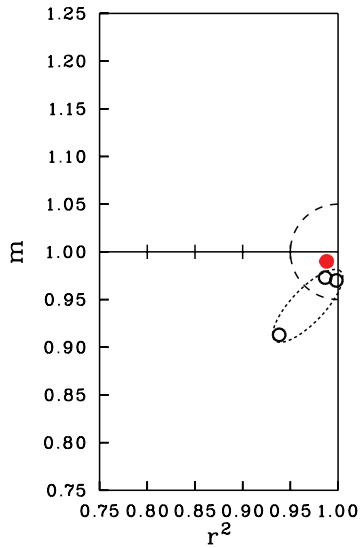


Figure 20. Accuracy map for three section normal forces for a repeat condition in the CH-34 wind tunnel test (Rabbott et al., 1966a); outlier is  $0.75R$ .

their figure, they show the mean value for the 128 revolutions and they represent the variance as dots.

Tom Norman provided the mean value and the  $+\sigma$ , and  $-\sigma$  time histories for the entire 128 revolutions. The linear regression between the  $+\sigma$  (dependent variables) and  $-\sigma$  (independent variables) was calculated to define an accuracy map for repeatability within the counter. The accuracy map in figure 23 shows considerable scatter in the pitching moments. For the moderate loading case, the worst scatter is not caused by dynamic stall, but is an artifact of the linear regression approach in cases where there is little loading change around the azimuth ( $0.40R$  in this case). But the large variance for the highly loaded dynamic stall case is a direct consequence of cycle-to-cycle variation caused by dynamic stall in the fourth quadrant.

The unsteadiness within a test point is similar between the flight and wind tunnel tests. As noted in the prior discussion of the flight test, present analyses cannot reproduce this unsteadiness, but they can do a fairly good job of calculating the mean behavior.

### Steady Thrust Comparisons

The steady (average) thrust can be obtained from pressure measurements by double integration. First, the blade pressures are integrated at each radial station to compute the normal force. Second, section normal forces along the blade are integrated to obtain the blade thrust. The rotor thrust is then the blade thrust multiplied by the number of blades.

For flight test, it is possible to calculate the rotor thrust based on the aircraft weight and correct for aircraft down-load and other relevant factors. Or in some cases, it is

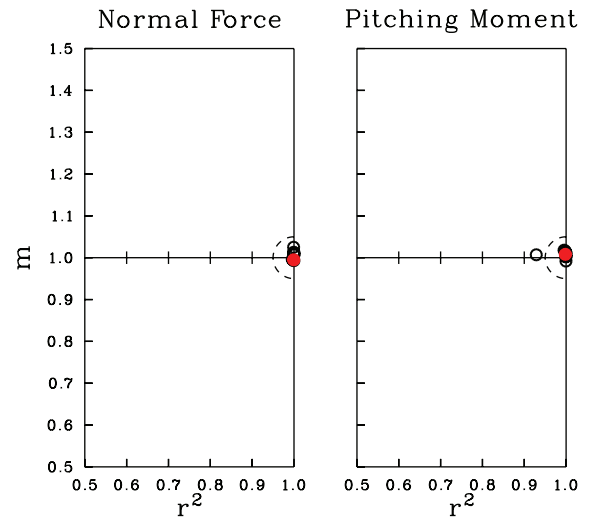


Figure 21. Normal force and pitching moment accuracy maps for UH-60A flight test, Counter 8534, based on difference between  $+\sigma$  and  $-\sigma$  time histories at nine radial stations; outlier is  $0.40R$ .

possible to estimate the rotor thrust from internal loads as was done for the XH-51A (Bartsch 1968a).

For a wind tunnel test, rotor thrust can be obtained from the wind tunnel balance or an internal rotor balance.

Nonetheless, the comparison of rotor thrust derived from blade pressures with rotor thrust obtained from other measurement approaches has numerous difficulties. The double integration of blade pressures requires quadrature approaches that have their own limitations. Moreover, steady measurements require accurate treatment of both the calibration scale factors and the measurement bias offset (Davis, 1981).

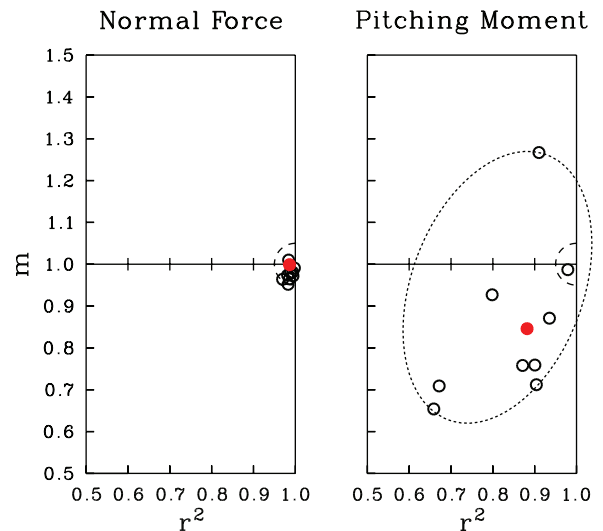


Figure 22. Normal force and pitching moment accuracy maps for UH-60A flight test, Counter 9017, based on difference between  $+\sigma$  and  $-\sigma$  time histories at nine radial stations.

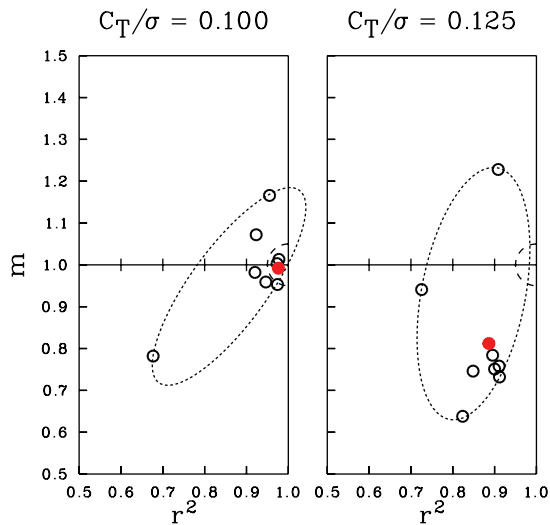


Figure 23. Section pitching moment accuracy maps for two loading conditions, UH-60A wind tunnel test (fig. 15, Norman et al., 2011).

The derivation of rotor thrust from aircraft weight means that the aircraft must be weighed before flight and the burnoff in fuel accounted for. Depending on the aircraft's pitch attitude, there will be either an upload or a download on the fuselage and the stabilator, elevator, or stabilizer. Moreover, in some flight conditions there may be rotor/airframe interference effects.

The derivation of rotor thrust from the wind tunnel balance requires an accurate balance calibration that accounts for both scale factor, bias offsets, and wind tunnel tare. Unless the rotor is very small relative to the wind tunnel, there is generally a need to account for wind tunnel wall effects. If an internal rotor balance is used, there is a similar need for balance calibration and corrections.

Steady thrust comparisons were examined for the NACA model rotor, the CH-34 wind tunnel test, the XH-51A compound flight test, the CH-53A flight test, the UH-60A flight test, and the UH-60A wind tunnel test. Some examples are described below.

**NACA Model Rotor.** Rabbott and Churchill (1956) integrated the blade pressures at five radial stations to obtain the section normal forces and then integrated the section normal forces to obtain the blade thrust. They compared this thrust with the measured lift from the wind tunnel balance in table 1 of their report. Prior testing had shown that lift corrections were not required in the open jet of the 30-by 60-Foot Wind Tunnel. Figure 24 shows the ratio of the rotor thrust obtained from integration of the pressure measurements to the rotor thrust measured by the wind tunnel balance as a function of  $\mu$  for the six advance ratios tested.

For this thrust/balance ratio, the mean and the standard deviation were calculated as accuracy metrics. (Linear

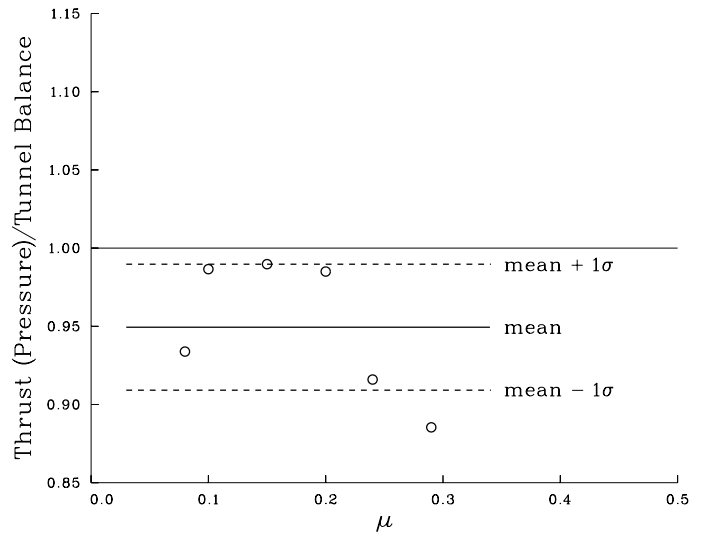


Figure 24. Thrust/balance comparison for for NACA model rotor as a function of advance ratio (Rabbott and Churchill, 1956);  $n = 6$ .

regression does not provide an accurate metric for cases where there is little variation; see Appendix 2.) The mean in this case is 0.949, that is, there is an offset of  $-5.1$  percent. The standard deviation ( $1\sigma$ ) is 0.044.

**CH-34 Wind Tunnel Test.** Rabbott et al. (1966a) did not compare their rotor thrust measurements with wind tunnel balance results in their test of the CH-34 in the 40-by 80-Foot Wind Tunnel. But they did provide the steady value of section normal force at each radial station for each of their 10 test conditions. Based on their tabulated steady harmonics of normal force, the second integration was computed to obtain blade thrust using Simpson's rule for non-equally spaced data. The lift and propulsive force as measured by the wind tunnel balance were given in table 1 of their report.

The ratio of the thrust obtained with integration of the pressure measurements to the tunnel balance measurement is shown in figure 25 for their 10 conditions. The mean of the ratio is 1.030, an offset of  $+3.0$  percent. The standard deviation ( $1\sigma$ ) is 0.054. The offset is less than for the NACA model rotor test, but the standard deviation is slightly greater.

**CH-53A Flight Test.** Davis and Egolf (1980) examined the CH-53A flight test airloads measurements to determine their suitability for use as inputs to acoustic calculations. As part of their examination, they compared the rotor thrust from pressure measurements with the aircraft gross weight for two advance ratios as shown in table 5. The thrust-to-gross-weight ratios show that the thrust derived from the pressure measurements was 30 to 40 percent low.

In calculating the rotor thrust, they attempted to increase the accuracy of the double integration in two ways. First,

TABLE 5. COMPARISON OF ROTOR THRUST FROM PRESSURE INTEGRATION WITH AIRCRAFT GROSS WEIGHT FOR THE CH-53A (FROM TABLE 12, DAVIS AND EGOLF, 1980)

Case	$\mu$	$GW$ , lb	Thrust, lb	$T/GW$
18	0.227	34,050	23,972	0.704
35	0.373	33,070	20,185	0.610

**UH-60A Wind Tunnel Test.** Norman et al. (2011) examined the thrust-to-balance ratio for the UH-60A rotor in the wind tunnel (their figure 13). They used a double integration similar to that used for the UH-60A flight test to obtain the rotor thrust from the blade pressure measurements. The rotor balance forces have been corrected for wind tunnel wall effects using an angle correction based on the Prandtl-Glauert equations (Langer et al., 1996).

The thrust-to-rotor-balance ratio is shown in figure 27 as a function of advance ratio for 85 test conditions. The data were obtained on Runs 40, 45, and 47. The measured rotor thrust for these cases varied from 8,400 to 28,000 pounds. The collective pitch varied from 2.3 to 13.2° and the shaft angle from zero to -6.9°. The mean of the ratio of pressure integration to rotor balance is 0.990, that is, an offset of -1.0 percent, a very good result. The standard deviation ( $1\sigma$ ) in this case is 0.017, almost the same as that observed for the UH-60A flight test in figure 26.

### Test-on-Test Cases

The 12 airloads tests discussed in this paper included 3 cases where the same rotor was tested a second time: the flight and wind tunnel test of the CH-34 rotor, the 2 flight tests of the AH-1G rotor, and the flight and wind tunnel test of the UH-60A rotor.

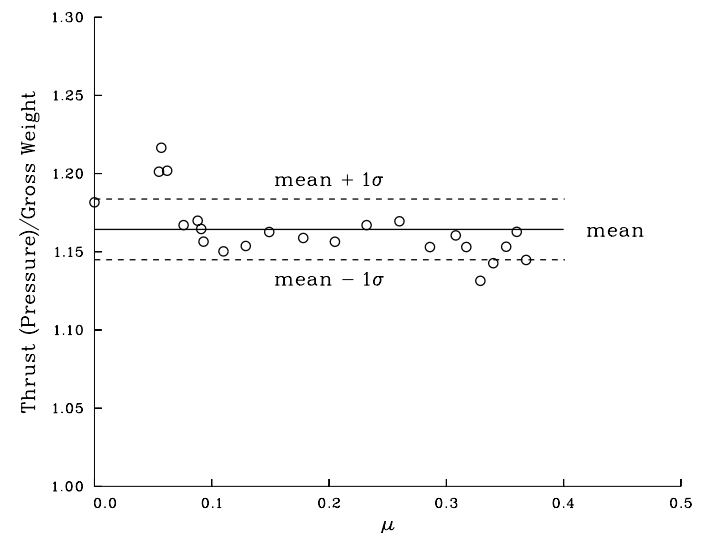


Figure 26. Thrust/weight comparison for the UH-60A flight test as a function of advance ratio; Flight 85,  $n = 23$ .

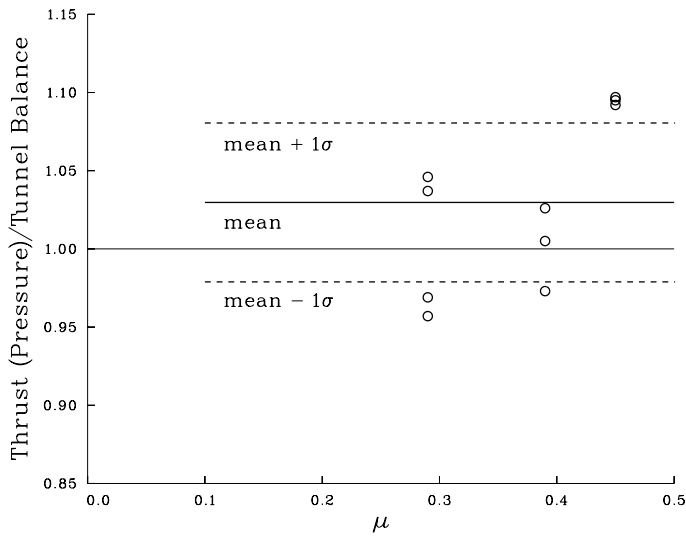


Figure 25. Thrust/balance comparison for the CH-34 wind tunnel test as a function of advance ratio (Rabbott et al., 1966a);  $n = 10$ .

at the five radial stations where there were pressure measurements at five chordwise points (the most forward being at  $0.042c$ ), they augmented the measurements with three additional chordwise stations based on an inviscid flow analysis. Second, at five additional radial stations where there was only a single pressure measurement, they used that measurement to estimate the normal force. There is no discussion as to whether any corrections were made to the aircraft gross weight to account for fuselage and stabilizer download or rotor/fuselage interference.

**UH-60A Flight Test.** Calculations of the thrust/gross weight ratio have been made for the UH-60A in the flight test. The thrust was obtained by a double integration. The section normal forces were obtained from an integration of the blade pressures using a quadrature based on Simpson's rule for non-equally spaced data. The blade thrust was obtained by an integration of the section normal forces, again using Simpson's rule quadrature.

Aircraft weight was measured prior to the flight using standard scales for each wheel. During flight, the fuel burn-off was continuously measured. Corrections were made to the aircraft weight to account for additional vertical forces including fuselage, stabilator, and tail rotor lift (the tail rotor is canted). These aerodynamic forces were based on quarter-scale wind tunnel tests performed early in the development program (Barnard, 1976). No correction was made for rotor/fuselage interference. The results of this calculation are shown in figure 26 for the 23 airspeed sweep measurements obtained on Flight 85. The mean of the ratio of pressure integration to gross weight is 1.164, that is, an offset of 16.4 percent. The standard deviation ( $1\sigma$ ) in this case is 0.020. The large offset and small variance suggest that there are significant bias errors in this calculation.

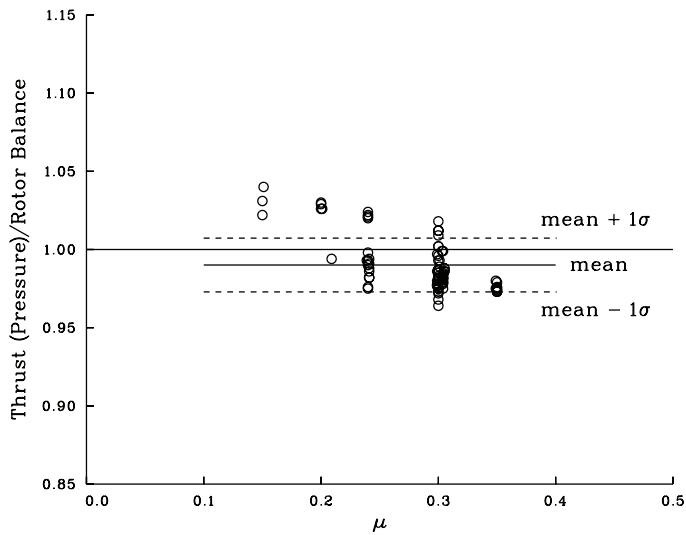


Figure 27. Thrust/rotor balance comparison for the UH-60A wind tunnel test as a function of advance ratio (Norman et al., 2011); n = 85.

**CH-34 Rotor.** Rabbott et al. (1966a) included one test condition in their wind tunnel test of the CH-34 rotor to match Flight 18 from Scheiman (1964). The pressure instrumented rotor was the one that was tested in flight, but additional pressure transducers were installed at  $0.97R$  and  $0.99R$ .

Because the wind tunnel test was designed to obtain forward speeds significantly higher than those possible in flight, modifications were made to the control systems. To a limited degree, these are discussed by Rabbott et al. (1966a), and additional detail is provided by Johnson (2011a,b).

The trim conditions for the two test points are shown in table 6. There is reasonable agreement in the advance ratio, tip speed, and lift, but there is a considerable discrepancy in the propulsive force. The agreement in the lift is misleading in that Scheiman (1964) did not record the aircraft weight for any test points, but reported instead a range of weight from 11,300 to 11,800 pounds.

As concerns the discrepancy in propulsive force, Rabbott et al. noted:

“A greater rotor propulsive force was inadvertently produced in the wind tunnel: 2144 pounds versus an estimated flight test value of 1390 pounds (based on 36.5 square feet of parasite for the H-34 helicopter). The increased propulsive force and the  $-9$ -degree rather than the  $-7.2$ -degree shaft angle reported in Reference 2 [Scheiman 1964] thus represent a different inflow and loading for the rotors, so these differences should be kept in mind in the following comparison of wind tunnel and flight test data.”

TABLE 6. COMPARISON OF TRIM CONDITIONS FOR THE CH-34 ROTOR TESTED IN FLIGHT, FLIGHT 18, AND THE WIND TUNNEL, CONDITION 10 (RABBOTT ET AL., 1966A)

	Flight	Tunnel	Difference, %
$\mu$	0.30	0.29	+3.5
$\Omega R$ , ft/sec	633	650	-2.6
$L$ , lb	11,500	11,800	-2.5
$D$ , lb	-1,390	-2,150	-35.3

Rabbott et al. (1966a) compared the measured normal forces at the seven common radial stations in their figure 33. They also included comparisons of flap, chord, and torsional stresses. They commented that “the agreement between flight and tunnel airload time histories is generally good.”

The linear regression between the normal forces measured in flight test (dependent variables) and the same forces measured in the tunnel (independent variables) were computed. An accuracy map for these airloads at seven radial stations is shown in figure 28. The dispersion is very low with  $r^2$  values ranging from about 0.93 to 0.97, thus the time histories appear very similar. But the  $m$  values (slopes) of the regression show that the flight values are lower, ranging from 0.76 to 0.96. The slope of the combined result is about 18 percent low.

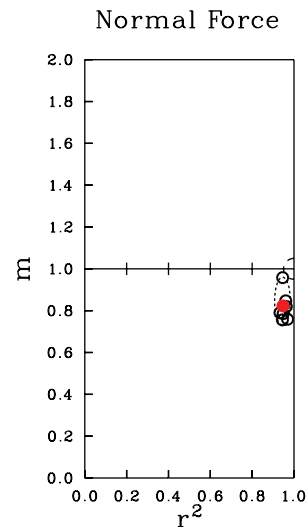


Figure 28. Accuracy map for the CH-34 normal force in flight as a function of that measured in the wind tunnel based on linear regression. Open circles show the seven individual radial stations, solid circle shows the combined analysis (1–12 harmonics). The dashed ellipse provides a qualitative idea of the scatter.

**AH-1G Rotor.** The AH-1G main rotor was first tested at Bell Helicopter Textron in the mid-1970s under U.S. Army sponsorship (Shockey et al., 1977). This test is often referred to as the Operational Loads Survey (OLS) test. The rotor was tested again in 1981 at NASA Ames Research Center (Cross and Watts, 1988). The second test is known as the Tip Aerodynamic and Acoustic Test (TAAT). Additional absolute pressure transducers were added to the rotor used in the OLS test, increasing the number of radial stations with measured airloads from five to eight.

A specific effort was made in the TAAT test to match a number of test conditions from the OLS test. Some airloads comparisons were carried out under the auspices of The Technical Cooperation Program (TTCP), a joint effort of the U.S., the U.K., Canada, Australia, and New Zealand. There is a limited discussion of these comparisons in restricted reports from the TTCP meetings, but there has never been a publication of the results in the open literature.

**UH-60A Rotor.** The highly instrumented UH-60A rotor was tested in flight at NASA Ames Research Center in 1993 and 1994 (Kufeld et al., 1994b). The same rotor was tested in the 40- by 80-Foot Wind Tunnel at Ames in 2010 (Norman et al., 2011).

During the 2010 wind tunnel test, a number of test conditions were selected to match flight test points. Three of these cases were compared in Norman et al. (2012). The trim values for the three conditions are shown in table 7. The first pair are for a high-speed case with moderate blade loading. The second pair are at moderate speed and low blade loading. The third pair are for a moderate speed and high blade loading with significant dynamic stall present.

Blade airloads data were obtained for eight radial stations for the first pair: Counter 8424 from the flight test compared to the wind tunnel point R47P21. Norman et al. (2012) showed the time histories in their figures 9 through 12 for six of the radial stations. Tom Norman provided these time histories, and the linear regression between the flight test point (dependent variable) and the tunnel point (independent variable) was calculated for both nondimensional

TABLE 7. COMPARISON OF THREE TRIM CONDITIONS FOR THE UH-60A ROTOR TESTED IN FLIGHT AND WIND TUNNEL (NORMAN ET AL., 2012)

	Flight	Tunnel	Difference, %
$\mu$	0.304	0.303	+0.3
$C_T/\sigma$	0.088	0.087	+1.1
$\mu$	0.233	0.232	+0.4
$C_T/\sigma$	0.077	0.077	0.0
$\mu$	0.244	0.245	-0.4
$C_T/\sigma$	0.118	0.118	0.0

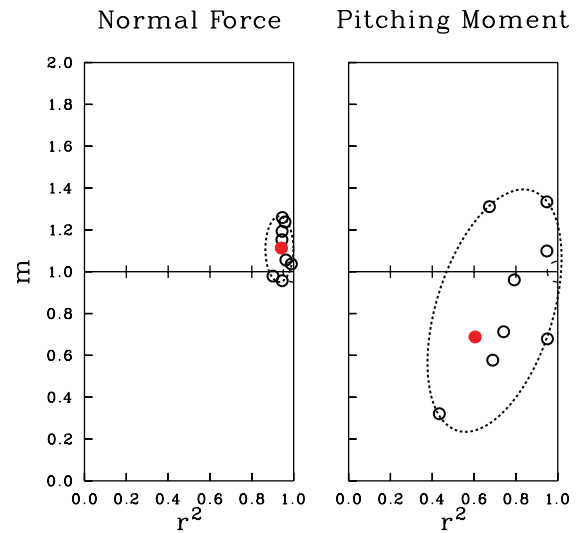


Figure 29. Accuracy map for the UH-60A nondimensional normal forces and pitching moments in flight as a function of that measured in the wind tunnel based on linear regression for Counter 8424 from the flight and R47P21 from the tunnel. Open circles show the eight individual radial stations, the solid circle shows the combined analysis (1–36 harmonics). The dashed ellipses provide a qualitative idea of the scatter.

normal forces and pitching moments. Whereas Norman et al. included the mean value in their comparisons, only 1–36 harmonics were used in the linear regression. Separate accuracy maps are shown for the normal forces and pitching moments in figure 29. The results for this moderate thrust, high-speed point are generally good for normal force. The slope ( $m$ ) for the combined analysis is about 11 percent high, and the average dispersion ( $r^2$ ) is about 0.94. The lack of dispersion reflects the good agreement in the time histories. The combined result is within an accuracy circle of 13 percent, slightly better than for the CH-34 comparison.

The pitching moment results are poor. Some of the radial stations show large scatter. In some cases, the pitching moments obtained in flight are less than those measured in the wind tunnel, in other cases more. The slope from the combined analysis is 31 percent low, and the dispersion is 0.60. The combined result is an accuracy circle of about 50 percent.

Blade airloads data were obtained for five radial stations for the second pair: Counter 8525 from the flight test compared to the wind tunnel point R60P18. Norman et al. (2012) showed the time histories in their figures 19 and 20 for three of the radial stations. Tom Norman provided these time histories, and the linear regression between the flight test point and the tunnel point for both nondimensional normal forces and pitching moments was calculated. Separate accuracy maps for normal force and pitching moment are shown in figure 30. The results for this low-thrust, moderate-speed point are generally good for normal force. The



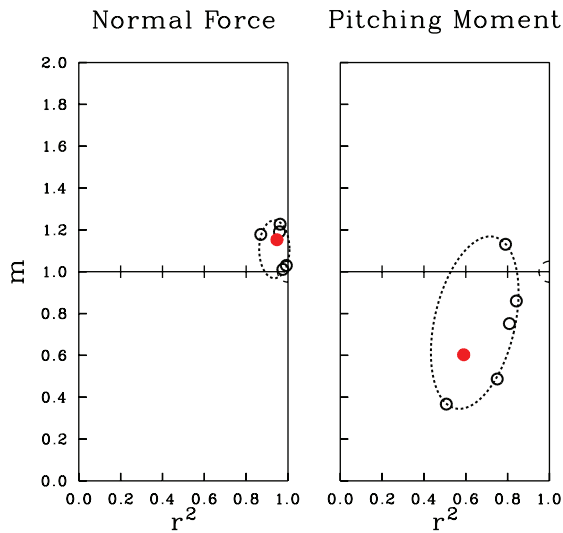


Figure 30. Accuracy map for the UH-60A nondimensional normal forces and pitching moments in flight as a function of that measured in the wind tunnel based on linear regression for the Counter 8525 from the flight and R60P18 from the tunnel. Open circles show the five individual radial stations, the solid circle shows the combined analysis (1–36 harmonics). The dashed ellipses provide a qualitative idea of the scatter.

slope ( $m$ ) for the combined analysis is about 15 percent high, and the average dispersion ( $r^2$ ) is about 0.95. The lack of dispersion reflects the good agreement in the time histories. The combined result is within an accuracy circle of 16 percent, about the same as for the CH-34 comparison. The pitching moment results are poor. The slope for the combined analysis is about 40 percent low, and the average dispersion is about 0.59. All of the radial stations show large dispersion, and the pitching moments in flight are mostly less than were measured in the tunnel. The combined result is an accuracy circle of 57 percent, which is similar to the previous case in figure 29.

Blade airloads data were obtained for six radial stations for the third pair: Counter 9020 from the flight test compared to the wind tunnel point R60P28. Norman et al. (2012) showed the time histories in their figures 21 and 22 for three of the radial stations. Tom Norman provided these time histories, and the linear regression between the flight test point and the tunnel point for both nondimensional normal forces and pitching moments was calculated. Separate accuracy maps for normal force and pitching moment are shown in figure 31.

The normal force shows more scatter for this highly loaded case. The slope ( $m$ ) for the combined analysis is about 8 percent high, and the average dispersion ( $r^2$ ) is about 0.78. The combined result is within an accuracy circle of 23 percent, which is poorer than was seen in the two moderately loaded cases.

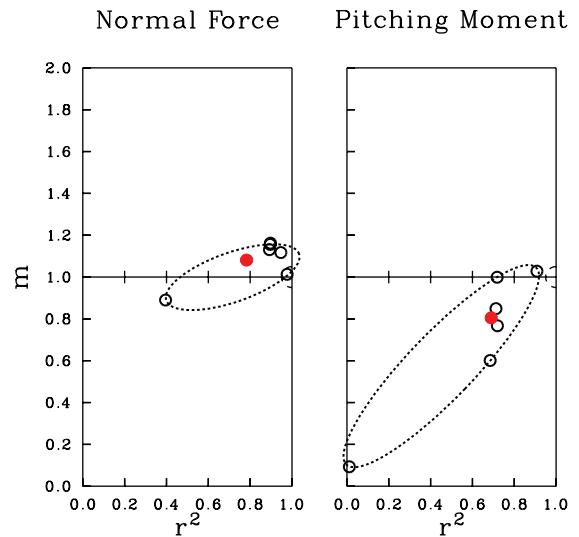


Figure 31. Accuracy map for the UH-60A nondimensional normal forces and pitching moments in flight as a function of that measured in the wind tunnel based on linear regression for the Counter 9020 from the flight and R60P28 from the tunnel. Open circles show the six individual radial stations, the solid circle shows the combined analysis (1–36 harmonics). The dashed ellipses provide a qualitative idea of the scatter.

The pitching moment results show more scatter than were seen for the moderately loaded conditions. The slope for the combined analysis is about 19 percent low, and the average dispersion is about 0.69. At most radial stations, the pitching moments in flight are less than were measured in the tunnel. But the combined result is within an accuracy circle of 37 percent, better than observed in the moderately loaded comparisons.

In most cases, test-on-test comparisons of normal force are good. This was true in the mid-1960s and it is true now. But the comparisons of pitching moments for the UH-60A are generally poor. In part, this is caused by the reduced accuracy in the integration of pitching moments as compared to the integration of normal force.

## BENEFITS OBTAINED FROM AIRLOADS TESTING

The Introduction discussed how, in order to be of value, airloads testing must provide the engineer with an understanding that becomes the basis for improved design tools that can be used in the development of new rotorcraft. It is desirable, therefore, to examine the history of these programs to understand both quantitatively and qualitatively the impact these measurements have made on the technology.

In using various technology metrics to understand this progress, it is useful to recognize that not all of the industry's advances are documented in the open literature. From the government's perspective, the funding for any of these research programs may be justified if it provides the industrial designers significant knowledge that will improve new rotorcraft. But in this paper, only those results that are in the public domain are addressed.

### Citations as a Measure of Benefits

One of the simplest ways to look at how the 12 airloads test data have been used is to count the number of citations in the literature. In preparation for this paper, as many citations were collected as possible for each of the test programs. Table 8 shows the 12 tests (ordered by test date), the date of first publication, and the number of citations. The greatest number of citations are for the UH-60A and CH-34 flight tests, flown about 30 years apart. Although citation indices are a popular means to assess progress in the sciences, they are too superficial to provide historical insight and, particularly, judgment of the benefits of these programs.

But insight into the uses of these data can be obtained by focusing more closely on the distribution of these citations over time. Such distributions are shown in figures 32 and 33, where the cumulative number of citations per year are plotted for each test, starting from the test date. The tests are divided into two groups. Figure 32 shows (mostly) the earlier tests, whereas the later tests are shown in figure 33. Different ordinate scales are also used for the two figures.

Figure 32 shows the cumulative citations for seven tests. In most of these tests the cumulative number of citations is fewer than 40. There is a similarity in the distributions for many of these tests, that is, there

TABLE 8. AIRLOADS TESTS, FIRST PUBLICATION DATE, AND NUMBER OF CITATIONS

Test	Date	Citations
NACA Model Rotor Test	1956	29
CH-34 Flight Test	1963	149
UH-1A Flight Test	1962	46
CH-34 Wind Tunnel Test	1966	68
CH-47A Flight Test	1967	26
NH-3A Flight Test	1970	27
XH-51A Flight Test	1968	29
CH-53A Flight Test	1970	42
AH-1G/OLS Flight Test	1977	97
AH-1G/TAAT Flight Test	1988	70
UH-60A Flight Test	1994	226
UH-60A Wind Tunnel Test	2011	42

is a rise in the number of cumulative citations analogous to a the first order time rise of an exponential function. The initial rise in the early citations has a number of causes. Many of these tests were contracted by the U.S. Government, and some of the publications represent contract requirements. In some cases there has been an immediate need for the data, and the government has encouraged the rapid dissemination and use of that data.

Following the first order-like rise in cumulative citations, subsequent citations tend to occur at a relatively slow rate. In some cases, these later citations are from survey papers rather than a direct use of the data. For example, the last paper using the CH-47A airloads data was published in 1968, and the flight test data were soon lost. The remaining citations refer to a few specific results published in the earlier literature or are citations of the test program.

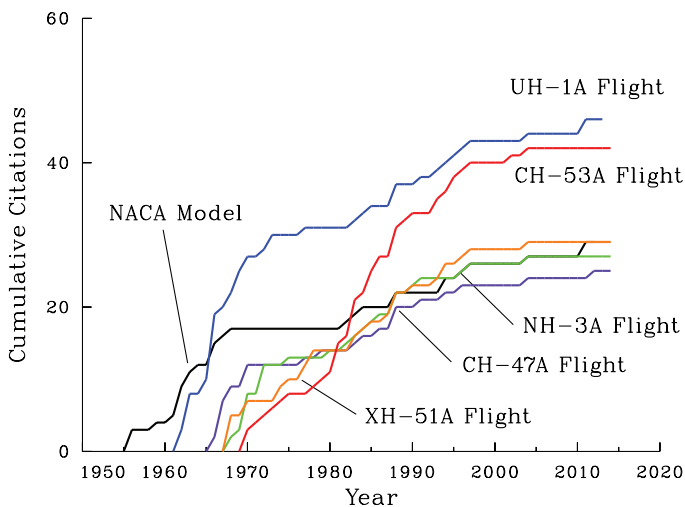


Figure 32. Cumulative citations as a function of time (mostly for earlier tests).

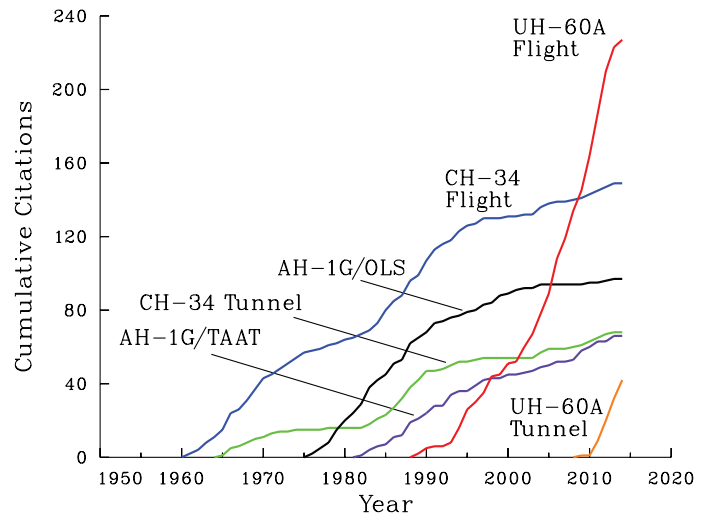


Figure 33. Cumulative citations as a function of time (mostly for later tests).

The CH-53A flight test data are an exception to the pattern of cumulative citations shown in figure 32. Both the airloads and structural data were used for many years after initial publications (almost exclusively by Sikorsky Aircraft authors).

The cumulative citation patterns for the later tests (and the early CH-34 flight and wind tunnel tests) in figure 33 show more variation. The CH-34 flight test data were used even before the original publication of the data reports because of the intense interest in the higher harmonic loading that could not be predicted at that time. The CH-34 wind tunnel test, on the other hand, focused on high-speed airloads and was not used very much after initial publication. This changed following the publication of Euan Hooper's masterly comparative paper looking at vibratory airloads (Hooper, 1983). His use of analysis and data visualization stimulated new interest in the CH-34 rotor, and both airloads data sets were used by investigators well into the 1990s.

The data from the AH-1G/OLS flight test was used in two phases. In the first phase, Bell Helicopter Textron was funded to reduce the airloads as well as ground-acoustic data that were recorded simultaneously. These data were then provided to various investigators (Nakamura, 1982; Succi, 1983) to compare radiated acoustic pressures based on the airloads with the microphone measurements. The second phase was an examination of vibration and structural loads data as a part of the Design Analysis Methods for Vibrations (DAMVIBS) program. This included tabulated structural load and vibration data (Dompka and Cronkhite, 1986) that were used extensively by the DAMVIBS collaborators (Kvaternik, 1993, and others). These data were also used in a series of papers by Yeo and Chopra (see for instance, Yeo and Chopra, 2001a,b). These structural and vibration data remain, but the airloads data are gone.

The follow-on AH-1G/TAAT test was used at a lower rate than the AH-1G/OLS data following its acquisition. But the publication of airloads data for a limited number of cases (Cross and Tu, 1990) has allowed analytical comparisons with these data to continue to the present.

The use of the UH-60A flight test data is quite different from the other tests in that the number of citations have increased in subsequent years rather than following the typical pattern and decreasing with the passage of time. The reason for the increasing use of the UH-60A flight test data in the last decade is a result of a number of factors and is the focus of much of the rest of this paper.

The UH-60A wind tunnel test was completed in 2010. Although it is too soon to predict the long-term trend of this test, it appears very much like the flight test cumulative citation distribution with its rapid initial rise.

## Understanding Airloads

An understanding of helicopter airloads developed as new and improved theoretical methods evolved, often using the airloads test data discussed in this paper. Those advances in understanding provide a better way of assessing the value of these experimental measurements rather than a list of citations or their cumulative distribution.

Datta and his colleagues reviewed the progress that had been made with recent advances in coupled Computational Fluid Dynamics (CFD) and Computational Structural Dynamics (CSD) analyses at the mid-point of the 2000s, mostly using the UH-60A flight test data (Datta et al., 2007). Figure 34 is a copy of their figure 2, with numbers added representing the three problems that they emphasized: (1) blade vortex loading at low speed and its effects on vibration, (2) dynamic stall at moderate speed or in maneuvers, and (3) vibratory loads at high speed. The use of flight measurements and the development of analytical methods for each of these three problems are discussed in turn. Each provide a window into the past.

### First Problem: Vortex Wake Loading at Low Speed

Throughout the late 1940s and the 1950s, helicopter developers encountered large-amplitude harmonic loads in flight that could not be predicted by the analytical methods of the day. In a series of flight experiments at the NACA at Langley Field using a bailed Sikorsky H-19A, LeRoy Ludi reported on flight conditions that caused high loads (Ludi, 1958b; Ludi, 1959). The H-19A had only limited strain-gauge instrumentation on a blade, but this was sufficient to show that large-amplitude blade flap bending moments occurred in low-speed flight.

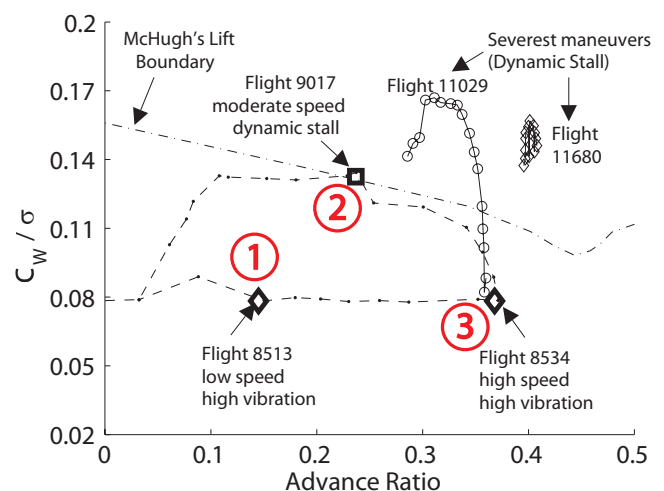


Figure 34. The three airloads problems used to measure progress in rotorcraft airloads theory (Datta et al., 2007).



Each of the helicopter companies had analysts working on these problems, but this was before the era of contract support for the companies for analytical developments. At that time, the U.S. Army Transportation Research Command (TRECOM) (now Aviation Applied Technology Directorate (AATD)) tended to use the Cornell Aeronautical Laboratory (CAL) to develop new methods (Ray Piziali, *pers. comm.*) and the U.S. Navy supported academic institutions such as the Massachusetts Institute of Technology (MIT).

The airloads measurements made on the NACA model rotor at Langley Field in 1954 (Rabbott and Churchill, 1956) showed higher harmonic loading at low speeds in the tunnel. Rabbott and Churchill, referring to this loading distribution, wrote “the magnitude of the loading varies by a factor of 3 to 4, with sharp gradients in the regions of 90° and 270° of azimuth.” These sharp gradients, caused by vortex wake loading, would soon be understood with the analytical developments using digital computers in the 1960s.

Concerning the prediction of these high loads, Professor Rene Miller later commented, “Attempts to obtain a closed form solution to this problem, or one based on tabulated integrals, were not successful and it was evident that extensive computer facilities would be required . . .” (Miller, 1963).

John McHugh at TRECOM (and, later, John Yeates) saw the need for airloads measurements in flight and instituted two test programs. The first was a Sikorsky CH-34 that was modified by Sikorsky and bailed to NASA (Scheiman and Ludi, 1963; Scheiman, 1964). The flight testing at Langley Field started in October 1960 and was completed in July 1961. The second program was a Bell Helicopter UH-1A modified and flown at Bell Helicopter (Burpo and Lynn, 1962). That testing was started in July 1961 and was completed in September of that year.

At the same time, McHugh talked with Frank DuWaldt at CAL about the need to develop calculation methods using the new digital computers, and a program was established in 1960 (Ray Piziali, *pers. comm.*). At about the same time, a similar effort started at MIT with Professor Miller under Navy sponsorship.

Truly useful data is rarely supplied in time to those that need it, and that has been true of all of the airloads tests. There were many complaints about the delays in publishing the CH-34 flight test data (Hooper, 1985), but there were significant efforts at NASA to informally provide early test results. Burpo and Lynn (1962), Piziali and DuWaldt (1962), and Wood and Hilzinger (1963) refer to a letter from F. L. Thompson, dated May 24, 1961, with initial results from the CH-34 flight test. Floyd L. Thompson was the Langley Research Center Director from May 23, 1960, to May 1,

1968, and it is undoubtedly the case that this was a service to the funding agency TRECOM (John Ward, *pers. comm.*). Ray Piziali (*pers. comm.*) recalls that the data that they used for correlation with their new prescribed wake model were supplied by TRECOM, but he does not remember seeing the Thompson letter. Similarly, Mike Scully (*pers. comm.*), a student working under Professor Miller in 1963, remembers using tabulated CH-34 loads data that had been provided to MIT, but he does not remember the Thompson letter either. It is likely that the results in the Thompson letter were the same data that were later published by Scheiman and Ludi (1963).

The UH-1A flight test program lagged the CH-34 flight test by a few months. Bell Helicopter had designed their test to sample the data every 30° to provide 6 harmonics, but TRECOM asked them to fly some cases with a sample every 15° to provide better resolution (the same sample rate used for the CH-34 test). The reason for the change was so that CAL could use the data in the validation of their new prescribed wake model (Burpo and Lynn, 1962).

Professor Miller compared his prescribed wake with data from the NACA model test and the CH-34 flight test (Miller, 1963; Miller, 1964). Ray Piziali and his colleagues also compared their prescribed wake model with data from the NACA model test, the CH-34 flight test, and the UH-1A flight test (Piziali and DuWaldt, 1962; Piziali et al., 1963; Piziali, 1966a,b). Ray credited CAL’s Walt Targoff for the “form in which the problem was cast and the method of solution” in the Foreword to Piziali and DuWaldt (1962).

Figure 35 shows a comparison of the Piziali model with CH-34 flight test data at seven radial stations. Qualitatively, the agreement is good and far superior to prior models that did not properly represent the vortex wake. This sort of agreement was typical for all three data sets for both the MIT and CAL models. The industry quickly made use of the benefits of a prescribed wake model (see, for example, Wood and Hilzinger, 1963).

The flight test data, the early digital computers, and the careful work of Miller and Piziali were all essential for the significant progress that occurred over just a few years in the early 1960s for the First Problem. Since then there have been many improvements in prescribed wake approaches. The free wake took a bit longer, but by the early 1970s successful efforts were coming in that development as well. This work has continued to the present and modern CFD methods using various wake capture methods have been successful.

## Second Problem: Dynamic Stall

It was clear to the early investigators that stall and compressibility were both factors that limited helicopter

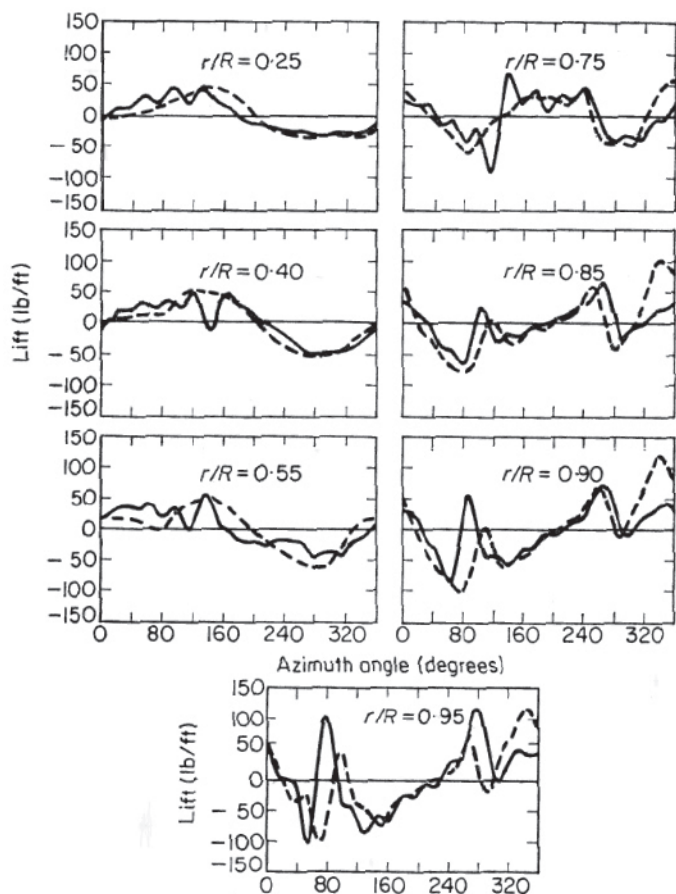


Figure 35. Prescribed wake model (dashed line) compared with CH-34 flight data (solid line);  $\mu = 0.18$  (Piziali, 1966b).

performance in forward flight (Gustafson and Myers, 1946). LeRoy Ludi's flight experiments at the NACA with the Sikorsky H-19A showed that the torsion loads increased significantly in maneuvering flight. But the mechanism of the stall on a rotor, and whether it was analogous to fixed-wing stall, was not clear at the start of the 1960s.

Both of the Army-sponsored flight tests in the early 1960s included maneuvers, and the UH-1A flight test also included high-altitude test points to increase the blade loading. From what is now known about flight limitations on helicopter rotors, both of these test aircraft encountered dynamic stall during their testing. Yet the  $15^\circ$  and  $30^\circ$  azimuth sample rates used on these tests probably lacked the resolution to allow a characterization of the dynamic stall behavior.

Norm Ham and his students at MIT provided significant insights into the dynamic stall phenomenon in a series of experiments in the 1960s (Ham and Young, 1966; Ham, 1967; Ham and Garelick, 1968). They examined pressure measurements from both a hover rotor test and a two-dimensional (2D) airfoil undergoing a ramp increase in angle of attack in the wind tunnel to characterize dynamic

stall. They concluded that under dynamic stall conditions an intense vortex was formed near the leading edge of the airfoil and passed aft along the upper surface. This vortex passage was the source of both moment and lift stall on the airfoil.

In complementary work, Harris and Pruyn (1968) used both pressure measurements from the CH-47A airloads test and model rotor data to show the effects of dynamic stall on rotor loading.

John Ward at NASA Langley took a second look at the CH-34 flight test data (Scheiman, 1964) obtained in the early 1960s. In the late 1960s, the original oscillograph rolls were still stored at the center. He re-digitized a limited number of flight cases to obtain better frequency resolution (Ward, 1971). He selected five of these, including both maneuvers and level flight. Rather than use a fixed sample rate for the re-digitization, he used a variable rate based on his inspection of the time histories. When rapid variation occurred, he sampled every two degrees, when there was less variation, he reduced the sample rate. He did this for all of the pressure measurements. He then integrated the blade pressures to provide both normal force and pitching moments (the first time that anyone had ever computed the moments for this data set).

An example of this effort is shown in figure 36, a reproduction of figure 8 from Ward's paper. The figure compares two cases, both from Flight 89, which was a combined collective and cyclic pull-up maneuver (Scheiman, 1964). The first case is the level flight entry to the maneuver at  $\mu = 0.24$  and  $C_w/\sigma = 0.088$ , and the second case is the revolution at the peak load factor of  $1.5g$  at  $\mu = 0.22$  ( $C_w/\sigma = 0.127$ ). In level flight, the normal force and pitching moment show largely 1/rev behavior at this radial station. But in the maneuver, three dynamic stall cycles are seen in the fourth quadrant with severe changes in the pitching moment near the blade tip and the concomitant changes in the torsion loads near the blade root. Ward postulated that the source of the torsional response was primarily caused by the vortex wake spacing, which was aggravated by dynamic stall. Based on analysis of the UH-60A airloads flight test (Bousman, 1998), it is now apparent that dynamic stall is the dominant source of the loading, not the rotor wake.

Ward's paper was an important step in understanding the source of the dynamic stall problem from flight test measurements. McCroskey and Fisher (1972) were able to increase this understanding by looking at the problem with a model rotor that included extensive aerodynamic measurements. They tested a model with absolute pressure transducers at the  $0.75R$  radial station on one blade and skin-friction gauges on a second blade. The angle of attack was estimated from differential pressure measurements on the lower surface of the airfoil near the leading edge

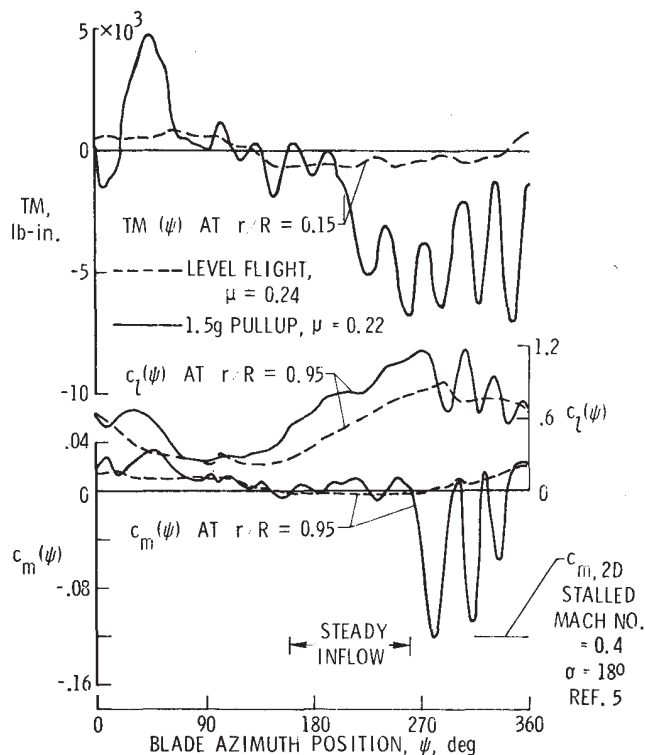


Figure 36. Re-digitization of CH-34 flight test data in level flight and maneuver (Ward, 1971).

(based on calibration of the blade from 2D airfoil tests). This angle-of-attack measurement was accurate at blade azimuths where the blade was not stalled. Over the range where the blade was stalled, they estimated the angle from “the blade cyclic input, elastic twist . . . , and theoretical flapping”.

The resulting angle of attack is shown as a function of the blade azimuth in figure 37 to illustrate the dynamic stall events. The test case was for  $\mu = 0.35$  and  $C_T/\sigma = 0.132$ , conditions beyond McHugh’s thrust limit boundary. The dynamic stall starts in the third quadrant and is characterized by the shedding of a leading edge vortex. As it passes back along the upper surface of the airfoil the pitching moment drops rapidly (“moment stall”), then as the vortex leaves the trailing edge the lift collapses (“lift stall”). Within the “stall flutter region” there are repeated stall cycles as the flow separates and reattaches while the blade undergoes elastic deformation in torsion.

The works of Ward (1971), and McCroskey and Fisher (1972), extended the insights of previous investigators to provide a basic understanding of the dynamic stall phenomenon and its importance to helicopter design. The following decades were fruitful in providing many 2D and three-dimensional (3D) tests of airfoil motions related to dynamic stall. Some of these tests provided new understanding of the dynamic stall phenomena through detailed and comparative measurements (McCroskey et al., 1982).

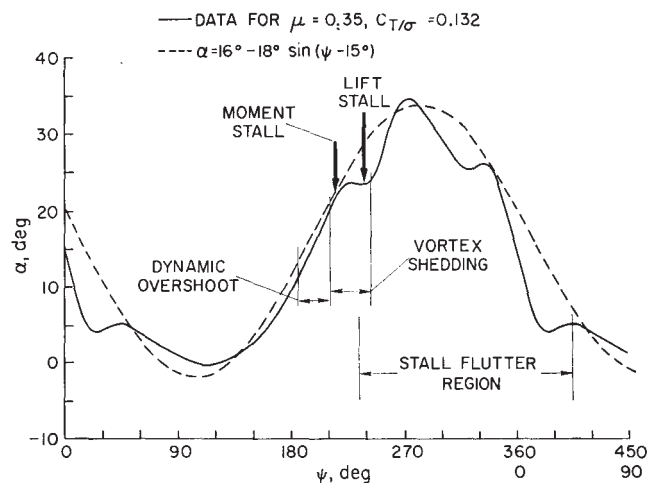


Figure 37. Angle of attack as a function of blade azimuth at 0.75R (McCroskey and Fisher, 1972).

Some provided data for semiempirical models of dynamic stall, which were then incorporated into analytical methods (Johnson, 1970; Gormont, 1973; Leishman and Beddoes, 1989; Petot, 1989; Truong, 1993). Other tests focused on airfoil designs that would provide improved dynamic stall characteristics, improved performance, and reduced loads.

Dynamic stall data from the UH-60A airloads flight test program became available in the 1990s, and it was possible to test some of the various semiempirical dynamic stall models. Leishman (2000) replotted the calculations made by Nguyen and Johnson (1998) as shown in figure 38 (color is used to show the flight data better). The flight test point in this case is the representative dynamic stall condition identified by Datta et al. (2007), see figure 34. None of the various semiempirical models agree well with the measured pitching moments. To some degree, the quasi-steady aerodynamic calculation (no dynamic stall model) does as well as any.

The semiempirical dynamic stall models developed from the early 1970s to the 1990s have been a disappointment. Whereas the result of the experimental measurements for the First Problem (vortex wake loading at low speed) were translated almost immediately into practical computational models, this did not happen for the Second Problem.

### Third Problem: High-Speed Structural Loads

From the beginning of helicopter development, the problem of increased drag on the advancing blade and the consequent performance limitations have been understood, at least to some degree. The airfoil drag will increase in a nonlinear manner beyond a certain Mach number (“drag divergence”), just as the pitching moments will decrease (“Mach tuck”). Adequate performance predictions have been made based on the steady 2D airfoil characteristics



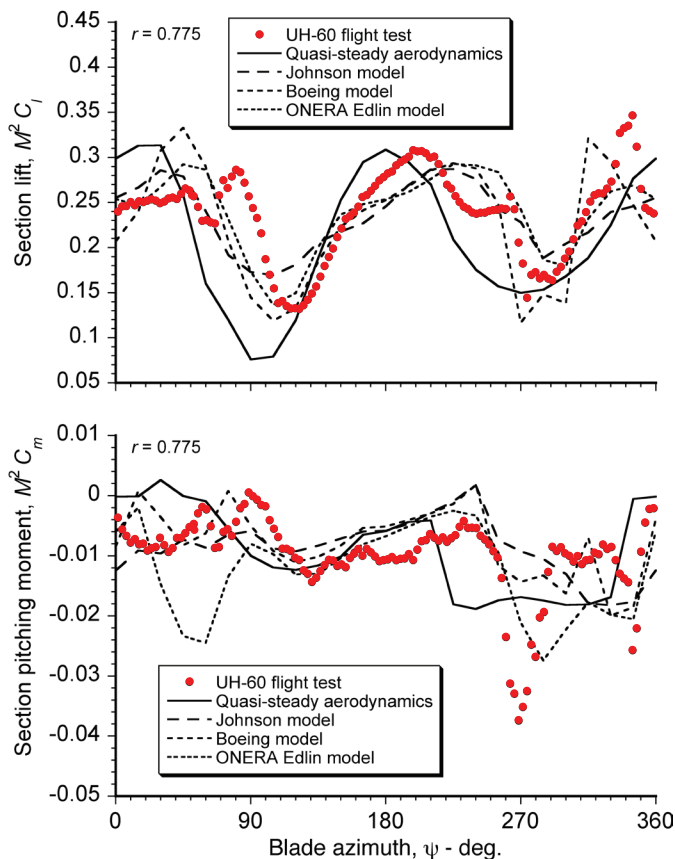


Figure 38. Calculations using five dynamic stall models in CAMRAD II compared to UH-60A airloads data for a condition with severe dynamic stall, Counter 9017 (Nguyen and Johnson, 1998; replotted by Leishman, 2000).

using a table look-up approach in the comprehensive analyses. But the unsteady transonic airloads at high speed have not begun to be understood until quite recently (Datta et al., 2007).

This Third Problem is considered to be “cryptic” because so much of the fundamentals were hidden until the development of better measurements, better experiments, and a realization that these high-speed loads were a separate problem from dynamic stall.

The first step in understanding that high-speed loads were not related to dynamic stall came from the experiments of McHugh and his colleagues at the Boeing Vertol Company (McHugh et al., 1977; McHugh, 1978). They tested a 1/10th-scale rotor of the CH-47B/C helicopter in their 20- by 20-Foot Wind Tunnel. The unique characteristic of the model was that it was designed with sufficient strength that it could determine the rotor’s aerodynamic limits. For example, at a high-speed test point, the collective pitch could be increased until the rotor thrust reversed without encountering any structural limit.

The importance of the McHugh test data is best understood by jumping back and forth in time over the decades from the 1960s to the 1990s (but without losing perspective of the time lines of these events).

In the late 1980s, inspired by Euan Hooper’s comparative study of airload measurements (Hooper, 1983), a similar comparison of structural measurements was made for eight rotor tests (Bousman, 1990). Figure 39 shows the range of level flight cases examined and compares these to the McHugh thrust boundary. What is new in this figure is the addition of the incipient stall boundary based on the UH-60A wind tunnel tests completed in 2010 (Norman et al., 2011). The incipient stall boundary marks the first evidence of stall on the rotor as thrust is increased.

What is now known is that none of these rotor tests encountered dynamic stall for these level flight conditions. Their level flight performance was limited by power or unsteady loads, but not by dynamic stall. The structural loads were rapidly increasing for each of these tests as shown for the pitch-link loads in figure 40. For most of these rotors the load increase becomes progressively greater as advance ratio increases. It is now understood that this load increase is a result of the transonic unsteady airloads on the rotor, but in the 1970s the common opinion was that these increased loads at high speed were a consequence of dynamic stall.

Bob Ormiston devised a comparative calculation test in 1973 for a hypothetical rotor (Ormiston, 1974). His purpose was to see what could be learned about the new comprehensive analyses by comparing calculations from as many companies and institutions as possible. The purpose of selecting a hypothetical rotor was to provide a level playing field for all of the analyses. In consultation with the contributing analysts, Bob selected three cases: (1) a low-speed case,  $\mu \sim 0.1$ , that would test the modeling of the low-speed vortex wake loading; (2) a moderate-speed case,  $\mu \sim 0.2$ , well removed from airfoil nonlinear behavior; and (3) a high-speed case,  $\mu \sim 0.33$ , that would result in dynamic stall. These three cases are overlaid on the plot of figure 39 in figure 41. It is apparent that the high-speed case is well short of incipient dynamic stall (but at that time there were no data to document rotor thrust limitations).

The calculations of the elastic torsional deflection at the blade tip that were made with six computational models are shown in figure 42. These differ widely from each other, and many show significant oscillations in the fourth quadrant as though dynamic stall was occurring. The results of these comparisons were first shown in a specialists’ meeting held at NASA Ames Research Center in February 1974, jointly sponsored by the American Helicopter Society and NASA (Rotorcraft Dynamics, NASA SP-352).

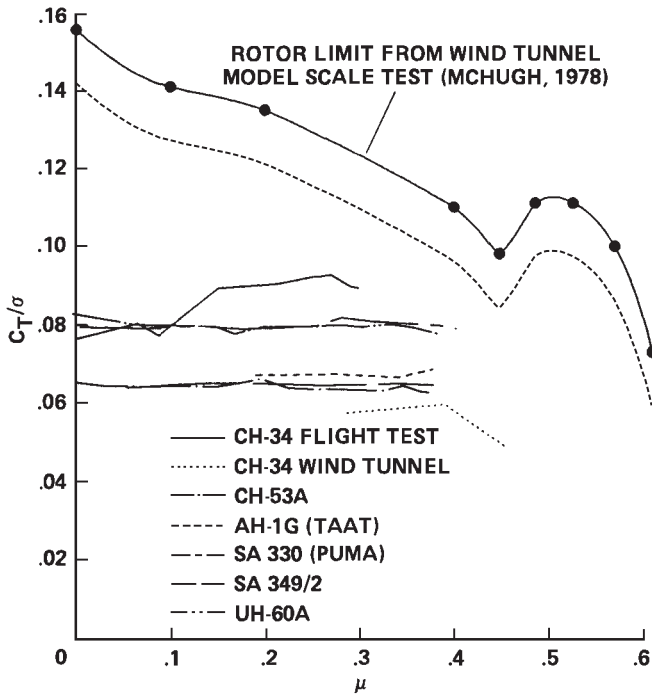


Figure 39. Flight and wind tunnel structural loads tests, nondimensional thrust as a function of advance ratio (Bousman, 1990). The rotor thrust limit is based on McHugh (1978), the incipient dynamic stall (dashed line) on Norman et al. (2011).

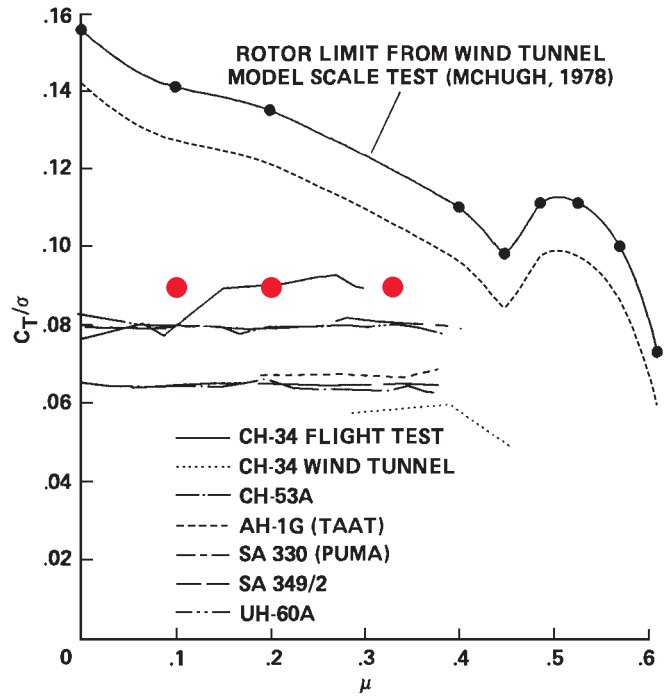


Figure 41. Calculation points for a hypothetical rotor (Ormiston, 1974) overlaid on figure 39.

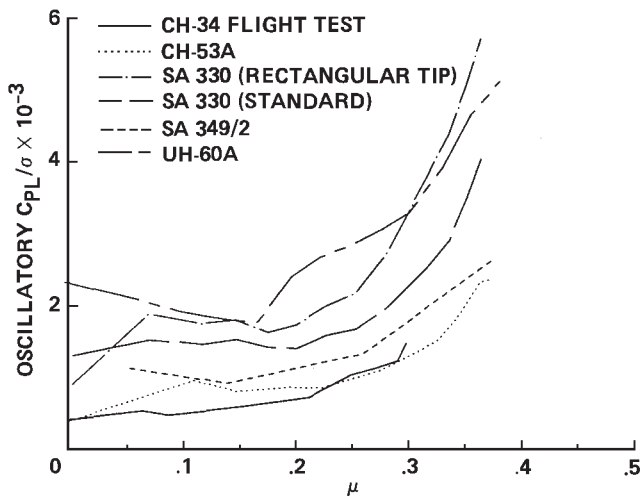


Figure 40. Nondimensional pitch-link loads as a function of advance ratio (Bousman, 1990).

One of the unusual features of the AHS/NASA conference was that the panel discussions, questions, and answers were taped, transcribed, and included in the NASA SP. It is particularly illuminating that in the transcribed comments there was no mention of the possibility that unsteady transonic loading was a cause of the loads at high speeds—an understanding of these loads was not understood at the time.

In the next decade, Hooper (1983) specifically addressed the problem of vibratory airloads in a remarkable

paper that compared measured airloads from seven airloads tests using novel visualization techniques. Figure 43 shows the normal forces as a function of both radius and blade azimuth for one of these rotors, the CH-34 in the Ames 40-by 80-Foot Wind Tunnel (Rabbott et al., 1966a). The use of a Cartesian grid provides a way of understanding both the azimuthal and radial loading. He made similar plots for six other rotor tests at both high and low speeds and concluded that the fundamental vibratory load behavior was similar for nearly all of these rotorcraft, particularly at low speed.

Hooper's comparative study was a significant accomplishment in many respects. His demonstration of the similarities in vibratory loading at low speed for different helicopter rotors in many ways provided a bookend for the First Problem. The early airloads data that had defined low-speed vortex wake loading and were instrumental in developing the prescribed wake models (and the later free wake models) were shown to be universal, but the high-speed vibratory loading was a different problem, and there was no obvious phenomenological explanation. Cowan et al. (1986) later remarked that Hooper's work showed that "the understanding of what causes these vibratory airloads was totally inadequate."

The lack of understanding to which Cowan et al. (1986) referred was related in part to limitations of the airloads data sets that Hooper had studied. First, six of the seven data sets used differential pressure measurements (only the AH-1G/OLS test relied on absolute pressure transducers). Although differential pressure measurements can provide

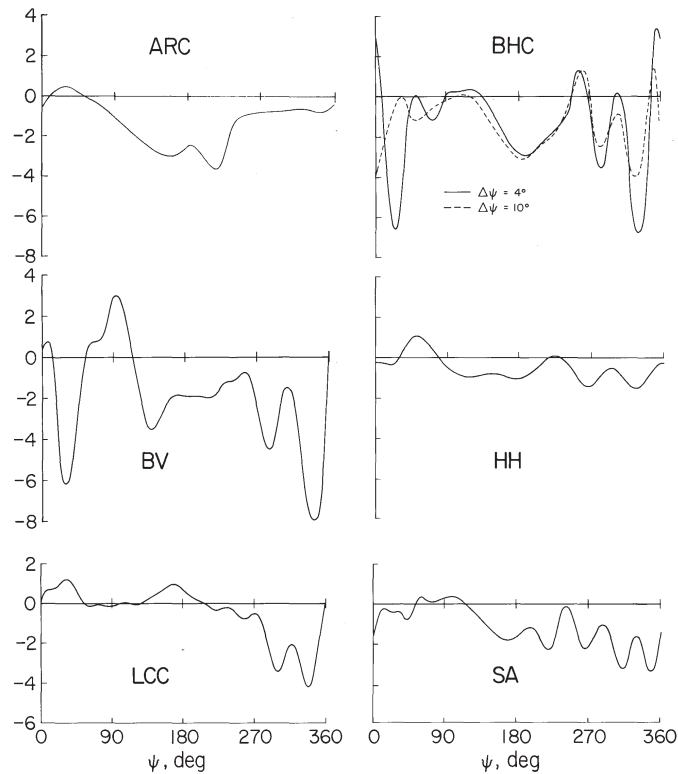


Figure 42. Comparison of calculated tip elastic torsional deflection (deg) for a hypothetical rotor,  $C_T/\sigma = 0.0897$ ,  $\mu = 0.33$  (Ormiston, 1974). Methods used: Ames Research Center (ARC), Bell Helicopter C81 (BHC), Boeing Vertol C60 (BV), Hughes Helicopters SADSAM (HH), Lockheed California 3110 (LCC), and Sikorsky Aircraft Normal Modes (SA).

accurate integrated normal forces and approximate pitching moments, they mask the behavior of the actual pressure distributions on the upper and lower surfaces. This is unimportant for subcritical flows, but the development of transonic or supersonic regions in high-speed flight creates unsteady loads that are difficult to understand without absolute pressure measurements.

Another difficulty in understanding the high-speed loads was the lack of pitching moment calculations for the airloads data sets that Hooper studied. Only one of those seven data sets, the XH-51A, included the calculation of the pitching moments (and with only five chordwise stations those moments may not have been trustworthy). Without knowing the measured pitching moments, the aeroelastic behavior of these rotors was hidden from us.

In the early 1980s, at about the same time that Hooper was looking at the early airloads data, the Royal Aircraft Establishment (RAE) in Britain and the Office National d'Études et de Recherches Aéropatiale (ONERA) and Aerospatiale in France embarked on a flight test program with a research Puma with absolute pressure transducers installed on a modified blade tip. The program was in two phases. The first used a mixed-bladed rotor with a swept

### H-34 AIRLOADING — LINEAR PLOT

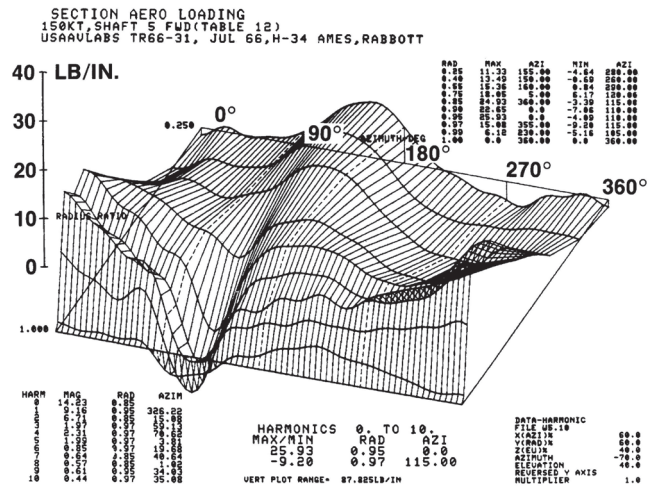


Figure 43. CH-34 section normal forces in wind tunnel test,  $\mu = 0.39$ ,  $\alpha_s = -5^\circ$  (courtesy of Euan Hooper).

tip opposite a rectangular “paddle” rotor and two standard blades (Riley and Miller, 1983). The second phase tested a rotor with four swept tip blades (Riley, 1986). A photo of the aircraft used in the second test is shown in figure 44. Between 12 and 21 absolute pressure transducers were installed at outboard radial stations at  $0.92R$ ,  $0.95R$ , and  $0.978R$ .

An international collaboration was formed in 1987 to compare the data from these tests with the most recent full-potential CFD codes. Investigators from the U.S. and Australia joined with researchers at the RAE, ONERA, and Aerospatiale. In this initial effort, the focus was primarily on comparison of measurements with CFD analyses, including a coupled CFD/CSD method based on Tung et al. (1986). A workshop was held in Farnborough in May 1988 and reported the next year in Amsterdam (Strawn et al., 1989; Bousman et al., 1989).



Figure 44. Research Puma with swept-tip blades at RAE Bedford.



A follow-on effort focused on additional comprehensive analysis calculations as well as coupled CFD/CSD approaches that included improvements to the coupling method developed by Tung et al. The new calculations were examined in a workshop at NASA Ames Research Center in May 1990 (Bousman et al., 1996).

An examination of the section normal forces on the research Puma at high speed shows that the advancing side dip pointed out by Hooper (1983) is also seen on this aircraft (see figure 45). The pressure distributions in this case (Bousman et al., 1996) show an area of transonic flow on the upper surface in the first quadrant as the local Mach number increases even as the lift is reduced. As the lift goes through zero near 90° there is transonic flow on both surfaces. Over the region of negative lift for the next 45°, there is significant transonic flow on the lower surface. Then, as the angle of attack becomes positive again, there

is an increasing supercritical flow on the upper surface until the reduction of the local Mach number allows the flow to become subcritical around the retreating side of the disk.

The unsteady nature of the supercritical flows on both the upper and lower surfaces has a profound effect on the airfoil section forces and moments. As shown in figure 45, both the comprehensive method (CSD) and the coupled calculation (CFD/CSD) are more or less able to capture the section normal forces (although the Comprehensive Analytical Model of Rotorcraft Aerodynamics and Dynamics/Johnson Aeronautics (CAMRAD/JA) is as good or better than the coupled analysis), but the pitching moment predictions for both methods are poor. The comprehensive method can deal with viscosity through its 2D table look-up approach at inboard locations, but not near the blade tip. The coupled CFD/CSD method used did not include viscosity, but was able to model 3D effects at the blade tip. From the two collaborations it was learned that both approaches were inadequate.

By the 1990s, the measurements were perhaps sufficient to understand some parts of the Third Problem. But to obtain accurate calculations one had to solve the aeroelastic problem, that is, one had to be able to accurately calculate the large pitching moments on the outer blade, calculate the torsional response, and obtain the correct elastic deformation (and tip angle of attack). The advent of the UH-60A flight test data, the series of workshops that followed that flight test program, and the new Navier–Stokes CFD models changed everything.

### UH-60A Airloads Program and Workshops

Flight testing accomplished in the UH-60A Airloads Program was envisioned as an integral part of a much larger effort sponsored by NASA and the U.S. Army called the Modern Technology Rotors (MTR) Program (Watts and Cross, 1986). Watts and Cross described a program of extensive testing of two modern rotors, the Boeing Vertol Model 360 and the Sikorsky Aircraft UH-60A. The testing would include multiple phases including flight tests, full-scale wind tunnel tests, model rotor wind tunnel tests, and ground vibration tests. They proposed that these systematic tests would be followed by testing of other new rotors from Bell Helicopter Textron and McDonnell Douglas.

A key part of the MTR program was that flight, wind tunnel, and model rotor tests would all include extensive pressure instrumentation. Looking back at the vision in their paper today, one can only be awed by their optimism considering the problems that followed. For the Model 360, wind tunnel testing of a pressure-instrumented rotor was accomplished (Cowan et al., 1986; Dadone et al., 1987), but a full-scale pressure instrumented blade was never

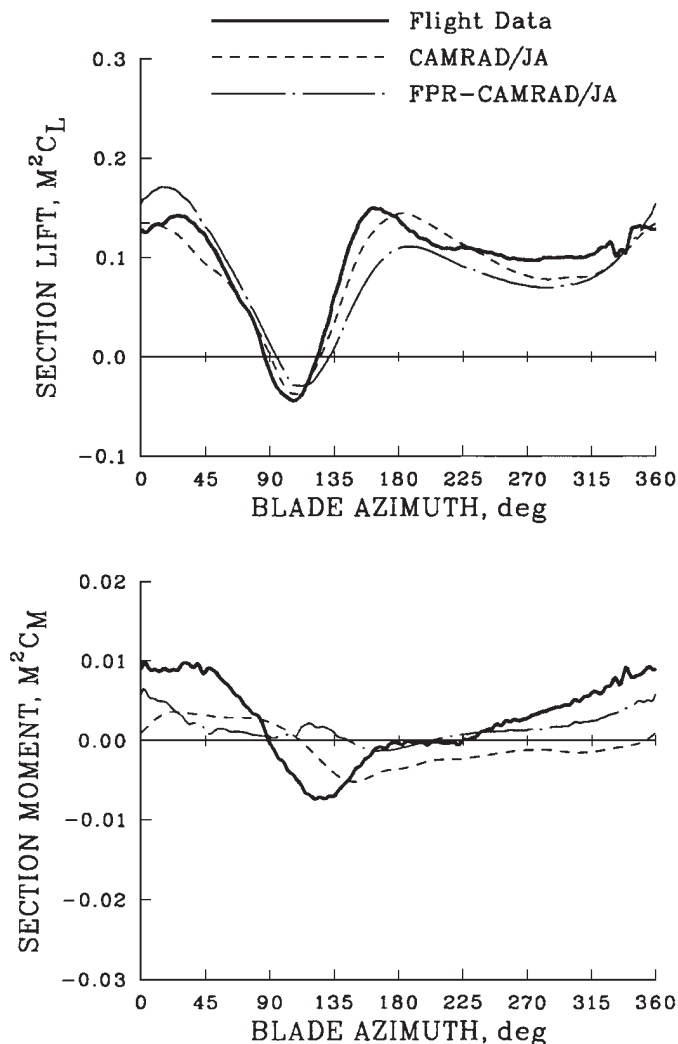


Figure 45. Comprehensive and CFD/CSD models compared to measured normal force and pitching moment on the research Puma with a swept tip at  $r/R = 0.95$ ,  $C_w/\sigma = 0.070$ ,  $\mu = 0.40$  (Bousman et al., 1996).

built. A pressure-instrumented blade for the UH-60A was fabricated, but the flight test program was cancelled before any data were obtained. How that program finally succeeded is a part of this paper.

### UH-60A Airloads Program

Under the MTR program, two instrumented blades were designed and built by Sikorsky Aircraft, and they were delivered to Ames Research Center in late 1988. One blade was instrumented with strain gauges and accelerometers and the other had 242 absolute pressure transducers. Two hundred and twenty-one of these transducers were installed at nine radial stations; the others were used to characterize blade vortex interactions at the blade leading edge.

The critical design path for the data processing system was to digitize the data in the rotating system and then split the pulse code modulated (PCM) data into 10 streams and pass it through slip rings to a multiplexer that combined the streams and recorded it on tape in the aircraft cabin (Kufeld and Loschke, 1991). That data processing system, referred to as the Rotating Data Acquisition System (RDAS), was designed and developed at Ames Research Center (see figure 46). The required data rates were about six times greater than the capability available at the time. The final data rate was about 7.5 MB/sec and was a major technological hurdle that caused no end of developmental problems. (Twenty years later, the data rate for streaming video to your smart phone is 1–2 MB/sec; technology moves fast.)

Initial work on the RDAS was started in April 1985, 3 years before the instrumented blades would be delivered. This work attempted to make use of already qualified hub-mounted hardware, the “mux bucket” used in the previous AH-1G/OLS and AH-1G/TAAT tests (albeit with a completely different data processing scheme). This was referred to as the RDAS I (Kufeld and Loschke, 1991). The mux bucket was modified to provide more room for components beneath the original envelope. By the time it was recognized that there was still not sufficient room in the mux bucket for the 10 PCM streams, nearly 54 months had elapsed. (The discarded RDAS I mux bucket was modified in the following years for use on the JUH-60A RASCAL aircraft, which is still doing flight control research in 2014.)

RDAS IIa (and all of the subsequent versions) used the same hub-mounted container as shown in figure 46. There was sufficient room for the 10 PCM streams, but stream synchronization could not be obtained. Attempts to fix this problem were not successful, and it was recognized after about 25 months that a redesign was required. NASA put together a committee of “wise old men” from the instrumentation side of the house under the chairmanship of Rod Bogue of NASA Dryden. They quickly generated a list of necessary changes. All of these were valuable; the most

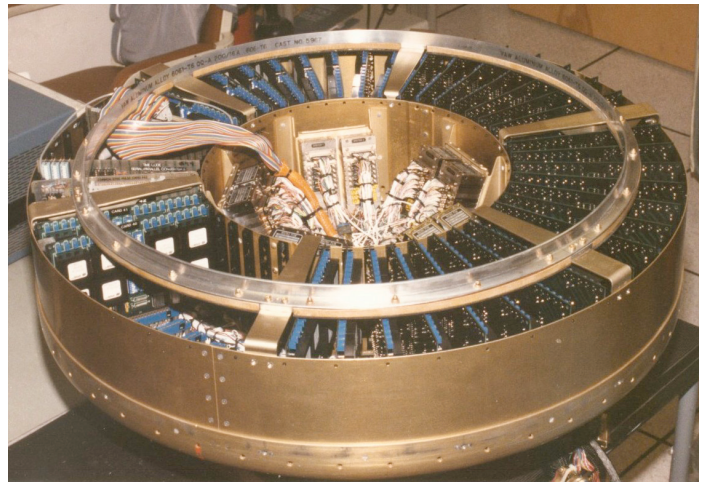


Figure 46. Rotating Data Acquisition System (RDAS) in the laboratory (NASA Ames Research Center).

important was the implementation of a master clock that cured the synchronization problem.

RDAS IIb was the redesigned system as recommended in the Bogue Report. A new problem of excessive high-frequency noise cropped up. This was less serious than the previous problems and was fixed by installing new shielding, but another 17 months had passed by.

The final configuration, RDAS III (or just RDAS) was installed on the aircraft for airworthiness testing during April 1993. The aircraft was flown through a series of critical maneuvers, but no maneuver limitations caused by the RDAS were observed and the aircraft was cleared for the flight test program at the end of the month.

Two weeks later, the flight test program was cancelled. All funding was eliminated as of September 30th, the end of the fiscal year. The cancellation was partly because of Administrator Golden’s insistence that all NASA flight testing be done at Dryden, but also because of the long series of development problems on the RDAS.

Optimistically, the best that could be done by the end of September was to make eight flights. So the new test plan was a description of those eight flights on a single sheet of paper. It was circulated to the companies and the universities and priorities were set. That summer five flights were managed, but only the last two had everything working properly.

NASA Ames Director of Aeronautics, Tom Snyder, made a deal. If the data acquisition problems could be solved and good data obtained by the end of September, he would transfer funds from the other divisions and branches in his directorate, and flight could continue until the end of the year. Bob Kufeld and Bill Bousman made a 3-hour presentation at the end of the month to a panel of Tom’s division and branch chiefs. The presentation went well, and



Tom gave the go-ahead. A collaborative ground acoustics program was flown with NASA Langley in November. After a rainy December, Tom granted two more months. The 31st flight was completed in late February 1994. By the summer, all of the data were stored and accessible, and the branch was dissolved. Tom had broken the primary promise of all “Big Science” projects—he had taken the funds needed to finish the project from the rest of his organization. Most of the UH-60A flight test data still being used today were obtained because of Tom’s decision.

## UH-60A Airloads Workshops

30 GB of airloads data were stored on an optical jukebox at NASA, but for what purpose? Bob Kufeld and Bill Bousman examined what were felt to be the most important parts of the data set (Kufeld and Bousman, 1995; Kufeld and Bousman, 1996) and in the process developed confidence in the validity of the data but still wanted to find a way to involve industry.

In 1995, the Airloads Working Group was created. A small amount of money was found and used to provide minimal support for Bell Helicopter Textron, Boeing Helicopters, McDonnell Douglas Helicopters, and Sikorsky Aircraft. Each company selected two cases and used visualization tools as a better way of understanding the data obtained. NASA and the U.S. Army at Ames Research Center did the same, and the results were exchanged. Discussions of a follow-on program did not lead to a continuation of this effort.

About 1999, Bob Ormiston developed a detailed plan for a series of airloads workshops that would be sponsored by the National Rotorcraft Technology Center (NRTC). This was a well planned, top-down approach that would use funds from both the NRTC and its industrial partner, the Rotorcraft Industry Technology Association (RITA). The need to assign funding based on a detailed plan caused political problems and the approach failed.

In 2001, Yung Yu, as part of his responsibilities at the NRTC, proposed a new format for the Airloads Workshop. He persuaded both the industry and academia to propose projects for the NRTC/RITA consortium that would take advantage of the UH-60A data. The Airloads Workshops would then be held twice a year in conjunction with the NRTC/RITA review and planning meetings. This ad hoc, bottom-up approach worked, and 26 workshops have been held from 2001 to early 2014.

In the initial years the meetings were organized by Yung Yu. After his retirement, Mike Rutkowski took over. From the beginning, the workshops were a mixture of researchers from industry, government labs, and the universities. Rules were developed slowly on an ad hoc basis and none were

written down. Each workshop tended to start out with outrageous goals, few of which were ever met. But enough was accomplished in the 12 years to maintain the interest of the participants.

The workshops have been enormously successful as described in the next section. Why this mix of people and ideas worked so well over such a long period is unclear, but a key ingredient has been the individual leadership of participants from industry, government, and academia.

## Airloads Workshops and the New Calculations

From the beginning, the workshops focused on the three problems that Datta et al. (2007) would later summarize, that is, the low-speed vortex wake loading, dynamic stall in level flight and maneuver, and unsteady transonic flow on the advancing blade tip at high speed. At first, the Third Problem, that of unsteady transonic flow, drew the most attention.

Calculations with a number of comprehensive analyses showed no improvement over past efforts. Although some of the predictions of normal force were fairly good, the pitching moments were unsatisfactory. The workshops focused on breaking the problem down into separate pieces by using the measured airloads to calculate the appropriate elastic response (see Ormiston, 2004, for example) and then use those elastic responses as inputs to the new Navier–Stokes CFD models. This work progressed quickly to the next stage, and soon a number of investigators were showing results using coupled CFD/CSD methods (Potsdam et al., 2004).

How well did the new calculations based on coupled CFD/CSD do? The next series of figures shows the workshop calculations for each of the three problems used as a theme of this paper. These figures are based on calculations made by workshop participants from early 2007 to the summer of 2009.

**First Problem.** This problem deals with the airloads caused by the low-speed vortex wake. The early airloads tests first stimulated the analytical developments of prescribed wake models, then eventually free-wake models. Present day methods are capable of reasonably accurate calculations although there are still a few problems in terms of the accuracy of the advancing and retreating side peak loads in both amplitude and phase.

Figure 47 compares four CFD/CSD calculations for the normal force at  $0.92R$  with the UH-60A flight test measurements for this problem. The four calculations are combinations of two CFD models (OVERFLOW and GT Hybrid) and three comprehensive methods (CAMRAD II, RCAS, and DYMORE).

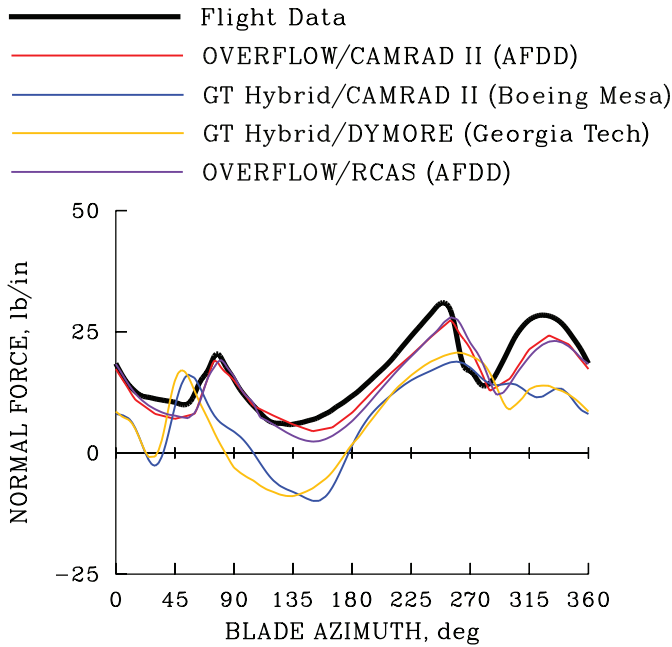


Figure 47. Comparison of measured normal force at  $0.92R$  for the UH-60A with four coupled CFD/CSD methods for the First Problem;  $\mu = 0.15$ ,  $C_w/\sigma = 0.079$ .

The calculations in figure 47 show that the major difference between the methods is in the CFD model, and no significant difference is observed in the comprehensive part. The two coupled calculations that use OVERFLOW show good agreement with the measurements, particularly in matching the peak disk vortex loading on the advancing and retreating sides. OVERFLOW includes the wake tip vortices within its solution grids and provides a good representation of the vortex wake loading. GT Hybrid, on the other hand, saves considerable computer time and cost by modeling the vortex wake in much the same manner as the comprehensive analyses, and this has caused differences in azimuths of the calculated and measured vortex-loading spikes.

The accuracy maps for the four sets of calculations at all nine radial stations are shown in figure 48. Again, the CFD model in this case is responsible for significant differences in the results, with more scatter seen for the GT Hybrid-based calculation than for the OVERFLOW-based calculation. The accuracy of GT Hybrid is much the same whether DYMORE or CAMRAD II is the CSD partner.

The coupled calculations using OVERFLOW provide slightly better results than have been obtained from a comprehensive analysis by itself, whereas the calculations using GT Hybrid are not as good.

What is more striking about the First Problem calculations is how well the methods agree with each other. That is, the OVERFLOW calculations are very similar whether the comprehensive model is CAMRAD II or RCAS. The same is seen for the GT Hybrid coupled calculation whether the

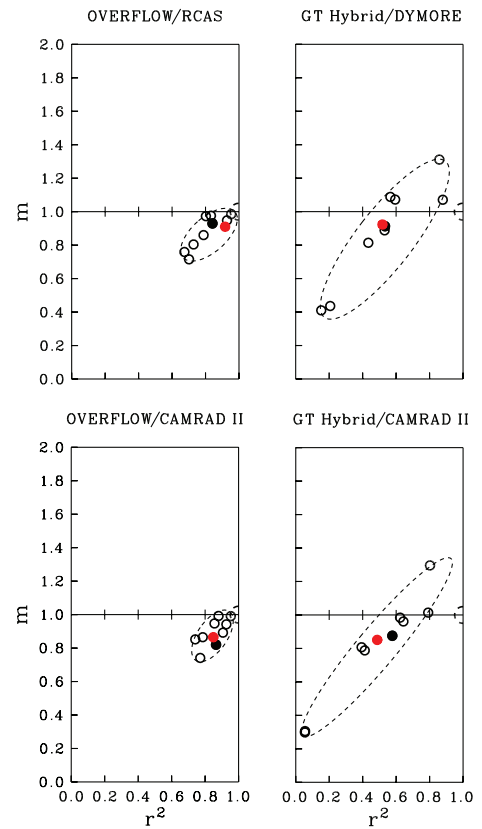


Figure 48. Accuracy maps of measured normal forces at nine radial stations (open circles) for the UH-60A with four coupled CFD/CSD methods for the First Problem;  $\mu = 0.15$ ,  $C_w/\sigma = 0.079$ . Solid black circles are  $0.92R$ , solid red circles show the combined accuracies.

comprehensive model is CAMRAD II or DYMORE. The state of the art has come a long way from the days of the hypothetical rotor comparisons (Ormiston, 1974).

**Second Problem.** The Second Problem deals with the effects of dynamic stall on the airloads. Through much experimentation a great deal has been learned about the phenomenon of dynamic stall, but that knowledge has not been translated into accurate calculations (see figure 38).

Figure 49 compares five CFD/CSD calculations for the normal force at  $0.92R$  with the UH-60A flight test measurements. For this problem there are five combinations for the coupled calculations. OVERFLOW is coupled with CAMRAD II, DYMORE, and RCAS, whereas GT Hybrid is coupled with CAMRAD II and DYMORE.

The calculations in figure 49 show that all of the methods produce similar results and roughly match the data. Each shows reduced loading on the advancing side, and most show a loss of lift caused by the first dynamic stall cycle at about  $280^\circ$ . But each calculation shows its own peculiarities, sometimes in amplitude and sometimes in phase shift, and few show satisfactory agreement in the phase of the second stall cycle at  $350^\circ$ .

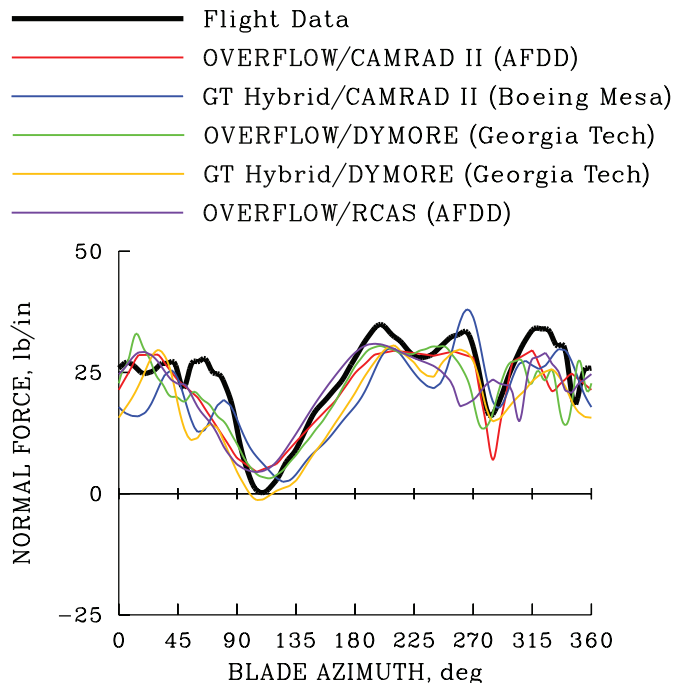


Figure 49. Comparison of measured normal force at  $0.92R$  for the UH-60A with five coupled CFD/CSD methods for the Second Problem;  $\mu = 0.24$ ,  $C_w/\sigma = 0.133$ .

The accuracy maps for the five sets of calculations at all nine radial stations are shown in figure 50. The ellipses in this figure indicate scatter in the results. The results with OVERFLOW are better than GT Hybrid, but the OVERFLOW results are not as good as were seen for the First Problem.

For the First Problem, it was striking how the accuracy of the results was independent of which comprehensive analysis was coupled to the CFD calculations. In terms of the accuracies shown in figure 50, that is also the case for this problem. But if the fine detail is examined in figure 49, differences are seen between the coupled calculations depending on which of the three comprehensive analyses is used.

**Third Problem.** The Third Problem deals with the high-speed vibratory loads caused by supercritical flows near the blade tip, a problem poorly understood over the past 40 years.

Figure 51 compares five CFD/CSD calculations for the normal force at  $0.92R$  with the UH-60A flight test measurements. For this figure there are five combinations for the coupled calculations. OVERFLOW is coupled with CAMRAD II, DYMORE, and RCAS, whereas GT Hybrid is coupled with CAMRAD II and DYMORE. All of the calculations in figure 51 show good predictions of the measured normal force and are in good agreement with each other. This is remarkable considering the great difficulty there has been with this problem over the last 40 years.

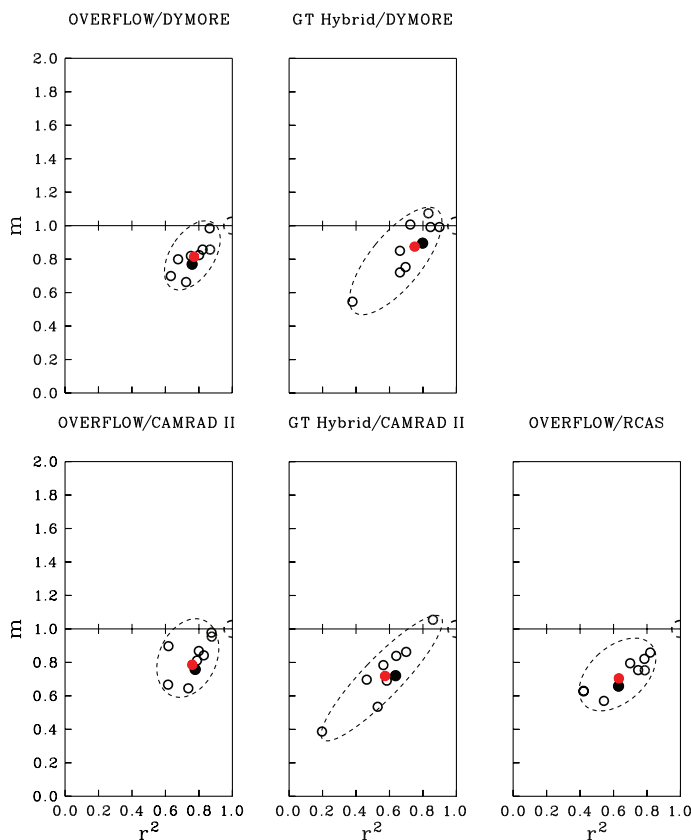


Figure 50. Accuracy maps of measured normal forces at nine radial stations (open circles) for the UH-60A with five coupled CFD/CSD methods for the Second Problem,  $\mu = 0.24$ ,  $C_w/\sigma = 0.133$ . Solid black circles are  $0.92R$ ; solid red circles show the combined accuracies.

The accuracy maps for the calculations at all nine radial stations are shown in figure 52. In most cases, the scatter ellipse is quite tight. The combined accuracy for the five coupled methods lies on an accuracy circle that ranges from 7 to 14 percent.

### The Airloads Workshops Transformation

The transformative event that has characterized the Airloads Workshops and the success of the new coupled calculations was the result of putting together many bits and parts that eventually led to these improved analyses. There is an old saying that “success has a thousand fathers, but failure is an orphan.” The success of the workshops has depended on many organizations and many people.

Figure 53 shows a schematic of the various parts that came together to allow the success that was obtained. These contributions are divided into seven categories. Starting on the left side, the first of these categories are the contributions of the UH-60A Airloads Program data, of which quite enough has already been said in this paper.

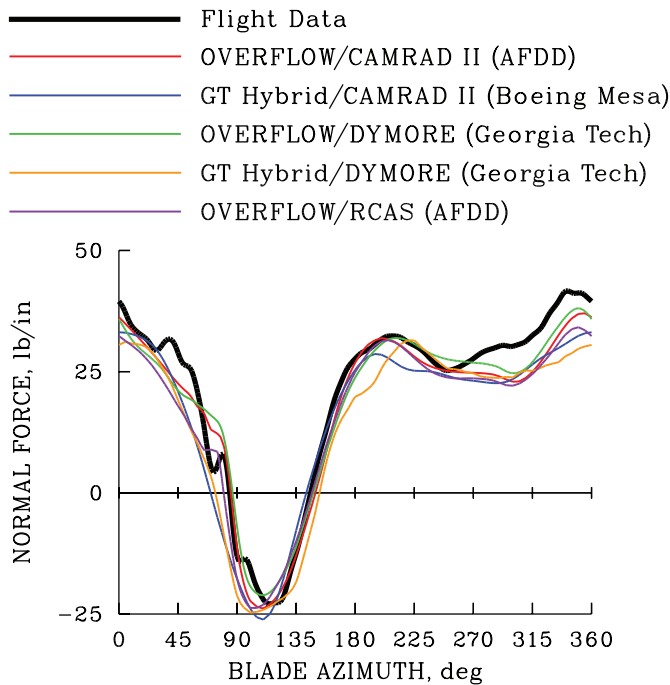


Figure 51. Comparison of measured normal force at 0.92R for the UH-60A with five coupled CFD/CSD methods for the Third Problem;  $\mu = 0.37$ ,  $C_w/\sigma = 0.078$ .

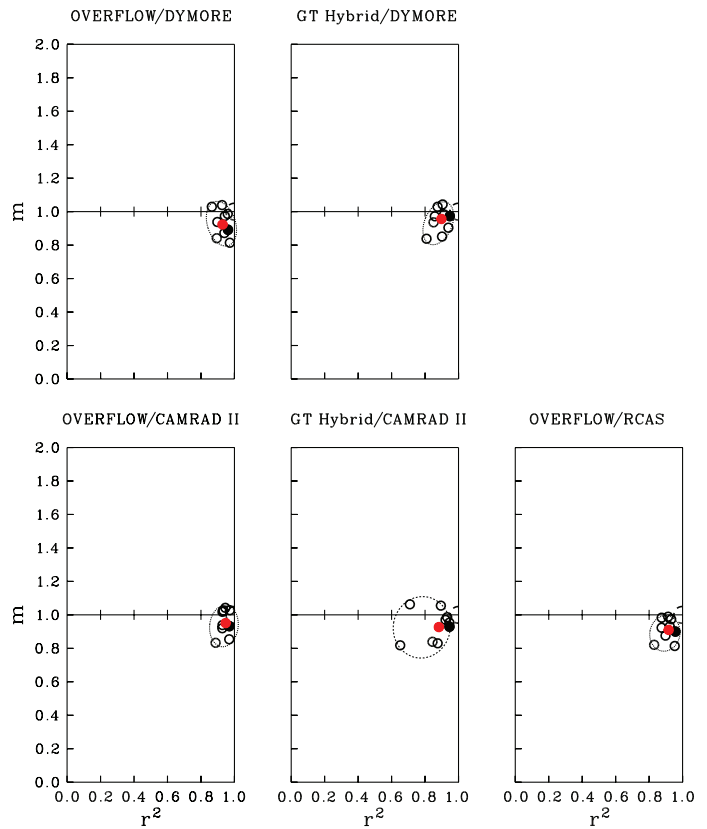


Figure 52. Accuracy maps of measured normal force at nine radial stations (open circles) for the UH-60A with five coupled CFD/CSD methods for the Third Problem;  $\mu = 0.37$ ,  $C_w/\sigma = 0.078$ . Solid black circles are 0.92R, solid red circles show the combined accuracies.

The second of the contributions were from the Rotorcraft Centers of Excellence (RCOE). Norm Augustine recommended the creation of academic centers for rotorcraft research in 1981 (Hirschberg, 2001). The purpose of the RCOEs was to develop long-term rotorcraft technology programs based on academic research at a few selected institutions. A competition to select the new centers was held in 1982 under the direction of the Army Research Office (ARO). The winners of the first competition were the University of Maryland, Georgia Tech, and Rensselaer Polytechnic Institute (RPI).

Program oversight changed when the National Rotorcraft Technology Center (NRTC) took over the program in the mid-1990s. At that time Penn State replaced RPI in the triumvirate of rotorcraft centers. In 2006, the program was restructured and named the Vertical Lift Research Centers of Excellence. Only Georgia Tech and Penn State remained as centers.

The RCOEs were a success for two reasons, both well understood when the centers were recommended in 1981. First, the centers provided academic capabilities with a long-term view of needed improvements in rotorcraft technology. Second, many graduates of the RCOEs have moved into industry and government positions where they have made significant contributions.

The third of the major contributors to the workshop transformations were the NRTC and the RITA. In the early 1990s, both the U.S. Army and NASA were pursuing

separate initiatives to increase the relevance of government Research and Development (R&D) efforts. The two initiatives were fused, and with the participation of the U.S. Navy and the Federal Aviation Administration (FAA), NRTC was formed in 1995. At the same time, the U.S. industry put together RITA to share resources for research into pre-competitive technologies. Money was the glue that held these two organizations together. It was under the NRTC and RITA that the Airloads Workshops were sponsored. The continuity provided by the NRTC and RITA was an important element in developing trust between researchers in industry, government, and academia.

The fourth contributor to the workshop's success was the addition of the Defense Advanced Research Projects Agency (DARPA) as a participant. In early 2004, DARPA started the Helicopter Quieting Program (HQP), working through NASA Ames Research Center. Prior to the program start, Dr. Lisa Porter, the DARPA Program Manager, attended the fall 2003 Airloads Workshop in Atlanta. She explained the objectives of the HQP and at the same time learned about the UH-60A data set. That data set became one of the HQP test cases and the additional funding broadened the efforts of the workshop (Newman et al., 2008).



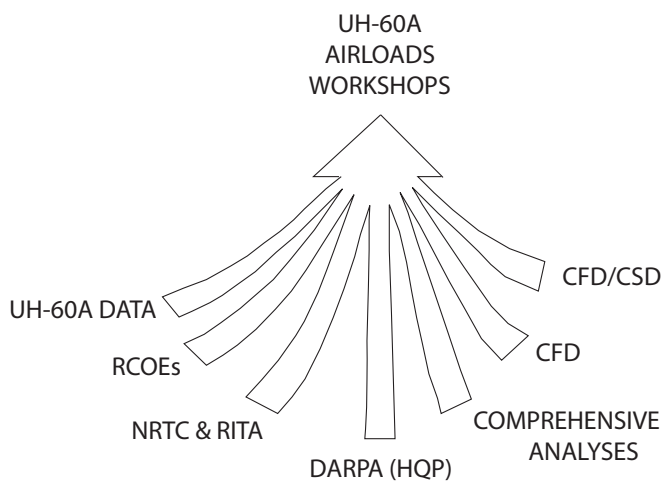


Figure 53. Factors contributing to the success of the UH-60A Airloads Workshops.

But DARPA's contribution extended beyond the additional funding. Jay Dryer, working for DARPA, dove into the UH-60A database on Tilt Rotor Engineering Database System (TRENDS). He uncovered a phase error made in extracting the data from TRENDS for use by the workshop participants (Kufeld and Bousman, 2005). Everyone working with that data was grateful for the error that Jay uncovered.

The final three contributions to the workshop's success deal with three aspects of rotorcraft modeling technology: comprehensive analyses (sometimes referred to as computational structural dynamics or CSD), computational fluid dynamics (CFD), and the coupling of CFD and CSD. Wayne Johnson's 30th Alexander Nikolsky Honorary Lecture (2011b) provides a detailed and insightful summary of each of these technology aspects. Here are a few brief comments on the three computational categories.

Digital computers were a main enabler of new helicopter analyses starting in the early 1960s. Bell Helicopter Textron developed a comprehensive analysis that became the C81 program, an early attempt to provide a balanced analysis that could model multiple configurations (Johnson, 2011b). The U.S. Army adopted C81 as its primary analysis program in 1973.

In February 1974, NASA Ames Research Center and the American Helicopter Society sponsored a meeting on Rotorcraft Dynamics. This conference included a comparison of a number of the early industry comprehensive analyses in the calculation for a "hypothetical" rotor (Ormiston, 1974). These calculations in many cases were divergent (see figure 42). Ormiston's paper was discussed by senior engineers from the helicopter companies, and a topic raised repeatedly was whether a standard analysis should be

developed for helicopters. Dick MacNeal, the developer of the NASA Structure Analysis (NASTRAN), said "No." When asked why, he elaborated (MacNeal, 1974):

"I think that there is great virtue in diversity, particularly when there is a great deal of doubt as to the physics of the problem, the methods of analysis, etc. If we settle on one particular approach, we will all use it and we will all go over the cliff together like lemmings going into the sea."

The Army pursued the notion that C81 should be a standard analysis over the next few years. They funded Bell Helicopter Textron, Boeing Vertol, and Sikorsky Aircraft to apply C81 to their own aircraft types and judge the utility of the analysis. Johnson (2011b) wrote that the "results were disappointing" and "the position against universal adoption of C81 was clear."

Despite the problems with developing a standard analysis, much had been learned by the late 1970s. In 1977, the Army embarked on the development of 2GCHAS, the Second Generation Comprehensive Helicopter Analysis System, a new comprehensive analysis that they believed would become the new standard. 2GCHAS, or "2-G-Charlie" as it quickly became known, never obtained that success. Instead, a number of other new comprehensive analyses were developed. These included CAMRAD and its successors from Johnson Aeronautics starting about 1980, UMARC from the University of Maryland beginning about 1988, DYMORE from Georgia Tech about 1996, and finally RCAS, the reincarnation of 2GCHAS, beginning about 1997. Each of these methods were different but, unlike the situation in 1974 where analytical predictions differed widely, these modern analyses provided much the same results and the rush into the sea of MacNeal's lemmings was avoided.

Computational Fluid Dynamics (CFD) became a major contributor to the success of the Airloads Workshops, particularly as more powerful computers became available in the 1990s. (These very powerful machines were a key to the success of the new analytical approaches, but rotorcraft technology was not the tail that wagged that dog.) As was the case for comprehensive analyses, Wayne Johnson's 30th Alexander Nikolsky Honorary Lecture (2011b) provides a critical summary of developments in CFD.

The effort progressed in a logical approach of looking first at calculations in hover, then non-lifting rotors in forward flight, and finally lifting rotors in forward flight. Much of this work was driven by the calculation methods at the U.S. Army Aeroflightdynamics Directorate at Ames Research Center and experimental work at ONERA, all under a cooperative international agreement.

Early CFD development using a small-disturbance method (Caradonna and Isom, 1976) showed the importance of the unsteady terms for a non-lifting rotor in forward flight, particularly for transonic flow on the advancing side. These methods were developed to the point where they could be applied to lifting model rotor data in forward flight (Caradonna et al., 1984). Wake effects and blade motion were accounted for by using the measured control angles and a simple inflow model. Figure 54 shows a sample of these calculations at six blade azimuth angles, and both the development and strength of the transonic flow are well represented. Johnson (2011b) has called the Caradonna et al. paper, “the start of this quest.”

These first results were followed by more accurate calculations using the full-potential and Euler equations in the mid-1980s. By the late 1980s, the first demonstrations occurred using the Navier–Stokes equations with a representation of viscosity.

The development of CFD methods up to the end of the 1990s was, in some respects, an “academic” exercise. The primary proof of predictive accuracy that was used was the comparison of pressure distributions (such as in figure 54). But the rotor designer had only a passing interest in pressure distributions. Instead, the designer wanted the distribution of lift, pitching moment, and drag along the blade span.

The CFD developers eventually provided their results in terms of the radial and azimuthal distributions of normal force as represented by  $C_N$  and pitching moment as represented by  $C_M$  but then stumbled over the baggage of the fixed-wing/rotary-wing divide. Because  $C_N$  is equal to the dimensional normal force divided by  $0.5\rho v^2 c$ , it is affected by the local velocity  $v$ . For a fixed-wing aircraft, the local velocity does not vary greatly over the entire aircraft, but for a helicopter rotor it varies with the blade radius and rotor azimuth. On the advancing side, where transonic effects are so important, the local velocity is high and  $C_N$  is low, whereas on the retreating side, the local velocity is low and  $C_N$  is high. Moreover, at the reverse flow boundary where the local velocity is zero,  $C_N$  becomes infinite. The dimensional reality is that the local normal forces are of the same order everywhere on the rotor and these cannot be represented by  $C_N$ .

This was not a new problem, but it took time to resolve. For example, in examining the AH-1G/OLS aerodynamics airloads data, Cox (1977) plotted the section normal forces as  $C_N$  for a high-speed case and described a “stall” event inboard at  $0.40R$ . But that stall event was an artifact of using  $C_N$  as the reverse flow boundary was approached. Charlie Morris (1978) used the White Cobra at NASA Langley Research Center in the late 1970s to evaluate three different

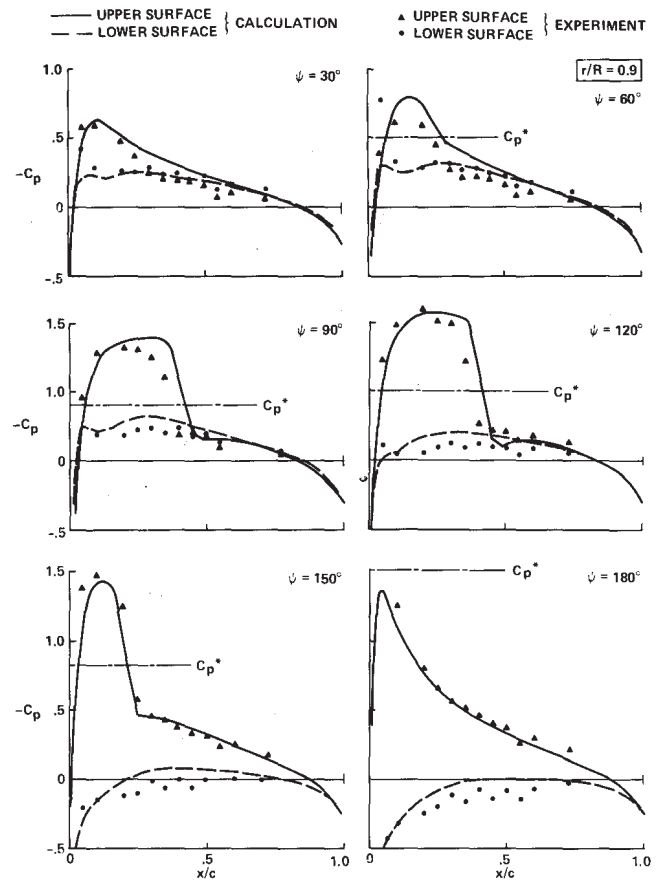


Figure 54. Comparison of measured and computed chordwise pressure distribution at different azimuth angles;  $\mu = 0.39$ ,  $C_T/\sigma = 0.0665$ ,  $r/R = 0.90$  (Caradonna et al., 1984).

airfoils on the AH-1G rotor. In one of these reports (Morris et al., 1980), he plotted normal force and pitching moments as  $M^2 C_N$  and  $M^2 C_M$ , where the speed of sound was used for nondimensionalization instead of the local velocity. No one picked up on Charlie’s idea.

Hooper (1983) recognized this problem in his study of the rotor loads measured on disparate aircraft. He simply showed the forces as dimensional data and selected appropriate axes to allow comparison.

The turnaround came in the late 1980s when an international program was started to compare CFD calculations with measurements obtained on the research Puma (Riley, 1986). In the planning discussions, Jim McCroskey suggested the use of  $M^2 C_N$  and  $M^2 C_M$  as a way of avoiding the distortion introduced by  $C_N$  and  $C_M$ . The use of  $M^2 C_N$  and  $M^2 C_M$  is now largely universal.

The last of the contributions to the workshops (but not the least) was the technique developed to couple the comprehensive analyses (also referred to as CSD) to the CFD analyses. The coupling between the two analyses is accomplished by a transfer of integrated airloads and blade

deformations. Over time, two basic schemes have been developed: (1) loose coupling, where the transfer takes place after a revolution, and (2) tight coupling, where the transfer is made at each time step (as driven by the CFD code).

The loose coupling efforts started in early 1984 when Chee Tung and Frank Caradonna decided to approach the problem of CFD calculations for a lifting rotor by using the transonic small-disturbance code called FDR as the means of calculating the lift on the outer blade on the advancing side to provide to the comprehensive analysis CAMRAD, which would then provide the rotor trim and blade deformations (Tung et al., 1986). They encountered difficulties in making the coupling work and asked Wayne Johnson for his help; Wayne developed the coupling methodology and made the necessary modifications to CAMRAD (Johnson, 2011b). A schematic of the coupling process is shown in figure 55. The FDR analysis provided only lift to the comprehensive analysis and only over a limited domain.

Datta et al. (2007) and Johnson (2011b) provide summaries of the development of these coupling methods. Strawn and Tung (1986) coupled the full-potential code

FPR with CAMRAD, and this time the lift was calculated by FPR over the entire rotor.

The next step was to have the CFD code provide pitching moments as well as lift, but this approach encountered many difficulties. Beaumier (1994) was one of the first to successfully accomplish this task, using an unsteady full potential code FP3D coupled with the comprehensive analysis R85/METAR. Although the coupling was successful, the pitching moment predictions were no better than the CSD predictions alone, a problem with many of the CFD codes at the time because they had no way of handling viscosity.

In the 1990s, a number of investigators had shown that Navier–Stokes calculations could be used to predict rotor airloads. The final step was in 2004 when Potsdam et al. (2004) coupled the Navier–Stokes code OVERFLOWD with CAMRAD II using the lift and chord forces, and the pitching moment simultaneously. The results obtained were basically those shown in figures 47 through 52.

## CONCLUDING REMARKS

This paper has focused on the history of the 12 major airloads measurements performed in the United States, and has shown how these measurements have supported new analytical approaches. It concludes that with the data from the UH-60A Airloads Program and the recent advances in computational methods the capability of these methods has undergone a transformation. But that transformation is not complete until these new methods are trusted and used by designers. Until that happens they remain an academic exercise.

There are five challenges in the next decade or two for the use of these new tools in order to truly obtain a transformation.

1. The new coupled CFD/CSD methods must be integrated into design.
2. Nonlinear aerodynamic loads at high speed and in maneuvers will depend on the rotor design—one must accept that each rotor is different.
3. The remaining deficiencies in prediction accuracy must be understood. One of these is the prediction of the higher harmonics of structural loads so that the problems of vibration can be addressed.
4. The loss of experimental data, particularly large data sets stored on digital media, must be addressed.
5. Finally, cheaper ways to obtain airloads from flight or wind tunnel tests must be found.

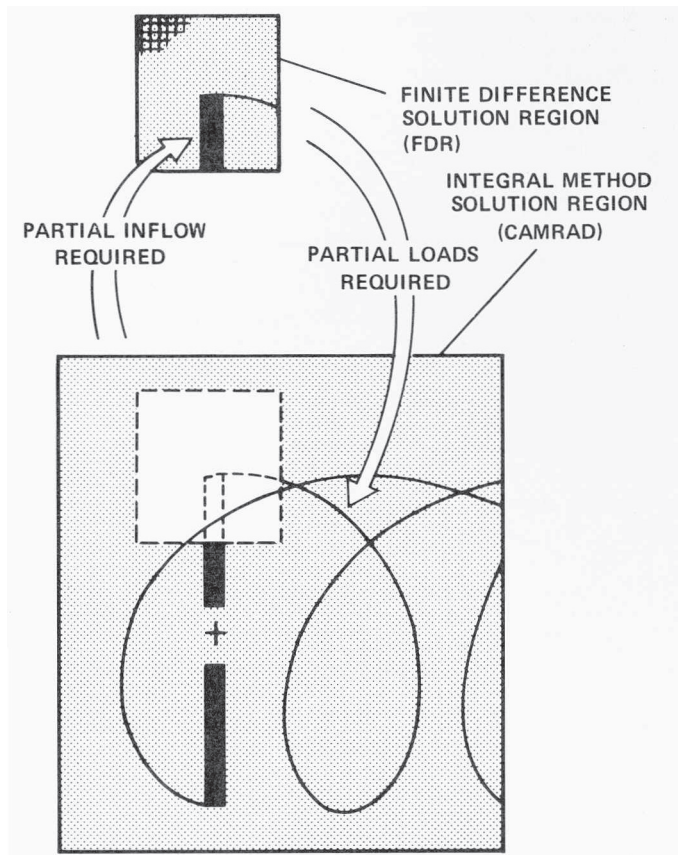


Figure 55. Schematic of loads exchange in CFD and CSD coupling (Tung et al., 1986).



## THE FIVE CHALLENGES

### Integrating the New Methods

There is a rule of thumb in the aviation business that it takes 20 years from the discovery of new materials or methods to their application in a successful commercial product. Roughly, this process follows a sigmoid curve as shown in the schematic in figure 56. In the beginning, there is a burst of enthusiasm for a new idea and there appears to be a clear and certain path to a final product—the “early exploration stage.” But then there is a long period of time where all aspects of the new idea must be tested for their efficacy, cost, and safety. Participants in this “main movement of technology” can become frustrated at the costs and delays that are always part of something new. At the end of the process are the “final details,” all of them essential, but frustrating with the goal so near at hand.

This process is still at the beginning stage, and hopefully this transformation in methods will provide improved designs in the future. Some of the funding for the main movement first occurred under the HI-ARMS program, a Department of Defense (DOD) initiative to bring computational methods to bear on many of the military system design problems. That program has transitioned to the present CREATE-AV program that sponsors the continuing work (Post, 2010). The UH-60A data set is now an integral part of the CREATE-AV program, and hopefully that program’s funding will push forward the integration of these new methods.

To achieve progress the rotor designer must also be convinced that the new methods are accurate, trustworthy, and practical. Each of the rotorcraft companies has cases where the predicted performance, loads, or vibration of one of its new helicopter rotors were missed and required redesign. Few of these rotor “skeletons” are public knowledge, but if the companies can be encouraged to test the new methods against a known design failure, the rotor designer may be convinced that the methods are accurate and practical.

A generation ago, Professor Richard Shevell examined his fixed-wing aircraft design experience at Douglas Aircraft and addressed the question as to whether the CFD methods available in the 1980s and earlier might have helped prevent some of the design problems encountered with such famed aircraft as the DC-8, DC-9, and DC-10 (Shevell, 1986). His answer was “no,” but in some cases those methods might have provided some useful information. Commercial aircraft and rotorcraft are far apart in the aviation spectrum, but Shevell’s experience with the complexity of the design process, and the overconfidence that is sometimes part of that process, provides a welcome cautionary note as these methods are implemented in the future.

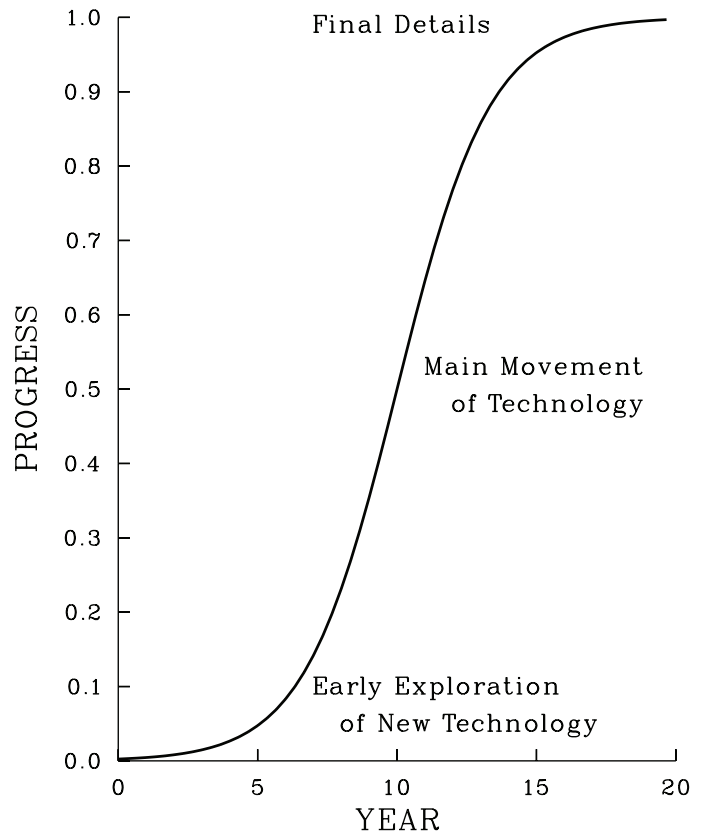


Figure 56. Curve of technology improvements.

### Nonlinear Aerodynamics—Each Rotor is Different

The problem of nonlinear aerodynamics can be referred to as the Tolstoy problem. In the novel *Anna Karenina*, published in Russia in 1888 (Tolstoy, 1965), the first sentence is “Happy families are all alike; every unhappy family is unhappy in its own way.” This is an apt description of nonlinearities if paraphrased: linear aerodynamics are all alike; every nonlinear aerodynamic problem is different in its own way.

Previously, John Ward’s re-digitization of data for the CH-34 was shown in figure 36 (Ward, 1971). That figure is repeated here as figure 57. By comparison, figure 58 uses Ward’s format, but with data substituted from the UH-60A flight test. The level flight rotor loading for the CH-34 is  $C_w/\sigma = 0.088$ , higher than for the UH-60A. The loading at the peak of the CH-34 maneuver is  $C_w/\sigma = 0.127$ , just below the level flight value for the UH-60A. Both rotors are at or near the rotor thrust limit for the highly loaded condition.

The comparison of the CH-34 and UH-60A test data is similar over the first three quadrants of the rotor, but quite different in the fourth. Dynamic stall on both rotors begins very close to  $270^\circ$ , but the CH-34 shows three cycles of dynamic stall whereas the UH-60A shows only two. Ward



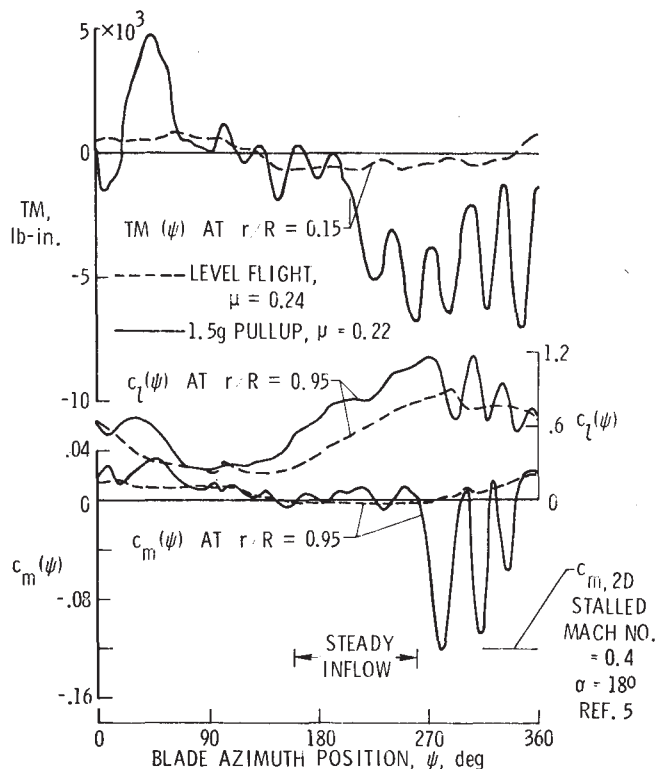


Figure 57. CH-34 flight test data in level flight and maneuver (Ward, 1971).

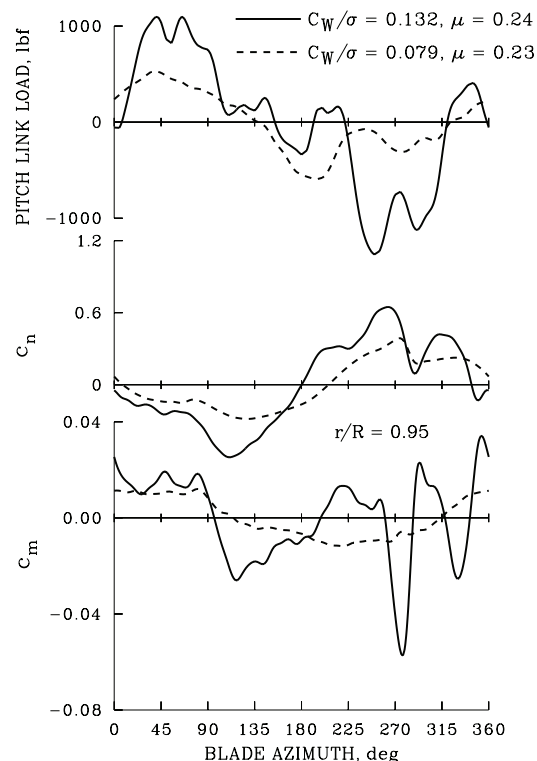


Figure 58. UH-60A flight test data, format based on Ward (1971).

(1971) has pointed out that dynamic stall for the CH-34 occurred at the second torsion mode frequency. But for the UH-60A, the dynamic stall occurs at the first torsion mode frequency. The initiation of dynamic stall is caused primarily by blade aerodynamics, but repetition of the dynamic stall cycles is caused primarily by dynamic response (Bousman, 1998).

The transformation that has been accomplished in the abilities to predict rotor loads in the last decade may lead to the hubris that Professor Shevell wrote about 30 years ago in the commercial aircraft business (Shevell, 1986). These new methods must be shown to be accurate across a broad range of rotorcraft design problems or the transformation described in figure 56 will not be obtained. Unfortunately for the challenge shown here, Ward's re-digitized data for the CH-34 have been lost. That is another challenge addressed below.

### Remaining Deficiencies

The significantly improved accuracy in the airloads calculation that has been accomplished in the last decade has not been fully extended to the calculation of structural loads. The normal force prediction at the maximum level flight speed for the UH-60A is shown in figure 59 (a repeat of figure 51) for five coupled CFD/CSD methods and is quite accurate (this figure and subsequent figures include the instrumentation phase corrections identified by Norman et al., 2012).

The structural loads at the blade midspan at  $0.50R$  are shown in figure 60 for four of the five methods. The prediction of peak-to-peak loading that is important for fatigue is quite good. But all of the calculations show a phase lead of about  $10^\circ$ . Vibration on this rotor is dominated by the 3 to 5/rev structural loads. Flap bending moments for 3/rev and above at the mid-span location are shown in figure 61. Here the phase lead in the calculations is more apparent, and the various methods show as much disagreement with each other as with the measurements.

The source of these differences is not presently understood. Is it in the CFD part of the calculation or the CSD part or both? Also, these results are for just one rotor—it is unknown whether similar differences would be seen on other rotors.

Beyond the problems with the structural load calculations, the good results in airloads predictions are not consistent. They appear to be most accurate in the prediction of unsteady transonic flows, less accurate when there is significant vortex wake loading, and poorest when dynamic stall is present. Uniformly, normal force is predicted better than pitching moment, a trend that is worrying to all aero-elasticians because the pitching moments directly affect the torsional elastic deformation.

In order to be successful in moving up the sigmoid curve, a better understanding of the present deficiencies is needed. Improved calculations will then be required and must be demonstrated.

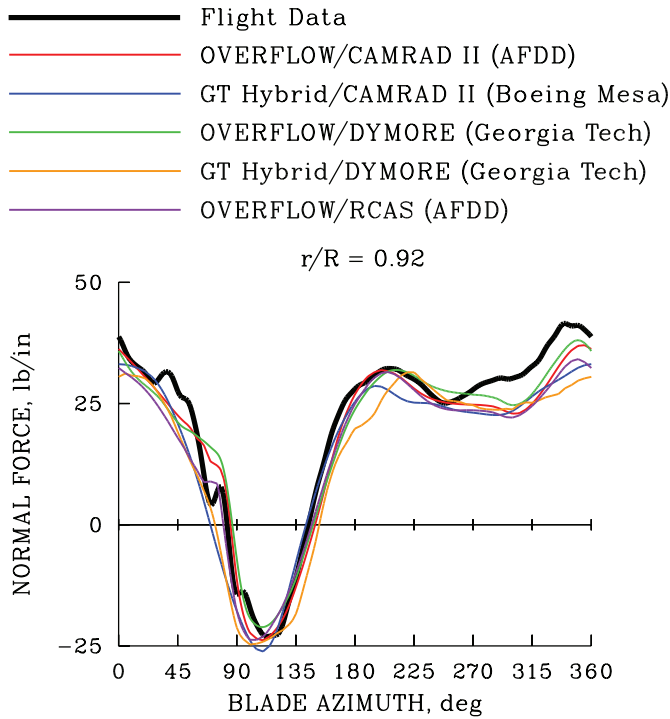


Figure 59. Comparison of measured normal force at 0.92R for the UH-60A with five coupled CFD/CSD methods;  $\mu = 0.37$ ,  $C_w/\sigma = 0.078$ , 0–36 harmonics.

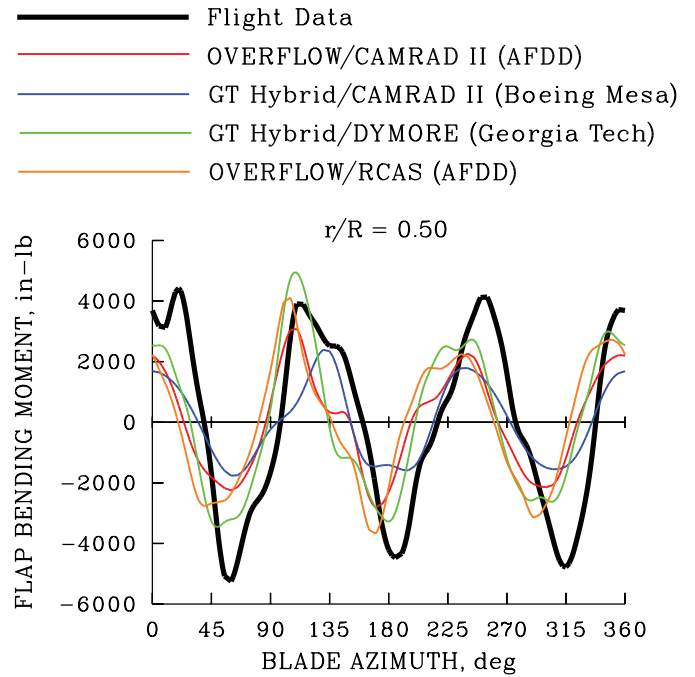


Figure 61. Comparison of measured flap bending moment at 0.50R for the UH-60A with five coupled CFD/CSD methods;  $\mu = 0.37$ ,  $C_w/\sigma = 0.078$ , 3–24 harmonics.

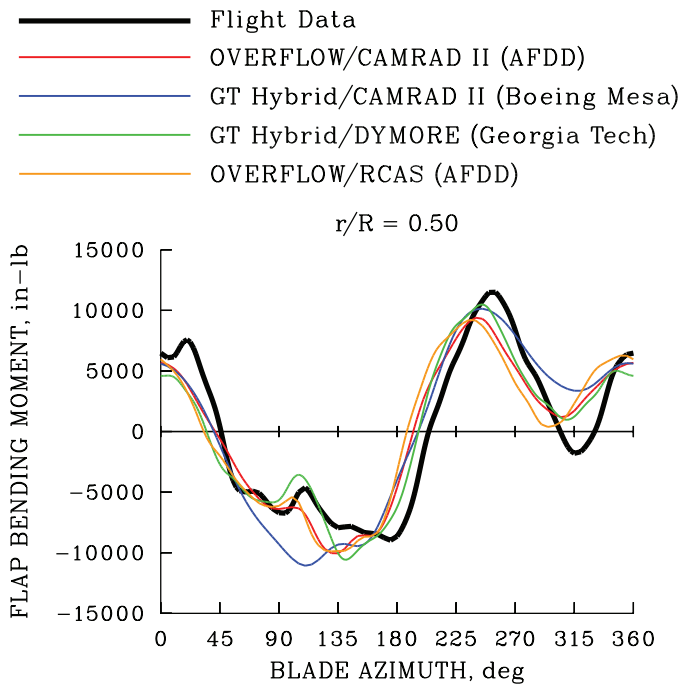


Figure 60. Comparison of measured flap bending moment at 0.50R for the UH-60A with five coupled CFD/CSD methods;  $\mu = 0.37$ ,  $C_w/\sigma = 0.078$ , 0–24 harmonics.

### Loss of Experimental Data

Euan Hooper chaired a panel at the 2nd Decennial Specialists' Meeting that was held at NASA Ames in November 1984 (Hooper, 1985). The timing of the panel

was appropriate considering Hooper's recent use of many of the airloads data sets that are the centerpiece of this paper (Hooper, 1983). In addition, the value of this panel was enhanced by the transcription of the panel presentations and all subsequent discussions.

Most of the presenters were aware of the history of the airloads databases. As shown in table 9, 10 of these databases had already been obtained by the date of the conference. Jim Biggers (p. 457) commented:

“... we are caught in a trap. The papers and things that we have heard the past couple of days indicate a need for increasingly detailed test information with which to compare our increasingly capable theories. And yet we are not terribly well equipped to handle the test information that we can go out and acquire. We also have the ability to go out and acquire a great deal of detailed test data with many surface pressures and things of the nature you have described. . . So we have a problem of data volume versus accessibility.”

By the time of the conference, data were available for all of the 10 airloads tests except the CH-47A. The AH-1G flight data were still in use at the time of the conference, although not equally accessible (Hooper, 1985). Ed Austin from the U.S. Army Applied Technology Laboratory (now AATD) was encouraged by their use of DATAMAP for the AH-1G/OLS data and encouraged others to consider using this tool for the storage and handling. He said (p. 464)

TABLE 9. AIRLOADS TESTS, TEST DATE, ROTATING SAMPLES, AND WHETHER DATA ARE STILL ACCESSIBLE; ROTATING SAMPLES BASED ON A SINGLE REVOLUTION OF DATA FOR EACH TEST POINT

Test	Test Date	Rotating Samples	Data Storage	Extant? (%)
NACA Model Rotor (Tunnel)	1954	14,496	figures	100
CH-34 Flight Test	1961	205,110	tables	100
UH-1A Flight Test	1961	20,616	tables	100
CH-34 Wind Tunnel Test	1964	48,480	tables	100
CH-47A Flight Test	1966	420,596	digital tape	0
NH-3A Flight Test	1967	479,520	tables	(100)
XH-51A Flight Test	1967	299,880	tables	100
CH-53A Flight Test	1969	439,438	tables	(100)
AH-1G/OLS Flight Test	1976	2,527,798	digital tape	0.1
AH-1G/TAAT Flight Test	1981	4,220,674	digital tape	2.2
UH-60A Flight Test	1994	64,198,493	digital memory	99.7
UH-60A Wind Tunnel Test	2010	1,444,243,200	digital memory	100

“... we have had a considerable amount of experience in converting various sets of data on to the DATAMAP database. And we have not found it to be a major problem.”

Concerning the permanence of test data, Mike Bondi, the program lead for the TRENDS database at NASA Ames, said somewhat wistfully (p. 464) “... industry should request NASA ... to support that function.” Jim McCroskey, unimpressed, said, “If you ask industry to set up congress to get NASA funded to preserve this stuff for 20 years, I don’t think it will happen.” The lasting words on the permanence of databases came from Wayne Johnson (p. 487).

“We have had paper for a couple of thousand years, printing presses for a couple of hundred, computers have been with us for maybe a couple of decades. . . . I think actually putting things down on paper and saving them has a lot to be recommended.”

The rotorcraft community is small compared to the larger world of science and engineering. Are its problems caused by its small size? Is all of its handwringing about unwieldy and lost data so much navel gazing? A special section in the 11 February 2011 issue of *Science* on “Dealing with Data” may provide some insight into the problems facing the larger scientific community.

In that special section of *Science*, Andrew Curry (2011) used the story of a 2-year search for data obtained in the 1980s by the PETRA collider in a high-energy physics lab near Hamburg, Germany. The project, called JADE, was an international collaboration. When funding was terminated in 1986, the shared data disappeared to the four winds. Siegfried Bethke, who had worked on the JADE project

as a young physicist at the time, was the head of the Max Planck Institute for Physics in Munich by the late 1990s. High-energy physics had moved on, but new theories had emerged in the meantime that could only be tested with data from lower energy experiments such as JADE. These data could not be replicated with something like the Large Hadron Collider at the CERN particle physics lab near Geneva, Switzerland.

The original data had been stored on magnetic tapes on the mainframes of that day. Eventually, much was recovered because of a “sentimental colleague” who copied a few gigabytes of the data to new storage media every few years. That fortunate outcome is not typical. Salvatore Mele, a physicist and data preservation expert at CERN has described the more typical case: “There’s funding to build, collect, analyze, and publish data, but not to preserve data.” Dr. Mele’s experience was no different from that of anyone in the rotorcraft community who has worked with some of the larger rotor data sets.

As Curry reports, things are changing within the high-energy physics community. In that community there is the need for a data archivist who would be a mix of librarian, IT expert, and physicist. For a modern physics experiment they estimate that it would cost only 1 percent of a collider’s total budget to archive and maintain the data. It is doubtful that costs for improved handling of rotorcraft experimental data would be any more expensive relative to testing budgets.

How well were the data sets of the 12 experiments shown in table 9 managed? The first four of these tests (the NACA model rotor, the CH-34 flight test, the UH-1A flight test, and the CH-34 wind tunnel test) published the data

either as figures or tables. To use these data, one only needs to find a copy of the report. If only limited data are required, the data can be transcribed directly from the report with little effort. If more data are needed then the pages can be scanned with an optical character reader. In some cases PDF files have been created from the printed copies and are available online.

For the fifth test, the CH-47A flight test, the data were reduced and written to digital tape. There were plans for printed reports, at least as internal Boeing Vertol documents (Pruyn, 1967, 1968). It has not been determined if these data reports were ever published and are still available. To the best of my knowledge, the data no longer exist either in printed form or on magnetic tape. The CH-47A airloads flight test was the most ambitious of the early airloads tests. It is now known as the first of the data sets to have disappeared.

The sixth, seventh, and eighth tests (NH-3A, XH-51A, and CH-53A) also provided data in printed tables. The XH-51A report was much like the earlier reports, and the tabulated data are legible. The two Sikorsky tests both included data in a separate volume. Using these data is difficult for two reasons. First, the U.S. Navy published the data as restricted reports, hence it is difficult to obtain a copy of the data volume. Second, the data were printed on a mainframe using a line (chain) printer. Anyone who worked with computers in the 1960s and 1970s remembers the sounds of the line printers as they chugged through reams of paper. Unfortunately, in using these line printers, the quality of the print degraded over time intervals between maintenance. This was not a problem if you were debugging code, but if you were printing tables for a 300-page data volume, the tables became more difficult to read. Optical character readers cannot handle the vertical character shifts typical of the line printers nor the poor inking. In a few cases, it is doubtful that an engineer with a magnifying glass can read the tables. The uncertainty for these two tests is indicated in table 9 with parentheses.

The ninth and tenth tests were both flight tests of the AH-1G Cobra. The flight data were recorded on FM analog tapes and then digitized and written to 9-track digital tapes. The 9-track digital tapes were an industry standard in the 1970s and early 1980s, but they were not particularly compact. For example, 23 FM analog tapes were sufficient for all the flight data obtained during the AH-1G/TAAT test. After data reduction, there was a total of 350 9-track tapes, a sizeable digital library. Toward the end of the 1980s, digital tape technology moved toward cassettes that could be easily loaded into cassette drives. The old 9-track tape machines became difficult to support and were abandoned along with the digital libraries that accompanied them.

Libraries based on print media have existed for thousands of years. They are not always permanent, as shown

by the history of the Royal Library of Alexandria first begun in 3000 BC. But by comparison to digital media, they are solid as rock. Moreover, there has always been the opportunity to save copies in multiple libraries and thus avoid the consequences of a single catastrophe. But digital data can disappear in an instant, sometimes by accident, sometimes on purpose.

The last two tests, the UH-60A flight test in 1993–94 and the UH-60A wind tunnel test in 2010, are both saved on digital media within the temperature-controlled computer centers at NASA Ames Research Center. The data are restricted and ephemeral. Since the data were placed on a DEC VAX using an optical jukebox for storage, four storage media changes have occurred and one operating system change. So far, only 0.3 percent of the data have been lost. But in August 2013, the current computer crashed and the data were inaccessible for the next 5 or 6 months. The data are now believed to be okay, but a certain demonstration of their adequacy is not trivial.

As for the most recent wind tunnel test, the data distribution system has already been shut down by hackers. It's a new world out there. As Dr. Johnson said in 1984, "putting things down on paper and saving them has a lot to be recommended."

### **Alternatives to Full-Scale Airloads Tests**

All of the airloads tests that have made up this paper have cost too much. Some worked and some did not. There is much to be learned from their failures, but more from their successes. There are alternatives. Here are four possibilities.

1. Model rotor tests.
2. Full-scale rotor tests, but with measurements at fewer radial stations.
3. Simplified measurements that use fewer pressure transducers.
4. New measurement techniques and technologies.

### **Model Rotor Tests**

There are a number of examples of successful Mach-scaled model rotor tests including a 1/5.73-scale rotor of the UH-60A tested in hover at Sikorsky Aircraft and in forward flight at the German-Dutch Wind Tunnel (DNW) (Lorber et al., 1989; Lorber, 1991), the 7A and 7AD rotors tested in ONERA's Modane tunnel (Petot et al., 1997), and the HART I and II tests, also in the DNW tunnel (Yu et al., 1994; van der Wall et al., 2002; Yu et al., 2002). All of these tests, to some degree, have been affected by lack of Reynolds number scaling.



Figure 62 shows a comparison of  $C_T/\sigma$  and  $\mu$  test points for the UH-60A model rotor tested in the DNW tunnel with  $C_W/\sigma$  and  $\mu$  for the UH-60A tested in level flight. The number of pressure transducers is roughly the same for both rotors. The model rotor distributed the pressure transducers over three blades, whereas in flight the pressure transducers were on a single blade. Because of structural limitations, high thrust and high advance ratio conditions were limited for the model rotor.

It would be interesting to know the relative costs between these two programs. It is not obvious that a model rotor test would be significantly cheaper. Because of structural limitations, the model rotor was not able to explore nonlinearities associated with high-speed flight and particularly with dynamic stall, but technology improvements have allowed a greater test envelope. For instance Lorber et al. (1994) report testing of a 9.4-foot-diameter rotor that achieved  $C_L/\sigma$  values to 0.12 and  $\mu$  values to 0.46.

The fully instrumented 7A and 7AD rotors, built and tested by ONERA, were 18.8-feet in diameter. They were tested to  $C_T/\sigma$  values as high as 0.125 and  $\mu$  values to 0.4. As with the UH-60A model rotor test, it is unclear how much less expensive this model rotor test was than an equivalent full-scale flight test.

The approach that was taken in the Higher-Harmonic-Control Aeroacoustic Rotor Test (HART) model rotor tests was different from the two previous examples. Both rotors were about 0.40-scale models of the German BO 105 helicopter. HART I, tested in June 1994, used 124 pressure transducers that were distributed at three radial stations: 0.75R, 0.87R, and 0.97R. HART II, tested in October 2001, employed 51 pressure transducers, most at 0.87R.

The two HART tests had fewer instrumented radial stations and focused most of their testing at one descent condition representing an approach in which there was extensive blade-vortex interaction. In contrast to the limited flight conditions examined, they added the capability of using higher-harmonic control of the rotor (to reduce noise radiation), and focused their measurements on the vortex intersections from previous blades using both wake visualization and extensive acoustic measurements.

The international nature of these tests allowed for extensive comparison of analytical methods with the measurements from the two tests. Initially the calculations used multiple comprehensive analyses, and that work has been followed with coupled CFD/CSD computations as well.

### Full-Scale Rotor Tests With Limited Instrumentation

The 12 tests that have been the focus of this paper had sufficient pressure transducers installed at five or more radial stations so that the normal force could be accurately

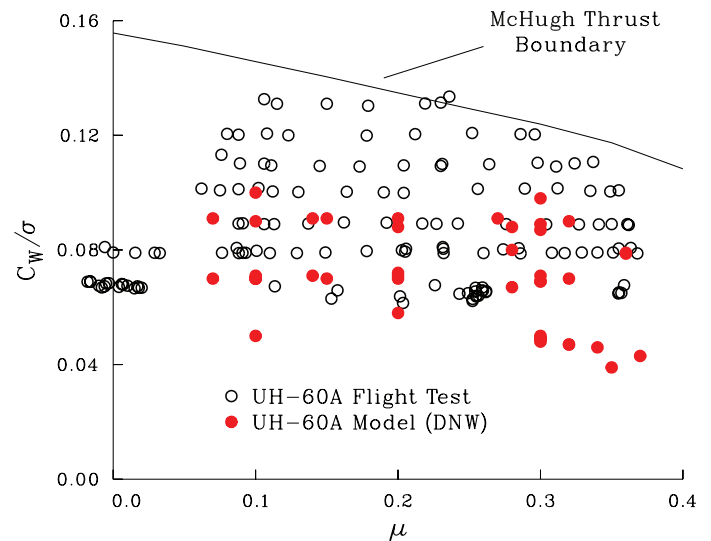


Figure 62. Comparison of thrust and advance ratio test points for UH-60A model in the DNW tunnel with level flight points for the flight test.

measured at these locations and the blade thrust calculated. Other flight tests have been accomplished with fewer radial measurement stations. Two that are notable were multiple tests including two different rotors on an Aerospatiale Puma (AS 330) at the Royal Aircraft Establishment (Riley and Miller, 1983; Riley, 1986) and tests of a special-purpose rotor on an Aerospatiale Gazelle (SA349/2) flown at Marignane, France (Heffernan and Gaubert, 1986).

The research Puma tests were undertaken in a cooperative program between the RAE and ONERA. The first test used an interesting mixed-bladed rotor with a rectangular tip opposite a swept tip, whereas the second test used four swept tips. Pressure measurements were obtained at three radial stations at the blade tip in both tests: 0.92R, 0.95R, and 0.978R. These radial stations were selected to better understand the unsteady transonic flow at the blade tip. Most of the correlation with the second test's data has been for a speed sweep at  $C_W/\sigma = 0.070$ , with  $\mu$  from 0.09 to 0.40 (see Bousman et al., 1996, for example).

The SA349/2 test was flown with special purpose Grand Vitesse blades designed for high speed. Pressure transducers were installed at three blade stations distributed over two blades: 0.75R, 0.88R, and 0.97R. A joint research program to examine these data was established between NASA and the French Ministry of Defense. Level flight cases were selected from  $C_W/\sigma = 0.062$  to 0.090 and  $\mu$  from 0.13 to 0.36. Maneuver cases were also examined.

An example from correlation with the research Puma data (Bousman et al., 1989) is shown in figure 63. In this particular case, the tip pressure measurements are well predicted by three of the four analyses. But most of the differences between the analyses occur more inboard on

the blade, roughly from  $0.6R$  to  $0.9R$ . This illustrates the problem that may occur in seeking a trade-off between the number of radial stations that are affordable and the reality that those measurements may not include the radial extent of important physical phenomena.

As before, where the UH-60A full-scale flight and wind tunnel model tests were compared, it would be interesting to know the relative costs of the two programs. As in that case, what is the relative cost reduction obtained in reducing the number of radial stations with pressure transducers from five or more stations down to three? What are the cost benefits as compared to the reduced data obtained?

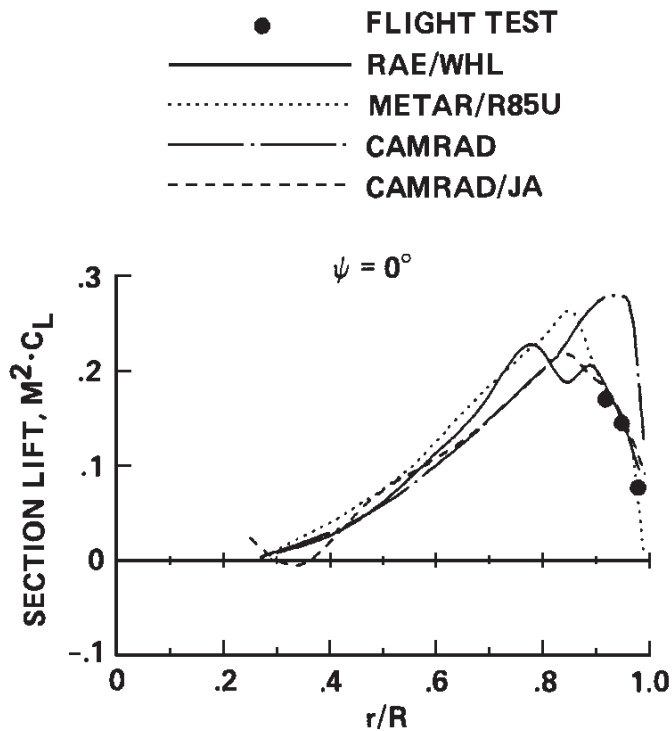


Figure 63. Comparison of four comprehensive analyses with flight test data for a swept-tip rotor on a research Puma;  $\mu = 0.38$ ,  $C_w/\sigma = 0.080$ ,  $\psi = 0^\circ$  (Bousman et al., 1989).

### Simplified Measurements

A number of simplified approaches have been tried that are cheaper than the fully instrumented rotors discussed in this paper, but each has its own limitations. Brotherhood (1982) demonstrated that two pressure transducers could be used to provide section normal force. One transducer was installed near the leading edge at about  $0.02c$  and the second near the trailing edge. An instrumented airfoil section was tested in a wind tunnel, and a linear relation between the section lift and the leading edge transducer was established. The linear relation was effective in the regime of linear aerodynamics, including blade vortex loading, but during blade stall (indicated by the blade trailing edge transducer), the linear relationship failed. The tradeoff, then, was a significant reduction in blade instrumentation but an inability to make measurements in the regimes of nonlinear aerodynamics.

Bousman (1987), using data from the airloads test of the CH-34 rotor in the wind tunnel (Rabbott et al., 1996a), demonstrated that flap bending structural measurements could be used to derive the distribution of section normal force by a least squares fit. Although the method was robust, it has not been applied to more complicated rotors nor have the blade torsion and chord bending moments been used to improve the fit.

### New Measurement Techniques and Technologies

Creativity in measurement techniques and technologies may provide some significant cost reductions in the future. The continuing miniaturization of pressure measurements and instrumentation, and related cost reductions as well, may provide opportunities for significantly less expensive testing.

New measurement techniques such as dynamic pressure sensitive paint measurements may also one day allow cost savings by eliminating the on-blade instrumentation.

## APPENDIX 1—AIRLOADS TEST DESCRIPTIONS

### Introduction

The 12 rotor airloads tests are each described in this appendix. For each experiment, the text is accompanied by a photograph of the test rotor, a table that lists rotor and test parameters, and figures that show the layout of the pressure instrumentation, the test data on a plot of  $C_w/\sigma$  or  $C_T/\sigma$  as a function of  $\mu$ , and the cumulative distribution of papers and reports from the test.

### NACA 15-Foot-Diameter Model Rotor

The first rotor airloads test was of a two-bladed teetering rotor tested in the 30- by 60-Foot Wind Tunnel at the NACA Langley Aeronautical Laboratory at Langley Field, Virginia, in the mid-1950s by Jack Rabbott (1956), and Jack Rabbott and Gary Churchill (1956). Based on tunnel run logs (Joseph Chambers, *pers. comm.*), the first test, Test 217, was the hover test (Rabbott, 1956), and ran from 1 Oct 1953 to 12 Mar 1954. The second test, Test 222, was the forward flight test (Rabbott and Churchill, 1956), and ran from 1 Sep 1954 to 13 Dec 1954. At some point, a third test was conducted by Mayo (1959); it was limited to structural instrumentation and repeated a limited number of the previous test cases, but this test is not listed in the logs and it is not certain when the testing took place. Figure A-1, from Rabbott and Churchill (1956), shows the rotor running in the tunnel.

It is possible that a photograph of the actual airloads test model rotor was never obtained. Based on recorded photo numbers, the photo shown here is part of a sequence of photos from a test by Harry Heyson (1956) of a different model rotor (smaller chord) that was tested at about the same time.

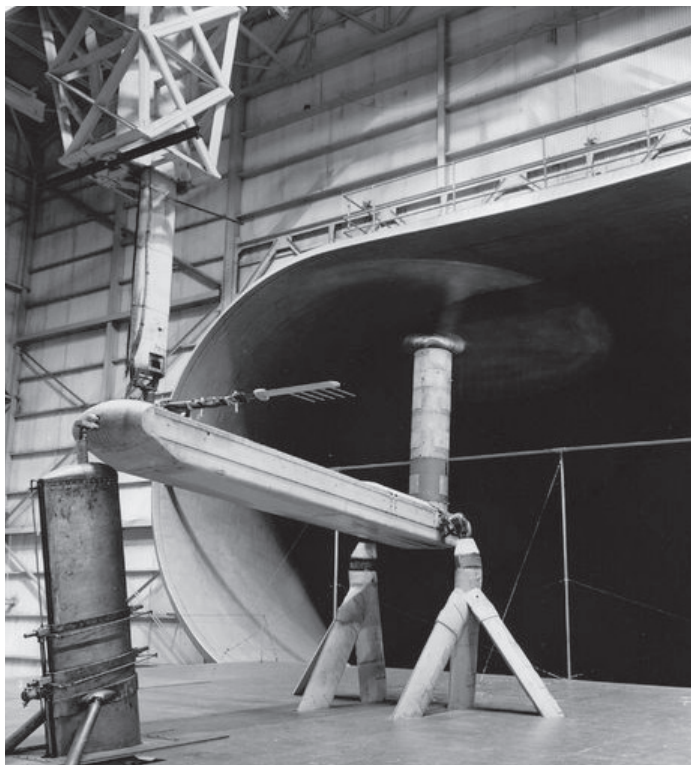


Figure A-1. NACA 15-Foot-Diameter Model Rotor being tested in 30- by 60-Foot Wind Tunnel at Langley Research Center (LAL 83264, <[http://crgis.ndc.nasa.gov/historic/30\\_X\\_60\\_Full\\_Scale\\_Tunnel](http://crgis.ndc.nasa.gov/historic/30_X_60_Full_Scale_Tunnel)>).

John Patterson's development of a miniaturized differential pressure transducer at Langley in the early 1950s (Patterson, 1952) was likely the stimulus that resulted in the model rotor development. Rabbott had 50 of the new differential pressure transducers installed in one blade of the model rotor. Ten pressure transducers were arranged at each of five radial stations as shown in figure A-2. The radial stations for the pressure transducers were  $r/R = 0.31, 0.56, 0.75, 0.85,$  and  $0.95$  (based on a radius of 7.625 ft). At each radial station, the pressure transducers were located at the same chordwise positions,  $x/c = 0.005, 0.010, 0.025, 0.050, 0.100, 0.250, 0.500, 0.700, 0.850,$  and  $0.950$ . Although the

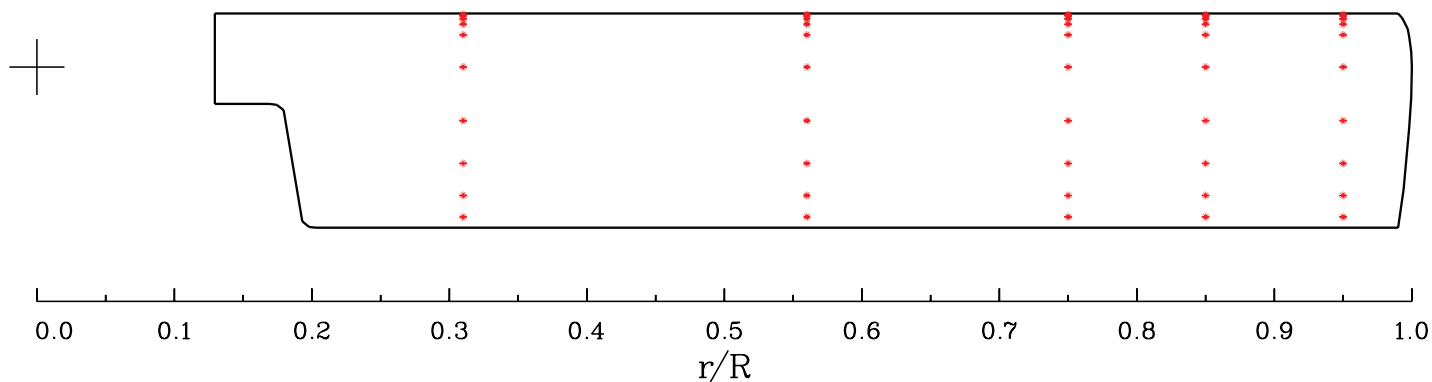


Figure A-2. NACA 15-Foot-Diameter Model Rotor planform showing locations of differential pressure transducers at five radial stations.

TABLE A-1. NACA 15-FOOT-DIAMETER MODEL ROTOR DESCRIPTION

Test number	1
Sponsor	NACA
Manufacturer	NACA
Number blades	2
Airfoil section	NACA 0012
Blade twist, deg	0.0
Blade chord, in.	14.0
Rotor diameter, ft	15.3
Rotor solidity	0.0974
Tip speed, ft/sec	481.
Instrumented radial stations	5
Transducers/radial station	10.0
Rotating sensors	57
Test points	6
Harmonic bandwidth	24
Rotating samples	15,936
Test hours	–
Test completion	December 1954

model rotor diameter for the test was described as being 15 feet, it was actually 15.25 feet. The chord was 14.0 inches, resulting in a calculated solidity of 0.0974. Additional details are provided in table A-1.

Rabbott and Churchill used 45-channel slip rings and a stepping switch to record the rotating data sequentially in two steps. In addition, they measured the pitch and flap angles.

Rotor forces were obtained with the tunnel balance, and the torque was measured on the drive shaft. Aero tares were measured with the blades off and the data were corrected.

The rotating measurements were made on a recording oscillograph, and the data were analyzed to provide 24 harmonics of pressure data (azimuth stepsize of  $7.5^\circ$ ). The measurements were then averaged over 10 cycles of data. At each spanwise station, the section normal force was calculated from the differential pressure measurements. The resulting normal forces were plotted in approximately 40 figures in Rabbott and Churchill (1956), but tabulated data were not provided. Pitching moments were not calculated.

It is unclear when Mayo (1959) installed strain gauges at five stations on one of the blades of the model and measured the flap bending moments at  $r/R = 0.25, 0.35, 0.50, 0.70,$  and  $0.90$ . He attempted to match one of the hover cases from Rabbott (1956) and two of the forward flight cases from Rabbott and Churchill (1956) for  $\mu = 0.076$  and  $0.15$ .

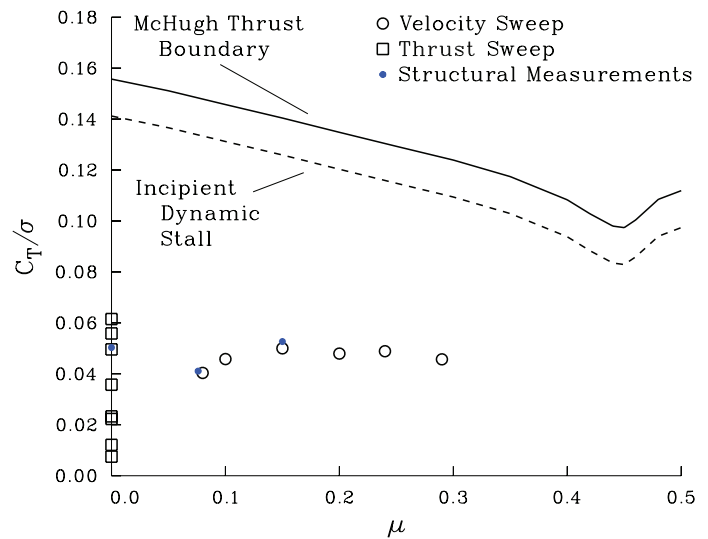


Figure A-3. NACA 15-Foot-Diameter Model Rotor nondimensional thrust coefficient as a function of advance ratio compared to the McHugh (1978) thrust boundary. Mayo (1959) repeated the first and third test points after adding strain-gauge measurements at five radial stations on the opposite blade.

The initial hover test obtained a number of thrust sweeps at different rotor speeds (Rabbott, 1956). One of these thrust sweeps is shown in figure A-3. Subsequently, Rabbott and Churchill (1956) obtained pressure measurements at six advance ratios, also shown in figure A-3. The thrust coefficients,  $C_T/\sigma$ , were between 0.04 and 0.05, which is low for a modern rotor and well away from the rotor thrust boundary and dynamic stall. But these remarkable data were ideal in showing the higher harmonic loads at low advance ratios caused by vortex wake loading of the rotor blades.

At first, citations of these data (fig. A-4) were just from the test reports. The Rabbott and Churchill (1956) report was initially classified CONFIDENTIAL, but was declassified about a year later. As often happens in engineering, the data were available, but could not be usefully employed because analytical methods were not suitable. Professor Rene Miller at the Massachusetts Institute of Technology (MIT) later commented (Miller, 1963):

“Attempts to obtain a closed form solution to this problem, or one based on tabulated integrals, were not successful and it was evident that extensive computer facilities would be required to explore this problem and, hopefully, to provide a basis for obtaining simplified solutions suitable for engineering applications.”

Once suitable computers became available in 1960 (Miller’s first was an IBM 709 with vacuum tubes), progress occurred quickly at both MIT and the Cornell Aeronautical



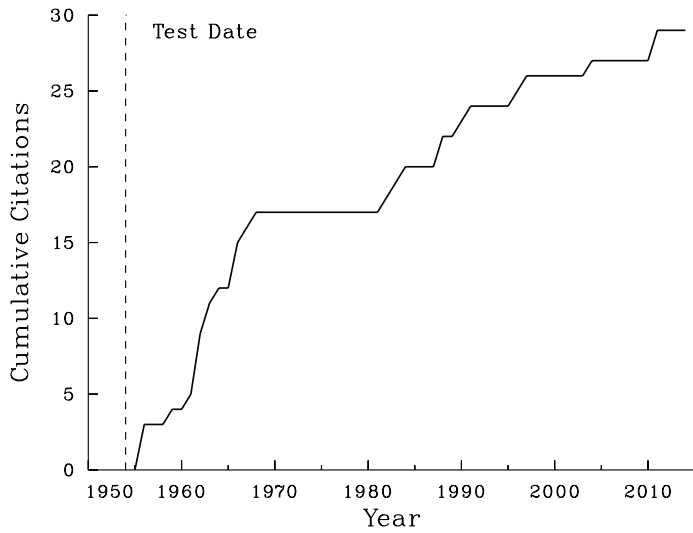


Figure A-4. Cumulative citations of the data obtained on the NACA 15-Foot-Diameter Model Rotor (Rabbott and Churchill, 1956).



Figure A-5. CH-34 flight test aircraft at Langley Research Center in 1961 (NASA photo, courtesy of Teresa Hornbuckle).

Laboratory (CAL), see Johnson (2011a,b). Most of the citations shown in figure A-4 were in the early 1960s as Professor Miller at MIT and Ray Piziali and his colleagues at CAL used these data to validate the prescribed wake theories that they had developed.

### CH-34 Flight Test

The CH-34 airloads program was the first test that used pressure transducers installed on a rotor blade to measure the forces on a full-scale rotor in flight. The test was part of an experimental program funded by the U.S. Army Transportation Research Command (USATRECOM, or just TRECOM) to examine in-flight airloads and included both the CH-34 test and that of the UH-1A (Burpo and Lynn, 1962). A photograph of the test aircraft is shown in figure A-5.

The pressure transducers and other instrumentation were installed by Sikorsky Aircraft, and the testing was performed by NASA at the Langley Research Center on a bailed U.S. Army aircraft. The testing was under the aegis

of the Vertical Takeoff and Landing (VTOL) Branch in the Langley Flight Research Division (Fred Gustafson was the branch head). LeRoy Ludi was the project leader and Jim Scheiman oversaw the flight test and data management (John Ward, *pers. comm.*). A description of the test program and the reduced data are in Scheiman and Ludi (1963) and Scheiman (1964).

The instrumented CH-34 blade is shown in figure A-6. The chordwise distribution and number of differential pressure transducers varied with radial location as given in table A-2. The chordwise distribution of transducers was based on the requirements of Gaussian integration. Each differential pressure transducer was connected to its upper and lower surface orifices by a 12-inch length of tubing so that the phase delays would be consistent over all transducers. At all radial stations, the transducers forward of about  $0.30R$  were on a slant of about  $25^\circ$ . There is no mention of why this was done in the references, but John Ward (*pers. comm.*) suggests that the slant was necessary because of the constraints of fitting and connecting all of the pressure transducers within the spar. Parameters describing the experiment are shown in table A-3.

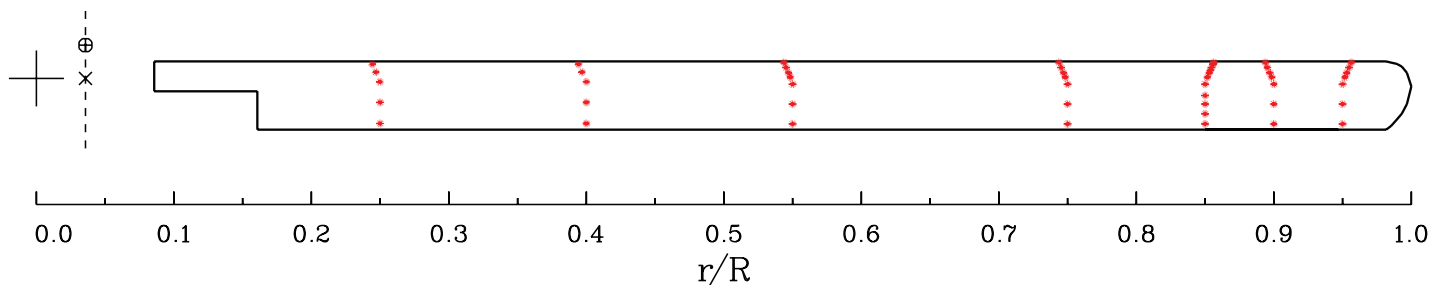


Figure A-6. CH-34 planform showing locations of differential pressure transducers at seven radial stations.

TABLE A-2. LOCATIONS OF PRESSURE TRANSDUCERS ON CH-34 BLADE USED IN FLIGHT TEST (ONE BLADE)

Radial	Chordwise	
	No.	
0.25, 0.40	5	0.042, 0.158, 0.300, 0.600, 0.910
0.55, 0.75, 0.90, 0.95	7	0.017, 0.090, 0.168, 0.233, 0.335, 0.625, 0.915
0.85	11	0.017, 0.040, 0.090, 0.130, 0.168, 0.233, 0.335, 0.560, 0.625, 0.769, 0.915

TABLE A-3. CH-34 FLIGHT TEST DESCRIPTION

Test number	2
Sponsor	U.S. Army, NASA
Manufacturer	Sikorsky Aircraft
Number blades	4
Airfoil section	NACA 0012
Blade twist, deg	-8.0
Blade chord, in.	16.4
Rotor diameter, ft	56.0
Rotor solidity	0.0622
Tip speed, ft/sec	650.
Instrumented radial stations	7
Transducers/radial station	7.0
Rotating sensors	67
Test points	129
Harmonic bandwidth	12
Rotating samples	205,110
Test Hours	<10*
Test completion	July 1961

\*Ward (2010)

By drilling holes in the CH-34 blade spar for the pressure transducer orifices, the fatigue life of the blade was reduced. The first job John Ward had after joining the VTOL Branch (*pers. comm.*) was to determine a safe life for the blade based on fatigue tests of a blade specimen. His analysis recommended a 10-hour lifetime for the blade.

Structural measurements were also obtained on the CH-34. Table A-4 shows the locations of strain-gauge bridges on the blade. In addition, the pitch-link load was measured on one of the pitch links.

TABLE A-4. STRAIN-GAUGE BRIDGE LOCATIONS ON CH-34 BLADE USED IN FLIGHT TEST (ONE BLADE)

Measurement	$r/R$
Flap bending moment	0.150, 0.275, 0.375, 0.450, 0.575, 0.650
Chord bending moment	0.150, 0.375, 0.575, 0.825
Torsion moment	0.150, 0.500

A 160-channel slip-ring assembly was used to bring the rotating measurements into the aircraft where they were recorded on an oscillograph. The oscillograph data were sampled every 15° to provide 12 harmonics. Data were obtained from three consecutive revolutions and then averaged to provide the tabulated data in the test reports. The section normal force at the seven radial stations was calculated using Gaussian integration. Differential pressures, the section normal forces, and the structural loads were tabulated in both reports. The integrated airloads are shown in about 10 figures in Scheiman and Ludi (1963), but only tabulated data are given in Scheiman (1964). There was no integration of the pressures to obtain the section pitching moments.

The CH-34 flight test conditions are shown in figure A-7 in terms of the weight coefficient modified by aircraft load factor,  $n_z C_w/\sigma$ , as a function of advance ratio,  $\mu$ . These values are compared with the McHugh thrust boundary and the line of incipient dynamic stall. All of the level flight cases are shown in the figure as open circles, and the three cases from Scheiman and Ludi (1963) are shown as solid blue symbols. The steady and unsteady maneuver cases reanalyzed by Ward (1971) are also included. The solid red circles are steady left and right coordinated turns, and the open red circles are three revolutions of a combined cyclic and collective pull-up. In these maneuver cases the ordinate weight coefficient is multiplied by the aircraft acceleration,  $n_z$ , so as to allow maneuvers to be compared with level flight cases. Note that the aircraft weight was not obtained, but reported as between 11,200 and 11,805 pounds. In the figure here it is assumed that the aircraft weight was approximately 11,500 pounds.

Just as Gustafson had done in the 1940s and Ludi in the 1950s, the rotor speed was reduced for a number of the level flight cases, resulting in an increase in both weight coefficient and advance ratio.

As of early 2014, 149 citations to the CH-34 flight test data have been collected, a remarkable number! The cumulative distribution of citations in figure A-8 shows that this data set was used at a fairly regular rate from the first use of the data in 1961 through the mid-1990s, a period

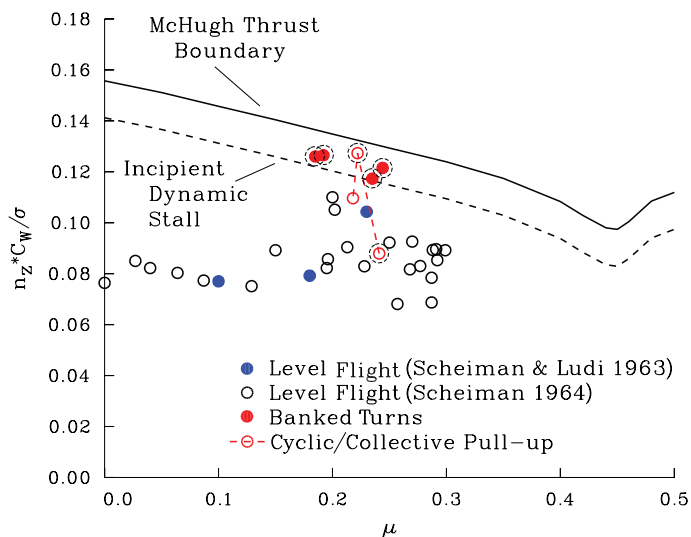


Figure A-7. CH-34 flight test nondimensional weight coefficient as a function of advance ratio compared to McHugh's (1978) thrust boundary. Dashed circles show test points re-analyzed by Ward (1971).

of 35 years. Initially, the data were used for the development of prescribed wake models. There appears to have been a slight tapering off of use in the late 1970s, but this was changed by Hooper's classic paper on rotor loads and data visualization (Hooper, 1983), and the data were used actively for another 15 years.

This data set also appears unusual in efforts that were made to informally provide early test results from the program. Both Burpo and Lynn (1962) and Piziali and DuWaldt (1962) refer to a letter from F. L. Thompson, dated May 24, 1961 (Thompson, 1961), with initial results from the CH-34 flight test. Floyd L. Thompson was the Langley Research Center Director from May 23, 1960, to May 1,

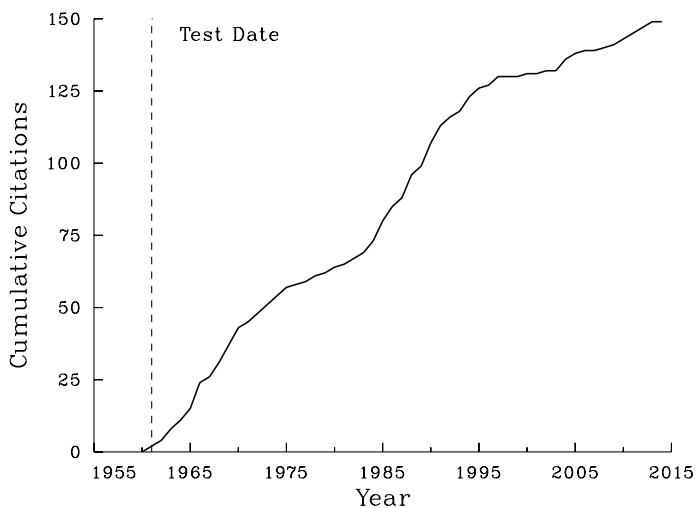


Figure A-8. Cumulative citations of the data obtained from the CH-34 flight test (Scheiman and Ludi, 1963; Scheiman 1964).

1968, and it is undoubtedly the case that this was a service to the funding agency TRECOM (John Ward, *pers. comm.*). Ray Piziali (*pers. comm.*) recalls that the data they used for correlation with their new prescribed wake model were supplied by TRECOM, but he does not recall seeing the Thompson letter. Similarly, Mike Scully (*pers. comm.*), a student working under Professor Miller in 1963, remembers using tabulated CH-34 loads data that had been provided to MIT, but he does not remember the Thompson letter. It is likely that the results in the Thompson letter were the same data that were later published in Scheiman and Ludi (1963).

Despite the efforts of NASA to provide test results even before the flight program was complete, many in the helicopter community were frustrated by the length of time it took to publish the main set of data (Scheiman, 1964). Hooper (1985) stated:

“But notice it was put out by Scheiman in March 1964. That was less than 3 years after the test was completed and I have spoken to both Scheiman and Ted Carter from the Sikorsky end and I understand that was at least a year longer than it should have been by both those guy's accounts because there was a great deal of delay. In fact, it's probably been forgotten by most of the participants, (and I wasn't one), but there were a lot of short tempers over that program because of the delay in getting out the data.”

Delays in publishing data and getting it out to the helicopter community, as well as the short tempers, have become the norm.

At the end of the 1960s, Ward (1971) returned to the Scheiman (1964) data to obtain “a clear understanding of the fundamental aerodynamic and structural response characteristics that impose the present maneuver limits.”

The bandwidth of the tabulated Scheiman data was 12 harmonics (samples every 15°). Ward went back to the original oscillograph rolls and re-digitized the data for six cases as shown in table A-5 (and shown with dashed circles in figure A-7). He sampled the data based on the frequency content of the trace, and the number of sample points varied from 10 to 170. He interpolated the data every 2°, providing a bandwidth of 90 harmonics. His reanalysis included all of the differential pressure and blade structural measurements. Based on the new differential time histories, he also calculated the section normal forces and pitching moments.

Ward's Case 1 provided a level flight condition as a baseline, whereas the rest of the cases were either steady or unsteady maneuvers. In the maneuver cases, there is clear evidence of three cycles of dynamic stall in the fourth quadrant. Figure A-9 is a copy of Ward's figure 8

TABLE A-5. REANALYZED CASES (WARD 1971)

Condition	Ward	Scheiman
Level flight	Case 1	Flight 89, Rev 1
Pull-up	Case 2	Flight 89, Rev 2
Steady left turn	Case 3	Flight 37
Steady right turn	Case 4	Flight 36
Steady left turn	Case 5	Flight 40
Steady right turn	Case 6	Flight 39

and shows comparisons between Case (1) and (2) for the torsion moment, the section lift at  $0.95R$ , and the pitching moment at  $0.95R$ , respectively. Ward reported that the three cycles of dynamic stall occurred at the second torsion mode frequency of the CH-34.

In his study, Ward concluded that the torsional loading was caused by the helical rotor wake and dynamic stall aggravated the problem. What is known of dynamic stall based on the UH-60A airloads dataset suggests that rotor wake loading has little affect on the dynamic stall limit (Bousman, 1998). The Ward reanalysis of the CH-34 flight data would be an excellent test case to examine the importance of helical wake effects. Unfortunately all of the reanalyzed data have been lost.

Although TRECOM's original purpose in funding the CH-34 flight test was to better understand the higher harmonic rotor airloads on rotor blades, acousticians at the various helicopter companies were intensely interested in the use of measured blade pressures as a means of understanding and validating their acoustic calculations. Loewy and Sutton (1966) used the measured hover airloads from Scheiman (1964) as an input to their acoustic model and compared the calculated acoustics with measurements on another CH-34 that were obtained in an extensive acoustic survey of U.S. Army aircraft (Sternfeld et al., 1961).

Schlegel et al. (1966) made acoustic measurements on a CH-34 at the Bridgeport Airport in 1965, obtaining data in both hover and forward flight. They attempted to match flight conditions with those of Scheiman (1964) and then used the Scheiman airload measurements as inputs to their acoustic models for validation.

### UH-1A Flight Test

The second of the two programs funded by TRECOM at the beginning of the 1960s used the Bell Helicopter UH-1A (known at the time as the HU-1A, but renamed the UH-1A in September 1962). Unlike the CH-34 flight test, Bell Helicopter was responsible for both the installation of

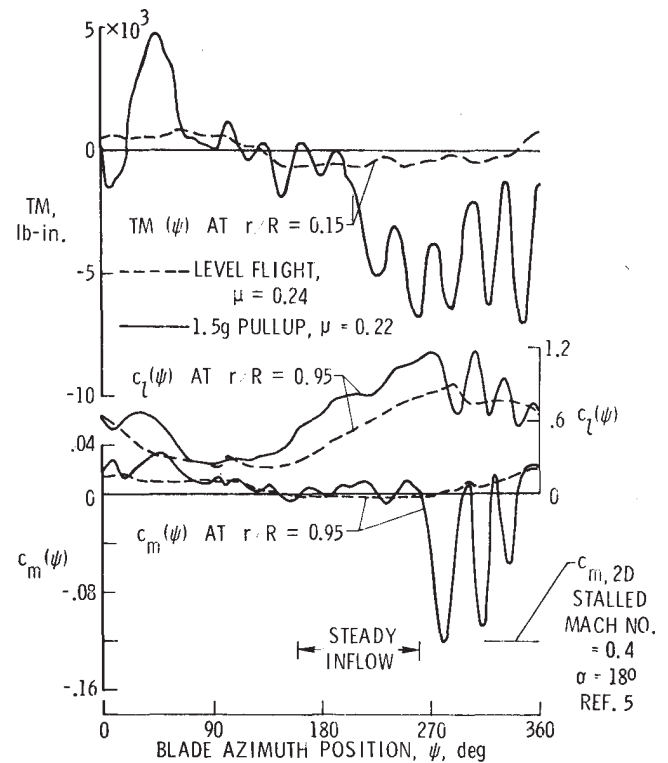


Figure A-9. Figure 8, Ward (1971).

the differential pressure transducers and the other instrumentation, and they were also responsible for the flight test, data reduction, and report publication. The UH-1A test aircraft, figure 1 from Burpo and Lynn (1962),<sup>2</sup> is shown in figure A-10. The Burpo and Lynn report provides a complete description of the test program and includes tabulated test data.

The instrumented UH-1A blade is shown in figure A-11. The chordwise distribution and number of differential pressure transducers are given in table A-6. The chordwise distribution of transducers was based on the requirements of Gaussian integration. A general description of the UH-1A and various test parameters is given in table A-7.

The differential pressure transducers installed in the blade of the UH-1A penetrated the blade spar and, as in the case of the CH-34, it was necessary to test blade specimens under fatigue loading. Four specimens incorporating instrumented sections were fatigue tested. Initial analyses indicated that the inboard section was critical. Based on these analyses, it was decided to locate the most inboard measurement station at  $0.40R$  rather than  $0.30R$  to increase

<sup>2</sup> In the 1960s, TRECOM did not list authors on the cover or title pages of their reports. Instead, they attached a page to the report on cardboard stock that could be removed and used as a library card to place in a card catalog. Unfortunately, the attached page was easily lost and these reports are sometimes referenced with "Anonymous" as the author.





Figure A-10. UH-1A flight test aircraft (Burpo and Lynn, 1962).

TABLE A-6. LOCATIONS OF PRESSURE TRANSDUCERS ON UH-1A BLADE USED IN FLIGHT TEST (ONE BLADE)

Radial	Chordwise	
	No.	
0.40	5	0.040, 0.170, 0.340, 0.640, 0.880
0.55, 0.75, 0.90, 0.95	7	0.020, 0.090, 0.170, 0.230, 0.340, 0.630, 0.90
0.85	11	0.020, 0.040, 0.090, 0.130, 0.170, 0.230, 0.340, 0.477, 0.630, 0.770, 0.900

TABLE A-7. UH-1A FLIGHT TEST DESCRIPTION\*

Test number	3
Sponsor	U. S. Army
Manufacturer	Bell Helicopter
Number blades	2
Airfoil section	NACA 0015
Blade twist, deg	-15.0
Blade chord, in.	15.2
Rotor diameter, ft	43.8
Rotor solidity	0.0369
Tip speed, ft/sec	716.
Instrumented radial stations	6 (5)
Transducers/radial station	7.3 (7.4)
Rotating sensors	78 (49)
Test points	17 (4)
Harmonic bandwidth	6 (12)
Rotating samples	21,015
Test hours	6.4
Test completion	October 1961

\*Parantheses refer to Type II data, see text.

blade fatigue life. But during flight test it was found that the most critical section was at  $0.75R$ . It was decided to restrict the blades to a 15-hour life, and this was sufficient for the flight test program.

Flap and chord bending moments, and torsion moments were obtained as shown in table A-8. Both pitch-link loads were measured as well.

The analog signals were brought down from the rotating system through a set of slip rings where they were recorded on an oscillograph. Initially, the plan was to sample the data every  $30^\circ$  to provide 6 harmonics, and these data were referred to as Type I data. Burpo and Lynn (1962) stated that

“During the course of the program, USATRECOM advised the contractor that a new rotor air load prediction technique was being developed by the Cornell Aeronautical Laboratory and that it was desirable to use data from the subject program for correlation purposes. During subsequent discussions with personnel from USATRECOM and the Cornell Aeronautical Laboratory, it was decided that the HU-1A data to be supplied to the Cornell

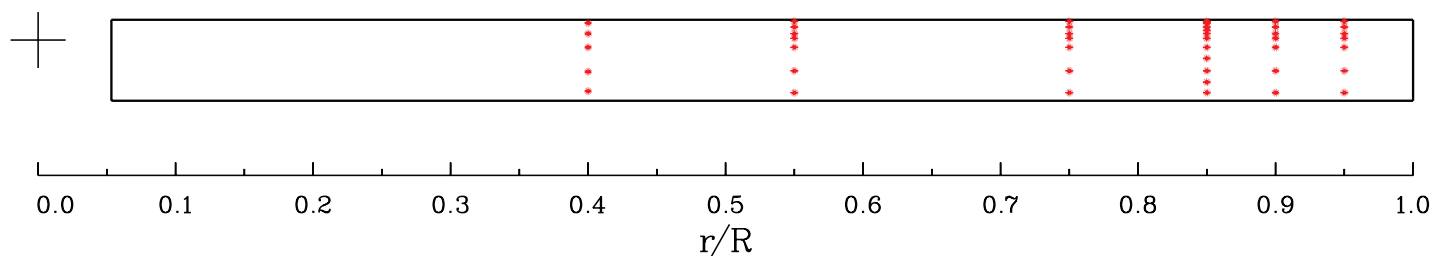


Figure A-11. UH-1A planform showing locations of differential pressure transducers at six radial stations.

TABLE A-8. STRAIN-GAUGE BRIDGE LOCATIONS ON UH-1A BLADES USED IN FLIGHT TEST

Measurement	$r/R$
Flap bending moment*	<u>0.150</u> , <u>0.280</u> , 0.360, 0.450, 0.600, 0.650, 0.800, 0.950
Chord bending moment*	<u>0.150</u> , <u>0.280</u> , 0.600, 0.800
Torsion moment	0.150, 0.500

\*Moments measured on both blades for underlined stations.

Aeronautical Laboratory should have a greater sensitivity than that originally planned; further, that a 24-point instead of a 12-point harmonic analysis should be used. To accomplish this, it was necessary to increase the sensitivity of the air load oscillograph traces, to delete some oscillograph traces (to allow for increased sensitivity), and to increase the oscillograph paper speed. The resulting four flight conditions and data are referenced to herein as Type II flights, conditions, data, etc. . .”

Consequently, for Type II data, no pressure measurements were made at  $0.55R$ , no chord bending measurements were obtained, and flap bending moments were recorded only on one blade.

Three revolutions of Type I and II steady data were digitized from the oscillograph rolls. The two best revolutions were averaged. For the two Type I maneuver cases, five revolutions were selected during the maneuver, approximately 1 second apart. Each of these revolutions was digitized. The section normal forces at the radial stations were calculated using Gaussian integration. There was no integration of the differential pressures to obtain the section pitching moments.

All of the differential pressures, integrated normal forces, and structural measurements are tabulated in the report. Most of these measurements are also shown in more than 80 figures.

The UH-1A flight test conditions are shown in figure A-12 in terms of the weight coefficient multiplied by the aircraft load factor,  $n_z C_w / \sigma$ , as a function of advance ratio,  $\mu$ , and are compared with the McHugh thrust boundary and the line of incipient dynamic stall. Type I flight data are shown with open circles and the Type II data are shown as closed blue circles. The Type I data included two cases that were flown at high altitude so that they would encounter stall in level flight. The two Type I maneuvers, a symmetric pull-up and a landing approach, are shown in red.

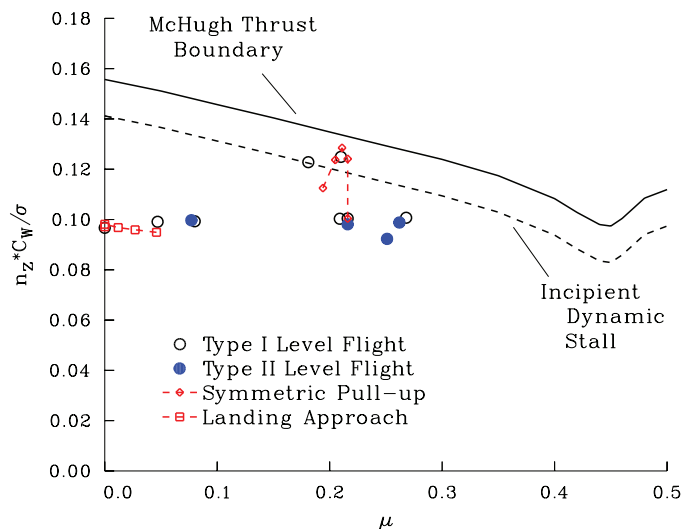


Figure A-12. UH-1A flight test nondimensional weight coefficient as a function of advance ratio compared to McHugh's (1978) thrust boundary.

At the time that TRECOM was funding the UH-1A airloads testing, they were also funding a major study at Bell Helicopter to better understand the origins of helicopter noise and ways in which it could be reduced (Cox and Lynn, 1963). As a part of this program, they funded additional testing of the UH-1A airloads aircraft and obtained acoustic measurements at the same time. Following the final test of the UH-1A airloads program on 7 Sept 1961, sound pressure measurements were made on this aircraft in ground tie-down conditions, in an in-ground-effect hover, and during a flyover at 50 feet. The blade pressures and internal cabin noise were recorded at the same time as ground acoustic measurements. The intent of these simultaneous measurements was to correlate the ground acoustic measurements with the blade aerodynamic measurements. Cox and Lynn (1963) reported:

“Within the scope of the subject program, the location of the helicopter with respect to the ground plane microphones and the azimuth positions of the rotor could not be established during the flyover tests. Therefore, the acoustical data of the ground plane microphones taken during these tests are not included.”

The measured blade pressure data for this follow-on test were never reduced.

The cumulative citations for the UH-1A airloads test are shown in Figure A-13. These data were used extensively into the early 1970s to assess the accuracy of the new prescribed wake models.

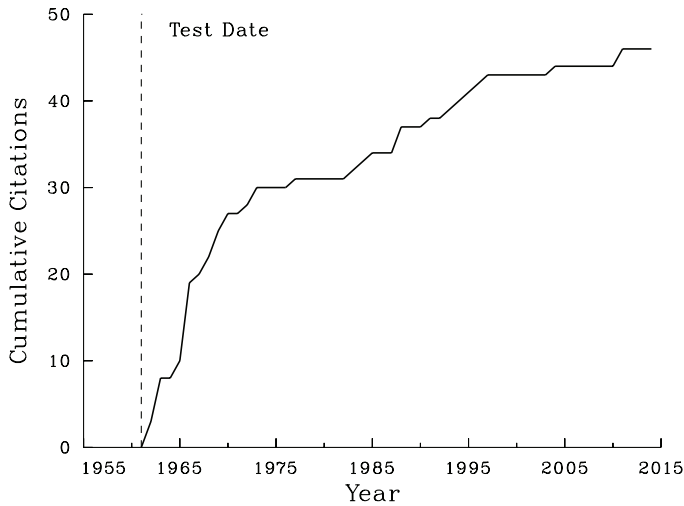


Figure A-13. Cumulative citations of the data obtained from the UH-1A flight test (Burpo and Lynn, 1962).

### CH-34 Wind Tunnel Test

The instrumented rotor tested in flight on the CH-34 at NASA Langley in 1960–61 under U.S. Army sponsorship (Scheiman, 1964) was modified and subsequently tested in the 40- by 80-Foot Wind Tunnel at NASA Ames (Rabbott et al., 1966a,b). The purpose of the test was “to extend the range of available aerodynamic and structural loading data to higher forward speeds” (Rabbott et al., 1966a). A photograph of the CH-34 rotor in the wind tunnel is shown in figure A-14.

A general description of the test, the major data obtained, and correlation with analysis is given in Rabbott et al. (1966a). The differential pressure data for the 10 test points are tabulated in Rabbott et al. (1966b).

The CH-34 wind tunnel test is the only one of the 12 airloads tests discussed in this paper that was not completely funded by agencies of the U.S. Government. Rabbott et al. (1966a) write in their introduction, “This program was jointly sponsored by the United States Army Aviation Material Laboratories and Sikorsky Aircraft, and the tests were conducted by the Ames Research Center of the National Aeronautics and Space Administration.” The actual division of costs and responsibility between the three organizations is unknown.

The instrumented CH-34 blade is shown in figure A-15. The chordwise distribution and number of differential pressure transducers are given in table A-9. Seven additional differential pressure transducers were installed for this test beyond those used in flight (as shown in figure A-6 and table A-2). Four of these were installed at 0.97R and the other three at 0.99R. The spanwise locations were selected to allow Gaussian integration. A general description of the CH-34 rotor and test is provided in table A-10.



Figure A-14. CH-34 pressure-instrumented rotor in the 40- by 80-Foot Wind Tunnel (courtesy of NASA Ames Research Center).

A reduction in the allowable test life of the pressure instrumented blade was discussed previously in the description of the flight test.

Flap and chord bending moments, and torsion measurements, were obtained as shown in table A-11. The radial locations of these measurements differ from those used in the flight test (see table A-4). There was no measurement of the pitch-link loads in the wind tunnel test.

The CH-34 control system was modified for the wind tunnel test to accommodate the higher control loads. The swashplate, scissors, and control horn were redesigned. The pitch links and servos from the Sikorsky S-61 were used instead of those for the CH-34. A consequence of these modifications was that there was “an unusual control system kinematic coupling such that two adjacent blades

TABLE A-9. LOCATIONS OF PRESSURE TRANSDUCERS ON CH-34 BLADE USED IN THE WIND TUNNEL TEST (ONE BLADE)

Radial	Chordwise	
	No.	
0.25, 0.40	5	0.042, 0.158, 0.300, 0.600, 0.910
0.55, 0.75, 0.90, 0.95	7	0.017, 0.090, 0.168, 0.233, 0.335, 0.625, 0.915
0.85	11	0.017, 0.040, 0.090, 0.130, 0.168, 0.233, 0.335, 0.560, 0.625, 0.769, 0.915
0.97	4	0.090, 0.230, 0.565, 0.850
0.99	3	0.101, 0.290, 0.737

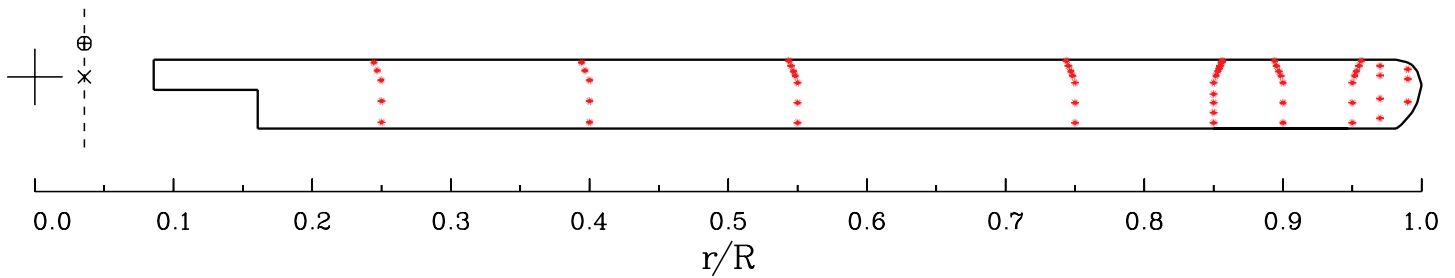


Figure A-15. CH-34 planform showing locations of differential pressure transducers at nine radial stations.

TABLE A-10. CH-34 WIND TUNNEL TEST DESCRIPTION

Test number	4
Sponsor	U.S. Army, Sikorsky Aircraft, NASA
Manufacturer	Sikorsky Aircraft
Number blades	4
Airfoil section	NACA 0012
Blade twist, deg	-8.0
Blade chord, in.	16.4
Rotor diameter, ft	56.0
Rotor solidity	0.0622
Tip speed, ft/sec	650.
Instrumented radial stations	9
Transducers/radial station	6.2
Rotating sensors	70
Test points	10
Harmonic bandwidth	36
Rotating samples	48,630
Test hours	-
Test completion	September 1964

TABLE A-11. STRAIN-GAUGE BRIDGE LOCATIONS ON CH-34 BLADE USED IN THE WIND TUNNEL TEST (ONE BLADE)

Measurement	$r/R$
Flap bending moment	0.375, 0.450, 0.650, 0.800
Chord bending moment	0.150, 0.375, 0.650, 0.800
Torsion moment	0.150, 0.375, 0.650

measured differential pressures (Rabbott et al., 1966b). These pressures were integrated using Gaussian quadrature to obtain the normal forces on the blade. The forces and the structural loads were tabulated in Rabbott et al. (1966a). No calculation of blade pitching moments was made.

The CH-34 wind tunnel test measurements are shown in figure A-16 for thrust coefficient,  $C_T/\sigma$ , as a function of advance ratio,  $\mu$ , and are compared with the McHugh thrust boundary and the line of incipient dynamic stall. The primary test data were obtained at three advance ratios ( $\mu = 0.29, 0.39, \text{ and } 0.45$ ) and three shaft angles ( $\alpha_s = 5.0, 0.0, \text{ and } -5.0^\circ$ ). The 10th test point was one selected to match a high-speed case in flight (Scheiman, 1964).

The cumulative citations for the CH-34 airloads testing in the wind tunnel are shown in figure A-17. As with most of the airloads tests, there was an initial use of the data following the test completion, but that use trails off after a few years. By 1980, there was little increase in citations for these data. But when Hooper (1983) wrote his important paper examining multiple sets of airloads data, he placed particular emphasis on the CH-34 wind tunnel test data at high advance ratio. Hooper's intent was to obtain a better understanding of the sources of vibratory loading, and his efforts inspired many of his colleagues to use these data as a basis of correlation over the following 20 or so years.

had a slightly different cyclic pitch from the other two adjacent blades, which resulted in a 'split' tip path plane whenever cyclic pitch was applied" (Rabbott et al., 1966a). Johnson (2011a,b) has discussed this modification and includes a sketch of the modified rotating scissors that was made at the time by the NASA test lead John L. McCloud III. Because of these changes it was not possible to trim the rotor to zero flapping, and resultant values for the test ranged from 0 to  $1.8^\circ$  for the longitudinal flapping and  $2.8$  to  $4.4^\circ$  for the lateral flapping.

The rotating system analog measurements were brought down through a set of slip rings and were recorded on a 14-track FM multiplex system. The analog data from the FM tape were digitized on a ground station at 72 samples/revolution, providing a harmonic bandwidth of 36/rev, three times that obtained in the flight test. Ten revolutions of data were averaged to generate data tables of the

### CH-47A Flight Test

Following the airloads testing of the CH-34 and the UH-1A under their sponsorship, the U.S. Army Aviation Materials Laboratories (AVLABS, formerly known as



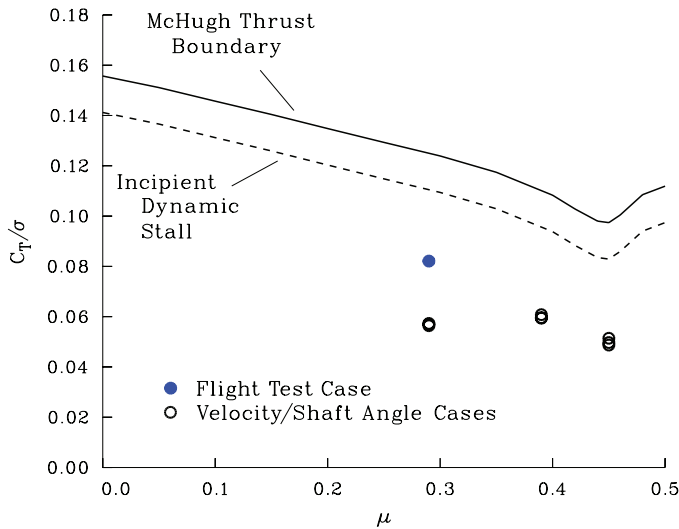


Figure A-16. CH-34 wind tunnel nondimensional thrust coefficient as a function of advance ratio compared to McHugh's (1978) thrust boundary.

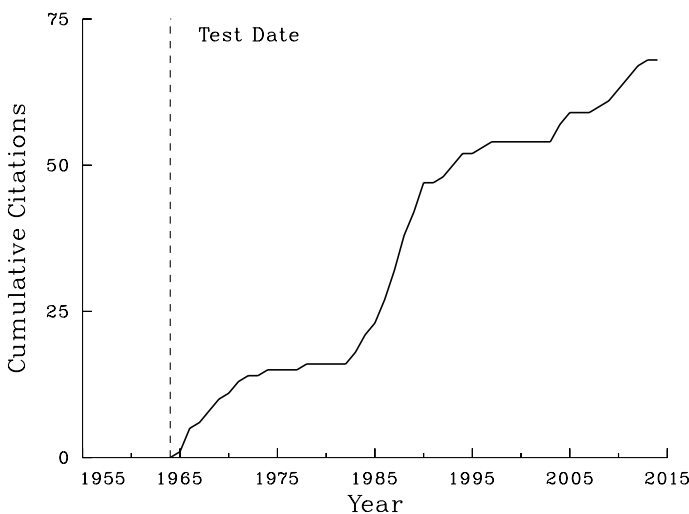


Figure A-17. Cumulative citations of the data obtained from the CH-34 wind tunnel test (Rabbott et al., 1966a, 1966b).

TRECOM) sponsored an airloads test of the CH-47A. Figure A-18 is a photograph of the prototype CH-47A (referred to as the YHC-1B) that was used as the airloads test vehicle. This was the most ambitious airloads test yet conceived. Both rotors were fully instrumented including a total of 108 pressure transducers and another 58 rotating sensors.

Documentation of the test was provided in four volumes: Golub and McLachlan (1967), Grant and Pruyn (1967), Obbard (1967), and Pruyn (1967). A related fifth volume (Pruyn, 1968) examined the most severe stall conditions tested.



Figure A-18. CH-47A flight test aircraft (courtesy of Boeing Rotorcraft Systems).

Both CH-47A blades had an identical suite of pressure transducers as shown in figure A-19. The chordwise distribution and number of pressure transducers are provided in table A-12. A general description of the CH-47A rotor is given in table A-13. The modification to the NACA 0012 airfoil noted in the table was the addition of a symmetrical leading edge cap and a flat plate trailing edge extension.

The previous four airloads tests had used differential pressure transducers, which required drilling multiple holes in the spar block during transducer installation. In those tests, to provide a safe life for the instrumented blades, it was necessary to fatigue test the instrumented blade sections. With advances in transducer technology, Boeing Vertol was able to procure miniaturized absolute pressure transducers that could be installed on the surface of the blade over the forward (structural) portion of the blade. These absolute transducers were installed on the top and bottom surfaces and were used to compute the differential pressure. Over the aft portion of the blade they used conventional differential pressure transducers.

Flap and chord bending moments, and torsion moments, were obtained as shown in table A-14. Additional rotating measurements included pitch-link loads, blade tension at  $0.13R$ , three hub accelerations, and seven rotor shaft loads and moments. A total of 32 accelerometers were installed in the fuselage to measure the fixed-system vibration.

The rotating system measurements were conditioned on the rotor hub and then brought down as analog signals through slip rings. The data from the forward and aft rotors were recorded alternately on a 14-track frequency modulation (FM) multiplex analog tape, with one cycle of data lost each time the rotor measurements were switched. Five cycles of data were obtained on each rotor but were non-contiguous, that is, every third revolution was recorded.

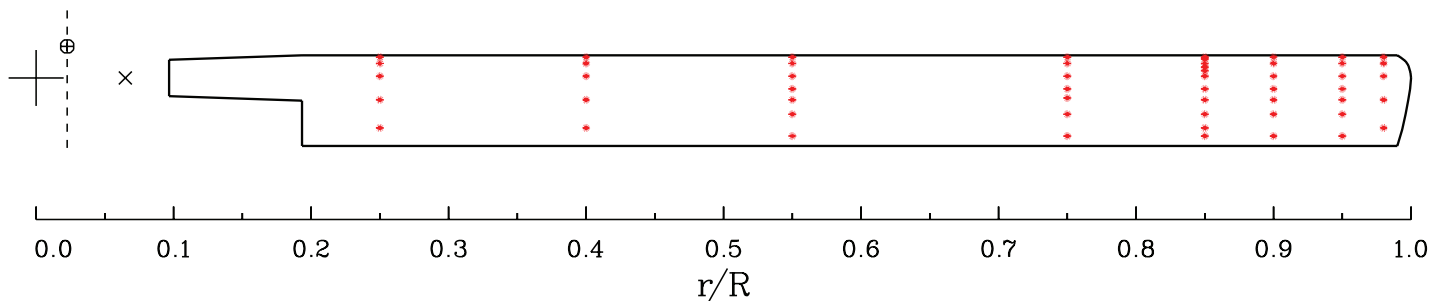


Figure A-19. CH-47A planform showing locations of pressure transducers at eight radial stations.

TABLE A-12. LOCATIONS OF PRESSURE TRANSDUCERS ON CH-47A BLADES USED IN FLIGHT TEST (BOTH ROTORS)

Radial	Chordwise	
	No.	
0.25, 0.40, 0.98	5	0.02, 0.09, 0.23, 0.49, 0.80
0.55, 0.75, 0.90, 0.95	7	0.02, 0.09, 0.23, 0.37, 0.49, 0.65, 0.89
0.85	11	0.02, 0.04, 0.09, 0.13, 0.17, 0.23, 0.37, 0.49, 0.65, 0.80, 0.89

TABLE A-14. STRAIN-GAUGE BRIDGE LOCATIONS ON CH-47A BLADES (BOTH ROTORS)

Measurement	$r/R$
Flap bending moment	0.25, 0.35, 0.45, 0.65, 0.75, 0.85, 0.95
Chord bending moment	0.25, 0.45, 0.65, 0.85
Torsion moment	0.13, 0.40

TABLE A-13. CH-47A FLIGHT TEST DESCRIPTION

Test number	5
Sponsor	U. S. Army
Manufacturer	Boeing Vertol
Number blades	3 (x2)
Airfoil section	mod NACA 0012
Blade twist, deg	-9.0
Blade chord, in.	23.0
Rotor diameter, ft	59.1
Rotor solidity	0.0619
Tip speed, ft/sec	712.
Instrumented radial stations	8
Transducers/radial station	6.8
Rotating sensors	166
Test points	121
Harmonic bandwidth	12
Rotating samples	420,956
Test hours	-
Test completion	July 1966

The analog data were digitized, and approximately 65 samples per revolution were obtained. After averaging, these data were harmonically analyzed and the mean and first 12 harmonics were saved. Both normal force and pitching moment were calculated using trapezoidal integration. Obbard (1967) checked the accuracy of the trapezoidal integration for normal force by using data from Scheiman (1964), which had used Gaussian integration. The agreement was quite good based on the magnitudes of the mean and first 10 harmonics at the 7 radial stations from the CH-34 flight test. There was a slight unexplained difference at 0.85R. Using linear regression for all of the data (Bousman and Norman, 2010), the slope,  $m$ , a measure of accuracy, was 0.97 (or -3 percent) and the coefficient of determination,  $r^2$ , a measure of scatter, was 0.9962.

The primary reports for the test (Pruyn 1967, 1968) show airloads results in about 90 figures, but none of the data were tabulated in these reports.

The CH-47A flight test cases are shown in figures A-20 and A-21 for the rotor weight coefficient,  $C_w/\sigma$ , as a function of advance ratio,  $\mu$ , and are compared with the McHugh thrust boundary and the line of incipient dynamic stall. The forward and aft rotor weight coefficients are shown separately, based on the thrust split in Tarzanin (1972). The aft rotor is the more heavily loaded.

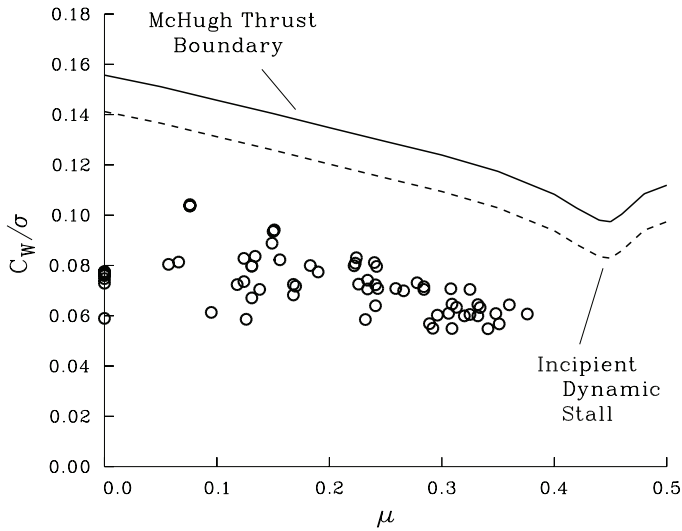


Figure A-20. CH-47A nondimensional weight coefficient for the forward rotor as a function of advance ratio compared to McHugh's (1978) thrust boundary.

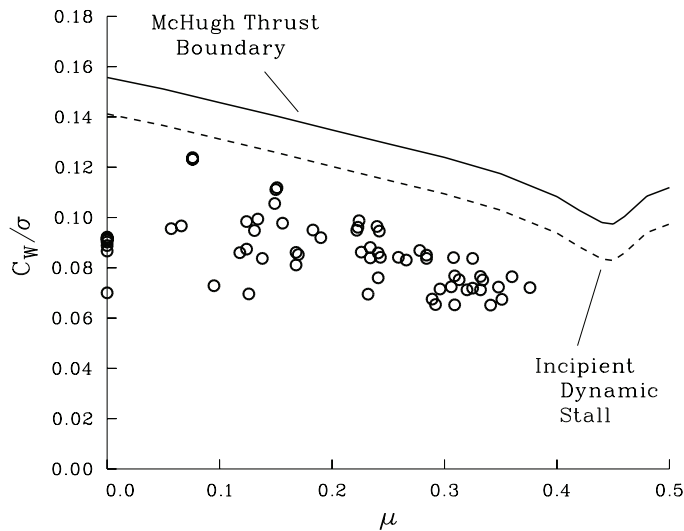


Figure A-21. CH-47A nondimensional weight coefficient for the aft rotor as a function of advance ratio compared to McHugh's (1978) thrust boundary.

The cumulative citations for the CH-47A airloads flight test are shown in figure A-22. Only five of these papers included analysis of the flight airloads data (Pruyn and Obbard, 1966; Pruyne and Alexander, 1966; Pruyne, 1967; Pruyne, 1968; Harris and Pruyne, 1968), the last publication in 1968. In discussing the data, Pruyne (1967) mentions the availability of the flight test data in an internal company document "to be published." A similar allusion is in Pruyne (1968). It has not been determined whether this data report was ever published or is still available; it appears the data no longer exist.

The CH-47A airloads flight test was the most ambitious of the early airloads tests. Now, it is known as the first of the data sets to have disappeared.

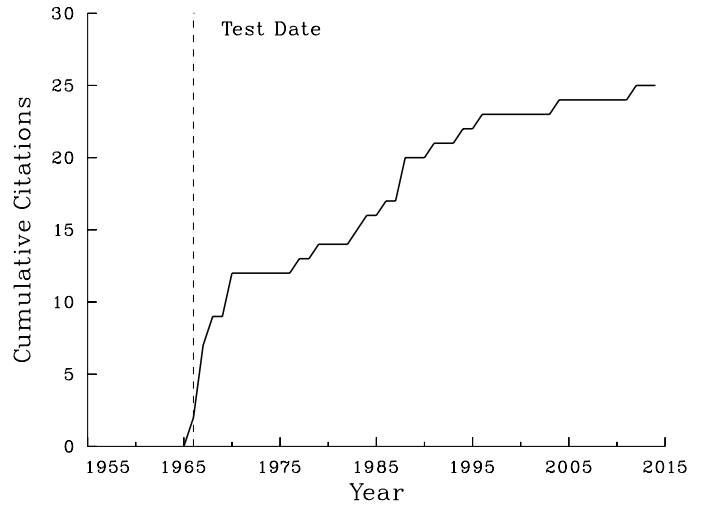


Figure A-22. Cumulative citations of the data obtained from the CH-47A flight test (Pruyn, 1967).

### NH-3A Compound Flight Test

The military services were very interested in the potential of compound helicopters in the 1960s (Prouty, 2009). These possibilities were studied by contracting with four manufacturers to add a wing and auxiliary propulsion to a current rotorcraft. For two of these aircraft, the Sikorsky Aircraft NH-3A and the Lockheed XH-51A, funding was provided to obtain airloads measurements.

The NH-3A compound airloads program was jointly funded by the U.S. Naval Air Systems Command (NASC) and the U.S. Army Aviation Materials Laboratories (AVLABS). Figure A-23 shows the NH-3A compound in flight. The NH-3A was based on the Sikorsky Aircraft SH-3A (S-61F), and included a wing with an adjustable flap and two Pratt & Whitney J-60-P2 turbojets mounted on either side of the fuselage. The empennage was modified to provide better streamlining. The horizontal and vertical tails were increased in area and both included controllable surfaces activated by "beeper" controls. The blade-folding hardware was removed from the rotor head (which made the configuration more like the CH-3C).

The test was described in Fenaughty and Beno (1970a) and the flight test data were provided in a separate volume (Fenaughty and Beno, 1970b).

Pressure transducers were installed on one blade as shown in figure A-24. The chordwise distribution and number of pressure transducers are provided in table A-15. A general description of the NH-3A rotor is provided in table A-16.

As was the case in the CH-47A flight test, absolute pressure transducers were bonded to the surface of the



Figure A-23. NH-3A compound flight test aircraft (Fenaughty and Beno, 1970a).

blade on the structural portion to avoid drilling holes for differential pressure transducers as had been required in the earlier tests. Measured absolute pressures on the upper and lower surfaces were used to create a differential pressure measurement.

Flap and chord bending moments, and torsion moments, were measured at the stations shown in table A-17. Additional rotating measurements included blade tension at  $0.111R$ , pitch-link and damper loads, blade root angles, and three blade accelerations. Fuselage accelerations were measured at 13 locations.

The rotating measurements were brought down to the flight recorder through slip rings, and a "burst" of approximately 30 revolutions of data were recorded on a 14-track FM multiplexed analog tape.

The FM tape was digitized in a ground station at approximately 72 samples/revolution and was written to digital tape. The normal forces at the five radial stations were obtained using Gaussian integration. In those cases with failed pressure transducers, trapezoidal integration was used. No calculations of pitching moment were made.

The digital tapes were subsequently processed to include all calibrations. Output tables were prepared and written to a printer, and included the 72 azimuthal steps for

TABLE A-15. LOCATIONS OF PRESSURE TRANSDUCERS ON THE NH-3A ROTOR (ONE BLADE)

Radial	Chordwise	
	No.	
0.40, 0.75, 0.85, 0.95, 0.98	5	0.042, 0.158, 0.300, 0.600, 0.910
0.25, 0.65, 0.80, 0.90	1	0.09

TABLE A-16. NH-3A COMPOUND FLIGHT TEST DESCRIPTION

Test number	6
Sponsor	U.S. Navy, U.S. Army
Manufacturer	Sikorsky Aircraft
Number blades	5
Airfoil section	NACA 0012
Blade twist, deg	-4.0
Blade chord, in.	18.3
Rotor diameter, ft	62.0
Rotor solidity	0.0781
Tip speed, ft/sec	660.
Instrumented radial stations	5
Transducers/radial station	5.0
Rotating sensors	90
Test points	74
Harmonic bandwidth	36
Rotating samples	475,524
Test hours	16.4
Test completion	March 1967

each parameter as well as the calculated steady and first seven harmonics. The primary volume that described the airloads test program (Fenaughty and Beno, 1970a) includes airloads measurements in three figures. This volume is in the public domain. The tabulated data were published in a

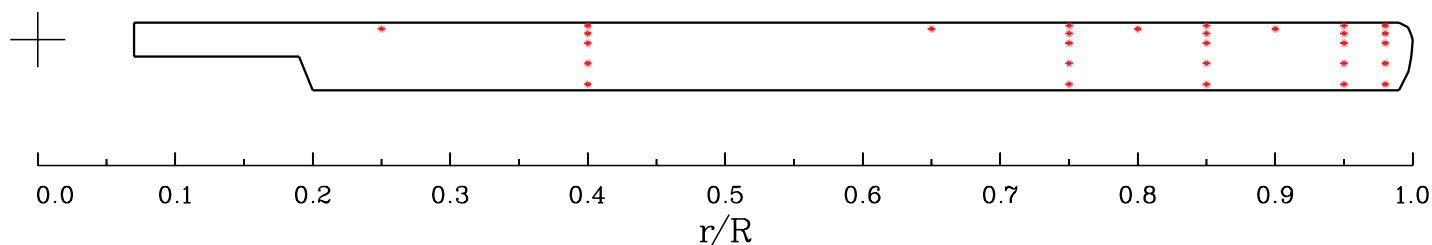


Figure A-24. NH-3A rotor blade planform showing locations of pressure transducers at five radial stations. Pressure transducers were also located at  $0.09c$  at four other radial stations.



TABLE A-17. STRAIN-GAUGE BRIDGE LOCATIONS ON NH-3A ROTOR (ONE BLADE)

Measurement	$r/R$
Flap bending moment	0.110, 0.137, 0.164, 0.267, 0.460, 0.653, 0.845
Chord bending moment	0.110, 0.137, 0.164, 0.267, 0.460, 0.653
Torsion moment	0.110, 0.653

separate restricted volume (Fenaughty and Beno, 1970b) and distribution was limited to U.S. Government agencies and their contractors. With the passage of time, many of the copies of the data volume have disappeared, but others have appeared in interesting places. The data volume has been digitized by Google Books courtesy of the Naval Air Systems Command.

The main rotor shaft was instrumented to measure both lift and torque. The nondimensional rotor thrust as multiplied by aircraft load factor,  $n_z C_T / \sigma$ , is shown as a function of advance ratio,  $\mu$ , in figure A-25, and the values are compared with the McHugh thrust boundary and the line of incipient dynamic stall. The majority of the data were obtained at just three advance ratios: 0.35, 0.41, and 0.47. Sixteen of the 74 data points were obtained with the wings off.

After the publication of the final reports for the NH-3A airloads tests and a subsequent airloads test of the CH-53A (discussed later), Sikorsky Aircraft obtained a contract from NASA at Langley Research Center to reanalyze the flight test data to better understand high-frequency blade loading (Beno, 1973). The original FM flight test tapes were reprocessed so as to provide 36 harmonics of data and plotted on oscillograph rolls. Based on the resulting time histories, Beno selected four cases from the NH-3A test (and two from the CH-53A test). The four cases for the NH-3A are indicated by a dashed open circle in figure A-25. Two of these were steady bank angle turns at 45° and 60° with the wings off. The other two were level flight cases with the wings on, one at  $\mu = 0.36$  and the other at 0.47.

Beno digitized the oscillograph rolls at 72 samples per revolution, but did not digitize all parameters. He processed all of the differential and absolute pressures at 0.75R, 0.85R, and 0.95R (see figure A-24). He also digitized the flap bending and chord bending moments at three radial stations, the torsion moments at two radial stations, and the pitch-link load. He calculated the normal forces using Gaussian quadrature (as was done for the NH-3A data volume) and also calculated the pitching moments using trapezoidal integration (which was not in the data volume).

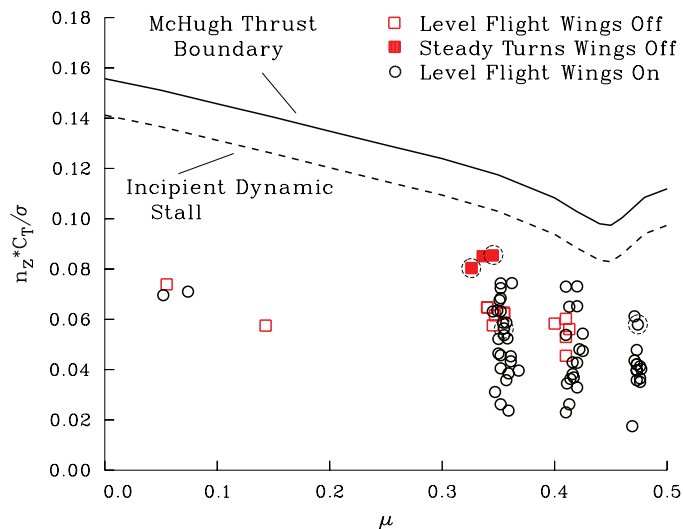


Figure A-25. NH-3A nondimensional thrust as a function of advance ratio compared to McHugh's (1978) thrust boundary. Dashed circles show test points reanalyzed by Beno (1973).

Beno focused his analysis on the torsional loads, but it is not clear how much of that loading was related to nonlinear effects of stall, blade vortex intersections, or other factors. Analytical results that were included did not provide much insight into the aerodynamic forcing. The problem of the NH-3A torsional loading still remains, although the reanalyzed data are gone.

During the period when the NH-3A was being tested, there was interest at Sikorsky Aircraft in obtaining acoustic data that could be compared with calculations based on the measured airloads (Schlegel et al., 1966). It has not been determined whether such acoustic measurements were ever made.

The cumulative citations for the NH-3A compound flight test airloads are shown in figure A-26. Following the initial publication of the test reports, structural loading data from the program were used over a number of years in Sikorsky Aircraft papers and reports. It appears that the published NH-3A airloads data were not used until Hooper's seminal paper in 1983 and have not been used subsequently.

### XH-51A Compound Flight Test

A flight test program to obtain measured airloads on the Lockheed California XH-51A compound aircraft was the second airloads test program using a compound helicopter (see the previous discussion of the NH-3A compound flight test program).

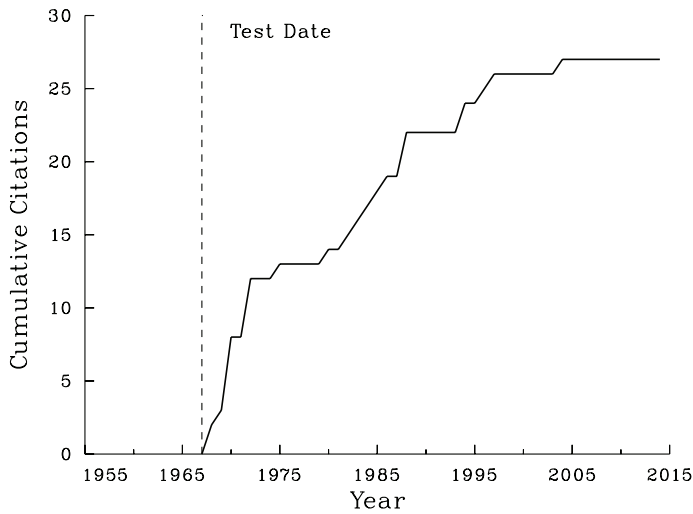


Figure A-26. Cumulative citations of the data obtained from the NH-3A compound flight test (Fenaughty and Beno, 1970a,b).



Figure A-27. XH-51A compound flight test aircraft (courtesy of Ray Prouty).

The XH-51A compound airloads program was funded by the U.S. Army Aviation Materials Laboratories (AVLABS). Figure A-27 shows a photograph of the XH-51A in flight. The basis of the XH-51A compound was the Lockheed California Model 286 helicopter. The changes made to this helicopter for the program were the “installation of a short-span wing and a [Pratt & Whitney] J-60 jet engine,” (Bartsch, 1968a). Spreuer (1968) provides an overview of the entire XH-51A compound program.

The flight test program, data, and correlation are described in Bartsch (1968a,b) and Sweers (1968). The flight data are tabulated in Bartsch (1968b).

Pressure transducers were installed on one blade as shown in figure A-28. The chordwise distribution and the number of pressure transducers are provided in table A-18. A general description of the XH-51A rotor is given in table A-19.

Differential pressure transducers were used at all chordwise stations on the blade. As with the CH-34 and UH-1A airloads programs, it was necessary to demonstrate a safe life for the instrumented blade. Analysis indicated that the blade would be good for at least 18 hours of testing. A blade specimen with holes drilled for the pressure

transducers was fatigue tested for 20 hours based on the expected flight test spectrum and no cracks were encountered. The specimen was then tested for an additional 20 hours with elevated loads, and showed no damage.

During flight test, the instrumented blade was removed after each 2 hours of testing and was x-rayed to ensure the blade’s structural integrity.

Flap and chord bending moments, and torsion moments, were measured at the stations shown in table A-20. Additional rotating structural measurements included the pitch-link load.

The differential pressure and strain-gauge bridge measurements were brought down from the rotating system through a 162-channel set of slip rings. They were recorded on two 50-channel oscillograph recorders.

The oscillograph data were digitized at arbitrary azimuth steps, and a cubic polynomial fit was used to calculate 72 azimuth samples per revolution.

The measured differential pressures were used to create estimated pressures at 53 chord points. A cubic polynomial was used to interpolate between the measurement stations. Pressures between the leading edge and the first

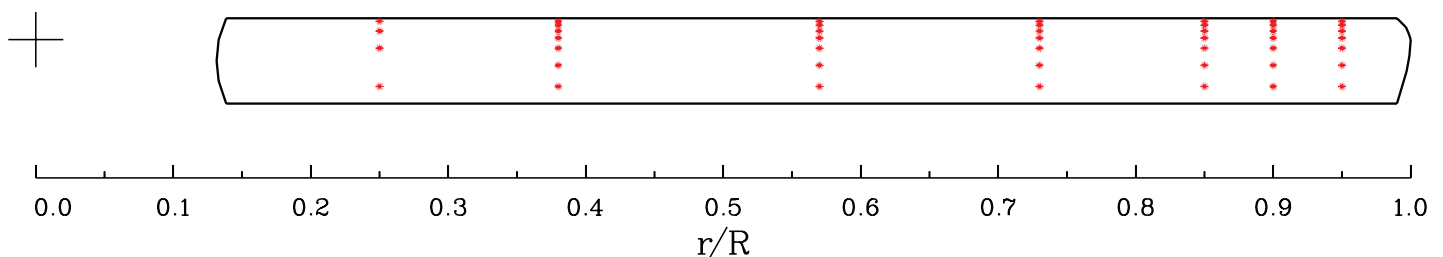


Figure A-28. XH-51A blade planform showing locations of pressure transducers at seven radial stations.

TABLE A-18. LOCATIONS OF PRESSURE TRANSDUCERS ON THE XH-51A ROTOR (ONE BLADE)

Radial	Chordwise	
	No.	
0.25	4	0.035, 0.150, 0.350, 0.800
0.38, 0.57, 0.73, 0.85, 0.90, 0.95	7	0.035, 0.080, 0.150, 0.230, 0.350, 0.550, 0.800

TABLE A-19. XH-51A COMPOUND FLIGHT TEST DESCRIPTION

Test number	7
Sponsor	U. S. Army
Manufacturer	Lockheed California
Number blades	4
Airfoil section	mod NACA 0012
Blade twist, deg	-5.0
Blade chord, in.	13.0
Rotor diameter, ft	35.0
Rotor solidity	0.0788
Tip speed, ft/sec	651.
Instrumented radial stations	7
Transducers/radial station	6.6
Rotating sensors	85
Test points	49
Harmonic bandwidth	10
Rotating samples	60,760
Test hours	-
Test completion	October 1967

measurement station at  $0.035c$  were calculated depending on whether the pressure at the first station,  $0.035c$ , was greater or less than the pressure at the subsequent station. If greater, the pressures were assumed to be the same as the measurement at  $0.035c$ . If less, the pressure at the leading edge was assumed to be zero, and a cubic polynomial interpolation was used for the other chord points. The pressure at the trailing edge was assumed to be zero, and a cubic polynomial interpolation was used from the final chordwise transducer to the trailing edge. The estimated pressures were integrated from the leading edge to the trailing edge to provide the normal force and pitching moments using the first three terms of Newton's interpolation formula.

The differential pressures, integrated loads, and structural loads were harmonically analyzed to provide the mean and first 10 harmonics, and these values are tabulated in Bartsch (1968b).

TABLE A-20. STRAIN-GAUGE BRIDGE LOCATIONS ON XH-51A ROTOR (ONE BLADE)

Measurement	$r/R$
Flap bending moment	0.038, 0.114, 0.214, 0.348, 0.548, 0.667, 0.748, 0.819, 0.881
Chord bending moment	0.038, 0.214, 0.548, 0.748
Torsion moment	0.548, 0.881

Four vertical links between the gearbox and the fuselage were instrumented to provide an estimate of the rotor thrust. The measured nondimensional rotor thrust multiplied by the aircraft load factor,  $n_z C_T / \sigma$ , is shown in figure A-29 as a function of advance ratio,  $\mu$ , and are compared with the McHugh thrust boundary and the line of incipient dynamic stall. Approximately half of the test points were taken with the jet off (shown as open circles for level flight and solid circles for maneuver). The symbols for the jet on are either open or solid squares.

Test flights with the jet on allowed data to be obtained at higher advance ratios than with any of the previous airloads tests. For these cases, the blade collective was fixed at  $4^\circ$  and most of the lift was provided by the wing, hence, the rotor thrust was reduced.

Bartsch (1968a) presented normal forces on the rotor in about 11 figures, and Sweers (1968) compared theoretical predictions with the normal force data in about 20 figures. The cumulative citations for the XH-51A compound flight test are shown in figure A-30. Rao and Schatzle (1978) compared their analysis with a hover case, and Hooper (1983) included five forward-speed cases in his examination of vibratory airloading. Otherwise, there has been limited use of these airload measurements.

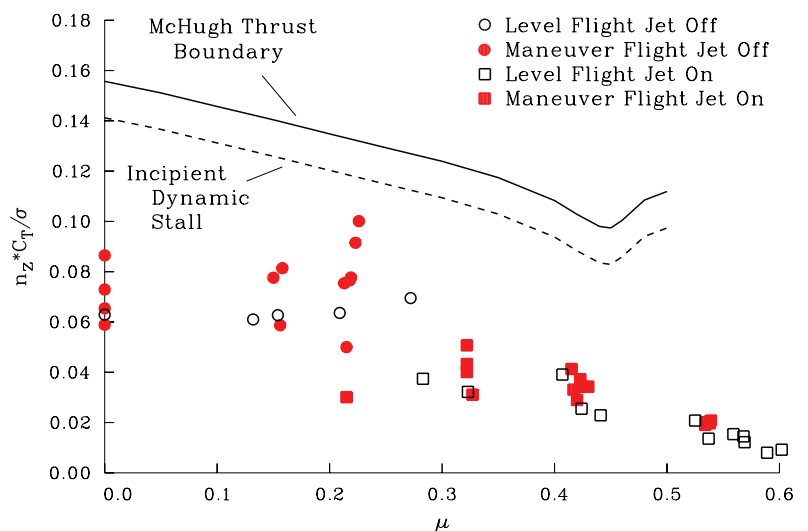


Figure A-29. XH-51A nondimensional thrust as a function of advance ratio compared to McHugh's (1978) thrust boundary.



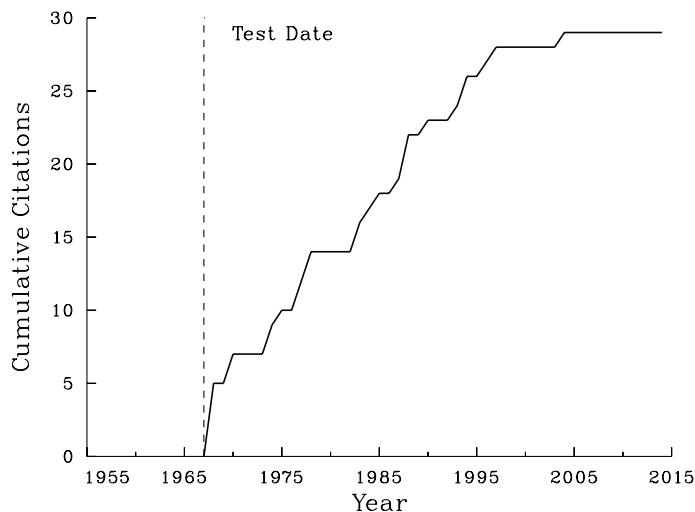


Figure A-30. Cumulative citations of the data obtained from the XH-51A compound flight test (Bartsch 1968a,b; Sweers 1968).

### CH-53A Flight Test

The CH-53A airloads program was funded by the U.S. Naval Air Systems Command. The purpose of the program was to measure pressures on one rotor blade and also on the horizontal stabilizer. This was the first airloads test of a six-bladed rotor. A photograph of the test aircraft is shown in figure A-31.

The test is described in Beno (1970a) and the flight test data are provided in a separate volume (Beno, 1970b).

The pressure transducers were installed on one blade as shown in figure A-32. The chordwise distribution and number of pressure transducers are provided in table A-21. The transducer arrangement is similar to that used on the NH-3A compound airloads test with a mixture of instrumented radial stations that used five chordwise measurement locations and single transducers at  $0.09c$  at other radial locations. This test included one more single transducer location at  $0.55R$ . The chordwise distribution and number of pressure transducers on the horizontal stabilizer are given in table A-22. A general description of the CH-53A rotor is provided in table A-23.

Absolute pressure transducers were used over the forward portion of the blade section (first three chordwise stations) out to  $0.95R$  to avoid structural problems. The absolute pressure transducer measurements were processed separately in the data reduction process with the calculation of the differential pressure delayed until the final step. Differential pressure measurements were obtained at the rear two chordwise locations at each radial station as well as all chordwise locations on the tip cap ( $0.98R$ ). Differential pressure transducers were used for all of the horizontal stabilizer measurements.



Figure A-31. CH-53A airloads test aircraft (Beno, 1973).

A fairing was used around the airfoil for the pressure transducer installation. The fairing extended on the lower surface from the trailing edge to the leading edge and then around to about  $0.50c$  on the upper surface. The fairing thickness was  $0.050$  in. (about 2.5 percent of the section thickness) and was  $\pm 4$  to  $5$  in. in radial extent (about 22- to 27-percent chord). The fairing was sanded at its juncture with the airfoil to provide a smooth transition. A similar approach was used for the pressure transducers on the horizontal stabilizer.

Flap and chord bending moments, and torsion moments, were measured at the stations shown in table A-24. Additional rotating measurements included blade tension at  $0.167R$ , pitch-link and damper loads, and blade root angles. Four load cells were used to measure the root loads on the horizontal stabilizer. Fuselage accelerations were measured with 19 accelerometers.

The rotating measurements were brought down to the flight recorder through slip rings and a “burst” of approximately 30 revolutions of data were recorded on a 14-track FM multiplexed analog tape.

The FM tape burst was initially used to create an oscillograph record that was hand checked to assess the adequacy of the data and determine the best cycles for subsequent data reduction. The FM tape was then digitized in a ground station at 72 samples/revolution, one FM track at a time, and written to a digital tape (all 30 revolutions). Subsequently, one cycle was selected and a final calibrated digital tape was written that was used for subsequent calculations and the published tables.

The normal forces at the five radial stations were obtained using Gaussian integration. In those cases with failed pressure transducers, an averaged quadratic integration was used. No calculations of pitching moment were made.

Most of the flight test conditions obtained during the test program were for level flight at two gross weights



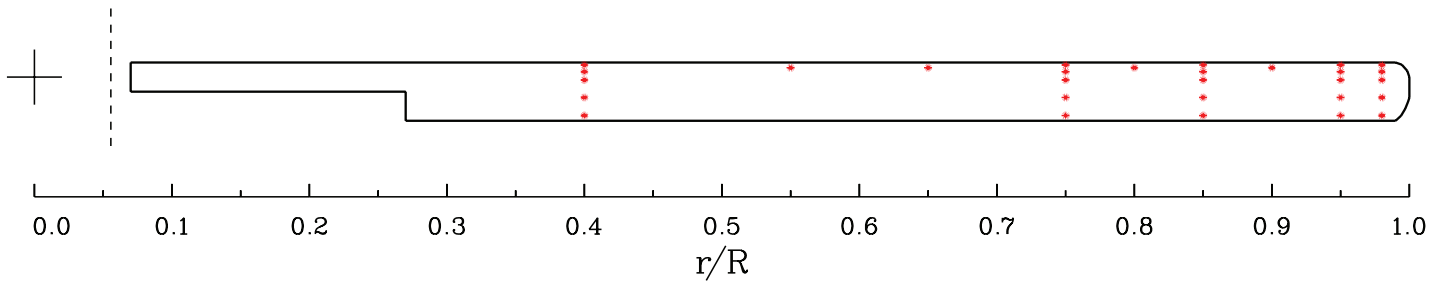


Figure A-32. CH-53A blade planform showing locations of pressure transducers at five radial stations.

TABLE A-21. LOCATIONS OF PRESSURE TRANSDUCERS ON THE CH-53A ROTOR (ONE BLADE)

Radial	Chordwise	
	No.	
0.40, 0.75, 0.85, 0.95, 0.98	5	0.042, 0.158, 0.300, 0.600, 0.910
0.25, 0.55, 0.65, 0.80, 0.90	1	0.09

TABLE A-22. LOCATIONS OF PRESSURE TRANSDUCERS ON THE CH-53A HORIZONTAL STABILIZER

Span	Chordwise	
	No.	
0.33, 0.60	5	0.042, 0.158, 0.300, 0.600, 0.910

TABLE A-23. CH-53A FLIGHT TEST DESCRIPTION

Test number	8
Sponsor	U. S. Navy
Manufacturer	Sikorsky Aircraft
Number blades	6
Airfoil section	NACA 0011 mod
Blade twist, deg	-6.0
Blade chord, in.	18.3
Rotor diameter, ft	72.0
Rotor solidity	0.1150
Tip speed, ft/sec	709.
Instrumented radial stations	5
Transducers/radial station	5.0
Rotating sensors	109
Test points	56
Harmonic bandwidth	36
Rotating samples	417,875
Test hours	10.8
Test completion	October 1969

and three centers of gravity (c.g.'s). The measured nondimensional weights multiplied by the aircraft load factor,  $n_z C_w / \sigma$ , are shown in figure A-33 as a function of advance ratio,  $\mu$ , and are compared with the McHugh thrust boundary and the line of incipient dynamic stall. Two test conditions were obtained at a  $60^\circ$  bank angle in a right turn, and these are shown in the figure as solid red circles. An examination of one of these cases (Beno, 1973) clearly shows two cycles of dynamic stall in the fourth quadrant (based on flow separation at the most aft pressure transducers), but the data from McHugh (1978) indicates that there should be no stall in this case. This suggests that the McHugh results may not apply to all rotors, and this may be especially true for the high-solidity CH-53A rotor.

As discussed in the NH-3A compound airloads test description, Beno (1973) obtained a contract from NASA at Langley Research Center to reanalyze flight test data from the NH-3A and CH-53A to better understand high-frequency blade loading. The original FM flight test tapes were reprocessed so as to provide 36 harmonics of data and plotted on oscillograph rolls. Based on the resulting time histories, Beno selected two cases from the CH-53A tests

(and four from the NH-3A test). These two cases are indicated by a dashed open circle in figure A-33. One was the highest speed case, but at a low blade loading ( $\mu = 0.38$ ,  $C_w / \sigma = 0.057$ ). The other was the most severe banked turn case ( $\mu = 0.24$ ,  $n_z C_w / \sigma = 0.099$ ). For the banked turn, Beno also digitized a cycle of the level flight entry to the turn as well as a cycle in transition.

Beno digitized the oscillograph rolls at 72 samples/revolution, but did not digitize all parameters. He processed all of the differential and absolute pressures at  $0.75R$ ,  $0.85R$ , and  $0.95R$  (see figure A-32). He also digitized the flap bending and chord bending moments at three radial stations, the torsion moments at two radial stations, and the pitch-link load. He calculated the normal forces using Gaussian quadrature (as was done in Beno, 1970b) and also calculated the pitching moments using trapezoidal integration.

TABLE A-24. STRAIN-GAUGE BRIDGE LOCATIONS ON CH-53A ROTOR (ONE BLADE)

Measurement	$r/R$
Flap bending moment	0.167, 0.190, 0.488, 0.571, 0.683, 0.794, 0.906
Chord bending moment	0.167, 0.190, 0.488, 0.571, 0.683, 0.794, 0.906
Torsion moment	0.167, 0.683

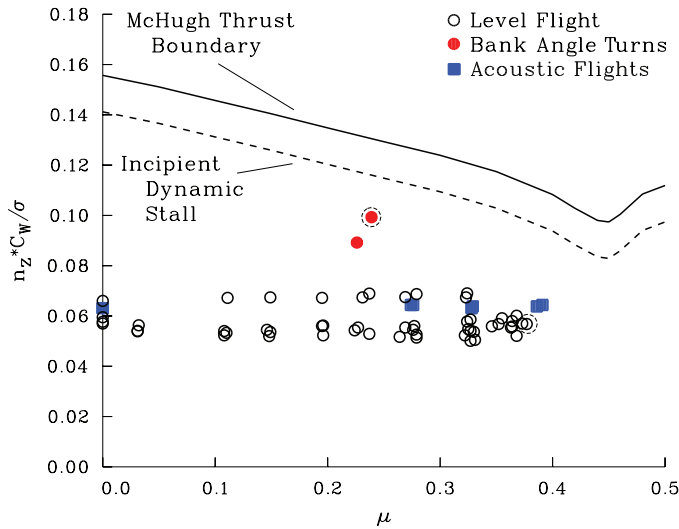


Figure A-33. CH-53A airloads flights nondimensional weight as a function of advance ratio compared to McHugh's (1978) thrust boundary. Dashed circles represent test points reanalyzed by Beno (1973).

Beno focused his analysis on the torsional loads, but it is not clear how much of that loading was related to non-linear effects of stall, blade vortex intersections, or other factors. The analytical results in his study did not provide much insight.

Sikorsky Aircraft obtained a contract from the U.S. Army Aviation Materials Laboratory (AVLABS) to extend the CH-53A flight testing to obtain acoustic measurements (Bausch et al., 1971). They flew the test aircraft on 15 Oct 1969, 5 days after the Navy contract was complete. They flew both hover (200 feet above the ground) and forward flight (1,000-foot altitude) and recorded both the blade pressures measured on the aircraft and the acoustics measured with the ground microphones.

They digitized the flight test data using a 2.5° azimuth stepsize (compared to the 5° stepsize used by Beno, 1970a) and retained the steady and first 30 harmonics. Of these tests, the data from three hover cases and six forward flight cases were included in an appendix to the Bausch report (the closed squares shown in figure A-33).

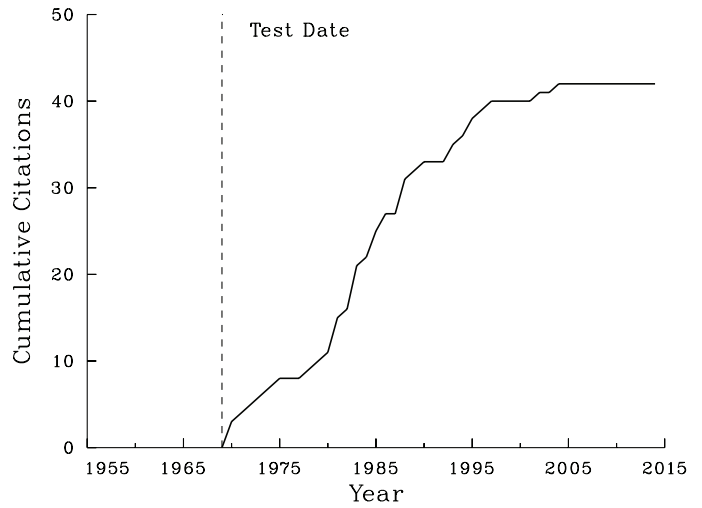


Figure A-34. Cumulative citations of the data obtained from the CH-53A airloads flight test (Beno, 1970a,b).

The cumulative citations based on the CH-53A airloads flight test are shown in figure A-34. There has been continuous use of these data, both the airloads and the structural loads, since the publication of the flight test data in 1970 through the mid-1990s, most of it by Sikorsky Aircraft investigators. They have used the airloads to examine both the aerodynamic loading on the stabilizer and to assess the accuracy of dynamic stall models.

### AH-1G/Operational Loads Survey

The AH-1G/Operational Loads Survey,<sup>3</sup> or AH-1G/OLS for short, was the most ambitious airloads test of its time. In addition to pressure transducers, other flow measuring devices were installed on the blade that could determine flow angularity and other details of the boundary layer. A hot-wire array was used to locate the stagnation point. Moreover, extensive measurements were obtained of blade and fuselage loads and accelerations. The test program was funded by the U.S. Army Air Mobility R&D Laboratory (AMRDL) at Fort Eustis (formerly known as AVLABS). A photograph of the AH-1G/OLS test aircraft is shown in figure A-35.

A summary of the test program is provided by Shockey et al. (1976). Shockey et al. (1977) contains the final report for the program. No tabulated data were included in either report.

<sup>3</sup> The original report (Shockey et al., 1977) describes the test as "Aerodynamic and Structural Loads Survey." The title "Operational Loads Survey," as it is known today, was used internally (for instance, in the data set-up sheets). The first published use is apparently in Van Gaasbeek and Austin (1978).



Figure A-35. AH-1G/OLS airloads test aircraft (Merkley et al., 1983).

TABLE A-25. COMPARISON OF AH-1G PRODUCTION AND GLOVED BLADE AIRFOIL SECTION MEASUREMENTS (SHOCKEY ET AL., 1977)

Measurement	Production	Gloved Blade
Chord, in	27.00	28.63
T.E. extension, in.	0.00	1.50
Thickness, in.	2.52	2.78
Thickness ratio, %	9.33	9.71
L.E. ratio, %	1.299	1.596

TABLE A-26. LOCATIONS OF ABSOLUTE PRESSURE TRANSDUCERS ON THE AH-1G/OLS ROTOR (ONE BLADE); UPPER AND LOWER SURFACE LOCATIONS ARE THE SAME

Radial	Chordwise	
	No.	
0.400	7	0.01, 0.03, 0.08, 0.25, 0.45, 0.70, 0.92
0.600	10	0.01, 0.03, 0.08, 0.15, 0.25, 0.35, 0.45, 0.55, 0.70, 0.92
0.750, 0.955	12	0.01, 0.03, 0.08, 0.15, 0.20, 0.25, 0.35, 0.40, 0.45, 0.55, 0.70, 0.92
0.864	14	0.01, 0.03, 0.08, 0.15, 0.20, 0.25, 0.35, 0.40, 0.45, 0.50, 0.55, 0.60, 0.70, 0.92

The U.S. Army AMRDL funded Bell Helicopter Textron for a series of experiments prior to the airloads test to verify that the new measurement techniques would work. A boundary layer button (BLB) was developed to measure flow direction and velocity within the boundary layer. At the same time, surface-mounted hot wire measurements were tested to locate the leading edge stagnation location (Tanner and Van Wyckhouse, 1968; Burpo and Tanner, 1968). These devices were then installed at one radial station on a UH-1H rotor and were tested in the NASA/Ames 40- by 80-Foot Wind Tunnel (Bowden and Shockey, 1970). The latter test also demonstrated that absolute pressure transducer measurements were essential to understanding supercritical flows on the upper and lower blade surfaces.

Bell solved the problem of installing pressure and other flow measurements on the blade by taking a “gloved blade” approach. A glove was added to the entire blade, and all transducers and wiring were contained between the glove and the production blade section. The dimensions of the gloved blade airfoil section are compared with the production blade in table A-25. Both airfoil sections were symmetric. As the gloved blade was 40 pounds heavier than the production blade, modifications were made to various blade weights to provide appropriate balancing. The natural frequencies of the gloved blades were close to the production blades.

Absolute pressure transducers were installed on one blade at five radial stations as shown in figure A-36. The chordwise distribution and number of pressure transducers are provided in table A-26. A general description of the AH-1G/OLS test is given in table A-27.

The BLBs were made of two total pressure tubes, each connected to a differential pressure transducer. Each of the miniature total pressure tubes was oriented at 45° to the chordline (hence 90° apart). Six BLBs were installed at each of the five radial stations on the opposite blade, three on the upper surface at 0.30c, 0.60c, and 0.90c, and three on the lower surface at the same chordwise locations.

Hot-wire arrays were mounted at the leading edge of the airfoil at the five radial stations where the absolute pressure transducers were located, but again on the opposite blade. Depending on radial location, between 10 and 19 elements were used to provide an estimate of the stagnation point.

Flap and chord bending moments, and torsion moments, were measured on both the blade and yoke as shown in table A-28. The inboard measurements at 0.023R and 0.045R are on the blade yoke. The most inboard yoke measurement was also measured on the opposite blade.

The AH-1G/OLS test was the first to use miniature accelerometers bonded to the blade and yoke. Accelerometers were installed to measure both flap and chord accelerations and were located as shown in table A-29.

Additional rotating measurements were obtained including both pitch-link loads, mast torque and bending, tail rotor torque, drag brace force, and blade flapping and feathering. In the fixed system, 23 fuselage and pylon accelerations were measured.

There were a total of 314 rotating system measurements. The signals were conditioned in a multiplex bucket (mux bucket) mounted on the main rotor trunion. In the

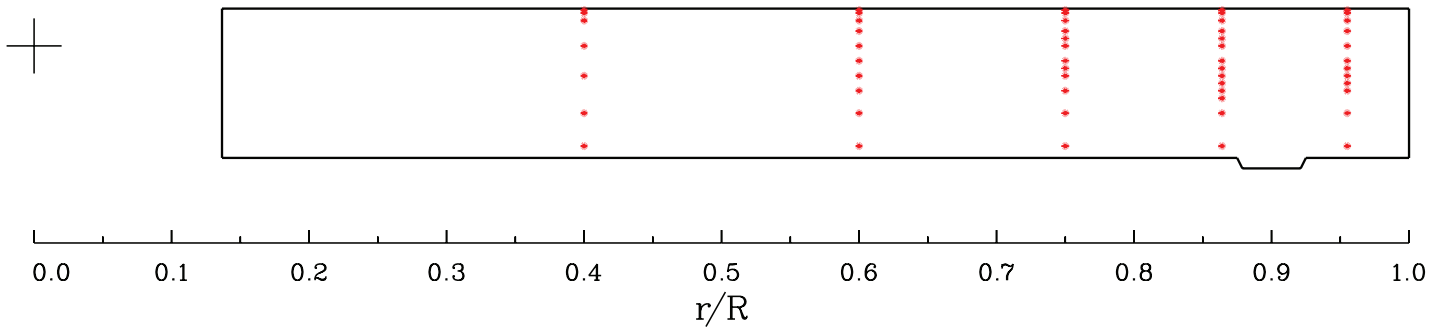


Figure A-36. AH-1G/OLS blade planform showing locations of absolute pressure transducers at five radial stations.

bucket, they were multiplexed into 20 16-band data channels using frequency modulation. The multiplexed data were passed down through 120-channel slip rings and recorded on a 28-track FM recorder. The flight test analog tapes were then converted to digital tapes on a ground station.

Acoustic measurements were obtained during portions of the AH-1G/OLS test. Five airborne microphones were mounted on the aircraft fuselage and were recorded on board the aircraft. A ground acoustic measurement system included three microphones in an array perpendicular to the aircraft flightpath. One microphone was in the aircraft flightpath and the other two were 500 feet to either side.

Figure A-37 shows the measured nondimensional aircraft weight multiplied by load factor,  $n_z C_w / \sigma$ , as a function of advance ratio,  $\mu$ , and compared with the McHugh thrust boundary and the line of incipient dynamic stall. Most level flight conditions were at either 8,100 or 9,000 pounds, hence there is only limited variation in the weight coefficient. Three unsteady maneuver cases are shown in the figure, and two of these should show nonlinear blade stall characteristics as they penetrated beyond the McHugh thrust boundary.

Sample results are provided in Shockey et al. (1977) for the aerodynamic measurements in about 10 figures and acoustic measurements in 2 figures. No tabulated data are included in the report.

The cumulative citations based on the AH-1G/OLS airloads flight test are shown in figure A-38. This data set was used extensively into the early 1990s. The primary use in the initial years was of the airload and acoustic data. Data were extracted from the aircraft and ground-acoustic measurements in internal Bell Helicopter Textron documents. Some of these data were compared with calculations by Nakamura (1982) and separately by Succi (1983) and various coauthors.

Later, vibration and loads data were used as part of the Design Analysis Methods for Vibrations (DAMVIBS). This included tabulated structural load and vibration data

TABLE A-27. AH-1G/OLS FLIGHT TEST DESCRIPTION

Test number	9
Sponsor	U. S. Army
Manufacturer	Bell Helicopter
Number blades	2
Airfoil section	9.7% symmetric
Blade twist, deg	-10.0
Blade chord, in.	28.6
Rotor diameter, ft	44.0
Rotor solidity	0.0690
Tip speed, ft/sec	746.
Instrumented radial stations	5
Transducers/radial station	11.0
Rotating sensors	280
Test points	238
Harmonic bandwidth	37
Rotating samples	4,931,360
Test hours	-
Test completion	April 1976

TABLE A-28. STRAIN-GAUGE BRIDGE LOCATIONS ON AH-1G/OLS BLADE AND YOKE (ONE BLADE)

Measurement	$r/R$
Flap bending moment	0.023, 0.045, 0.200, 0.300, 0.400, 0.500, 0.600, 0.700, 0.800, 0.900
Chord bending moment	0.023, 0.045, 0.200, 0.300, 0.400, 0.500, 0.600, 0.700, 0.800, 0.900
Torsion moment	0.023, 0.300, 0.500, 0.700, 0.900

(Dompka and Cronkhite, 1986) that were used extensively in the DAMVIBS program (Kvaternik, 1993, and others). These data were also used in a series of papers by Yeo and Chopra (see for instance, Yeo and Chopra, 2001a,b).



TABLE A-29. ACCELEROMETER LOCATIONS ON AH-1G/OLS BLADE AND YOKE (ONE BLADE)

$r/R$
0.013, 0.042, 0.061, 0.142, 0.227, 0.309, 0.390, 0.500, 0.700, 0.902, 0.996

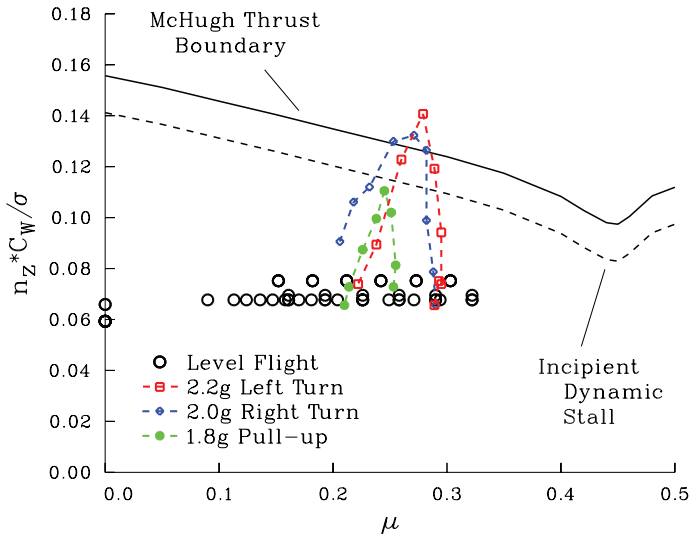


Figure A-37. AH-1G/OLS nondimensional weight as a function of advance ratio compared to McHugh's (1978) thrust boundary.

The original purpose of the test program was to provide the U.S. Army with an analog and digital tape library of all of the flight test data (Shockey et al., 1977). There were 175 digital tapes in this library and in the initial years after the test, the access was difficult (Don Merkley, *pers. comm.*) The Army funded Bell to develop tools that would make the process easier, and they created a software interface that came to be known as DATAMAP (Philbrick and Eubanks, 1979; Philbrick, 1980). DATAMAP improved the ease of access and data use. But eventually the large machines required to read the digital tapes became obsolete, and subsequently the tapes were abandoned. The only published data that remain are the structural loads and vibration data used for the DAMVIBS Program (Dompka and Cronkhite, 1986). Limited pressure data may still remain in internal reports at Bell Helicopter Textron.

### AH-1G/Tip Aerodynamics and Acoustics Test

The AH-1G/Tip Aerodynamics and Acoustic Test, shortened to AH-1G/TAAT or just TAAT, was a follow-on to the AH-1G/OLS airloads test using, for the most part, the same measurement systems. The test program was funded and conducted at the NASA Ames Research Center. A photo of the TAAT rotor flown on the NASA AH-1G is shown in figure A-39.

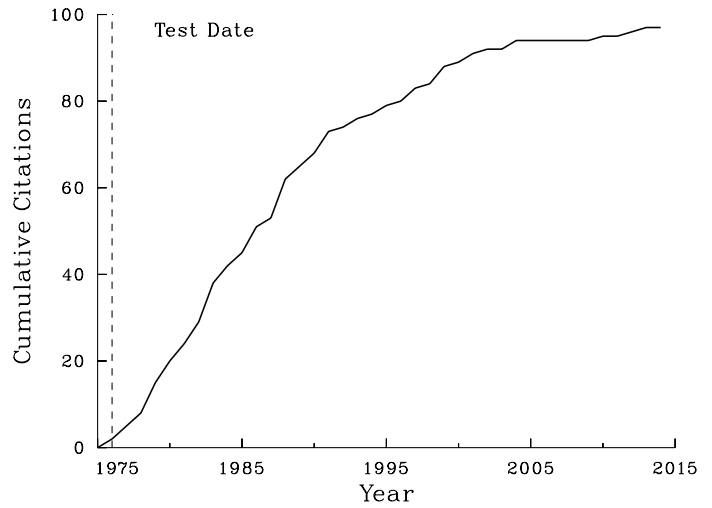


Figure A-38. Cumulative citations of the data obtained from the AH-1G/OLS airloads flight test (Shockey et al., 1977).

A summary of the test program was provided in Cross and Watts (1988). Data for six level flight and five descent cases was published in Cross and Tu (1990).

The aircraft used in the program was called the "White Cobra." This aircraft was the first production AH-1G, serial number 20004 (Cross and Watts, 1988). It had been used in a number of research programs at NASA Langley; see, for example, Morris (1978), which summarizes tests of three different airfoil sections on the aircraft. The White Cobra was moved to NASA Ames in the late 1970s as part of a NASA reorganization that consolidated rotary wing flight testing at Ames (Ward, 2010).

NASA Ames employed the same blade and instrumentation approach that was used for the AH-1G/OLS test program. Because the objectives of the program were more closely focused on blade tip aerodynamics and acoustics (Snyder et al., 1990), absolute pressure transducers were added at three additional radial stations, 0.91R, 0.97R, and 0.99R (compare figure A-40 with figure A-36). The pressure transducer locations for the modified installation are shown in table A-30. The total number of pressure transducers increased from 110 to 188. Prior to the flight test program, all of the transducers flown in the AH-1G/OLS program were removed from the blade, tested, recalibrated and reinstalled.

The other blade aerodynamic measurements on the blade were the same as used on the AH-1G/OLS test, that is the BLBs and leading edge hot-wire arrays, but they were reduced in number. The BLBs were made of two total pressure tubes, each connected to a differential pressure transducer. Each of the miniature total pressure tubes was oriented at 45° to the chordline (hence 90° apart). Six BLBs were installed at each of three radial stations (0.750R, 0.866R,



Figure A-39. AH-1G/TAAT airloads test aircraft (courtesy of NASA Ames Research Center).

TABLE A-30. LOCATIONS OF ABSOLUTE PRESSURE TRANSDUCERS ON THE AH-1G/TAAT ROTOR (ONE BLADE); UPPER AND LOWER SURFACE LOCATIONS ARE THE SAME

Radial	Chordwise	
	No.	Stations
0.400	7	0.01, 0.03, 0.08, 0.25, 0.45, 0.70, 0.92
0.600	10	0.01, 0.03, 0.08, 0.15, 0.25, 0.35, 0.45, 0.55, 0.70, 0.92
0.750, 0.955	12	0.01, 0.03, 0.08, 0.15, 0.20, 0.25, 0.35, 0.40, 0.45, 0.55, 0.70, 0.92
0.864, 0.970, 0.990	14	0.01, 0.03, 0.08, 0.15, 0.20, 0.25, 0.35, 0.40, 0.45, 0.50, 0.55, 0.60, 0.70, 0.92
0.910	13	0.01, 0.03, 0.08, 0.15, 0.20, 0.25, 0.35, 0.40, 0.45, 0.50, 0.55, 0.60, 0.70

and 0.955R) on the opposite blade, three on the upper surface at 0.30c, 0.60c, and 0.90c, and three on the lower surface at the same chordwise locations.

Hot-wire arrays were mounted at the leading edge of the airfoil at the same radial stations as the BLBs, again on the opposite blade. The most inboard array used 9 elements, and the 2 outer arrays used 19 elements.

A general description of the AH-1G/TAAT aircraft and test is provided in table A-31.

Flap and chord bending moments, and torsion moments, were measured on both the blade and yoke as shown in table A-32. The inboard measurements at 0.023R and 0.045R are

TABLE A-31. AH-1G/TAAT FLIGHT TEST DESCRIPTION

Test number	10
Sponsor	U. S. Army
Manufacturer	Bell Helicopter
Number blades	2
Airfoil section	9.7% symmetric
Blade twist, deg	-10.0
Blade chord, in.	28.6
Rotor diameter, ft	44.0
Rotor solidity	0.0690
Tip speed, ft/sec	746.
Instrumented radial stations	8
Transducers/radial station	11.8
Rotating sensors	305
Test points	292
Harmonic bandwidth	37
Rotating samples	6,590,440
Test hours	26.3
Test completion	July 1981

on the blade yoke. The most inboard yoke measurement was also measured on the opposite blade.

Miniature accelerometers were bonded to the blade and yoke. These accelerometers, also reduced in number from the OLS test, measured both flap and chord accelerations. The locations are shown in table A-33.

Additional rotating measurements were obtained including both pitch-link loads, mast torque and bending, tail rotor torque, and drag brace force.

A multiplex bucket (mux bucket) was mounted on the main rotor trunion and provided a maximum of 314 rotating system measurements. The signals were conditioned in the mux bucket and multiplexed into 20 16-band data channels using frequency modulation. The multiplexed data were passed down through 120-channel slip rings and recorded on a 28-track FM recorder.

Because the TAAT test added an additional 78 absolute pressure transducers, it was necessary to remove other measurements to stay within the 314 parameter limit. Most of the excised measurements were inboard BLBs, hot-wire arrays, and blade accelerometers.

The analog flight tapes from the AH-1G were digitized at Bell Helicopter Textron. There were a total of 23 analog flight tapes from the test program. Digitization expanded the number of tapes to 350.

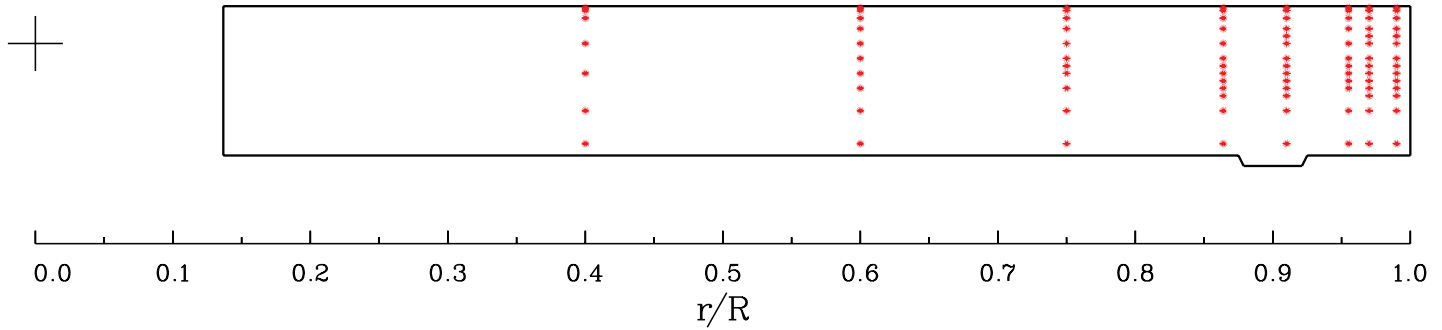


Figure A-40. AH-1G/TAAT blade planform showing locations of absolute pressure transducers at eight radial stations.



Figure A-41. AH-1G/TAAT airloads test aircraft trailing the YO-3A (courtesy of NASA Ames Research Center).

Two approaches were taken to measure the rotor acoustics. The first was to obtain in-flight measurements using the YO-3A Acoustic Research Aircraft as a microphone platform as shown in figure A-41. The YO-3A is a powered glider specifically designed to have a low acoustic signature. The in-flight acoustic measurement technique was pioneered by Schmitz and Boxwell (1976) and Boxwell and Schmitz (1980).

The second approach used ground-based microphones. Three microphones were mounted in a standard Federal Aviation Administration (FAA) array on a line perpendicular to the flightpath with one microphone on the centerline and the other two 150m to each side. Two additional microphones were installed on 40-foot towers instead of the 4-foot towers of the primary array. One was mounted to the right and the other on the centerline.

Both of the acoustic measurement approaches recorded acoustic data to analog tapes using the same formats. Selected test points were digitized at NASA Langley (Cross and Watts, 1988).

TABLE A-32. STRAIN-GAUGE BRIDGE LOCATIONS ON AH-1G/TAAT BLADE AND YOKE (ONE BLADE)

Measurement	$r/R$
Flap bending moment	0.023, 0.042, 0.227, 0.311, 0.390, 0.500, 0.701, 0.803, 0.902
Chord bending moment	0.023, 0.042, 0.227, 0.311, 0.390, 0.500, 0.701, 0.803, 0.902
Torsion moment	0.023, 0.311, 0.500, 0.701, 0.902

TABLE A-33. ACCELEROMETER LOCATIONS ON AH-1G/TAAT BLADE AND YOKE (ONE BLADE)

$r/R$
0.013, 0.500, 0.591, 0.697, 0.902, 0.996

The AH-1G/TAAT tests were organized in four phases. Phase I (performance) examined steady level flight conditions that matched the OLS test data. These also included a limited number of steady turns. For the Phase II (In-flight Acoustics) the TAAT aircraft flew in formation with the YO-3A in both level flight and for a range of descent conditions. Ground-acoustic or flyover testing (Phase III) over the ground microphones also included both level flight and descent cases. Phase IV testing was a detailed Aerodynamic Survey that attempted to match specific  $\mu$  and  $C_w$  conditions based on measurements of pressure, temperature, and fuel burnoff.

Figure A-42 shows the measured nondimensional weight multiplied by aircraft load factor,  $n_z C_w / \sigma$ , as a function of advance ratio,  $\mu$ , for the four phases, and these are compared with the McHugh thrust boundary and the line of incipient dynamic stall. The majority of the data are for steady level flight with a range of  $0.056 \leq C_w / \sigma \leq 0.095$ . The four steady-turn cases may have encountered stall.



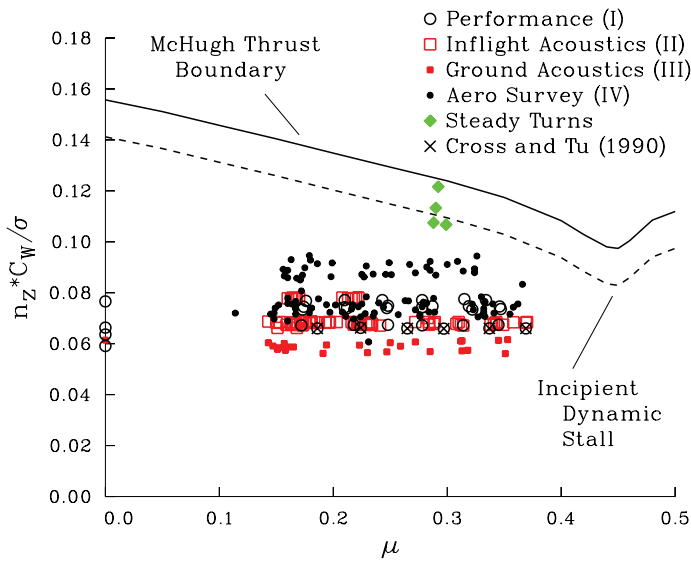


Figure A-42. AH-1G/TAAT nondimensional weight as a function of advance ratio compared to McHugh's (1978) thrust boundary.

Sample aerodynamic results are provided by Cross and Watts (1988) in about 159 figures for 7 flight conditions. Cross and Tu (1990) tabulate the steady and first 15 harmonics of pressures, moments, and accelerations on the blade for 6 level flight cases and 5 descent cases.

The cumulative citations on the AH-1G/TAAT airloads flight test are shown in figure A-43. About a quarter of these citations were published before the test report (Cross and Watts, 1988). Some of these early citations included papers that used TAAT data for correlation; NASA helped individuals acquire these data early in the publication process. From 1985 to the present there has been continuous use of some of the data that was published by Cross and Tu (1990), particularly the lowest speed level flight condition.

The development of DATAMAP (Philbrick, 1980) made the use of the 350 TAAT digital tapes easier than had been the case in the first years after the OLS data became available. But problems with maintaining the large tape machines needed to read these tapes, and the related difficulties of housing such a quantity of tapes, became overwhelming. Both the machines and the tapes were abandoned. Except for the six level flight cases ( $0.19 \leq \mu \leq 0.38$ ) and five descent cases at  $\mu = 0.22$  (level flight to 800 ft/min rate of descent) published in Cross and Tu (1990), none of the data remain.

### UH-60A Airloads Program Flight Test

In the mid-1980s, NASA proposed an extensive series of tests of recently developed helicopter rotors (Watts and Cross, 1986). The "Modern Technology Rotors Program"

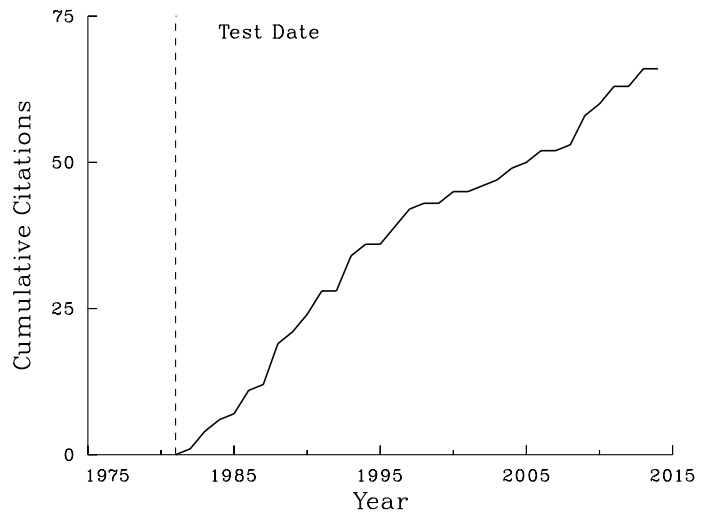


Figure A-43. Cumulative citations of the data obtained from the AH-1G/TAAT airloads flight test (Cross and Watts, 1988).

would include flight and wind tunnel tests at both full scale and model scale. Auxiliary tests would include fuselage shake tests and other tests to define the rotor characteristics. The first of the tests under the program was the UH-60A. The test program was funded and conducted at NASA Ames Research Center. A photo of the flight test aircraft is shown in figure A-44.

The flight test program has been described in a series of papers (Kufeld et al., 1994b; Balough, 1994; Coleman and Bousman, 1994; Kufeld et al., 1994a; Studebaker, 1994) and these papers have included representative results. A systematic description of the majority of test points obtained is in Bousman and Kufeld (2005). The data are stored at NASA Ames Research Center in a database (Bjorkman and Bondi, 1990). The data continue to be available to approved investigators.

The flight test rotor included a pressure blade with 242 absolute pressure transducers, a strain-gauge blade with both strain gauges and accelerometers, and two standard blades. The instrumented blades were built by Sikorsky Aircraft and delivered to NASA in late 1988. Figure A-45 shows an upper view of the layout of the pressure transducers on the pressure blade. The pressure transducer locations for the nine radial arrays are shown in table A-34. The locations for the BVI arrays are shown in table A-35. Although not readily discernible in figure A-45, some pressure transducers near the leading edge at  $0.775R$ ,  $0.865R$ , and  $0.92R$  were shifted inboard radially on the upper and lower surfaces by about 0.5 in. ( $0.0016R$ ). On the upper surface, the transducers at  $0.010c$ ,  $0.049c$ , and  $0.107c$  were shifted inboard, whereas on the lower surface the shifted transducers were located at  $0.030c$  and  $0.080c$ .





Figure A-44. UH-60A flight test aircraft (courtesy of NASA Ames Research Center).

The pressure blade included 50 distributed temperature measurements to allow temperature compensation of the pressure measurements, but the pressure measurements have shown limited sensitivity to temperature changes and compensation has not been used.

A general description of the UH-60A aircraft and test is given in table A-36.

The strain-gauge blade was located opposite to the pressure blade and included flap and chord bending moment and torsion moment measurements at the radial stations given in table A-37. The inboard flap and chord bending measurements at  $0.113R$  were on the blade root outboard of the grip, and the rest of the moment measurements were on the blade spar (installed before final assembly of the blade). The same inboard flap and chord bending measurements at  $0.113R$  were also obtained on the pressure blade.

Accelerometers were installed at four radial stations in the strain-gauge blade before final assembly. At each station, two accelerometers measured flapping accelerations and one accelerometer measured lead-lag (chordwise)

TABLE A-34. LOCATIONS OF ABSOLUTE PRESSURE TRANSDUCERS' RADIAL ARRAYS ON THE UH-60A PRESSURE BLADE (UPPER AND LOWER SURFACE TRANSDUCER LOCATIONS SHOWN SEPARATELY WHEN DIFFERENT)

Radial	Chordwise	
	No.	
0.225, 0.400, 0.550, 0.675	10	0.010, 0.049, 0.107, 0.164, 0.203, 0.250, 0.395, 0.607, 0.818, 0.939
0.775	12	0.010, 0.030, 0.049, 0.080, 0.107, 0.164, 0.203, 0.250, 0.395, 0.607, 0.818, 0.939
0.865U, 0.920U, 0.965, 0.990	15	0.010, 0.030, 0.049, 0.080, 0.107, 0.164, 0.203, 0.250, 0.320, 0.395, 0.450, 0.530, 0.607, 0.818, 0.939
0.865L	13	0.010, 0.030, 0.049, 0.080, 0.107, 0.164, 0.203, 0.250, 0.320, 0.395, 0.607, 0.818, 0.939
0.920L	14	0.010, 0.030, 0.049, 0.080, 0.107, 0.164, 0.203, 0.250, 0.320, 0.395, 0.450, 0.607, 0.818, 0.939

acceleration. The two accelerometers that measured flapping accelerations were located on both sides of the blade elastic axis such that differencing of the signals provided torsion acceleration. The four stations used were  $0.300R$ ,  $0.500R$ ,  $0.700R$ , and  $0.900R$ .

External accelerometers were also placed at two radial locations on three of the blades to measure flapping acceleration that could be used in blade motion studies (Balough, 1994). These accelerometers were located at  $0.112R$  and  $0.964R$  (within the tip cap).

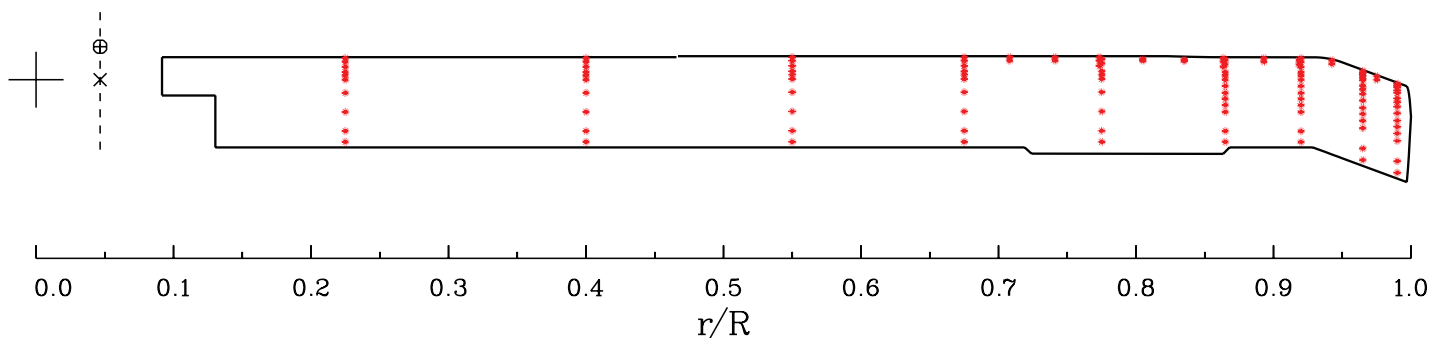


Figure A-45. Upper surface of UH-60A pressure blade, showing nine radial arrays and leading edge transducers at seven other radial stations to characterize BVI interactions.

TABLE A-35. LOCATIONS OF ABSOLUTE PRESSURE TRANSDUCERS' BVI ARRAYS ON THE UH-60A BLADE (UPPER AND LOWER SURFACE TRANSDUCER LOCATIONS SHOWN SEPARATELY WHEN DIFFERENT)

Radial	Chordwise	
	No.	
0.708U, 0.741U, 0.891U, 0.943U, 0.975U	2	0.010, 0.049
0.708L, 0.741L, 0.805L, 0.835L, 0.891L, 0.943L, 0.975L	1	0.049
0.805U, 0.835U	2	0.030, 0.049

TABLE A-36. UH-60A FLIGHT TEST DESCRIPTION

Test number	11
Sponsor	NASA, U.S. Army
Manufacturer	Sikorsky Aircraft
Number blades	4
Airfoil section	SC1095, SC1094R8
Blade twist, deg	-16.0 (nonlinear)
Blade chord, in.	20.8
Rotor diameter, ft	53.7
Rotor solidity	0.0826
Tip speed, ft/sec	719.
Instrumented radial stations	9
Transducers/radial station	12.3
Rotating sensors	361
Test points	962
Harmonic bandwidth	120
Rotating samples	126,453,472
Test hours	57
Test completion	February 1994

Additional rotating system measurements included the pitch-link and damper loads on all four blades, blade root angles on all four blades, the hub-mounted bifilar vibration absorber accelerations, mast torque and bending, and three components of hub acceleration. Fixed-system fuselage accelerations were measured with 32 accelerometers.

All of the rotor rotating signals were conditioned in the Rotating Data Acquisition System (RDAS) that was bolted to the top of the rotor hub (see figure A-44). The digitized signals were combined into 10 pulse code modulation (PCM) streams that were brought down to the aircraft

TABLE A-37. RADIAL LOCATIONS OF STRAIN-GAUGE BRIDGE LOCATIONS ON UH-60A STRAIN-GAUGE BLADE

Measurement	<i>r/R</i>
Flap bending moment	0.113, 0.200, 0.300, 0.400, 0.500, 0.600, 0.700, 0.800, 0.900
Chord bending moment	0.113, 0.200, 0.300, 0.400, 0.500, 0.600, 0.700, 0.800
Torsion moment	0.300, 0.500, 0.700, 0.900

through slip rings where they were recorded on digital tape. Within the RDAS, there were two primary data rates: nominally 502 samples/rev for the pressure measurements, and 84 samples/rev for the rest of the rotating measurements.

Two sets of acoustic measurements were made during the program: measurements over an array of ground microphones and in-flight measurements using the YO-3A Acoustic Research Aircraft (as was used with the AH-1G/TAAT aircraft, see figure A-41).

Early in the program, researchers from NASA Langley Research Center came west and set up an acoustic array at Crows Landing Airfield (across the Diablo Range from Ames Research Center). The microphone layout used 18 microphones in a T, with 15 of the microphones in the upper bar of the T. All measurements were made as the UH-60A flew perpendicular to the upper bar of the T. Data were obtained for a wide range of level, climb, and descent cases as shown in figure A-46.

The UH-60A acoustic data are classified and are stored at Langley Research Center. The primary papers that reported the use of these data were Muller et al. (1995), Rutledge et al. (1995), and Wilson et al. (1995).

The in-flight acoustic tests used the YO-3A as a microphone platform, just as had been done for the AH-1G/TAAT testing. Figure A-47 shows the flightpath angles and advance ratios obtained during these tests (and compares them to the ground acoustic test points). The in-flight measurements were selected to match as closely as possible those data conditions tested at model scale in the 1989 German-Dutch Wind Tunnel (DNW) test (Yu et al., 1990). The in-flight acoustic data are classified and are controlled by the U.S. Army Aeroflightdynamics Directorate at Ames Research Center.

Figure A-48 provides an overview of the UH-60A Airloads Program flight test measurements. The figure shows the measured nondimensional weight multiplied by aircraft load factor,  $n_z C_w / \sigma$ , as a function of advance ratio,  $\mu$ , and compares these with the McHugh thrust boundary

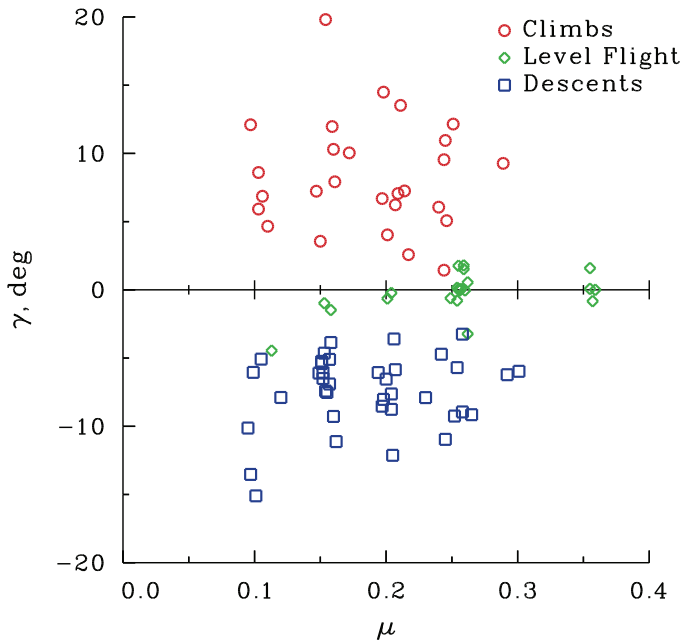


Figure A-46. Flightpath angle as a function of advance ratio for level flight, climbs, and descents during the ground-acoustic testing at Crows Landing Airfield.

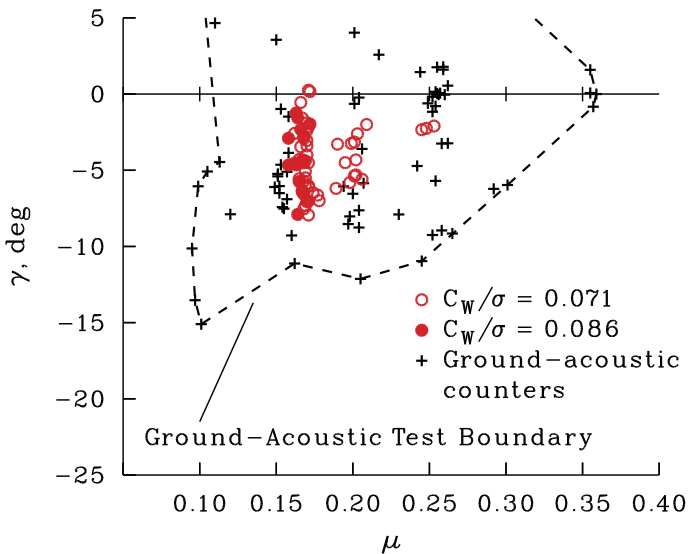


Figure A-47. Flightpath angle as a function of advance ratio for level flight and descent during in-flight acoustic testing.

and the line of incipient dynamic stall. All of the steady level flight cases in the program are shown by open circle symbols. In general, the maximum and minimum advance ratios were limited by engine power. The primary matrix of weight coefficient values were obtained in steps of  $\Delta C_w/\sigma = 0.01$  from 0.08 to 0.13 by flying at progressively higher altitudes to reduce the air density. For the two highest weight coefficients, it was necessary to install the standard UH-60A oxygen kit for the pilots and crew.

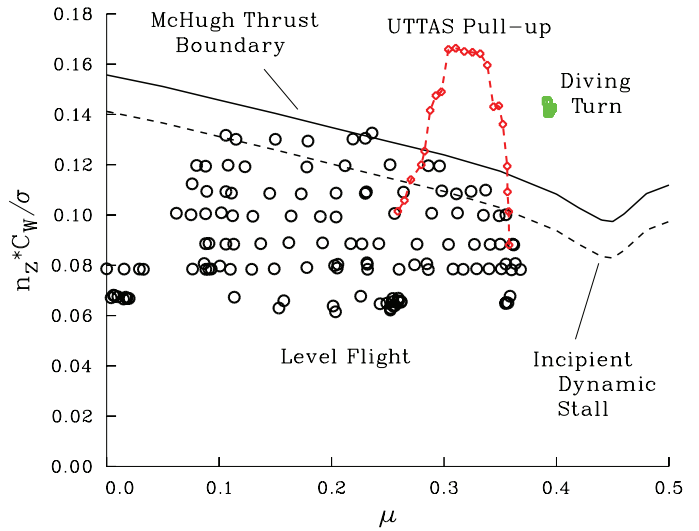


Figure A-48. UH-60A nondimensional weight as a function of advance ratio compared to McHugh's (1978) thrust boundary.

Multiple maneuvers were flown during the test program (Bousman and Kufeld, 2005). Two examples are shown in figure A-48: a relatively steady diving turn, and an unsteady pull-up that approximated the UTTAS pull-up that was a contract guarantee for the UH-60A development.

The primary reports for the test (Kufeld et al., 1994a,b; Coleman and Bousman, 1994; Bousman and Kufeld, 2005) include aerodynamic results in approximately 45 figures.

Cumulative citations of the UH-60A Airloads Program data are shown in figure A-49. The cumulative curve is unlike the other airloads tests in that the number of citations has been increasing with time rather than decreasing. This is probably a consequence of a number of factors, including the start of the Airloads Workshops in 2002, DARPA's Helicopter Quieting Program in 2004, and a National Rotorcraft Technology Center (NRTC) Technical Area of Joint Investigation (TAJI) in aeromechanics that started in 2010.

The inadequacy of digital storage techniques in the 1970s and 1980s that plagued the two AH-1G airloads tests were still troublesome when the UH-60A data were being obtained in 1993. The primary computer used in the flight research organizations at that time was a DEC machine using a VAX operating system. System storage was on large and expensive disk drives. The development of an optical storage system that included 110 optical disks in a "jukebox" was an improvement, and all of the data were stored on the jukebox after being acquired. In subsequent years, the database has gone through three storage media and at least one operating system change. Through 2013, only about 0.3 percent of the database has been lost during

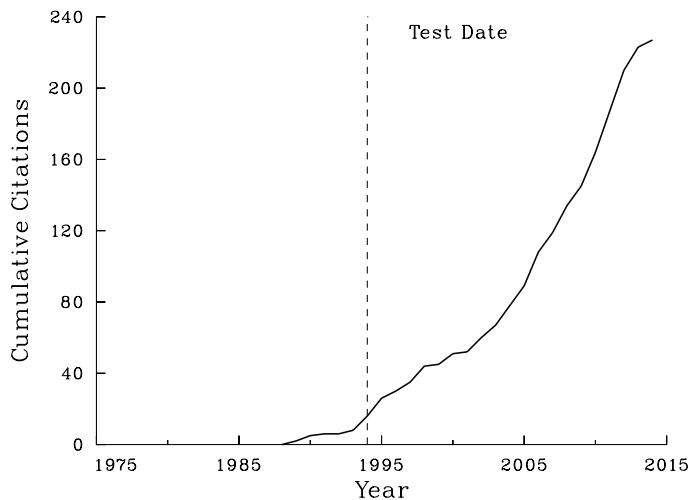


Figure A-49. Cumulative citations of the data obtained from the UH-60A airloads flight test (Kufeld et al., 1994b).



Figure A-50. UH-60A rotor in the NFAC 40- by 80-Foot Wind Tunnel (courtesy of NASA Ames Research Center).

these changes, but the ephemeral nature of electronic storage remains as evidenced in August 2013 when the computer system crashed. Most of these data are available once more in early 2014.

### UH-60A Airloads Wind Tunnel Test

As described in the introductory paragraph of the UH-60A Airloads Program flight test description, NASA proposed a series of tests of recently developed helicopter rotors in the mid-1980s (Watts and Cross, 1986). These tests would use extensive pressure instrumentation on the rotor blades and include both model-scale and full-scale tests. The first rotor selected under this program was the UH-60A rotor. A pressure-instrumented 5.73-scale model was built by Sikorsky Aircraft under a U.S. Army contract from the Aviation Applied Technology Directorate (AATD) at Ft. Eustis, Virginia. After a hover test at Sikorsky (Lorber et al., 1989), the model rotor was tested in the Netherlands in the DNW wind tunnel in 1989 (Yu et al., 1990; Lorber, 1991). A pressure-instrumented full-scale rotor was flight tested at NASA Ames Research Center in 1993–94 (Kufeld et al., 1994b). A planned test of that same pressure-instrumented rotor in the National Full-Scale Aerodynamics Complex (NFAC) 40- by 80-Foot Wind Tunnel at Ames Research Center would complete the first test series.

Before a wind tunnel test of the UH-60A rotor could take place, it was necessary to build a new test stand capable of testing such a large-scale rotor. The new test stand, the Large Rotor Test Apparatus (LRTA), was designed and fabricated by Dynamic Engineering, Inc. for NASA and the U.S. Army, and was delivered in 1995.

The first test of the LRTA was performed in 2001 in the NFAC’s 80- by 120-Foot Wind Tunnel with a UH-60A rotor installed (Norman et al., 2002). The installation included Individual Blade Control (IBC) controls, but did not use the pressure-instrumented blade.

The period from 1990 to 2007 has been characterized as a time of “severe budget pressures” (Ward, 2010), and that period was particularly difficult for aerodynamics and rotary wing programs. In 2003, NASA closed the NFAC, placing it in a mothball status. In 2006, the U.S. Air Force signed an agreement with NASA to reopen the facility. Under that lease, the facility is managed by the Air Force’s Arnold Engineering Development Center. Operational capability was regained in 2008. The first rotor research test to use the LRTA in the reopened NFAC was the Boeing-SMART rotor test (Straub et al., 2009).

The UH-60A pressure-instrumented rotor was tested in the NFAC 40- by 80-Foot Wind Tunnel in 2010. A photograph of the rotor on the LRTA is shown in figure A-50. The primary summary of the test program is in Norman et al. (2011). The tunnel test data are stored at NASA Ames Research Center and are accessible to approved users.

The same instrumented blades used in the flight test were also used in the wind tunnel although with some changes. Figure A-51 shows the layout of the pressure transducers on the upper surface of the pressure blade. The pressure transducer locations for the nine radial arrays are shown in table A-38, and the locations of the BVI arrays are provided in table A-39. Some of the transducers near the leading edge were offset inboard about 0.5 in. ( $0.0016R$ ) because of space limitations. At  $0.775R$  and  $0.865R$ , the offset transducers were at  $0.010c$ ,  $0.049c$ , and  $0.107c$ . At  $0.920R$  the transducers at  $0.030c$  and  $0.080c$  were offset.



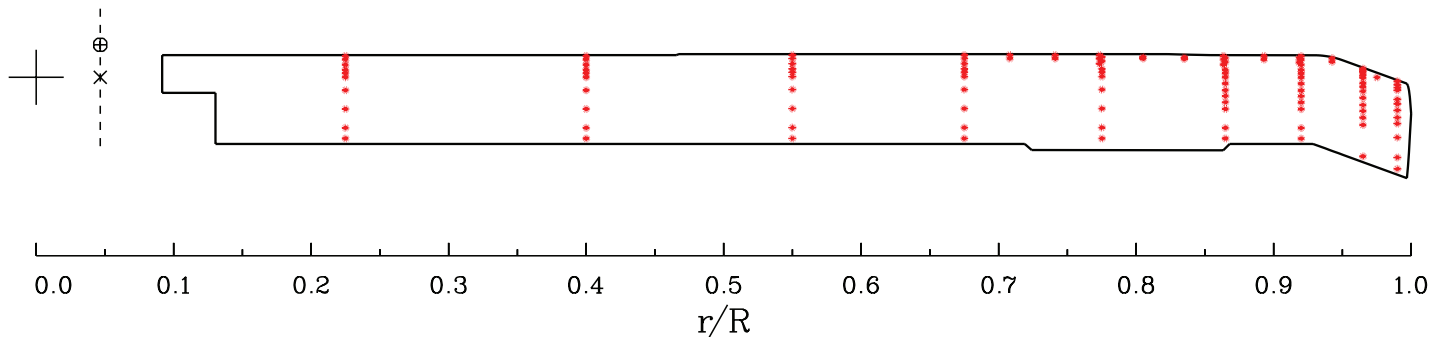


Figure A-51. Upper surface of UH-60A pressure blade, showing nine radial arrays and leading edge transducers at seven other radial stations to characterize BVI interactions.

TABLE A-38. LOCATIONS OF ABSOLUTE PRESSURE TRANSDUCERS' RADIAL ARRAYS ON THE UH-60A BLADE (UPPER AND LOWER SURFACE TRANSDUCER LOCATIONS SHOWN SEPARATELY WHEN DIFFERENT)

Radial	No.	Chordwise
0.225, 0.400, 0.550, 0.675	10	0.010, 0.049, 0.106, 0.164, 0.203, 0.250, 0.395, 0.607, 0.819, 0.939
0.775	12	0.010, 0.030, 0.049, 0.080, 0.106, 0.164, 0.203, 0.250, 0.395, 0.607, 0.819, 0.939
0.865U, 0.920U, 0.990L	15	0.010, 0.030, 0.049, 0.080, 0.106, 0.164, 0.203, 0.250, 0.320, 0.395, 0.450, 0.530, 0.607, 0.819, 0.939
0.865L	13	0.010, 0.030, 0.049, 0.080, 0.106, 0.164, 0.203, 0.250, 0.320, 0.395, 0.607, 0.819, 0.939
0.920L	14	0.010, 0.030, 0.049, 0.080, 0.106, 0.164, 0.203, 0.250, 0.320, 0.395, 0.450, 0.607, 0.819, 0.939
0.965U	14	0.010, 0.030, 0.049, 0.080, 0.106, 0.164, 0.203, 0.250, 0.320, 0.395, 0.450, 0.530, 0.607, 0.939
0.965L	14	0.030, 0.049, 0.080, 0.106, 0.164, 0.203, 0.250, 0.320, 0.395, 0.450, 0.530, 0.607, 0.819, 0.939
0.990U	12	0.010, 0.049, 0.080, 0.106, 0.164, 0.250, 0.320, 0.395, 0.450, 0.607, 0.819, 0.939

TABLE A-39. LOCATIONS OF ABSOLUTE PRESSURE TRANSDUCERS' BVI ARRAYS ON THE UH-60A BLADE (UPPER AND LOWER SURFACE TRANSDUCER LOCATIONS SHOWN SEPARATELY WHEN DIFFERENT)

Radial	No.	Chordwise
0.708U, 0.741U, 0.893U, 0.942U	2	0.010, 0.049
0.708L, 0.741L, 0.805L, 0.835L, 0.893L, 0.942L	1	0.049
0.805U, 0.835U	2	0.030, 0.049

pressure transducers were remeasured. Figure A-52 and tables A-38 and A-39 include all of these changes.

A general description of the UH-60A rotor for the wind tunnel test is given in table A-40.

The strain-gauge blade was located opposite to the pressure blade and included flap and chord bending moment and torsion moment measurements at the radial stations shown in table A-41. The inboard flap and chord bending measurements at 0.113R are mounted on the blade root just outboard of the grip; the rest of the moment measurements are on the blade spar (installed before final assembly of the blade). The same inboard flap and chord bending measurements at 0.113R were also obtained on the pressure blade.

Torsion moment bridges were added to the blade surface at 0.20R, 0.30R, 0.40R, 0.60R, and 0.80R. These augmented the torsion moment bridges (on the blade spar) used in the flight test.

The blade-mounted accelerometers used during the flight test were not connected for the wind tunnel test.

Additional rotating system measurements included the pitch-link and damper loads on the four blades, blade root angles on the four blades (using two different measurement

All of the 242 pressure transducers from the flight test were checked prior to putting the rotor into the wind tunnel. Inoperable transducers were replaced or wiring modified and this resulted in 235 operational transducers at the beginning of the test. In addition, the locations of all

TABLE A-40. UH-60A WIND TUNNEL TEST DESCRIPTION

Test number	12
Sponsor	NASA, U. S. Army
Manufacturer	Sikorsky Aircraft
Number blades	4
Airfoil section	SC1095, SC1094R8
Blade twist, deg	-16.0 (nonlinear)
Blade chord, in.	20.8
Rotor diameter, ft	53.7
Rotor solidity	0.0826
Tip speed, ft/sec	719.
Instrumented radial stations	9
Transducers/radial station	11.9
Rotating sensors	322
Test points	2,755
Harmonic bandwidth	1028
Rotating samples	1,444,243,200
Test hours	83
Test completion	May 2010

approaches), hub arm vertical shears on the four blades, rotor shaft bending moments at two locations, drive shaft torque, and three orthogonal hub accelerations.

The primary data systems used for rotating measurements in the wind tunnel were the NFAC Data Acquisition System (NFAC DAS) and the Rotor Mounted Data Acquisition and Transmission System (RMDATS). The NFAC DAS was used for low-sample-rate channels (256 samples/rev), whereas the RMDATS was used for the high-sample-rate channels (2048 samples/rev), primarily the pressure measurements. The RMDATS data were conditioned and sampled in the rotating system, and the digital streams were transferred to the fixed system using a capacitive data coupler. The digital data were then integrated with the NFAC DAS data.

In addition to the rotor-system measurements, three independent image-based measurement systems were used external to the rotor: the Blade Displacement system, the Retro-Reflective Background Oriented Schlieren (RBOS) system, and the large-field Particle Image Velocimetry (PIV) system.

The blade displacement measurements were made using photogrammetry. Four pairs of cameras were used, and each blade had 48 retro-reflectors, resulting in displacement measurements from blade root to tip and around the entire azimuth (Barrows et al., 2011).

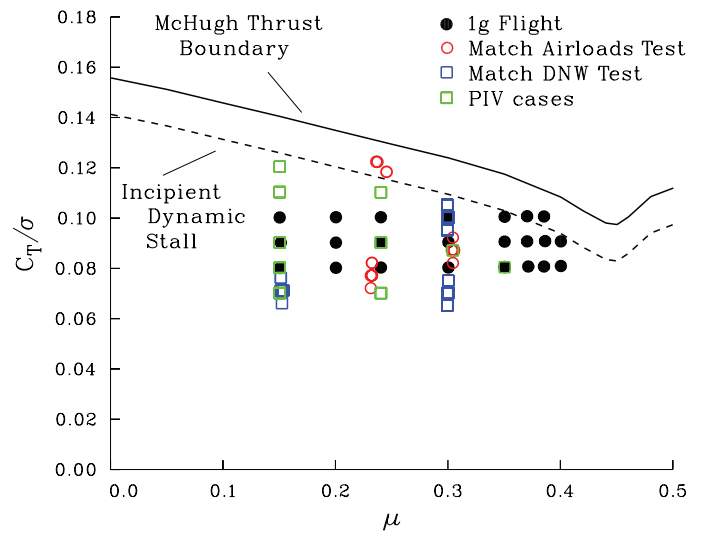


Figure A-52. UH-60A nondimensional weight as a function of advance ratio compared to McHugh's (1978) thrust boundary, test phases 1, 3, 4, and 6.

TABLE A-41. RADIAL LOCATIONS OF STRAIN-GAUGE BRIDGE LOCATIONS ON UH-60A STRAIN-GAUGE BLADE

Measurement	$r/R$
Flap bending moment	0.113, 0.200, 0.300, 0.400, 0.500, 0.600, 0.700, 0.800, 0.900
Chord bending moment	0.113, 0.200, 0.300, 0.400, 0.500, 0.600, 0.700, 0.800
Torsion moment	0.200, 0.300, 0.400, 0.500, 0.600, 0.700, 0.800, 0.900

The RBOS system is an optical system that can trace density variations in the blade tip vortices by comparing wind tunnel on and off images of the vortices against a speckled, retro-reflective background (Heineck et al., 2010).

PIV systems are optical approaches that are able to measure all three components of velocity in a plane using a seeded flow. This approach is now a well-established technique, particularly at small scales. For the UH-60A wind tunnel test, a plane was defined that was 0.13R high by 0.52R wide, the largest PIV "region of interest" so far attempted in the NFAC tunnels (Wadcock et al., 2011). Because of tunnel constraints, only one azimuth was used for the PIV testing, approximately at 90°.

The wind tunnel testing was divided into six phases: (1) 1-g level flight sweeps, (2) parametric sweeps, (3) airload flight test simulations, (4) small-scale wind tunnel simulations, (5) slowed rotor test, and (6) PIV testing (Norman et al., 2011).

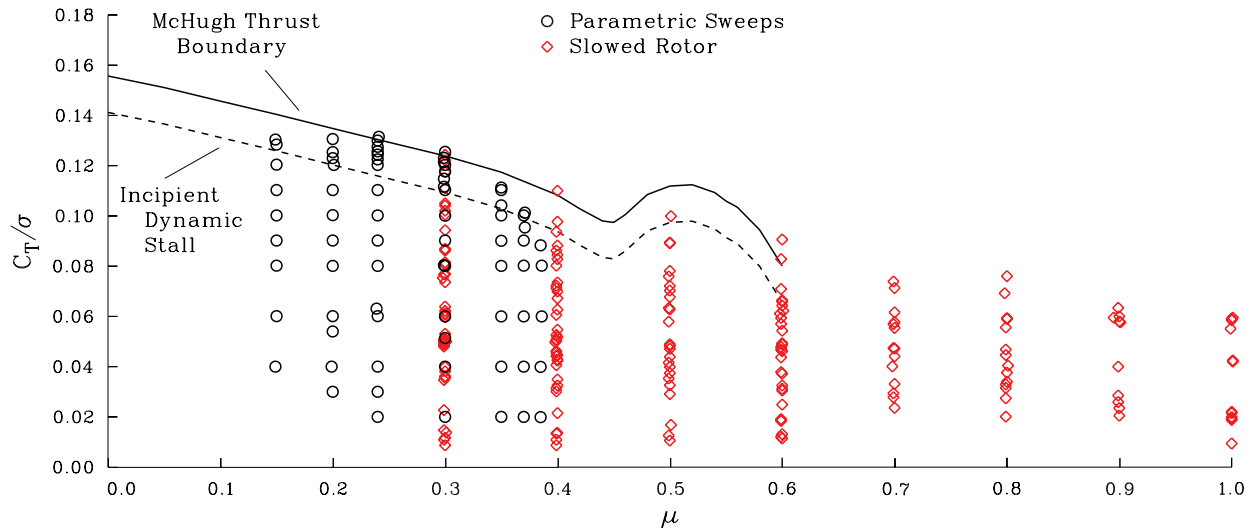


Figure A-53. UH-60A nondimensional thrust as a function of advance ratio compared to McHugh's (1978) thrust boundary, test phases 2 and 5.

The first phase, the 1-g level flight sweeps, examined the rotor trimmed for a constant vehicle weight and propulsive force as would occur for a helicopter in forward flight. The required rotor trim hub moments were calculated from CAMRAD II. The second phase, the parametric sweeps, looked at variations in thrust, advance ratio, Mach number, and shaft angle with the rotor hub moments set to zero. The third and fourth phases trimmed the rotor to match a limited number of the flight and wind tunnel test points. This testing included derivative conditions around each baseline point.

The fifth test phase examined the effects of high-advance-ratio conditions (up to  $\mu = 1.0$ ) using reduced rotor speeds. The sixth phase, PIV testing, used selected conditions based on previous test points, and the data were obtained with various blade azimuthal delays with respect to the PIV optical plane.

The six phases are shown on plots of the nondimensional thrust coefficient,  $C_T/\sigma$ , as a function of advance ratio,  $\mu$ , and are compared with the McHugh thrust boundary and the line of incipient dynamic stall in figures A-52 and A-53. The data from test phases 1, 3, 4, and 6 are shown in figure A-52 for a conventional range of advance ratios up to  $\mu = 0.4$ , whereas phases 2 and 5 are shown in figure A-53 with values up to  $\mu = 1.0$ .

Parametric sweep data included testing to define the rotor thrust limit at  $\mu = 0.24$  and  $0.30$ . Figure A-53 shows good agreement between the UH-60A rotor and McHugh's model test results. The line of incipient dynamic stall is

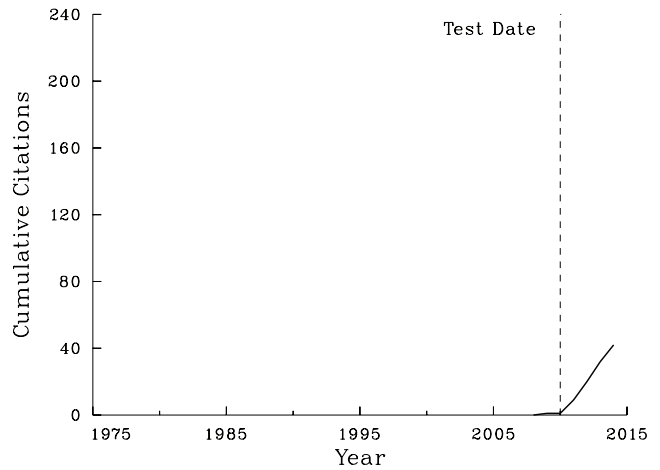


Figure A-54. Cumulative citations of the data obtained from the UH-60A wind tunnel test (Norman et al., 2011).

based on these test data and indicates the thrust value where there is evidence of dynamic stall on the rotor.

The initial papers reporting on the wind tunnel test (Norman et al., 2011; Datta et al., 2011; Romander et al., 2011) have between them approximately 35 figures that show airload measurements.

Cumulative citations for the UH-60A wind tunnel test are shown in figure A-54. Although there are only 42 citations at the time of this writing, the expectation is that this massive data set will provide a wealth of use in the coming years.

## APPENDIX 2—CORRELATION ACCURACY

### Introduction

There is value in applying uniform, quantitative metrics to judge correlation accuracy rather than relying on qualitative evaluations alone. Bousman and Norman (2010) have used an accuracy metric based on the linear regression of a set of dependent variables with respect to a set of independent variables. They have applied this approach to a wide range of rotorcraft aeromechanics problems, generally using experimental measurements as the independent variables and calculations as the dependent variables. But one can also compare experimental measurements to each other by arbitrarily selecting one data set as the dependent one and the other set as the independent variables.

This appendix reviews the approach used by Bousman and Norman (2010) and includes some modifications. As will be shown, linear regression provides three metrics: (1) an accuracy or scale metric, (2) a scatter or dispersion metric, and (3) a steady offset or bias metric. The application of this approach is described separately for (1) steady data and (2) time history data, however, the mechanics of linear regression metrics are much the same in either case.

### Steady Data

An example of steady data correlation is shown in figure B-1. The comparison shows the UH-60A power measured in six airspeed sweeps at differing weight coefficients. The measured values (symbols) are considered the independent variables, and the CAMRAD II calculations (lines) are the dependent variables.

Figure B-2 shows the linear regression for the case of  $C_w/\sigma = 0.079$ . The black 45° line represents a perfect fit between the calculations and measurements. If that were the case, the slope  $m$  would be 1.0. Qualitatively, there is good agreement between the calculations and the measurements. In this case, the accuracy metric,  $m$ , is 1.037, an overprediction of 3.7 percent. Scatter is expressed either by the coefficient of determination,  $r^2$ , or the standard error of estimate,  $S_e$ . For this example,  $r^2 = 0.9751$  and  $S_e = 2.7$  percent. The standard error of estimate requires a reference value whereas the coefficient of determination does not. In Bousman and Norman (2010), the  $S_e$  reference value was chosen to be the ordinate scale. Here only  $r^2$  is used as a measure of scatter. The third metric, the offset, also requires a reference value. In this case, the average of the difference between the dependent and independent variables is taken, and it is referenced to the ordinate scale ( $C_p/\sigma = 0.014$ ). For this example the average percent offset difference is -1.9 percent.

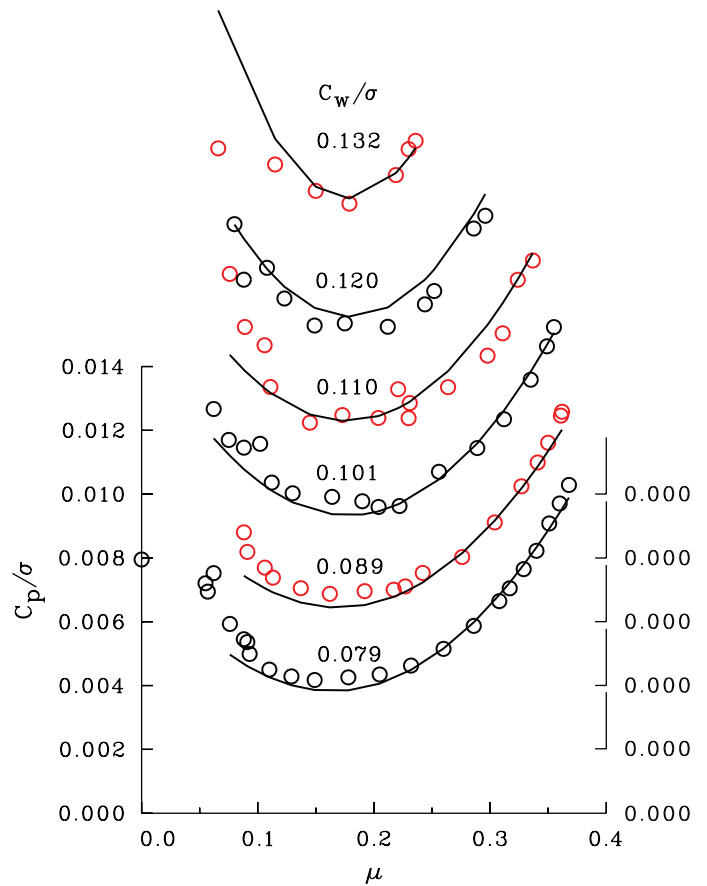


Figure B-1. Offset plot of engine power coefficient for the UH-60A with calculations using CAMRAD II for six airspeed sweeps (Yeo et al., 2004). Color is used to discriminate between airspeed sweeps.

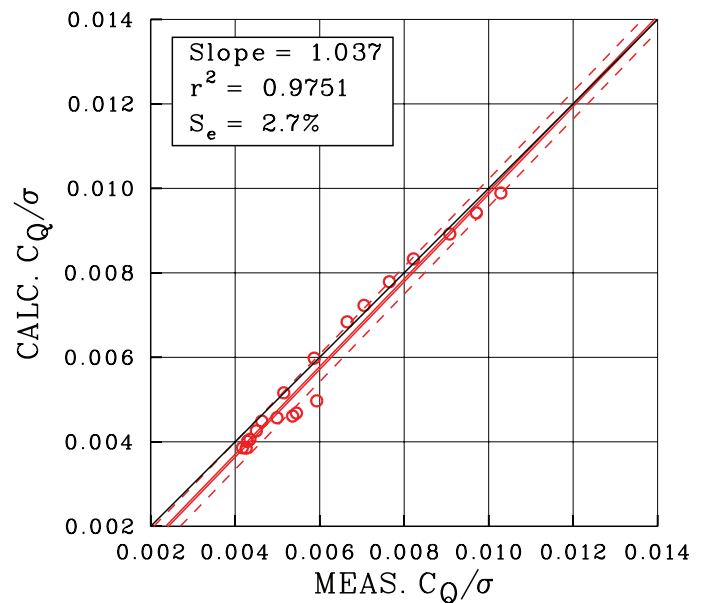


Figure B-2. Linear regression of CAMRAD II calculation of engine power coefficient against UH-60A flight test data for  $C_w/\sigma = 0.079$ .



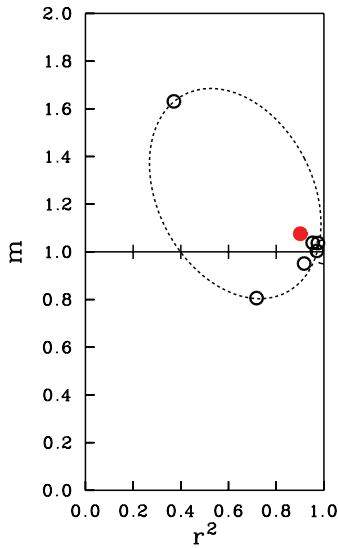
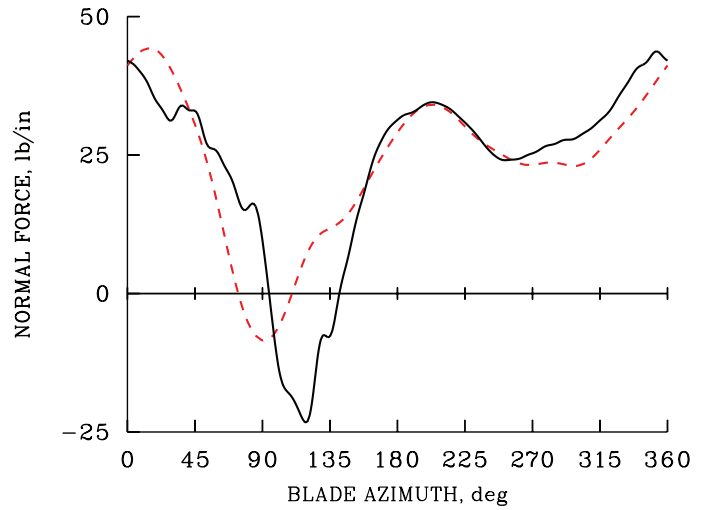


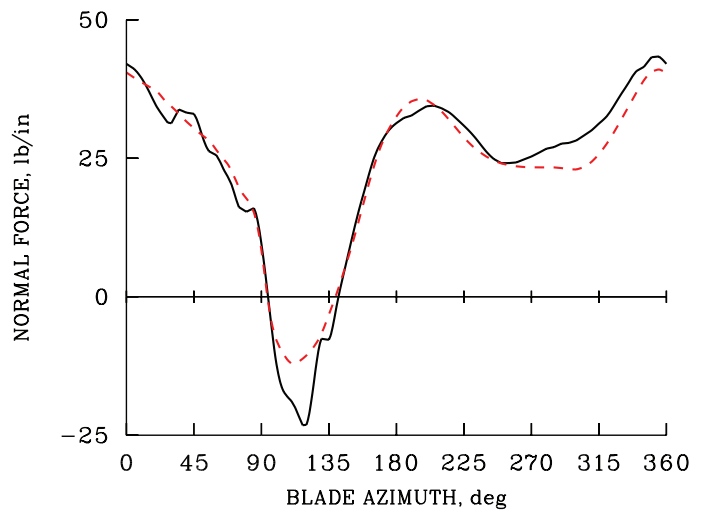
Figure B-3. Accuracy map for six airspeed sweeps for engine power coefficient for the UH-60A. The solid red circular symbol represents an accuracy metric for combined analysis.

The linear regression calculation is repeated for each airspeed sweep, thus there are six sets of metrics. Graphically these can be shown on an accuracy map as indicated in figure B-3. The accuracy map is a plot of  $m$  as a function of  $r^2$ . If the calculations and measurements agreed exactly, all of the values would lie at the point where  $m = r^2 = 1.0$ . If the agreement is not exact, then the error can be represented by half circles that are concentric about the  $m = r^2 = 1.0$  center. The map in figure B-3 shows a half circle for an accuracy of 5 percent with a dashed line. An arbitrary dashed ellipse has also been added to illustrate the scatter in the power calculation results.

The solid red circular symbol in the accuracy map in figure B-3 is a result of combined analysis of all of the data, that is all of the airspeed sweep data are lumped together and the linear regression is calculated for the combined data set. Both the individual and combined linear regression values have their usefulness. The combined value gives an overall assessment of accuracy, whereas the individual values may provide insight into sources of error. In this example, the accuracy at  $C_w/\sigma = 0.079$  is quite good. The small errors for this weight coefficient are probably related to the difficulty in making accurate measurements at low speeds, as well as making calculations at the highest speeds where supersonic flow over the airfoil may cause difficulties. The accuracy of the three lower weight coefficients are reasonably good, but as the weight coefficient (rotor thrust) increases, the accuracy is degraded. In the figure B-3, the largest error (accuracy circle of 89 percent) is for the highest weight coefficient,  $C_w/\sigma = 0.132$ . The next largest error (34 percent) is for  $C_w/\sigma = 0.110$ .



a. CAMRAD II and UH-60A flight data.



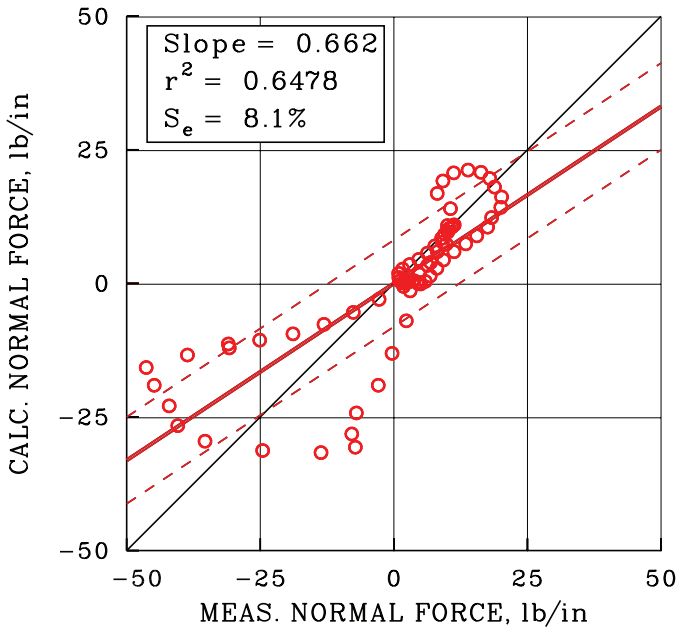
b. OVERFLOW/CAMRAD II and UH-60A flight data.

Figure B-4. Comparison of CAMRAD II and coupled OVERFLOW/CAMRAD II calculations with flight data for Counter 8534 at  $0.865R$ , 1–36 harmonics.

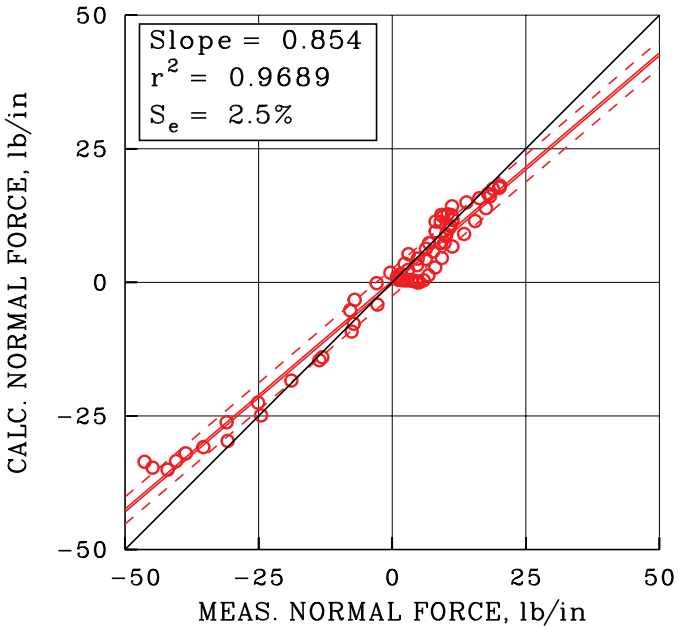
### Time History Data

An example of unsteady data correlation (time histories) is shown in figure B-4. The comparison shows the UH-60A normal force data at  $0.865R$  over one revolution. Figure B-4a shows calculations made with the comprehensive analysis CAMRAD II using a free wake model, whereas figure B-4b shows the calculation from an analysis that couples OVERFLOW and CAMRAD II (CFD/CSD coupling).

The linear regression data sets are created by sampling the time histories at a specified sample rate, in this case 72 samples per revolution (every 5 degrees). Hence, there are 72 dependent and 72 independent variables.



a. CAMRAD II and UH-60A flight data.



b. OVERFLOW/CAMRAD II and UH-60A flight data.

Figure B-5. Linear regression of CAMRAD II and coupled OVERFLOW/CAMRAD II calculations against flight data from Counter 8534 at 0.865R, 1–36 harmonics.

The linear regression plots are shown for this example in figure B-5. Using CAMRAD II alone, the slope is 0.662, an underprediction of about 34 percent. The calculation shows fairly good agreement over about three quadrants of the rotor, but there is a considerable phase error with regards to the strong negative loading on the advancing side. Because of the phase error there is considerable dispersion, and the coefficient of determination is 0.6478, a low value.

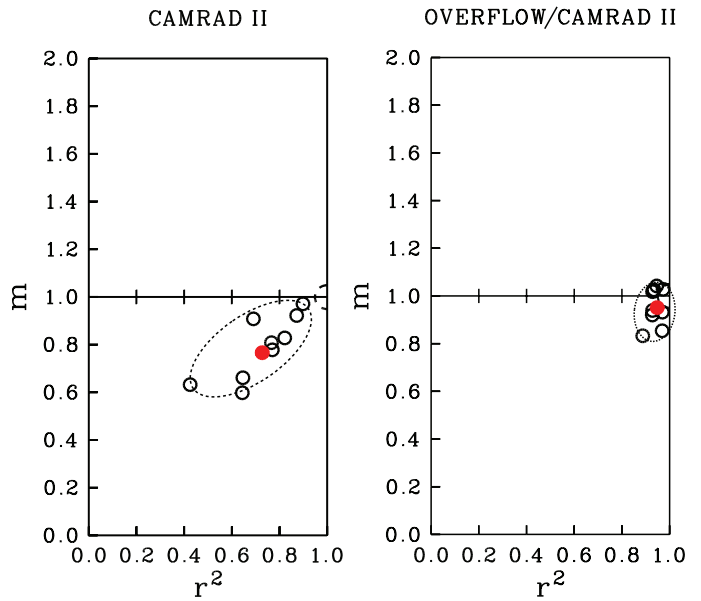


Figure B-6. Accuracy maps based on linear regression of CAMRAD II and coupled OVERFLOW/CAMRAD II calculations against flight data from Counter 8534 at 0.865R, 1–36 harmonics.

The linear regression for the coupled calculation, as shown in figure 5b, is better. Here the slope is 0.854, an underprediction of about 15 percent, and the coefficient of determination is 0.9689, indicating little scatter.

The correlation examined in figures B-4 and B-5 are for one radial station. Calculations were also made at the other measurement stations, and a better judgment of accuracy can be made by looking at all of these analysis results. One way of doing this is to plot the  $m$  and  $r^2$  values of the calculations at all of the radial stations on a single accuracy map, just as was done for the steady data. The maps for the two cases are shown below in figure B-6.

The CAMRAD II calculations are in the accuracy map on the left in figure B-6. The results are fairly good at some radial stations, but there is considerable variation as indicated by an ellipse that encloses all of the calculations. The coupled OVERFLOW/CAMRAD II results are significantly better, as shown on the right-hand side of the figure. The answers are quite near the 5-percent error half circle, and there is very little variation in accuracy between the nine stations.

## REFERENCES

- Balough, D. L. 1994. Estimation of Rotor Flapping Response Using Blade-Mounted Accelerometers. Amer. Hel. Soc. Aeromechanics Specialists Conference, San Francisco, CA.
- Barnard R. 1976. YUH-60A/T700 IR Suppressor Full Scale Prototype Test Report. SER 70094.
- Barrows, D. A., A. W. Burner, A. I. Abrego, and L. E. Olson. 2011. Blade Displacement Measurements of the Full-Scale UH-60A Airloads Rotor. 29th AIAA Applied Aerodynamics Conference, Honolulu, HI.
- Bartsch, E. A. 1968a. In-Flight Measurement and Correlation with Theory of Blade Airloads and Responses on the XH-51A Compound Helicopter Rotor, Volume I—Measurement and Data Reduction of Airloads and Structural Loads. USAAVLABS TR 68-22A.
- Bartsch, E. A. 1968b. In-Flight Measurement and Correlation with Theory of Blade Airloads and Responses on the XH-51A Compound Helicopter Rotor, Volume II—Measurement and Data Reduction of Airloads and Structural Loads Appendixes V Through IX. USAAVLABS TR 68-22B.
- Bausch, W. E., C. L. Munch, and R. G. Schlegel. 1971. An Experimental Study of Helicopter Rotor Impulsive Noise. USAAVLABS TR 70-72.
- Beaumier, P. 1994. A Coupling Procedure Between a Rotor Dynamics Code and a 3D Unsteady Full Potential Code. Amer. Hel. Soc. Aeromechanics Specialists Conference, San Francisco, CA.
- Beno, E. A. 1970a. CH-53A Main Rotor and Stabilizer Vibratory Airloads and Forces (Vol. I). Sikorsky Aircraft SER 65593.
- Beno, E. A. 1970b. CH-53A Main Rotor and Stabilizer Vibratory Airloads and Forces (Vol. II). Sikorsky Aircraft SER 65593.
- Beno, E. A. 1973. Analysis of Helicopter Maneuver-Loads and Rotor-Loads Flight Test Data. NASA CR-2225.
- Bhattacharjee, Y. 2011. House Panel Would Kill Space Telescope. *Science*, 330, pp. 275–76.
- Bjorkman, W. S. and M. J. Bondi. 1990. TRENDS: The Aeronautical Post-Test Database Management System. NASA TM 101025.
- Bousman, W. G. 1987. Estimation of Blade Airloads From Rotor Blade Bending Moments. Thirteenth European Rotorcraft Forum, Arles, France.
- Bousman, W. G. 1990. The Response of Helicopter Rotors to Vibratory Airloads. *J. Amer. Hel. Soc.*, 35 (4).
- Bousman, W. G. 1998. A Qualitative Examination of Dynamic Stall from Flight Test Data. *J. Amer. Hel. Soc.*, 43 (4).
- Bousman, W. G. and D. H. Hodges. 1979. An Experimental Study of Coupled Rotor-Body Aeromechanical Instability of Hingeless Rotors in Hover. *Vertica*, 3, pp. 221–244.
- Bousman, W. G. and R. M. Kufeld. 2005. UH-60A Airloads Catalog, NASA TM 2005–212827.
- Bousman, W. G. and T. Norman. 2010. Assessment of Predictive Capability of Aeromechanics Methods. *J. Amer. Hel. Soc.*, 55 (1).
- Bousman, W. G., C. Young, N. Gilbert, F. Toulmay, W. Johnson, and M. J. Riley. 1989. Correlation of Puma Airloads—Lifting-line and Wake Calculation. Fifteenth Eur. Rotorcraft Forum, Amsterdam, The Netherlands.
- Bousman, W. G., C. Young, F. Toulmay, N. E. Gilbert, R. C. Strawn, J. V. Miller, T. H. Maier, M. Costes, and P. Beaumier. 1996. A Comparison of Lifting-Line and CFD Methods With Flight Test Data From a Research Puma Helicopter. NASA TM 110421.
- Bowden, T. H. and G. A. Schockey. 1970. A Wind-Tunnel Investigation of the Aerodynamic Environment of a Full-Scale Helicopter Rotor in Forward Flight. USAAMRDL TR 70-35.
- Boxwell, D. A. and F. H. Schmitz. 1980. Full-Scale Measurements of Blade-Vortex Interaction Noise. Amer. Hel. Soc. 36th Annual Forum, Washington, D.C.
- Brotherhood, P. 1982. An Appraisal of Rotor Blade-Tip Vortex Interaction and Wake Geometry From Flight Measurements. *In* Prediction of Aerodynamic Loads on Rotorcraft, AGARD CP 334, London, U.K.
- Bugos, G. E. 2010. *Atmosphere of Freedom: 70 Years at the NASA Ames Research Center*. NASA SP-2010-4314.
- Burpo, F. B. and R. R. Lynn. 1962. Measurement of Dynamic Air Loads on a Full-Scale Semirigid Rotor. TCREC TR 62-42.

- Burpo, F. B. and W. H. Tanner. 1968. Two-Dimensional Tests of Advanced Instrumentation for Rotors. Bell Helicopter Company Report 606-099-001.
- Caradonna, F. X. and M. P. Isom. 1976. Numerical Calculation of Unsteady Transonic Potential Flow Over Helicopter Rotor Blades. *AIAA J.*, 14 (4).
- Caradonna, F. X., C. Tung, and A. Desopper. 1984. Finite Difference Modeling of Rotor Flows Including Wake Effects. *J. Amer. Hel. Soc.*, 29 (2).
- Coleman, C. P. and W. G. Bousman. 1994. Aerodynamic Limitations of the UH-60A Rotor. Amer. Hel. Soc. Aeromechanics Specialists Conference, San Francisco, CA.
- Cowan, J., L. Dadone, and S. Gangwani. 1986. Wind Tunnel Test of a Pressure Instrumented Model Scale Rotor. Amer. Hel. Soc. 42nd Annual Forum Proceedings, Washington, D.C.
- Cox, C. R. 1977. Helicopter Rotor Aerodynamic and Aeroacoustic Environments. AIAA Preprint No. 77-1338, 4th Aeroacoustics Conference, Atlanta, GA.
- Cox, C. R. and R. R. Lynn. 1963. A Study of the Origin and Means of Reducing Helicopter Noise. TREC Technical Report 62-73.
- Cross, J. L. and W. Tu. 1990. Tabulation of Data From the Tip Aerodynamics and Acoustics Test. NASA TM 102280.
- Cross, J. L. and M. E. Watts. 1988. Tip Aerodynamics and Acoustics Test. NASA RP 1179.
- Curry, A. 2011. Rescue of Old Data Offers Lesson for Particle Physicists. *Science* 331, pp. 694-695.
- Dadone, L., S. Dawson, and D. Ekquist. 1987. Model 360 Rotor Test at DNW – Review of Performance and Blade Airload Data. Amer. Hel. Soc. 43rd Annual Forum, St. Louis, MO.
- Datta, A., M. Nixon, and I. Chopra. 2007. Review of Rotor Loads Prediction with the Emergence of Rotorcraft CFD. *J. Amer. Hel. Soc.*, 52 (4).
- Datta, A., H. Yeo, and T. R. Norman. 2011. Experimental Investigation and Fundamental Understanding of a Slowed UH-60A Rotor at High Advance Ratios. Amer. Hel. Soc. 66th Annual Forum, Virginia Beach, VA.
- Davis, S. J. 1981. Predesign Study for a Modern 4-Bladed Rotor for the RSRA. NASA CR 166155.
- Davis, S. J. and T. A. Egolf. 1980. An Evaluation of a Computer Code Based on Linear Acoustic Theory for Predicting Helicopter Main Rotor Noise. NASA CR 159339.
- Dompka, R. V., and J. D. Cronkhite. 1986. Summary of AH-1G Flight Vibration Data for Validation of Coupled Rotor-Fuselage Analysis. NASA CR-178160.
- Fenaughty, R. and E. Beno. 1970a. NH-3A Vibratory Airloads and Vibratory Rotor Loads. Sikorsky Aircraft SER 611493, Vol. I.
- Fenaughty, R. and E. Beno. 1970b. NH-3A Vibratory Airloads and Vibratory Rotor Loads. Sikorsky Aircraft SER 611493, Vol. II.
- Golub, R. and W. McLachlan. 1967. In-flight Measurement of Rotor Blade Airloads, Bending Moments, and Motions, Together with Rotor Shaft Loads and Fuselage Vibration, on a Tandem Rotor Helicopter, Vol. I, Instrumentation and In-Flight Recording System. USAAVLABS TR 67-9A.
- Gormont, R. E. 1973. A Mathematical Model of Unsteady Aerodynamics and Radial Flow for Application to Helicopter Rotors. USAAVLABS TR 72-67.
- Grant, W. J. and R. R. Pruyn. 1967. In-Flight Measurement of Rotor Blade Airloads, Bending Moments, and Motions, Together With Rotor Shaft Loads and Fuselage Vibration, on a Tandem Rotor Helicopter, Vol. II, Calibrations and Instrumented Component Testing. USAAVLABS TR 67-9B.
- Gustafson, F. B. 1945. Flight Test of the Sikorsky HNS-1 (Army YR-4B) Helicopter, I-Experimental Data on Level-Flight Performance with Original Rotor Blades. NACA Memorandum Report L5C10 (re-issued as L-595).
- Gustafson, F. B. and A. Gessow. 1945. Tests of the Sikorsky HNS-1 (Army YR-4B) Helicopter, II – Hovering and Vertical-Flight Performance with the Original and an Alternate Set of Main-Rotor Blades, Including a Comparison with Hovering Performance Theory. NACA Memorandum Report L5D09a (reissued as L-596).
- Gustafson, F. B. and A. Gessow. 1947. Effect of Blade Stalling on the Efficiency of a Helicopter Rotor as Measured in Flight. NACA TN 1250.
- Gustafson, F. B. and G. C. Myers, Jr. 1946. Stalling of Helicopter Blades. NACA Report No. 840.
- Ham, N. D. 1967. Stall Flutter of Helicopter Rotor Blades: A Special Case of the Dynamic Stall Phenomenon. *J. Amer. Hel. Soc.*, 12 (4).



- Ham, N. D. and M. S. Garelick. 1968. Dynamic Stall Considerations in Helicopter Rotors. *J. Amer. Hel. Soc.*, 13 (2).
- Ham, N. D. and M. I. Young. 1966. Torsional Oscillations of Helicopter Blades Due to Stall. *J. Aircraft*, 3 (3).
- Harris, F. D. and R. R. Pruyn. 1968. Blade Stall—Half Fact, Half Fiction. *J. Amer. Hel. Soc.*, 13 (2).
- Heffernan, R. and M. Gaubert. 1986. Structural and Aerodynamic Loads and Performance Measurements of an SA349/2 Helicopter With an Advanced Geometry Rotor. NASA TM 88370.
- Heineck, J. T., E. T. Schairer, L. K. Kushner, L. K., and L. A. Walker. 2010. Retroreflective Background Oriented Schlieren (RBOS) as Applied to Full-Scale UH-60 Blade Tip Vortices. Amer. Hel. Soc. Aeromechanics Specialists' Conference, San Francisco, CA.
- Heyson, H. H. 1956. Analysis and Comparison With Theory of Flow-Field Measurements Near a Lifting Rotor in the Langley Full-Scale Tunnel. NACA TN 3691.
- Hirschberg, M. 2001. The Rotorcraft Centers of Excellence. *Vertiflite*, 47 (2).
- Hooper, W. E. 1983. The Vibratory Airloading of Helicopter Rotors. Paper No. 46, Ninth Eur. Rotorcraft Forum, Stresa, Italy.
- Hooper, W. E. 1985. Panel Two: Data Bases—The User's Viewpoint, Prepared Comments. *In Rotorcraft Dynamics 1984*, NASA CP 2400.
- Johnson, W. 1970. The Response and Airloading of Helicopter Rotor Blades Due to Dynamic Stall. Massachusetts Institute of Technology, ASRL TR 130-1.
- Johnson, W., Discussion in Hooper, W. E. 1985. Panel Two: Data Bases—The User's Viewpoint, Prepared Comments. *In Rotorcraft Dynamics 1984*, NASA CP 2400, p. 487.
- Johnson, W. 2011a. Milestones in Rotorcraft Aeromechanics. NASA/TP-2011-215971.
- Johnson, W. 2011b. Milestones in Rotorcraft Aeromechanics, Alexander A Nikolsky Honorary Lecture. *J. Amer. Hel. Soc.*, 56 (3).
- Kufeld, R. and P. Loschke. 1991. UH-60 Airloads Program: Status and Plans. AIAA-91-3142, AIAA Aircraft Design Systems and Operations Meeting, Baltimore, MD.
- Kufeld, R. M., D. L. Balough, J. L. Cross, K. F. Studebaker, C. D. Jennison, and W. G. Bousman. 1994b. Flight Testing the UH-60A Airloads Aircraft. Amer. Hel. Soc. 50th Annual Forum Proceedings, Washington, D.C.
- Kufeld, R. M. and W. G. Bousman. 1995. High Load Conditions Measured on a UH-60A in Maneuvering Flight. Amer. Hel. Soc. 50th Annual Forum Proceedings.
- Kufeld, R. M. and W. G. Bousman. 1996. UH-60A Helicopter Rotor Airloads Measured in Flight. 22nd Eur. Rotorcraft Forum, Brighton, England.
- Kufeld, R. M. and W. G. Bousman. 2005. UH-60A Airloads Program Azimuth Reference Correction. *J. Amer. Hel. Soc.*, 50 (2).
- Kufeld, R. M., J. L. Cross, and W. G. Bousman. 1994a. A Survey of Rotor Loads Distribution in Maneuvering Flight. Amer. Hel. Soc. Aeromechanics Specialists Conference, San Francisco, CA.
- Kvaternik, R. G. 1993. The NASA/Industry Design Analysis Methods For Vibrations (DAMVIBS) Program—A Government Overview. In A Government/Industry Summary of the Design Analysis Methods for Vibrations (DAMVIBS) Program, NASA CP 10114.
- Langer, H. J., R. L. Peterson, and T. H. Maier. 1996. An Experimental Evaluation of Wind Tunnel Wall Correction Methods for Helicopter Performance. Amer. Hel. Soc. 52nd Annual Forum, Washington, D.C.
- Lawler, A. and Y. Bhattacharjee. 2010. Massive Cost Overrun to Webb Threatens Other NASA Missions. *Science*, 330, pp. 1028–29.
- Leishman, J. G. 2000. *Principles of Helicopter Aerodynamics*. Cambridge University Press, Cambridge, U.K.
- Leishman, J. G. and T. S. Beddoes. 1989. A Semi-Empirical Model for Dynamic Stall. *J. Am. Hel. Soc.*, 24 (3).
- Loewy, R. G. and L. R. Sutton. 1966. A Theory for Predicting the Rotational Noise of Lifting Rotors in Forward Flight, Including a Comparison With Experiment. USAA-VLABS TR 65-82.
- Lorber, P. F. 1991. Aerodynamic Results of a Pressure-Instrumented Model Rotor Test at the DNW. *J. Amer. Hel. Soc.*, 36 (4).
- Lorber, P. F., R. C. Stauter, R. J. Haas, T. J. Anderson, M. S. Torok, and F. W. Kohlhepp. 1994. Techniques for Comprehensive Measurement of Model Helicopter Rotor Aerodynamics. Amer. Hel. Soc. 50th Annual Forum Proceedings, Washington, D.C.

- Lorber, P. F., R. C. Stauter, and A. J. Landgrebe. 1989. A Comprehensive Hover Test of the Airloads and Airflow of an Extensively Instrumented Model Helicopter Rotor, Amer. Hel. Soc. 45th Annual Forum, Boston, MA.
- Ludi, L. H. 1958a. Flight Investigation of Effects of Atmosphere Turbulence and Moderate Maneuvers on Bending and Torsional Moments Encountered by a Helicopter Rotor Blade. NACA TN 4203.
- Ludi, L. H. 1958b. Flight Investigation of Effects of Retreating-Blade Stall on Bending and Torsional Moments Encountered by a Helicopter Rotor Blade. NACA TN 4254.
- Ludi, L. H. 1959. Flight Investigation of Effects of Transition, Landing Approaches, Partial-Power Vertical Descents, and Droop-Stop Pounding on the Bending and Torsional Moments Encountered by a Helicopter Rotor Blade. NACA MEMO 5-7-59L.
- Ludi, L. H. 1961. Flight Investigation of Effects of Additional Selected Operating Conditions on Bending and Torsional Moments Encountered by a Helicopter Rotor Blade. NASA TN D759.
- Lunn, K. and J. L. Knopp. 1981. Real Time Analysis for Helicopter Flight Testing. *Vertica* 5 (3).
- MacNeal, R. H. 1974. Panel 1: Prediction of Rotor and Control System Loads. Question and Answers. *In* Rotorcraft Dynamics 1974, NASA SP-352.
- Mayo, Alton P. 1959. Comparison of Measured Flapwise Structural Bending Moments on a Teetering Rotor Blade With Results Calculated From the Measured Pressure Distribution. NASA MEMO 2-28-59L.
- McCroskey, W. J. and R. K. Fisher, Jr. 1972. Detailed Aerodynamic Measurements on Model Rotor in the Blade Stall Regime. *J. Amer. Hel. Soc.*, 17 (1).
- McCroskey, W. J., K. W. McAlister, L. W. Carr and S. L. Pucci. 1982. An Experimental Study of Dynamic Stall on Advanced Airfoil Sections Volume 1. Summary of Experiments. NASA TM 84245.
- McHugh, F. J. 1978. What Are the Lift and Propulsive Force Limits at High Speed for the Conventional Rotor? Amer. Hel. Soc. 34th Annual National Forum Proceedings, Washington, D.C., Preprint 78-2.
- McHugh, F. J., C. Ross, and M. Solomon. 1977. Wind Tunnel Investigation of Rotor Lift and Propulsive Force at High Speed—Data Analysis. NASA CR 145217-1.
- Merkley, D. J., M. J. Riley, and C. Young. 1983. Summary Report of the Second TTCP/HTP-6 Joint Working Session on Rotor Loads. USAAVRADCOM-TR-83-D-29.
- Miller, R. H. 1963. A Discussion of Rotor Blade Harmonic Airloading. CAL/TRECOM Symposium on Dynamic Load Problems Associated with Helicopters and V/STOL Aircraft, Buffalo, NY.
- Miller, R. H. 1964. Unsteady Air Loads on Helicopter Rotor Blades. *J. Royal Aircraft Soc.*, 68:640.
- Morris, C. E. K., Jr. 1978. Rotor-Airfoil Flight Investigation: Preliminary Results. Amer. Hel. Soc. 34th Annual National Forum Proceedings, Washington, D.C.
- Morris, C. E. K., Jr., D. D. Stevens, and R. L. Tomaine. 1980. A Flight Investigation of Blade-Section Aerodynamics for a Helicopter with NLR-1T Airfoil Sections. NASA TM 80166.
- Mueller, A. W., D. A. Conner, C. K. Rutledge, and M. R. Wilson. 1995. Full-Scale Flight Acoustic Results for the UH-60A Airloads Aircraft. Amer. Hel. Soc. Vertical Lift Aircraft Design Conference, San Francisco, CA.
- Nakamura, Y. 1982. Prediction of Blade-Vortex Interaction Noise from Measured Blade Pressure. *Vertica*, 6 (4).
- Newman, D., T. Doligalski, and R. Minniti. 2008. Advances in Modeling and Simulation of Rotorcraft Noise and Associated Impacts on Survivability. DARPA.
- Nguyen, K. and W. Johnson. 1998. Evaluation of Dynamic Stall Models with UH-60A Airloads Flight Test Data. AHS International 54th Annual Forum Proceedings, Washington, D.C.
- Norman, T. R., R. L. Peterson, T. H. Maier, and H. Yeo. 2012. Evaluation of Wind Tunnel and Scaling Effects with the UH-60A Airloads Rotor. AHS International 68th Annual Forum, Fort Worth, TX.
- Norman, T. R., P. Shinoda, C. Kitaplioglu, S. A. Jacklin, and A. Sheikman. 2002. Low-Speed Wind Tunnel Investigation of a Full-Scale UH-60 Rotor System. Amer. Hel. Soc. 58th Annual Forum, Montreal, Canada.
- Norman, T. R., P. Shinoda, R. L. Peterson, and A. Datta. 2011. Full-Scale Wind Tunnel Test of the UH-60A Airloads Rotor. AHS International 67th Annual Forum, Virginia Beach, VA.
- Obbard, J. W. 1967. In-Flight Measurement of Rotor Blade Airloads, Bending Moments, and Motions, Together With

- Rotor Shaft Loads and Fuselage Vibration, on a Tandem Rotor Helicopter, Vol. III, Data Processing and Analysis System. USAAVLABS TR 67-9C.
- Ormiston, R. A. 1974. Comparison of Several Methods for Predicting Loads on a Hypothetical Helicopter Rotor. *J. Amer. Hel. Soc.*, 19 (4).
- Ormiston, R. A. 2004. An Investigation of the Mechanical Airloads Problem for Evaluating Rotor Blade Structural Dynamics Analysis. Amer. Hel. Soc. 4th Decennial Specialists' Conference on Aeromechanics, San Francisco, CA.
- Patterson, J. L. 1952. A Miniature Electrical Pressure Gage Utilizing a Stretched Flat Diaphragm. TN 2659.
- Petot, D. 1989. Differential Equation Modeling of Dynamic Stall. *La Recherche Aerospatiale*, No. 1989-5.
- Petot, D., G. Arnaud, R. Harrison, J. Stevens, D. Teves, B. G. van der Wall, C. Young, and E. Szechenyi. 1997. Stall Effects and Blade Torsion—An Evaluation of Predictive Tools. 23rd Eur. Rotorcraft Forum, Dresden, Germany.
- Philbrick, R. B. 1980. The Data from Aeromechanics Test and Analytics—Management and Analysis Package (DATAMAP), Vol. 1 – User's Manual. USAAVRADCOTR-80-D-30A.
- Philbrick, R. B. and A. L. Eubanks. 1979. Operational Loads Survey – Data Management System, Vol. 1 User's Manual. USARTL TR 78-52A.
- Piziali, R. A. 1966a. A Method for Predicting the Aerodynamic Loads and Dynamic Response of Rotor Blades. USAAVLABS TR 65-74.
- Piziali, R. A. 1966b. Method for the Solution of the Aeroelastic Response Problem for Rotating Wings. *J. Sound and Vibration*, 4, (3).
- Piziali, R., H. Daughaday, and F. DuWaldt. 1963. Rotor Airloads. CAL/TRECOM Symposium on Dynamic Load Problems Associated With Helicopters and V/STOL Aircraft, Buffalo, NY.
- Piziali, R. A. and F. DuWaldt. 1962. A Method for Computing Rotary Wing Airload Distributions in Forward Flight. TRECOM Report No. TCREC TR 62-44.
- Post, D. E. 2010. Highlights of the CREATE Program. DoD HPCMP User Group Conference, Schaumburg, IL.
- Potsdam, M. A., H. Yeo, and W. Johnson. 2004. Rotor Airloads Prediction Using Loose Aerodynamic/Structural Coupling. Amer. Hel. Soc. 60th Annual Forum, Baltimore, MD.
- Prouty, R. W. 2009. The Lockheed Helicopter Experience. Amer. Hel. Soc. 65th Annual Forum Proceedings, Grapevine, TX.
- Pruyn, R. R. 1967. In-flight Measurement of Rotor Blade Airloads, Bending Moments, and Motions, Together With Rotor Shaft Loads and Fuselage Vibration, on a Tandem Rotor Helicopter, Vol. IV, Summary and Evaluation of Results. USAAVLABS TR 67-9D.
- Pruyn, R. R. 1968. In-Flight Measurement of Rotor Blade Airloads, Bending Moments, and Motions, Together with Rotor Shaft Loads and Fuselage Vibration, on a Tandem Rotor Helicopter, Vol. V, Investigation of Blade Stall Conditions. USAAVLABS TR 67-9E.
- Pruyn, R. and W. T. Alexander, Jr. 1966. The USAAVLABS Tandem Rotor Airloads Measurement Program. AIAA Aerodynamic Testing Conference, Los Angeles, CA.
- Pruyn, R. R. and J. Obbard. 1966. The Measurement and Analysis of a Rotor Blade Airloads and the Resulting Dynamic Response of a Large Tandem Rotor Helicopter. The Fourth International Instrumentation Symposium, Cranfield, England.
- Rabbott, J. P., Jr. 1956. Static-Thrust Measurements of the Aerodynamic Loading on a Helicopter Rotor Blade. NACA TN 3688.
- Rabbott, J. P., Jr. and G. B. Churchill. 1956. Experimental Investigation of the Aerodynamic Loading on a Helicopter Rotor Blade in Forward Flight. NACA RM L56107.
- Rabbott, J. P., Jr., A. A. Lizak, and V. M. Paglino. 1966a. A Presentation of Measured and Calculated Full-Scale Rotor Blade Aerodynamic and Structural Loads. USAAVLABS TR 66-31 (also Sikorsky Aircraft SER 58398).
- Rabbott, J. P., Jr., A. A. Lizak, and V. M. Paglino. 1966b. Tabulated Sikorsky CH-34 Blade Surface Pressures Measured at the NASA/Ames Full Scale Wind Tunnel. Sikorsky Aircraft SER 58399.
- Rao, B. M. and P. R. Schatzle. 1978. Analysis of Unsteady Airloads of Helicopter Rotors in Hover. *J. Aircraft*, 15 (4).
- Riley, M. J. 1986. Measurements of the Performance of a Helicopter Swept Tip Rotor in Flight. Twelfth Eur. Rotorcraft Forum, Garmisch-Partenkirchen, Germany.

- Riley, M. J. and J. V. Miller 1983. Pressure Distributions on a Helicopter Swept Tip From Flight Testing and From Calculations. Ninth Eur. Rotorcraft Forum, Stresa, Italy.
- Romander, E., T. R. Norman, I-C. Chang. 2011. Correlating CFD Simulation With Wind Tunnel Test for the Full-Scale UH-60A Airloads Rotor. Amer. Hel. Soc. 67th Annual Forum, Virginia Beach, VA.
- Rutledge, C. K., A. W. Mueller, and M. Wilson. 1995. A Study of the Variability Difference Between Model Scale Wind Tunnel and Full Scale Flight Test Airloads Data. Amer. Hel. Soc. Vertical Lift Aircraft Design Conference, San Francisco, CA.
- Scheiman, J. 1964. A Tabulation of Helicopter Rotor-Blade Differential Pressures, Stresses, and Motions as Measured in Flight. NASA TM X-952.
- Scheiman, J. and L. H. Ludi. 1963. Qualitative Evaluation of Effect of Helicopter Rotor-Blade Tip Vortex on Blade Airloads. NASA TN D-1637.
- Schlegel, R., R. King, and H. Mull. 1966. Helicopter Rotor Noise Generation and Propagation. USAAVLABS TR 66-4.
- Schmitz, F. H. and D. A. Boxwell. 1976. In-Flight Far-Field Measurement of Helicopter Impulsive Noise. *J. Amer. Hel. Soc.*, 21 (4).
- Shevell, R. S. 1986. Aerodynamic Anomalies: Can CFD Prevent or Correct Them? *J. Aircraft*, 23 (8).
- Shockey, G. A., J. W. Williamson, and C. R. Cox. 1976. Helicopter Aerodynamics and Structural Loads Survey. Amer. Hel. Soc. 32nd Annual National V/STOL Forum, May 10–12, Washington, D.C.
- Shockey, G. A., J. W. Williamson, and C. R. Cox. 1977. AH-1G Helicopter Aerodynamic and Structural Loads Survey. USAAMRDL-TR-76-39.
- Snyder, W. J., J. L. Cross, and R. M. Kufeld. 1990. NASA/Army Rotor Systems Flight Research Leading to the UH-60 Airloads Program. Amer. Hel. Soc. Specialists Meeting “Innovations in Rotorcraft Test Technology for the 90’s,” Phoenix, AZ.
- Spreuer, W. E. 1968. Experimental Flight Tests of the 300 MPH XH-51A Compound Helicopter. Amer. Hel. Soc. 24th Annual National Forum, Washington, D.C.
- Stepniewski, W. Z. 1982a. Alexander A. Nikolsky. *J. Amer. Hel. Soc.*, 27 (2), pp. 3–5.
- Stepniewski, W. Z. 1982b. Factors Shaping Conceptual Design of Rotary-Wing Aircraft. *J. Amer. Hel. Soc.*, 27 (2), pp. 6–20.
- Sternfeld, H., Jr., R. H. Spencer, and E. G. Schaeffer. 1961. Study to Establish Realistic Acoustic Design Criteria for Future Army Aircraft. TREC Technical Report 61-72.
- Straub, F. K., V. R. Anand, T. S. Birchette, and B. H. Lau. 2009. Wind Tunnel Test of the SMART Active Flap Rotor. Amer. Hel. Soc. 65th Annual Forum, Grapevine, TX.
- Strawn, R. C., A. Desopper, J. Miller, and A. Jones. 1989. Correlation of Puma Airloads—Evaluation of CFD Prediction Methods, 15th Eur. Rotorcraft Forum, Amsterdam, The Netherlands.
- Strawn, R. C., and Tung, C. 1986. The Prediction of Transonic Loading on Advancing Helicopter Rotors. AGARD CP 412.
- Studebaker, K. 1994. A Survey of Hub Vibration for the UH-60A Airloads Research Aircraft. Amer. Hel. Soc. Aeromechanics Specialists Conference, San Francisco, CA.
- Succi, G. P. 1983. Limits on Prediction of Helicopter Rotor Noise Using Thickness and Loading Sources: Validation of Helicopter Noise Prediction Technique. NASA CR-166097.
- Sweers, J. E. 1968. In-Flight Measurement and Correlation With Theory of Blade Airloads and Responses on the XH-51A Compound Helicopter Rotor, Vol. III—Theoretical Prediction of Airloads and Structural Loads and Correlation with Flight Test Measurements. USAAVLABS TR 68-22C.
- Tanner, W. H. and J. F. Van Wyckhouse. 1968. Wind-Tunnel Tests of Full-Scale Rotors Operating at High Advancing Tip Mach Numbers and Advance Ratios. USAAVLABS TR 68-44.
- Tarzanin, F. J., Jr. 1972. Prediction of Control Loads Due to Blade Stall. *J. Amer. Hel. Soc.*, 17 (2).
- Thompson, F. L. 1961. Letter to USATRECOM, Subject: Information and Preliminary Data on Helicopter Rotor Blade Air Loads and Moments as Measured in Flight.
- Tolstoy, L. 1965. *Anna Karenina*. Random House, New York.
- Truong, V. K. 1993. A 2-D Dynamic Stall Model Based on a Hopf Bifurcation. 19th Eur. Rotorcraft Forum, Cernobbio, Italy.



- Tung, C., F. X. Caradonna, and W. Johnson. 1986. The Prediction of Transonic Flows on an Advancing Rotor. *J. Amer. Hel. Soc.*, (31) 3.
- van der Wall, B. G., B. Junker, C. L. Burley, T. F. Brooks, Y. Yu, C. Tung, M. Raffel, H. Richard, W. Wagner, E. Mercker, K. Pengel, H. Holthusen, P. Beaumier, and Y. Delrieux. 2002. The HART II Test in the LLF of the DNW—A Major Step Towards Rotor Wake Understanding. 28th Eur. Rotorcraft Forum, Bristol, UK.
- Van Gaasbeek, J. R. and E. E. Austin. 1978. Digital Simulation of the Operational Loads Survey Flight Tests. Amer. Hel. Soc. 34th Annual National Forum Proceedings, Washington, D.C.
- Wadcock, A. J., G. K. Yamauchi, E. Solis, and A. E. Pete. 2011. PIV Measurements in the Wake of a Full-Scale Rotor in Forward Flight. 29th AIAA Applied Aerodynamics Conference, Honolulu, HI.
- Ward, J. F. 1971. Helicopter Rotor Periodic Differential Pressures and Structural Response Measured in Transient and Steady-State Maneuvers. *J. Amer. Hel. Soc.*, 16 (1).
- Ward, J. F. 2010. NACA-NASA and the Rotary Wing Revolution. *NASA's Contributions to Aeronautics* (R. P. Hallion, ed), Vol. 1, NASA/SP-2010-570-Vol 1, pp. 134–179.
- Watts, M. E. and J. L. Cross. 1986. The NASA Modern Technology Rotors Program. AIAA Paper No. 86-9788.
- Wilson, M. R., A. W. Mueller, and C. K. Rutledge. 1995. A New Technique For Estimating Ground Footprint Acoustics for Rotorcraft Using Measured Sound Fields. Amer. Hel. Soc. Vertical Lift Aircraft Design Conference, San Francisco, CA.
- Wood, E. R. and K. D. Hilzinger. 1963. A Method for Determining the Fully Coupled Aeroelastic Response of Helicopter Rotor Blades. Amer. Hel. Soc. 19th Annual National Forum, Washington, D. C.
- Yeo, H., W. G. Bousman, and W. Johnson. 2004. Performance Analysis of a Utility Helicopter with Standard and Advanced Rotors. *J. Amer. Hel. Soc.*, 49 (3).
- Yeo, H., and I. Chopra. 2001a. Coupled Rotor/Fuselage Vibration Analysis for a Teetering Rotor and Comparison with Test Data. *J. Aircraft*, 38 (1).
- Yeo, H., and I. Chopra, I. 2001b. Coupled Rotor/Fuselage Vibration Analysis Using Detailed 3-D Airframe Models. *Mathematical Modeling and Analysis of Rotary-Wing Systems*, Vol. 33, Issues 10-11.
- Yu, Y., B. Gmelin, H. Heller, J. J. Phillipe, E. Mercker, and J. S. Preisser. 1994. HHC Aeroacoustics Rotor Test at the DNW – The Joint German/French/US HART Project. 20th Eur. Rotorcraft Forum, Amsterdam, Netherlands.
- Yu, Y., S. R. Liu, D. E. Jordan, A. J. Landgrebe, P. F. Lorber, M. J. Pollack, and R. M. Martin. 1990. Aerodynamic and Acoustic Test of a United Technologies Scale Model Rotor at DNW. Amer. Hel. Soc. 46th Annual Forum, Washington, D.C.
- Yu, Y. H., C. Tung, B. van der Wall, H.-J. Pausder, C. Burley, T. Brooks, P. Beaumier, Y. Delrieux, D. Mercker, and K. Pengel. 2002. The HART-II Test: Rotor Wakes and Aeroacoustics with Higher-Harmonic Pitch Control (HHC) Inputs—The Join German/French/Dutch/US Project. Amer. Hel. Soc. 58th Annual Forum, Montreal, Canada.